THE UNIVERSITY *of* EDINBURGH

THE UNIVERSITY OF EDINBURGH
College of Science and Engineering
School of Chemistry

Biocompatible Polymer Microarrays for Cellular High-Content Screening

By

Salvatore Pernagallo

Doctor of Philosophy

January 2010

When the Emperor Joseph II first listened to *The Abduction from the Seraglio*, he reportedly said, “My dear Mozart, that is too fine for my ears; there are too many notes.” When viewing the dauntingly expanding list of focal-adhesion components, it is also easy to conclude that there are too many molecular domains in cell–matrix adhesions. However, to continue the story, Mozart replied, “I ask your Majesty’s pardon, but there are just as many notes as there should be.”

Nature Reviews Molecular Cell Biology **2001**, 2, (11), 793-805.

THE UNIVERSITY OF EDINBURGH
College of Science and Engineering
School of Chemistry

Abstract

Biocompatible Polymer Microarrays for Cellular High-Content Screening

by Salvatore Pernagallo

The global aim of this thesis was to study the use of microarray technology for the screening and identification of biocompatible polymers, to understand physiological phenomena, and the design of biomaterials, implant surfaces and tissue-engineering scaffolds. This work was based upon the polymer microarray platform developed by the Bradley group.
Polymer microarrays were successfully applied to find the best polymer supports for:
(i) mouse fibroblast cells and used to evaluate cell biocompatibility and cell morphology. Fourteen polyurethanes demonstrated significant cellular adhesion.
(ii) Analysis of the adhesion of human erythroleukaemic K562 suspension cells onto biomaterials with particular families of polyurethanes and polyacrylates identified. A DNA microarray study (to access the global gene expression profiles upon cellular binding) demonstrated that interactions between cells and some polyacrylates induced a number of transcriptomic changes. These results suggested that, during these interactions, a chain of cellular changes is triggered, most notably resulting in the down-regulation of membrane receptors and ligands.
(iii) Identification of polymers with potential applications in the field of stem cell biology. Polymers were identified that showed attachment, promotion and stabilisation of hepatocyte-like cells. A polyurethane support (PU-134) was pinpointed, which significantly improved both hepatocyte-like cell function and "lifespan". A second project investigated biomaterials that promoted adhesion, growth and function of endothelial progenitor cells. A new polymer matrix was identified which contained the necessary signals to promote endothelial phenotype and function. This has potential application in the creation of blood vessels and the endothelialisation of artificial vessel prostheses and stent coatings for improving angioplasty therapy.
(iv) The study of bacterial adhesion, focusing on the adhesion of food-borne pathogenic bacterium *Salmonella enterica* serovar *typhimurium*, strain SL1344, and the commensal bacterium *Escherichia coli*, strain W3110. Several polymers were found to support selective bacterial enrichment, as well as others that minimised bacterial adhesion.

Declaration of Authorship

The studies described in this thesis were carried out by the author, except where stated in the thesis, under the supervision of Prof. Mark Bradley at the University of Edinburgh between April 2006 and April 2009. No part of this thesis has been previously submitted at this or any other University for any other degree or a professional qualification.

Parts of this work have been published or in the process of being published in the scientific literature and parts of it are subject to a current patent application:

Patent:

Use of polymer for cell growth (GB 0904834.9).

Articles:

- Pernagallo, S.; Unciti-Broceta, A.; Diaz-Mochon, J. J.; Bradley, M. Deciphering cellular morphology and biocompatibility using polymer microarrays. *Biomedical Materials* **2008**, 3, 034112.
- Pernagallo, S.; Diaz-Mochon, J. J.; Bradley, M. A cooperative polymer - DNA microarray approach to biomaterial investigation. *Lab on a Chip* **2009,** 9, (3), 397-403.
- Hay, D. C.; Pernagallo, S.; Diaz-Mochon, J. J.; Fletcher, J.; Black, J.; Thompson, A.; Hannoun, Z.; Newsome, P.; Forbes, S.; Ross, J.; Bradley, M.; Iredale, J. P. A simple polyurethane matrix promotes hepatic endoderm viability and inducible drug metabolism. **2010,** submitted.
- Pernagallo S.; Wu M.; Gallagher M.P.; Bradley M. Colonising new frontiers - microarrays reveal novel biofilm modulating polymers. **2010**, submitted.

Date:……

Signed:……

Acknowledgements

Should I write down all the people whom in some way have made this possibility a reality, this work would resemble an endless list of names, rather than thesis of science so I will mention only a few. Those unmentioned, remember you may not be recorded, but you are far from forgotten.

Firstly I would like to thank my supervisor, Professor Mark Bradley, without whom this thesis would never have happened, for taking me on as a research student in the first place and always pushing me to achieve more. He has taught me a huge amount about high-throughput technologies, biochemistry, and molecular biology. His concern, enthusiasm and encouragement were valuable for the successful completion of this thesis. I know it probably wasn't obvious at the time, but your efforts have been thoroughly appreciated!

I gratefully acknowledge the EPSRC (Engineering and Physical Sciences Research Council) for financial support, and all the previous PhDs of the Bradley group (Jasmine, Hitoshi, Jeff and Yucheng), without whom my research would not have been possible, since they synthesised all of the polymers that I have used. I am also very grateful to Guilhem who has contributed, particularly with his previous work onto polymer microarray technology, to the success of my PhD.

Thanks to everybody in the Bradley group (both past and present). Thanks especially to Mei and Mentxu who worked with me on the bacteria project and the synthetic biology project, respectively. I am also indebted to Asier for always being there when I needed someone to talk and offering unconditional support as a friend. Thanks to Albert, Ferdous and Rong for taking over the polymer microarray work and their dedication in

its improvement. Juanma, “it has been a great pleasure to share flat with you”, I really appreciated the contribution of you to bring me through the dark days - thank you my dear friend!-. Thanks to Jose for all the unforgettable evenings together at work and for his valuable data analysis help. Thanks to Jeff and Mariona who helped me with the Endnote software. Adam, Frank, Rahimi and Geraldine for their good daily humours and for making the time so special and enjoyable

Here come my big thanks to our collaborators who have allowed us to develop practical applications for our method: Dr. David Hay who worked with me to the hepatocute-like cells project; Dr Olga Tura and Kay Samuel, who worked with me on the Endothelial Progenitor Cells project; Dr Maurice Gallagher who, not only, collaborated with me on the bacteria project, but also for giving me invaluable advice and for his proof-reading. I have to say a massive thanks to Dr. Joshua Brickman and Dr Alessandra Livigni for always taking the time to chat with me and for giving me invaluable advice and allowed me to use their facilities.

I want to thank also all my friends from back home (Danilo, Elisa, Salvo, Marco, Maria, Aberto, Marilene, Rocco and Rosita) to remind me that science isn’t everything in life and for sharing with me fantastic moments.

An enormous thank you goes out to the Lovell’s family (especially to Madeleine) for their steadfast support, proof-reading, patience and love that have made it possible for me to get through this PhD.

Special (but insufficient) thanks to my Spanish family (JuanJo, Rosario, Alba and the little Jorge) for bringing me through the unhappy days and for all their love, support and help until the very end of this thesis, it could not have been achieved without you.

Finally I would like to say a big thank you to my family (mum and dad, Giusi, Maria Concetta, Marco and my little Giorgia) for their never-ending love (on all levels), to them I dedicate this thesis.

Contents

Supplementary Informations are provided on a CD inside the back cover.

Abbreviations

a.u.	Arbitrary units
APC	Allophycocyanin
BM	Bone marrow
BPO	Benzoyl peroxide
CB	Cord blood
cDNA	Complementary DNA
CFU	Colony-forming unit
cRGD	Cyclic Arg-Gly-Asp
CTG	CellTracker green
CTG-CMFDA	CellTracker Green 5-chloromethylfluorescein diacetate
CTG-CMF	CellTracker Green 5-chloromethylfluorescein
Cy3	N,N'-(dipropyl)-tetramethylindocarbocyanine
Cy5	N,N'-(dipropyl)-tetramethylindodicarbocyanine
CYP3A4	Cytochrome P450 3A4
DAPI	4’,6-Diamidino-2-phenylindole
DES	Drug-eluting stent
DNA	Deoxyribonucleic acid
EBI	European bioinformatics institute
EC	Endothelial cell
ECM	Extracellular matrix
EDTA	Ethylenediaminetetraacetic acid
ELISA	Enzyme-linked immunosorbent assay
em	Emission
eNOS	Endothelial nitric oxide synthase
EOC	Endothelial outgrowth cell

EPC	Endothelial progenitor cell
ESC	Embryonic stem cell
EU	European union
ex	Excitation
FACS	Fluorescence activated cell sorting
FAK	Focal adhesion kinase
FCS	Fetal calf serum
FE	Feature extraction
FITC	Fluorescein isothiocyanate
FT-IR	Fourier transform infra red
GFP	Green fluorescent protein
GO	Gene ontology
GPC	Gel permeation cromatography
GX	Gene spring
HCS	High-content screening
hESC	Human embryonic stem cell
HLC	Hepatocyte-like cell
HMGCS1	3-Hydroxy-3-methylglutaryl-coenzyme A synthase 1
hMSC	Human mesenchymal stem cell
HPLC	High performance liquid chromatography
hRNF7	Human ring finger protein 7
HSC	Hematopoietic stem cell
HUVEC	Human umbilical vein endothelial cell
IGFBP-3	Insulin-like growth factor binding protein 3
IGF-II	Insulin-like growth factor II
IgG	Immunoglobulin-G
KEGG	Kyoto encyclopedia of genes and genomes
LB	Luria-bertani
MAb	Anti-human monoclonal antibodie
MAPK	Mitogen-activated protein kinase
MED18	Mediator complex subunit 18
MEF-CM	Mouse embryonic fibroblast conditioned-medium

MEM	Modified Eagle’s medium
mESC	Mouse embryonic stem cell
MG	Matrigel
MHC	Major histocompatibility complex
MNC	Mononuclear cell
MSC	Mesenchymal stem cell
MT1B	Metallothionein 1B
MT1E	Metallothionein 1E
MT1H	Metallothionein 1H
MT1X	Metallothionein 1X
MT2A	Metallothionein 2A
NK	Natural killer
NMP	1-Methyl-2-pyrrolidinone
PA	Poly(acrylate)
PBS	Phosphate buffered saline
PCR	Polymerase chain reaction
PE	Phycoerythrin
PerCP	Peridin chlorophylla protein
PFC	Polyfibre core
PHA	Polyhydroxy acids
PHEMA	Poly(2-hydroxyethyl methacrylate)
PHHs	Primary human hepatocyte
PI	Photo-initiator
PLA	Poly(lactic acid)
PMMA	Poly(methyl methacrylate)
PTK	Protein-tyrosine kinases
PU	Poly(urethane)
RLU	Relative light units
RIN	RNA integrity number
RNA	Ribonucleic acid
RT	Room temperature
RT-PCR	Real-time polymerase chain reaction

SEM	Scanning electron microscopy
SNP	Single nucleotide polymorphisms
SREBP	Sterol-regulatory element binding protein
Ta	Annealing temperature
TF	Tissue factor
THF	Tetrahydrofuran
TOF	Time-of-flight
TOF-SIMS	Time-of-flight secondary ion mass spectrometry
TTR	Transthyretin
UCB	Umbilical cord blood
VEGF	Vascular endothelial growth factor
vWF	Willebrand factor
XPR1	Xenotropic and polytropic retrovirus re

Chapter 1

Introduction

1.1 Biomaterials

The concept of a biomaterial has been defined as "*any substance (other than a drug) or a combination of substances, synthetic or natural in origin, which can be used for any period of time, as a whole or as part of a system which treats, augments, or replaces any tissue, organ, or function of the body*".[1] This definition was later refined as: "*a material conceived to interface with biological systems to evaluate, treat, augment or replace any tissue, organ or function of the body*".[2]

The use of man-made materials for the replacement of body parts dates back to well before Christianity, with metals such as gold being used extensively in dentistry.[3] "It is intuitive to think that, throughout history, anyone who had the misfortune to suffer a seriously debilitating injury would have tried to provide themselves with a prosthesis adapted to compensate for the anatomical and functional damage sustained, and consequently to remedy, at least in part, their incapacity by profiting from such a device".[4] As might be expected, evidence of use of biomaterials as prostheses from the classical period are scarce, as indeed it is in the early part of the Middle Ages. However, there are several representations of prostheses used by disabled and lepers dating from the thirteenth to fifteenth centuries, as is shown, for example, in some frescoes in the baptisteries of Parma and Florence, and in various works by Brueghel, Cornelius, Mastys and Hieronymous Bosch.[5] It was only in the sixteenth century, however, that the disabled were accorded a new interest, which removed them from the isolation to which they had been confined.

One of the most important historical studies is found in the work of Ambroise Paré, titled "*Treatise on Surgery*", in which, for the first time, the problem of prosthetic intervention became a medical problem, even if the doctor had recourse only to the blacksmith for practical solutions. In this same work, a series of prostheses are discussed, such as artificial eyes made of gold, dental prostheses, palatal prostheses, prostheses for the tongue, for the outer ear, for the genito-urinary tract and so on.[6] For centuries, iron, wood and leather were the dominant materials used in such applications – the use of, for instance, noble metals was rare. In the modern sense, biomaterials hardly existed – these materials were simply confined to use outside of the organism.[4] The advance towards true biomaterials was essentially the result of an imaginative leap; people such as Lister, Pasteur, Klebs and Koch who opened a new chapter in medicine and indirectly created new hypotheses, because the 'insides' of the human body became a new territory to be conquered by technology.[7]

The use of biomaterials grew rapidly from the end of the nineteenth century, in particular after the advent of antiseptic surgical techniques developed by Lister in 1860.[8] The first metal devices for correcting bone fractures were introduced at the beginning of the twentieth century; the first replacement prosthesis for an entire hip bone was implanted by Wiles in London in 1938,[9] and between 1950 and 1960 polymers were introduced for the replacement of the cornea and blood vessels.[10]

In many cases, biomaterials did not begin as materials destined for medical applications, but were originally used in other fields, and their entry into the biomedical field came as a result of the attempt to solve specific clinical and surgical problems. For instance, many new materials were developed in the 1940s and '50s as a response to military and aerospace needs, and these materials were subsequently found to have applications in the field of biomedicine.[11] In the 1960s, with advances in the fields of chemistry, biology and physics, an entirely new, collaborative area of research was initiated purposely for the design of new biomaterials with improved biological performance.[12] Biomaterials have now contributed to improved quality of life for millions of people.[3, 4, 12] Over the past two decades focus has shifted gradually to generating materials that are considered "bioactive" and elicit a controlled response. Current applications include: (a) prostheses for functional replacement; (b) supportive scaffolds for guided tissue growth; (c) external

communicating devices; and (d) surface coatings.[13-16] The biomaterial field continues to grow, and new applications are continually being developed.

In spite of this, there is much still to understand, in particular the biological response biomaterials elicit and their role in driving the regeneration of tissue. These relatively unresolved areas continue to motivate researchers to develop new products.[16, 17]

1.1.1 Biomaterial classification

In accordance with their medical applications, materials can be classified in the following way:[18]

1. Class I: not used in direct contact with body tissues.
2. Class II: come into contact with tissues only at the initial stage, or intermittently.
3. Class III: constantly in contact with the host tissue.

It is materials of Class III which are today defined as biomaterials or biomedical materials, and these can be subdivided into three categories according to their biological interaction with surrounding tissue:[19]

1. Inert materials: these do not produce an immune response in the host and their structure remains unaltered in the body after implantation.
2. Active materials: these have biological function by which they mimic the tissue in which they are implanted.
3. Degradable or resorbable materials: these are slowly biodegraded by the host and replaced with the natural, regenerated tissue.

Another more traditional classification is that which subdivides biomaterials according to their chemical-structural characteristics. Following this classification it is possible to group different materials into three main categories: metals, ceramics and polymers.[19]

Metals have been used to make simple prosthetic devices to repair the teeth and bones.[3] However, many metals are vulnerable to corrosion and exhibit brittleness, while the release of metal ions may cause adverse tissue reaction. More recently, the development of new metal alloys and coatings has led to materials with improved corrosion resistance and strength, allowing a wider range of applications such as orthopaedic prostheses.[20]

Ceramics (for example, types of glass which may be inert, active or resorbable) are widely used inside the body (for instance, the application of bioglass in titanium bone replacement)[21] and outside the body (for example, lenses, or porcelain crowns in dentistry).[22] Hydroxyapatite (a naturally occurring ceramic material) is commonly used as a filler to replace amputated bone or as a coating to promote bone growth in prosthetic implants.[23] Although used in medical applications throughout history, the disadvantages of ceramics include brittleness and difficulty of manufacture. However, over the last two decades some of these issues have been resolved, allowing the development of many different classes of bioceramics, which are now used successfully as orthopaedic materials.[22, 24]

Polymers represent the most significant class of biomaterials in medical application, as they can be inert, active and resorbable. Polymers can encompass a wide range of physical and chemical properties; they can be used either directly or coated onto other materials, they are readily functionalised and they can be degraded by the body after a desired period. Additionally, they are easily processed and come in many different forms including solids, fibres, films and gels.[25] As a result, biopolymers are currently the materials of choice for thousands of medical applications (**Table 1.1**).

Polymers	Applications
Cellulose and derivatives	Membranes for dialysis
Poly(alkyl cyanoacrylates)	Wound closure adhesives
Poly(amides)	Sutures
Poly(carbonates)	Device housings
Poly(ethylene terephthalate)	Surgical mesh, vascular prostheses
Poly(lactic acid)	Tendon repair, sutures, drug delivery
Poly(lactic/glycolic acid)	Drug delivery, sutures
Poly(urethanes)	Catheters, vascular prostheses, coatings, heart valves
Poly(vinyl chlorides)	Tubing, blood bags
Poly(acrylates)	Contact lenses, artificial teeth and bone cements
Ultra high molecular weight poly(ethylene)	Hip & knee bearing surfaces

Table 1.1 *Some of the most widely used "biocompatible" polymers and their biomedical application.*

Initially utilised for their mechanical properties and high chemical resistance, biocompatible polymers are used as components of prosthetic devices including hip implants, artificial lenses, vascular graft and catheters.[10, 19] More recently, new drugs (protein or peptide-based) have been developed that require novel formulations for efficient delivery. This discovery has led to the widespread use of biodegradable polymers for the controlled release of drugs and gene therapy. Additionally, in tissue engineering, polymers provide structures onto which three-dimensional tissues and organs can theoretically be generated.[10, 19, 25, 26]

1.1.2 Introduction to polyurethanes and polyacrylates

This thesis focuses principally on two categories of synthetic polymers: polyurethanes[27] and polyacrylates,[28] which are often used because of their transparency, resistance to breakage and elasticity.

1.1.2.1 A brief history of polyurethanes and their applications

Polyurethanes are copolymers composed by diol segments (for example, polyethylene glycol (PEG), polybutylene glycol (PTMG)) and hard segments of diisocyanates (for example, toluene diisocyanate (TDI), diphenylmethane diisocyanate (MDI), hexamethylene 1,6-diisocyanate (HDI)), and contain a carbamate or urethane linkage (-NH-CO-O-). They have been widely used in medical applications such as tubing, storage bags, dressings, pacemaker coatings and precisely controllable drug release from a biodegradable stent coating.[29, 30]

Polyurethanes were first made in 1937 by Bayer.[31] However, it was not until 1961 that a polyurethane was first used as a biomaterial as a component in an artificial heart valve. This, however, gave disappointing results and was abandoned because, after implant, thrombus appeared first on the suture line and then grew and covered the entire surface of the artificial heart valve.[32]

In recent years, advances have been made in the synthesis of polyurethanes, improving their mechanical resistance to abrasion, their tissue-compatibility, and the ways in which they are processed. Researchers have sought to alleviate the difficulties caused by biodegradability by optimising the ratio between hard components and soft in the polymeric chain.[29, 33, 34]

1.1.2.2 A brief history of polyacrylates and their applications

An acrylate polymer belongs to a group of polymers which could be referred to generally as plastics. They are noted for their transparency, elasticity and resistance to breakage. There are a number of common acrylates whose basic chemical formula is showed in **Figure 1.1 A**. These polymers can be prepared using a wide range of acrylic monomers as shown in **Figure 1.1 B**. These monomers can be polymerized by a free radical chain reaction process in which the reaction is started by an *initiator* such as benzoyl peroxide (BPO).[35] Polymethyl methacrylate (PMMA) has high tensile strength and softening temperature, excellent light transparency, and high refractive index.[36, 37]

A

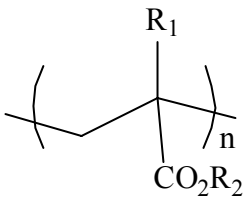

B

R_1	R_2	Name
H	H	Acrylic acid
CH_3	H	Methacrylic acid
H	CH_3	Methyl acrylate
CH_3	CH_3	Methyl methacrylate
CH_3	C_2H_5	Methyl ethylacrylate

Figure 1.1 *A) Basic chemical structure of acrylates. B) Some acrylate monomers.*

Acrylic acid was first synthesised in 1843 and polymerisation of its esters is well known. The polymerisation of acrylics was extensively studied by Rohm in 1901, who took out a patent for polyacrylic esters as a paint binder in 1915.[38]

Commercial production of acrylate polymers began around 1927 as Acryloid and Plexigum and as an intermediate layer in "safety glass" Luglas. Chalmers' discovery of the much harder methacrylate polymers led to the development of PMMA by Crawford in the mid 1930s. Around 1934, Rohm and Haas developed the first stable acrylic emulsion. A paint laboratory was established in 1938 but aqueous all-acrylic emulsions were not commercially produced until the 1950s. In around 1970, weather resistant acrylic emulsion paints were developed for use on timber, and have now largely replaced oil based paints.[38, 39]

Polyacrylates have multiple applications in the modern field of biomedicine: PMMA, for example, has been used to prepare hard contact lenses, artificial teeth, dental fillings and bone cements;[37, 40, 41] while polyhydroxyethyl methacrylate (PHEMA) is used in soft contact lenses, drug delivery systems and dressings.[42, 43]

1.1.3 Global biomaterial market and legislation

The biomaterial market is continually expanding, and the 50 years of successful development in materials is reflected in an improved quality of life for countless numbers of patients and the economic growth of the industry, now valued in excess of $100 billion.[12] Due to this constant growth, the EU has felt the need to make medical devices conform to high standards of safety.[44] Newly developed biomaterials, before receiving approval for clinical application development, must, therefore fulfil rigorous criteria laid out by governmental authorities and international agencies, for example, the US Food and Drug Administration and the International Organization for Standardization.[15] Testing begins with standard cell-based toxicity assays *in vitro*, which are performed in order to remove high-risk materials, with subsequent testing at both a pre-clinical and clinical level to ascertain where, and for how long, the material will be present in the body.[15, 45] It is standard practice for new biomaterial implants to undergo testing for a number of years.[46]

1.2 Biocompatibility

Biocompatible materials must, by definition, minimise any adverse reactions occurring at the materials interface, and must not provoke problems such as embolism, tissue necrosis, or even cancer. The most widely accepted definition of biocompatibility has been formulated by Williams as "*the ability of a material to perform with an appropriate host response in a specific application*".[47] Normally biomaterials come into contact either with the cardiovascular blood system (the intravascular system) or soft and hard tissues (the extravascular system), or with both. Thus, in order to design materials for biomedical use, it is necessary to comprehend fully the events initiated when a biomaterial is implanted into the body.[48]

1.2.1 Blood response

An essential aspect of biocompatibility is the complex interaction between blood and foreign materials. The greatest danger in any blood-material interaction is coagulation with the formation of thrombosis, which may cause embolisms (**Figure 1.2**).[19] It has been shown that when foreign materials come into contact with blood, the surface may, first, adsorb small molecules such as water and ions. This is followed by adsorption of blood plasma proteins such as albumin, fibrinogen, immunoglobulin G and fibronectin. These proteins may subsequently be desorbed and/or displaced by other proteins. This first adsorption on a biomaterial's surface determines the initiation of a complex sequence of reactions. This can lead to the coagulation of platelets as well as their fragments (microparticles).

This set of reactions initiates the coagulation cascade, which culminates in the production of thrombin (Factor II), which acts on fibrinogen, converting it into the insoluble protein fibrin, which forms fibres. Blood cells and platelets get caught up in the fibres, forming a clot. The generation of thrombin occurs *via* two pathways, intrinsic and extrinsic, that provide alternative routes for the generation of Factor X (**Figure 1.3**).

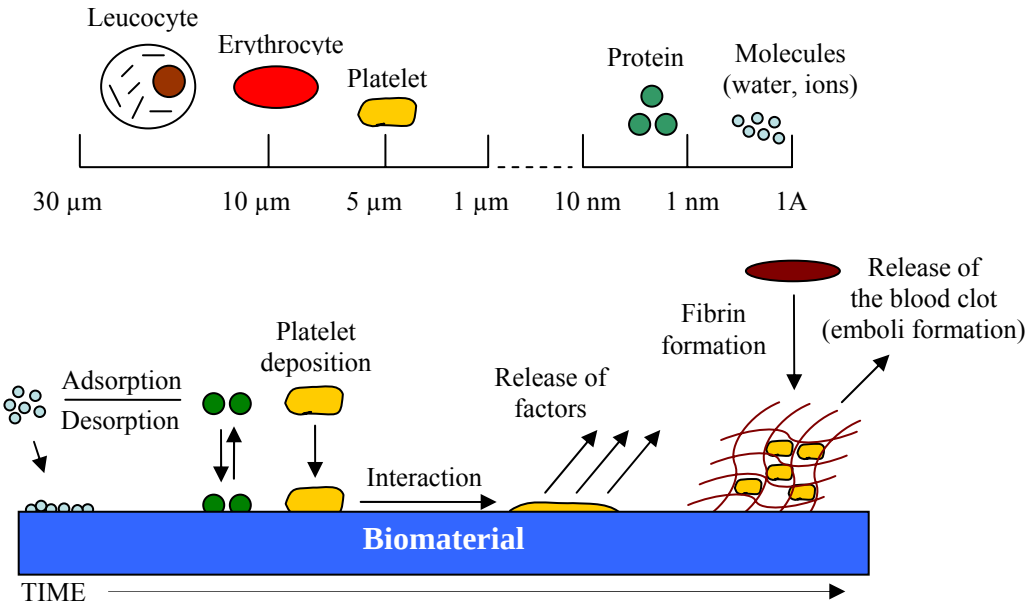

Figure 1.2 *General scheme of blood coagulation with formation of thrombosis.*

The intrinsic pathway begins with the interaction of Factor XII, caused by contact with abnormal surfaces produced by injury. The extrinsic pathway is triggered by trauma, which releases Tissue Factor (TF) VII. Both pathways converge to a common pathway leading to the formation of thrombin, which in turn induces the formation of fibrin monomers from fibrinogen, and consequently the adhesion, activation and aggregation of platelets (**Figure 1.3**).[19, 47]

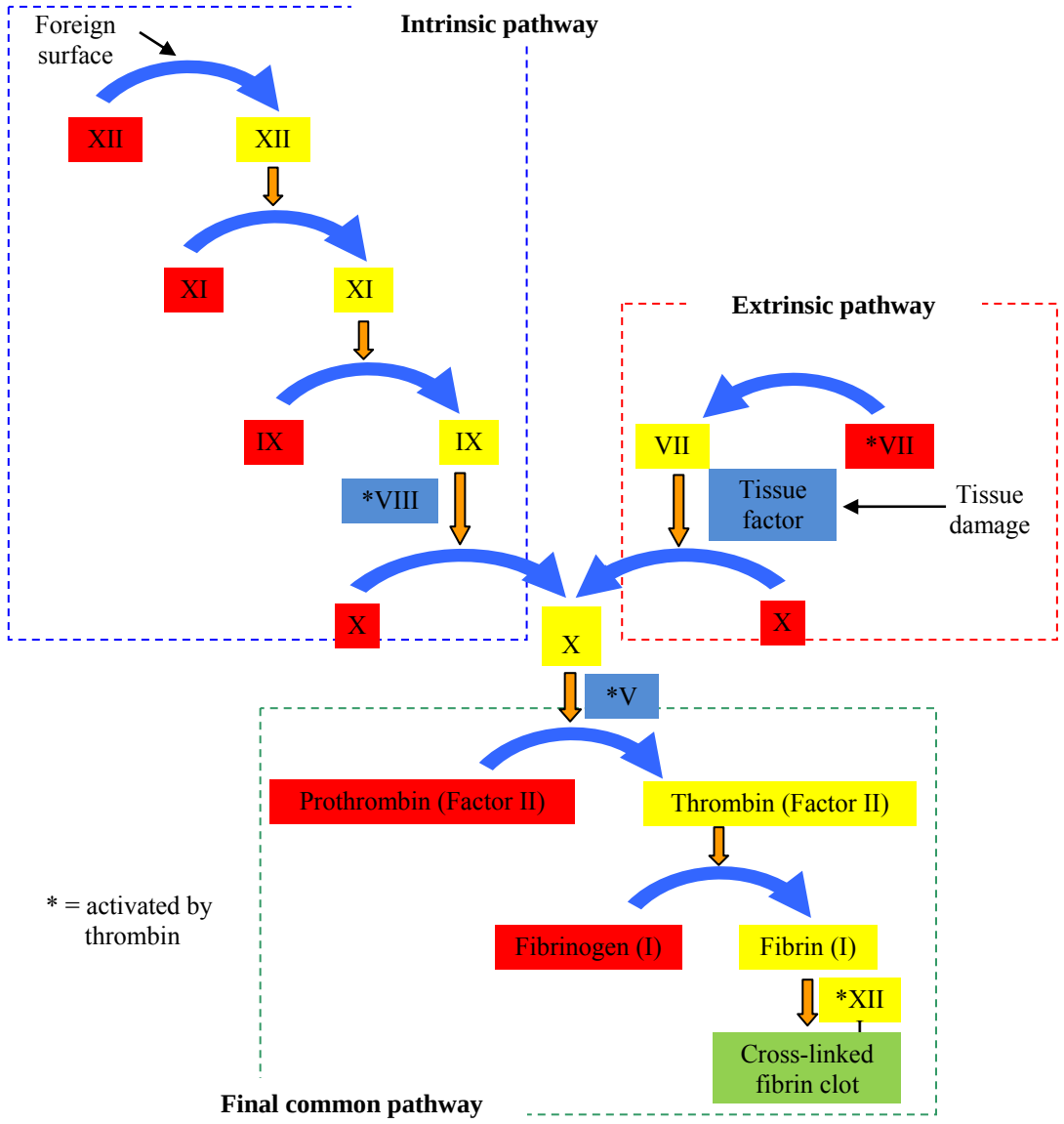

Figure 1.3 *Scheme of alternative intrinsic and extrinsic pathways that provide routes for the generation of factor X, by activation of Factor XII. Inactive forms of clotting factors are shown in red; their activated counterparts are in yellow; stimulatory proteins that are not themselves enzymes are shown in blue boxes. A striking feature of this process is that the activated form of one clotting factor catalyzes the activation of the next factor.*

1.2.2 Tissue response

Materials implanted in tissues always generate a response. The major tissue response in the extravascular system is inflammation, which starts as a local reaction to injury, insult or infection (**Figure 1.4**).[49] The classic foreign body response involves initially a non-specific adsorption of plasma proteins onto the surface of the implanted material. These proteins then promote the adhesion of blood cells, which may subsequently instigate a proinflammatory process through the up-regulation of certain cytokines with the migration of neutrophils/macrophages to the implant site. As a consequence of this process, monocytes often differentiate into macrophages as the cell attempts through phagocytosis to clear the wound site of foreign bodies, dead cells and bacteria. The macrophages in turn fuse in order to form multinucleate giant cells. These giant cells then coordinate the secretion of derivative agents such as superoxides and free radicals that can damage the implant. The last stage of the reaction to a foreign body occurs when a poorly vascular collagen shell forms around the foreign body in order to separate it from the host tissue. This isolation of the foreign material can provoke several unwanted reactions such as chronic pain, device rejection and device failure (**Figure 1.4**).[49, 50]

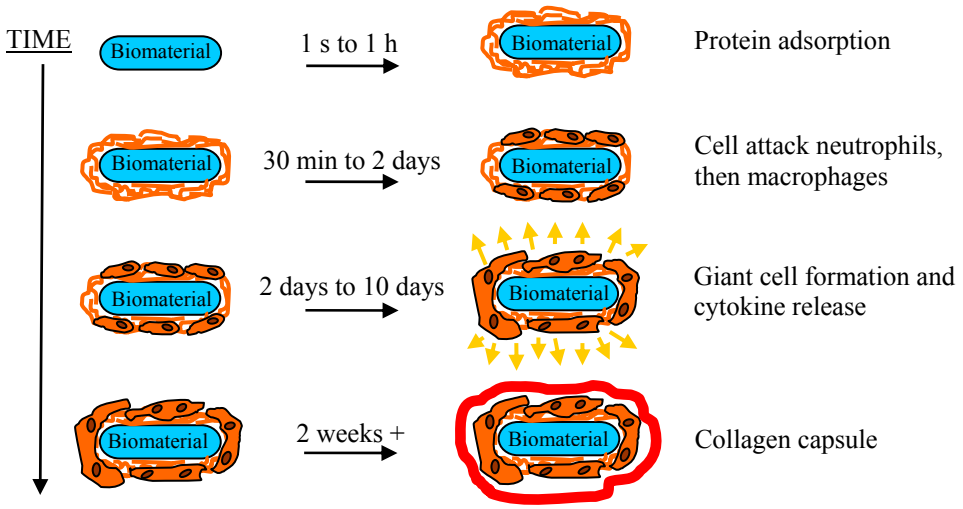

Figure 1.4 *Illustration of the classic foreign body response.*

1.2.3 Strategies to enhance biocompatibility

There are several strategies for enhancing the biocompatibility of foreign surfaces, such as controlling protein adsorption by regulating the hydrophilicity or hydrophobicity of the material surface, and increasing cellular recognition by controlling the interaction of extracellular matrix (ECM) proteins with cell-surface receptors such as integrins and selectins.[51] In the case of foreign materials only interacting with blood, haemocompatibility is enhanced by interfering directly with the coagulation cascade and inflammatory response. A widely used methodology for this purpose consists of immobilising the anticoagulant heparin onto the surface of implanted materials, resulting in the neutralisation of thrombin.[52]

1.2.3.1 Controlling protein adsorption

Adsorption of proteins onto hydrophilic surfaces is usually limited and reversible, whereas proteins irreversibly bind onto hydrophobic surfaces. Therefore, a typical method for reducing protein adsorption consists of increasing the hydrophilicity of the surface by functionalisation of the surface with hydrophilic polymers such as PHEMA, PEG and their derivatives in both a covalent and non-covalent manner using methodologies such as grafting,[53] coating, and self-assembly.[48]

Instead of functionalising the surface of materials, another approach aims to improve biocompatibility by producing bulk polymers which are able to control protein adsorption.

Hydrogels are water-swollen polymeric networks prepared from hydrophilic monomers, which are insoluble due to the presence of chemical or physical cross-links.[42] They have been widely used as biomaterials as they present tissue-like properties and good biocompatibility.[50, 54]These hydrogels can be synthesised from cross-linked acrylate and methacrylate monomers **Figure 1.1 B** (Chapter 1.1.2.2), or from the crosslinking of polymers such as PEG with polyhydroxy acids (PHA)[55] or polylactic acid (PLA).[56] Modification of synthetic procedures, such as polymerisation conditions and amount of cross-linker, can afford easy control of a wide range of properties.

Microdomain containing polymers are co-polymers composed of both hydrophilic and hydrophobic moieties. The presence of "microdomains" allows these materials to control protein adsorption more easily. These materials have been shown to provide reversible platelet attachment while preventing platelet activation.[54] The most popular of these polymers are polyurethanes, which contain both hard (hydrophobic) and soft (hydrophilic) segments (Chapter 1.1.2.1). Other examples are co-polymers of hydroxyethylmethacrylate (HEMA) and styrene.[40] An advantage of these co-polymers over hydrogels is that they demonstrate good elasticity, tensile strength and durability and for this reason, these materials are frequently used in blood-contacting applications where long-term non-thrombogenicity is required.[57]

1.3 Polymer microarrays

1.3.1 A brief history of microarrays

In science a microarray is a tool for analysing a group of molecules or materials arranged as microscopic spots in a regular pattern on either a membrane or, more typically, a glass slide. The molecules or materials in an array are attached to their support, in order to be able to co-register each spot on the array with a specific material entity.

The first microarrays as defined above were developed in 1991 by Fodor and co-workers, who fabricated a miniaturised array of oligopeptides, which was employed to screen for potential binding sequences with a monoclonal antibody.[58] The same research group later developed a strategy for the rapid synthesis and analysis of DNA sequences.[59] Prior to Fodor's discovery, in 1987 a related technology had already been described as a refinement of Southern blotting by Kulesh. This research group made an array by spotting cDNAs onto filter paper with a pin-spotting device in order to identify interferon-modulated proliferation-related cDNA sequences.[60] In 1995, Schena described a miniaturised microarray for gene expression measurements of 45 *Arabidopsis* genes by simultaneous two-colour fluorescent hybridisation.[61] Two years later, a high-density DNA microarray of the complete eukaryotic genome (*Saccharomyces cerevisiae*) was published.[62] Since this time, DNA microarrays have dramatically accelerated many types of investigation, creating a powerful tool for

gene expression profiling, comparative genomic hybridization,[63] SNP detection,[64] and in discovering useful biomarkers of human diseases.[65, 66]

Over the last two decades, researchers have formulated alternative uses for the multiple properties of arrays, and new areas have been developed, such as protein,[67] small-molecule[68] and carbohydrate microarrays.[69] Arrays have also been exploited in an increasing number of fields, such as the characterisation of tissue analysis,[70] and cell-based screening.[71]

1.3.2 A brief history of polymer microarrays

Polymers, as already stated, are essential in the area of biomaterials and have been used in a myriad of applications.[19, 25] However, the nature of the interactions between a polymer and its biological environment is highly complex. For example, due to the multiplicity of the cell surface components (lipid bilayer, membrane proteins, glycoproteins and small molecules), the principles of immobilisation of cells on a surface are more difficult to predict than the immobilisation of single biomolecules. In fact, cell-biomaterial interactions should be considered as the result of a wide range of co-operative and dynamic non-covalent interactions (ionic bonds, hydrophobic interactions, hydrogen bonds, Van der Waals forces and dipole-dipole bonds) between these components and a given substrate. Surface characteristics, such as hydrophobicity, roughness and charge, and chemical composition, are all known to play key roles in regulating the response of cells that interact with biomaterials.[72] Due to the immense diversity of cells present in our bodies, there is no universal material suitable for studying cellular adhesion. It would appear, however, that the most efficient strategy for binding cells on polymers is to try to predict which properties each type of cell requires for binding and manufacture the polymer accordingly.[73]

There has been a long-term reliance in the biomaterial industry on the use and study of conventional materials. Traditional methods of screening, identification and testing of new polymers are slow, yet over recent years the field of automated and parallel screening of polymers has grown enormously.

The use of a high throughput approach, such as microarraying, to allow the rapid screening of chemically diverse polymers offers an important tool for finding

correlations between the design and performance of such materials.[74, 75]

The use of polymer microarrays for cell-biomaterial screening has recently been developed by two independent research groups, Langer (2004)[76] and Bradley (2004).[40]

The Langer approach:[76]

Langer and co-workers reported polymer microarrays for applications with human embryonic stem cells (hESCs). First, they mixed monomers using a liquid handling system and then contact printed in triplicate 576 different combinations of 25 different acrylates, diacrylates, dimethacrylate and triacrylate monomers with a radical initiator onto a layer of PHEMA, on top of an epoxide-coated slide. These spots were then exposed to UV irradiation in order to polymerise them. Using this method 1,728 (576 x 3) polymer spots were manufactured in order to study the interaction between the newly formed polymers and the growth of hESCs.

In general, cell attachment and spreading to display typical cellular morphology was supported by the majority of these materials. However, certain monomers inhibited hESC cell attachment and spreading, in particular monomers m-phenylene diacrylate, 3-methacryloyloxy-2-hydroxypropyl methacrylate and 6-acryloxy-perfluorohexyl acrylate. To examine the polymer effect on other cell types, Langer and co-workers tested the arrays with C2C12, an embryonic muscle cell line. Unlike the hESCs, C2C12 cells attached to and grew on almost all the materials, including those containing 70% monomers m-phenylene diacrylate and 6-acryloxy-perfluorohexyl acrylate.

An important aspect of Langer's approach was related to the equipment used for polymer synthesis and the fabrication of microarrays. Langer discussed in detail the problems and solutions of liquid handling in a highly miniaturised manner, necessitating significant modification of existing robotic technology, including:

1. The effect of viscous acrylate monomers on liquid handling equipment (during the pre-formulation of monomers) and printing and pin washing (during monomer contact printing).
2. The radical polymerisation of monomers, which can be subject to oxygen-mediated inhibition. This is particularly significant at small volumes, and as a

consequence printing must be performed in an atmosphere of humid argon.

3. Due to the difficulty of controlling the speed of monomer spreading, in some cases irregular polymer spots form.
4. The PHEMA would mix with the polymers being synthesised would generate a blent of all the polymers being synthesied.

In 2005, in order to study human mesenchymal stem cells (hMSCs)-biomaterials interaction, Langer and co-workers generated polymer microarrays by blending 24 different polymers in various proportions, producing 1152 polymer blends.[77]

The Bradley approach:

1. Contact printing of pre-formed polymers:[40, 78-80]

The Bradley research group developed an alternative approach *via* the contact printing of pre-formed polymers (from a polymer library) onto cytophobic (agarose-coated) slides to generate well-defined polymer microarrays. All the polymer libraries used were prepared on gram-scale by parallel synthesis, and all individual members were fully characterised by gel permeation chromatography (GPC), differential scanning calorimetry (DSC) and contact angle measurements. Before printing in a microarray-type format each library member was dissolved in a common, non-volatile solvent 1-methyl-2-pyrrolidinone (NMP) in order to minimise the formation of so-called "rings" during evaporation. Furthermore, a number of printing parameters, such as inking and printing time, were optimised in this process to ensure uniformity of polymer spot within the array. Since each library member was synthesised on a scale that allowed characterisation prior to array fabrication there was full confidence in any structure-activity relationship generated while allowing immediate scale-up following polymer identification. Several cell lines were studied, such as stem cells, primary cells, suspension cells, adherent cells, and prokaryotic cells.

2. Inkjet fabrication of polymer microarrays:[81]

More recently an inkjet printing approach was developed by the Bradley group in order to prepare, in a highly miniaturised manner, polymer microarrays on glass

slides, through the use of *in situ* pico-nano litre-scale polymerisation (**Figure 1.5**). This method used a redox initiator system and inkjet printing to print rapidly both an initiator and monomers that contained the reductant onto pre-treated glass slides. This system allowed 2280 hydrogels to be prepared, while the non-contact nature of the printing approach gave excellent morphology and size control (spot diameters of polymer printed 220 μm). This allowed rapid identification of "smart hydrogels" for the binding and release of several cell lines, such as HeLa cells.

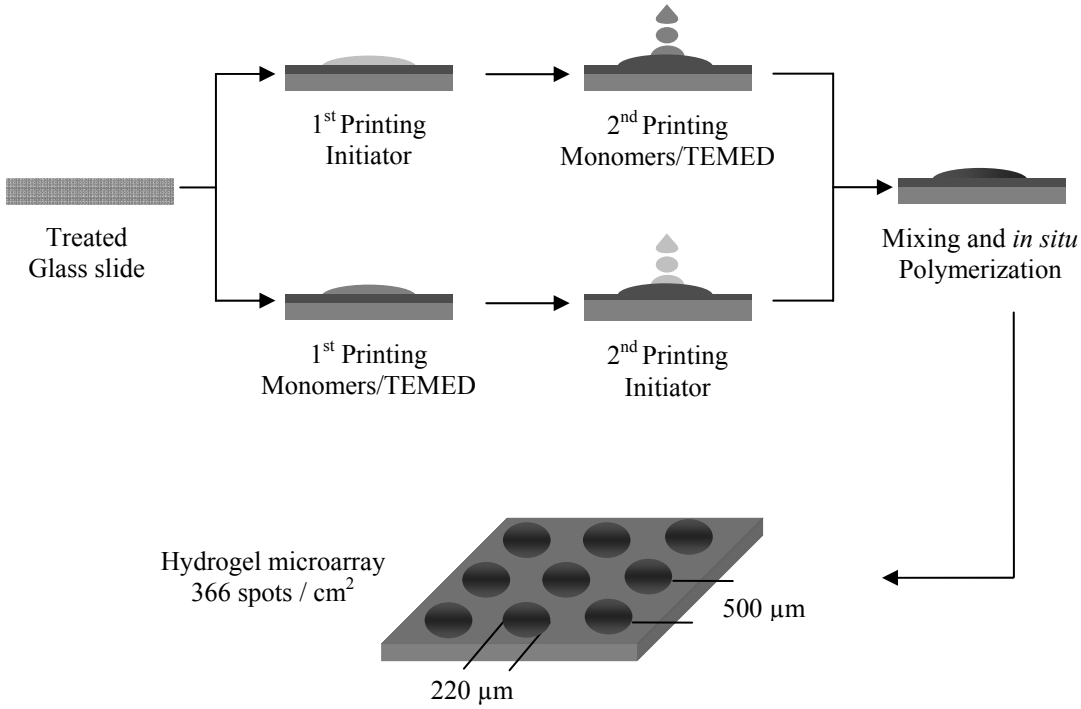

Figure 1.5 *The two approaches used for inkjetting mediated hydrogel (synthetic) on a microarray via in situ polymerization.*[81]

The main disadvantage of this method, however, was that it was limited to the use of water-compatible polymerisations.

These difficulties were solved through the development of a second method of inkjet printing, which overcame the problem of evaporation.[82] It consisted of inkjet printing (independently) both a photo-initiator (2,2-dimethoxy-2-phenylacetophenone) and monomers (or a mixture of initiators and monomers) onto agarose-coated glass slides, which had been pre-coated with a thin layer of paraffin oil (**Figure 1.6**).

Once printed the monomer drops (all dissolved in NMP) sank and settled onto the agarose layer where they were polymerised. Using this approach a polymer microarray of 1100 polymers was fabricated *in situ* on a single microscope glass slide with feature sizes of ~0.62 mm and a density of 100 spots/cm^2. The advantage of this method is that it allows for the use of a much wider range of monomers, which do not have to be water-compatible. These arrays of polymers were used to identify polymers for selective mouse embryonic stem cells (mESCs) binding.

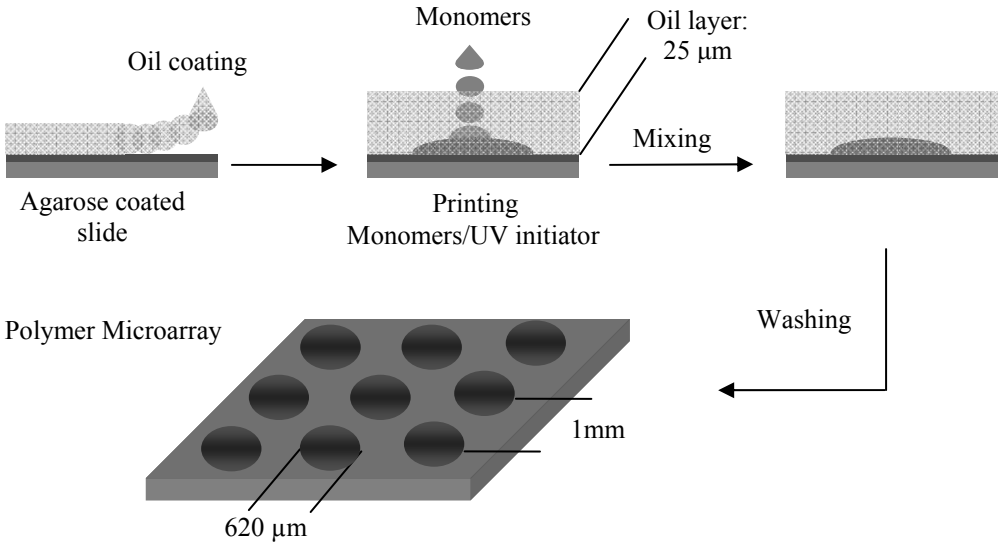

Figure 1.6 *Approach used to prepare polyacrylate microarrays. An oil film was used to prevent evaporation of the nanolitre volumes of the printed monomer solutions while maintaining the pattern on the glass surface. Following UV photo-polymerisation and removal of the oil film the polyacrylate library was left attached on the slide.*[82]

1.3.3 Contact printing polymer microarrays[78, 80]

The work reported in this thesis used contact printing methods rather than inkjet printing in order to prepare more rapidly the arrays of polymers. In contrast to the inkjet method, contact printing has been shown to be the fastest method for mass production of arrays.

1.3.3.1 Polymer microarray fabrication

There are three parameters essential in order to generate polymer microarrays with uniform and reproducible features:

1. The surface onto which the polymers are printed.
2. The solvent used to prepare the polymer solutions.
3. The printing conditions used.

It is important to note that three parameters are not independent of each other and will influence the quality and reproducibility of the final polymer microarray.

1.3.3.1.1 Surfaces

In order to develop a cell-based microarray, the substrate has to comply with several requirements:

1. The substrate must be unaltered by the contact printing of the polymer solution.
2. The substrate must be stable to UV-irradiation to allow sterilisation prior to the plating of the cells.
3. Substrates with low levels of background binding must be developed to facilitate data analysis.

As a result of previous work[80] several functionalised and gold-coated glass slides were investigated for this application, most of which provide a suitable surface for polymer printing, and could be readily sterilised under UV-irradiation, but unfortunately did not prevent cellular adhesion. The following substrates were prepared and tested: C18-functionalised slides, aluminium slides, and perfluoroalkylthiol-modified slides. The best results were obtained by dip-coating aminoalkylsilane slides with a thin film of agarose. Importantly agarose is readily sterilised by UV irradiation and does not dissolve in most organic solvents.

1.3.3.1.2 Solvents

As a result of previous work[80] a variety of solvents and solvent mixtures were investigated. As a result of this study, n-methyl-pyrrolidinone (NMP) was selected due to the solubility of over 90% of the polymers from both the polyurethane and polyacrylate libraries. Its boiling point (202 ºC/1 atm) also radiuses solvent evaporation, which allows large numbers of polymers and microarrays to be printed

in a single run. In order to fully remove the solvent following microarray fabrication, the arrays were dried under vacuum at 45 ºC overnight.

1.3.3.1.3 Printing and washing of the polymer microarray

Polymer printing was carried out using a Q-Array Mini contact microarrayer with 150 μm solid pins (**Figure 1.7**).

Using solid pins, the main factors effecting the shape and uniformity of the printed spot were the nature of the solvent and the substrate used. This array allows the control of a variety of parameters including inking time, stamping time, number of stamps per spot and washing conditions. Importantly, washing of the printing station can only be carried out with ethanol and water. However, this does not remove the trace amounts of NMP and dissolved polymers. Hence, this results in cross-contamination between samples during printing. To remedy this, pins must be removed and washed manually with acetone.

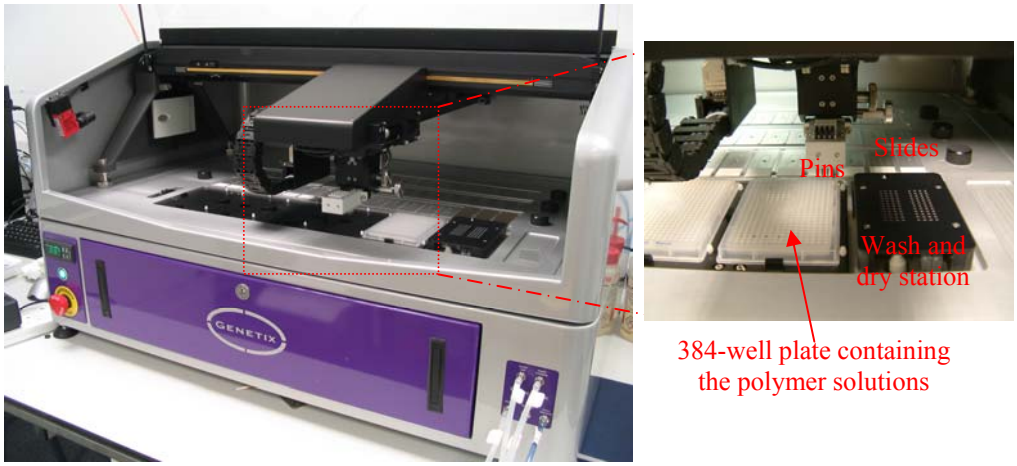

Figure 1.7 *Q-Array Mini contact microarrayer.*

Through the work of Mizomoto,[40] Jose[79] and Tourniaire,[80] polymer microarrays were also studied in order to evaluate the properties of the printed polymers. Specifically, the morphology of the printed polymer spots was studied using scanning electron microscopy (SEM), chemical functionality and composition analysis were undertaken using Fourier Transform Infra Red (FT-IR) microscopy and Time-of-

Flight Secondary Ion Mass Spectrometry (TOF-SIMS).[83] These techniques successfully characterised the functional groups present on the surface of the printed polymer spot, and in this way not only have polymer microarrays shown their versatility in biological uses, but also have allowed high throughput chemical analysis.[83]

1.3.4 Detection methods

Most of the detection and imaging systems used in the field of polymer microarrays rely on fluorescence. With the drive towards increasing throughput, such systems have required automation for both detection and image analysis.

The detection methods used by Bradley, in order to allow the screening of polymer microarrays, can be divided into two main categories, depending on the level of resolution necessary. Low resolution systems (2-10 μm), where individual cells do not need to be observed, are based on standard DNA microarray scanners. These systems are compatible with a range of fluorophores and generate single images of a whole microarray. Subsequent analysis is generally carried out with commercial software (for example, LaVision BioTech GmbH) allowing quantification of fluorescence for each spot (**Figure 1.8**).[78]

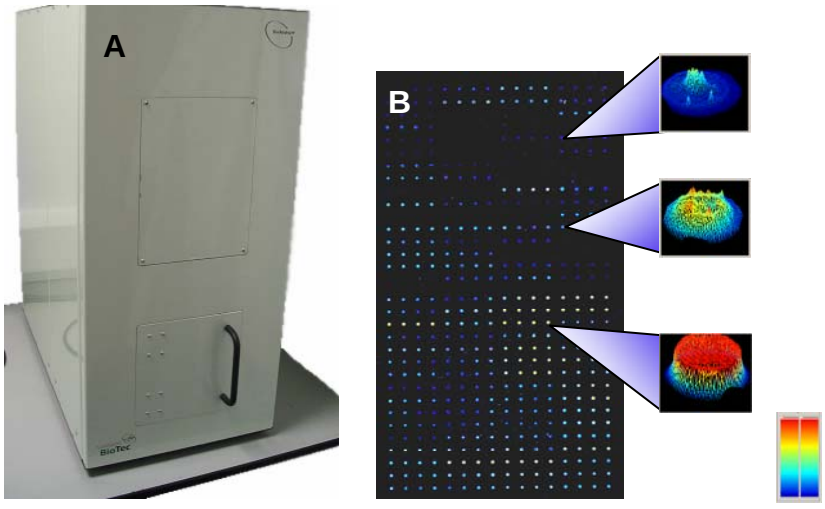

Figure 1.8 *A) Bioanalyser 4F/4S scanner (LaVision BioTech GmbH) with CCD camera allowing the rapid determination of fluorescence intensities. B) Scanning of a polymer microarray, containing 15 polyurethanes each printed as 24 identical spots after incubation with fibrinogen labeled with AlexaFluor.*[80]

High resolution high-content screening (HCS) systems (down to 0.2 µm) was based on a conventional microscope fitted with a motorised stage allowing the automated capture of high-resolution images for each spot (**Figure 1.9 A** and **B**).

The use of these systems, initially developed for microplate assays, is essential when individual cells need to be visualised or sub-cellular localisation is necessary.

The main inconvenience of these systems comes from the handling and analysis of the data sets generated. However, with the development of high-content screening, several software packages (for example, Pathfinder™**)** have been developed to carry out automated image analysis (**Figure 1.9 C**).

Such packages allow rapid analysis of multiple parameters (cell number, shape and size, fluorescent intensities etc.) from hundreds of images in order to provide accurate and meaningful interpretations of various assays.[84]

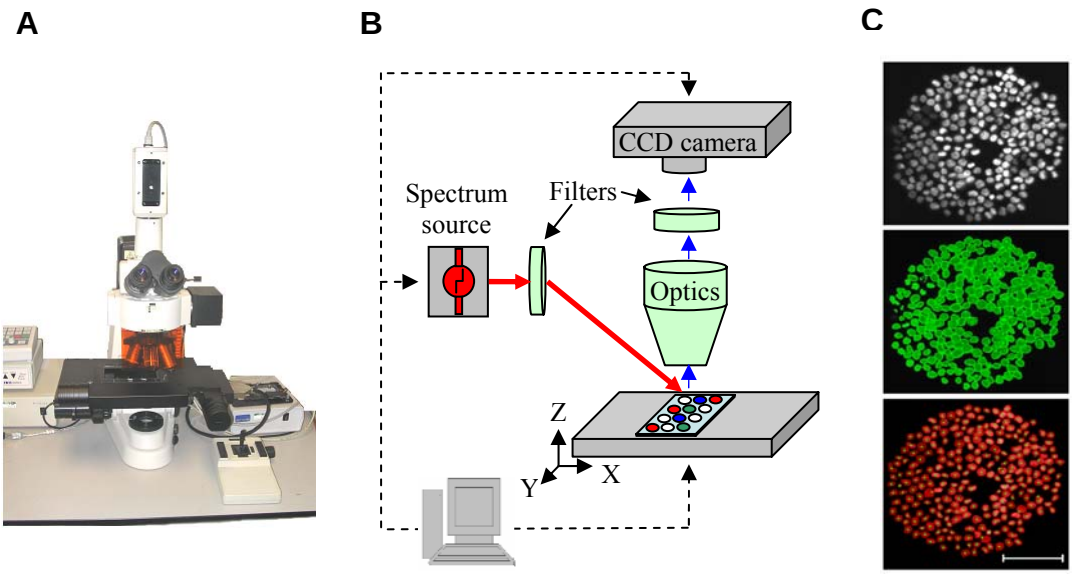

Figure 1.9 *A) Nikon 50i fluorescence microscope with a motorised X–Y–Z stage; B) general scheme of an IMSTAR HCS device equipped with the Pathfinder™ software package; C) pathfinder™ software automated cell quantification. Fluorescent images of K562 cells grown on a representative PA374 spot. From top to bottom: DAPI channel, pathfinder™ software automatic cell quantification. Scale bar 100 µm.*

1.4 Summary

The development of biomaterials for the biomedical field, especially in the case of polymers, represents a major opportunity to improve quality of life. For this reason great quantities of resource have been spent with the intention of synthesising and improving biocompatible materials. However, due to the complexity and diversity of biocompatibility testing, it has been difficult to find a universal method which permits high throughput determination of *in vitro* properties. It is impossible to theoretically predict cellular response, and thus every time a new material is generated it is vital to test its biocompatibility using cells with which it will come into contact. Researchers need to create new systems and techniques which allow the acceleration of this type of screening, and which minimise expenditure of time and money.

This issue has been addressed by the Bradley group with the development of a new system of screening, based on microarray technology. The technique of polymer microarrays has had, and will continue to have, a significant impact on the study and development of new biomaterials with diverse applications. Thousands of new polymers have been tested for their interaction with different cell lines, as will be discussed in future Chapters. The polymer microarray approach also appears to offer a significant advance when allied with cellular biology and the area of tissue engineering.

1.5 Aim for the thesis

The aim of this thesis was to apply polymer microarrays to the screening of polymer libraries with three main purposes: firstly, identifying substrates upon which specific cell lines would adhere and grow; secondly, gaining an understanding of the interactions between the cells and the biomaterials; and thirdly, to provide materials with potential applications. DNA-microarray analysis was undertaken in order to facilitate understanding of the changes in gene expression after suspension cell immobilisation.

Specific avenues of research included:

(i) The control of fibroblast adhesion and morphology;
(ii) The binding of suspension cells (erythroleukaemic K562 cells) with analysis to access the global gene expression profiles;
(iii) The attachment, promotion and stabilisation of hepatocyte-like cells applicable to cell culture and bioartificial liver models;
(iv) The promotion of adhesion, growth and function of endothelial progenitor cells to create living blood vessels and to mediate the endothelialisation of artificial vessel prostheses;
(v) Selective bacterial enrichment or the prevention of surface contamination.

It was hoped that the results of these investigations would offer practical applications for biomaterials, such as: developing new implant surfaces and tissue-engineered scaffolds while enhancing the study of cell-biomaterial interactions, and creating surface treatments for the prevention of bacterial contamination.

Chapter 2

Cellular Adhesion, Morphology and Biocompatibility Studies

2.1 Introduction

One of the fundamental requirements for a biomaterial in tissue engineering, cell therapy and regenerative medicine is the capacity to control efficiently the adhesion of cells.[85-88] Such adhesion requires an initial phase in which the cell recognises the substrate and it is essential to understand the mechanisms which determine this initial phase of adhesion, as well as how to control it.[86, 89-91] Both the mechanical properties and the chemistry of the biomaterial determine the efficiency and success with which cells recognise and respond to it.[92] Only by quantifying the relative success or failure of a given biomaterial to bind a specific cell type can biomaterials, implant surfaces and tissue-engineering scaffolds be designed.[93] Cells exist in a complex and dynamic microenvironment which includes the surrounding ECM, growth factors and cytokines, as well as adjacent cells.[94] Cell adhesion to the biomaterial involves firstly the physical interaction of ECM proteins in the given media with the biomaterial surface, and then the covalent connection of ECM proteins to cell surface receptors.[95] Integrins are the principal transmembrane receptors, which initiate the connection of the intracellular cytoskeleton to the ECM.[94-96] This allows cells to react in an appropriate manner to extracellular events (outside-in signalling), while cell adhesion molecules are capable of transmitting signals from inside the cells to the extracellular environment (inside-out signalling).[97] Binding of integrins to ligands on the ECM causes integrins to group into localised adhesions.[98] These adhesive processes initiate a cascade of intracellular signalling events that can provoke changes in cellular behaviour, such as morphology, growth, migration, and differentiation.[94, 97, 98]

2.2 Scope of this study

In this Chapter, cell adhesion studies were realised using a library of polyurethanes[99] to try and find optimal polymer support for mouse connective tissue cells (fibroblast cells (L929)). These cells are of interest in biomedical research since fibroblasts provide a structural framework (stroma) for many tissues and play a critical role in wound healing.[100] For example, the healing of full-thickness skin defects requires extensive synthesis and remodelling of dermal and epidermal components. Fibroblasts play an important role in this process and are being incorporated in the latest generation of artificial dermal substitutes.[101] Numerous physical parameters such as elasticity, surface topography[102] and biochemical properties (in particular the ability to absorb ECM)[103] are expected to play a relevant role in cellular adhesion and biocompatibility. In addition, the surface of a polymer often changes the conformation of the adsorbed ECM proteins which may partially or completely lose their bioactivity.[104] All these factors are dependent on the chemical structure of the polymer and are, therefore, not easy to predict. The versatile, and time-saving, method of polymer microarray allows the simultaneous study of both cellular morphology and cell viability in relation to the polymers to which the cells adhere.[105]

2.2.1 High content screening of L929 cells

Cell-adhesion experiments used the mouse fibrosarcoma cell line, L929, and included incubation on a 214-member polymer microarray for 48 h and 72 h. In order to study the biocompatibility of the polymer support, cells were incubated with CellTracker Green-(CTG) one hour before fixing (CellTracker Green is an indicator of cell viability (see Chapter 2.2.2)).[106] Subsequently, the cells were fixed, and cell nuclei and the cytoskeleton stained with Hoechst-33342 and AlexaFluor 568 phalloidin respectively. Cell permeable Hoechst-33342 is an adenine-thymine-specific dye that binds to the minor groove of DNA, and is used to enable the counting of cells.[107] AlexaFluor 568 phalloidin is a fluorescent bicyclic peptide with high-affinity for F-actin, which is an important component of the cytoskeleton, and is used to study cell morphology.[108] This fluorescent probe does not cross the

membrane of living cells and requires permeation of the cells. Once the cells are fixed, the staining of the cells with Hoechst-33342 is also accelerated, due to enhanced cellular permeability. Cell number, biocompatibility and morphology of each polyurethane member was determined using fluorescent (DAPI, fluorescein, and rhodamine-like band-pass filters) and brightfield channels by automated scanning of polymer spots (**Figure 2.1**).

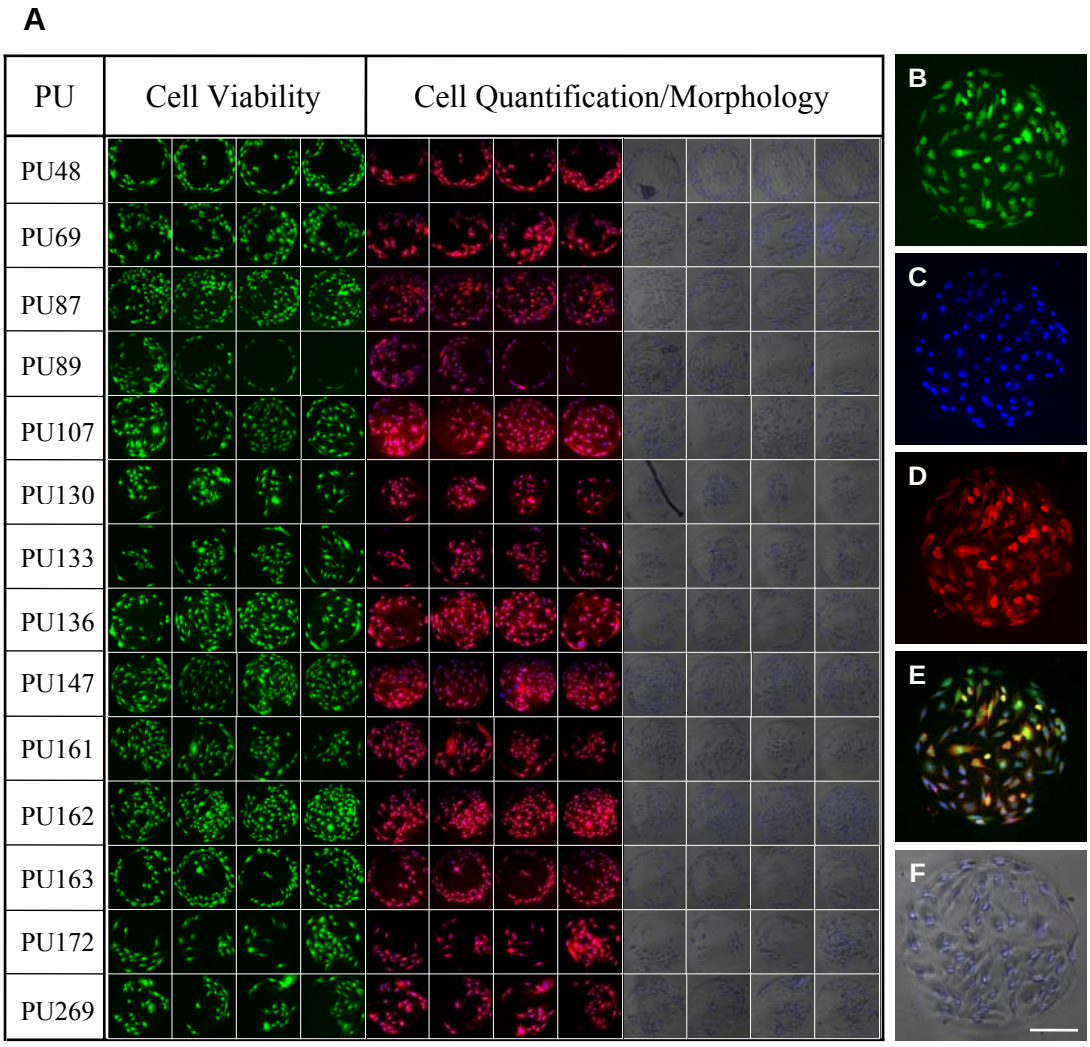

Figure 2.1 *L929 cells grown on polymer microarrays after 72 h incubation. A) The top polymers for L929 cells. All polymers supported a minimum of 200 cells/mm^2. Fluorescein channel images are shown in the cell viability column. Rhodamine/DAPI merged images and brightfield/DAPI composites are shown in the Cell Quantification/Morphology column. B–F) Fluorescent images of L929 cells grown on PU107: B) FITC channel; C) DAPI channel; D) rhodamine channel; E) FITC/DAPI/rhodamine channel, merged image; F) DAPI/brightfield channel merged, image (scale bar 100 µm).*

2.2.2 Analysis of cell viability

The viability of cells (i.e. the number that survived)[109] was measured by CTG fluorescent emission of the content of each spot through the FITC-like channel. CellTracker Green 5-chloromethylfluorescein diacetate (CTG-CMFDA) is non-fluorescent and able to diffuse freely through the membrane of live cells. Once inside the cell, intracellular esterases convert nonfluorescent CTG-CMFDA to fluorescent 5-chloromethylfluorescein (CTG-CMF) to produce cells that are fluorescent. Cells are also covalently modified, due to the chloromethyl group which react with thiols on proteins and peptides to form aldehyde-fixable conjugates (**Figure 2.2**).[106]

CellTracker Green is a useful indicator for showing whether or not cells are living. If cells have died, esterases will be denatured (just like any other protein in the cell) and unable to initiate the process of fluorescent marking. This, therefore, acts to determe the success of a biomaterial substrate. In general all polymers with the ability to support L929 cells were found to have high biocompatibility with this cell line.

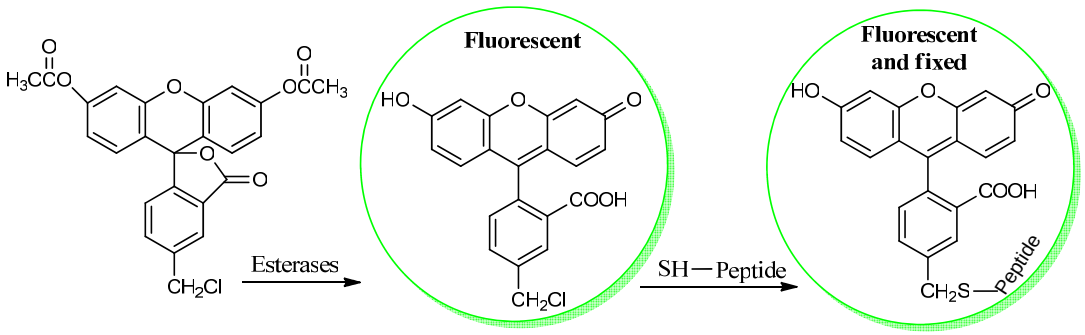

Figure 2.2 *Intracellular reactions of CTG-CMFDA.*

2.2.3 Analysis of cell adhesion and competitive affinity

In order to quantify cellular adhesion on each polymer the average number of cells across the four spots was calculated, with values for L929 cells recorded at two time points, 48 h and 72 h. This was done by fluorescence analysis of images from the DAPI channel (**Figure 2.1 C**).

Pathfinder™ was used to automatically count cell nuclei. In general, significant cellular adhesion was supported by a number of the polyurethane library members (**Figure 2.3**). PU87, PU147 and PU162, with difference in their polymer construction (**Table 2.1**), were the best substrates, providing an average of cell binding (over the 4 identical polymer spots) higher than 1000 cells/mm^2 mouse fibroblast cells. Thirteen out of the fourteen best polymer supports contained a chain extender, except PU172 (**Table 2.1**).

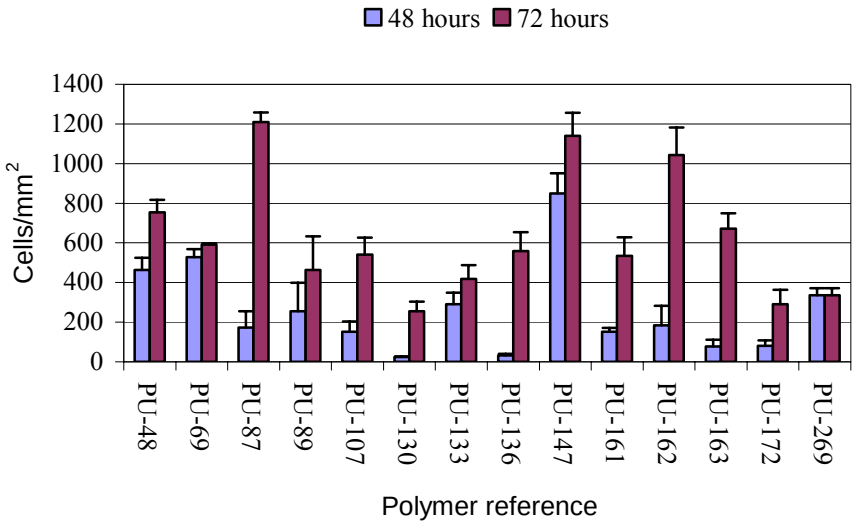

Figure 2.3 *Polyurethanes cell binding after 48 and 72 h (average from 4 spots of same polymer). The number of cells/mm^2 was calculated assuming a spot diameter of 300 µm. The error bars represent the standard error of the average. Complete L929 cell-polyurethane binding analysis is reported on CD (Supplementary Information, excel folder named "Chapter 2").*

The diol, PTMG, although with different molecular weights (650, 1000, 2000), was a common component of ten of the "hit" polymers (**Table 2.1**), thus indicating correlation between polymer structure and cell binding. Although two different polymers could have similar capacity for binding a specific cell line, the cell adherence process could be faster on one polymer than on the other. Consequently, in order to quantify the cell proliferation, the average number of cells and the standard deviation across the replicates were determined at two different incubation times (48 h and 72 h) on two separate polymer microarrays.

PU	Polymer Structure			
	Diol	Mn	Diisocyanate	Chain Extender
48	PPG	2000	BICH	ED
69	PTMG	2000	MDI	BD
87	PPG	2000	HMDI	BD
89	PTMG	2000	HMDI	BD
107	PTMG	650	HDI	DEAPD
130	PTMG	650	TDI	DMAPD
133	PHNGAD	1800	HDI	BD
136	PTMG	250	BICH	DEAPD
147	PTMG	250	HDI	DEAPD
161	PTMG	650	MDI	EG
162	PTMG	1000	MDI	EG
163	PTMG	2000	MDI	EG
172	PTMG	650	HDI	none
269	PPG	2000	MDI	DEAPD

Table 2.1 *L929 cell binding polymers with polymer composition: Diol/Diisocyanate/Chain Extender (1:2:1), except PU172 which is: Diol/Diisocyanate (1:1).*

Monomers abbreviations:

Diol:
PHNGAD: poly[1,6-hexanediol/neopentyl glycol/diethylene glycol-*alt*-(adiptic acid)]diol
PPG: poly(propylene glycol)
PTMG: poly(butylene glycol)

Diisocyanate:
BICH: 1,3-bis(isocyananatomethyl)cyclohexane
HDI: 1,6-diisocyanohexane
HMDI: 4,4'-methylenebis(cyclohexylisocyanate)
MDI: 4,4'-methylenebis(phenylisocyanate)
TDI: 4-methyl-1,3-phenylene diisocyanate

Chain Extender:
BD: 1,4-butanediol
DEAPD: 3-diethylamino-1,2-propanediol
DMAPD: 3-dimethylamino-1,2-propanediol
ED: ethylene diamine
EG: ethylene glycol

A comparative analysis of cell number per polymer over time would thus be a measure of the proliferation ability of L929 on the polymers. Data analysis revealed different behaviors for the polymers (**Figure 2.3**). For example, some polymers showed low cell binding after the first 48 h and then showed a "burst of growth" over the following 24 h.

The 160 series (PU161,162 and 163), which has the same monomer structure (**Table 2.1**), only differing in the molecular weight of the diol used (PTMG 650, 1000 and 2000 respectively), showed similar cell attachment trends (**Figure 2.3**). Low cell binding was observed within the first 48 h followed by vigorous growth for the next 24 h. On the other hand, polymers PU48, 69 and 147 (**Table 2.1)** showed steady cell numbers over time, associated with rapid cell immobilization achieved by these polymers (**Figure 2.3**). The number of cells on PU269 for both observation times was identical, with high affinity of these polymers for L929 after 48 h but, over the following 24 h, cellular proliferation was absent (**Figure 2.3**).

2.2.4 Correlation between polymer wettability and cell adhesion abilities

Bradley previously reported a high throughput method for evaluating the wettability of polymer libraries by measuring the spreading area of water droplets deposited onto spin-coated films of the polymer. The entire polyurethane library, was, therefore characterized with spreading areas determined after a contact time of 20 s. Analysis showed that 90% of the PU library members were relatively hydrophobic, with a spreading area ranging from 8 to 12 mm^2 (equivalent to a contact angle from 90º to 70º, respectively).[99] These values were shown to be strongly correlated with the cell binding (**Figure 2.4**) with all hydrophilic polymers (having a spreading area > 15 mm^2, equivalent to contact angle < 50º) found to impede cell adhesion. This analysis emphasizes the significant role of the polymer's physical properties on cell adhesion and indicates that L929 cells require a relatively hydrophobic substrate for adherence.

2.2.5 Analysis of cell morphology

Cells in contact with a binding surface will first attach and then spread according to the interactions created between the surface, the proteins from the growth serum and the ECM proteins. The nature of this adhesion will influence their morphology and their capacity for proliferation and differentiation. Fibroblasts are slow-moving cells in which the cytoskeleton plays a very important role in cell motility and shape.

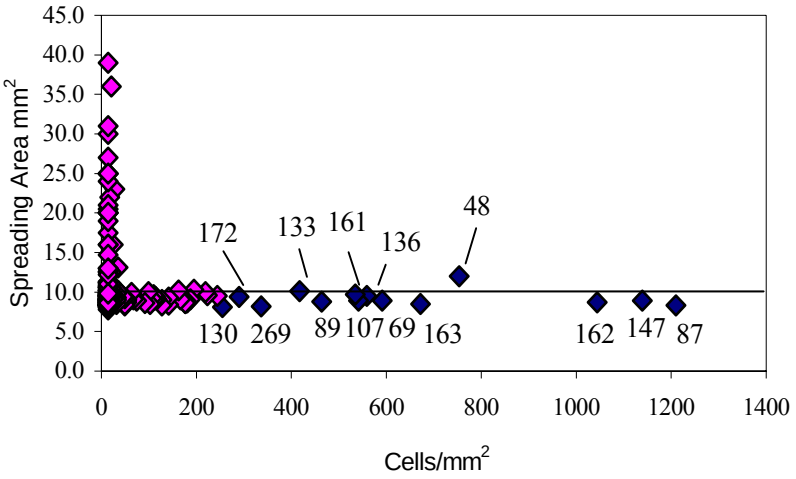

Figure 2.4 *Analysis of polymer wettability in relation to the average number of cells/mm^2 per polymer. Polymer wettability is expressed as the area over which a droplet of water of defined volume spreads over a cover slip spin-coated with the polymer (and was determined in this case after a contact time of 20 s). The numbers of the hit polymers described in* ***Figure 2.3*** *are shown (blue diamonds).*

To observe the effects of polyurethanes on the typical morphology of this cell-type, confocal microscopy studies were carried out on cultured L929 fibroblasts. Cells cultured on the majority of the spots maintain their characteristic morphology (**Figure 2.5 A**). Closer analysis revealed alternative cell morphologies (**Figure 2.5 B-D**). In spots showing low density cell binding a rounded morphology was typically observed (**Figure 2.5 C**), due presumably to the lack of suitable attachment points needed for the development of a "normal phenotype" (**Figure 2.5 A**).

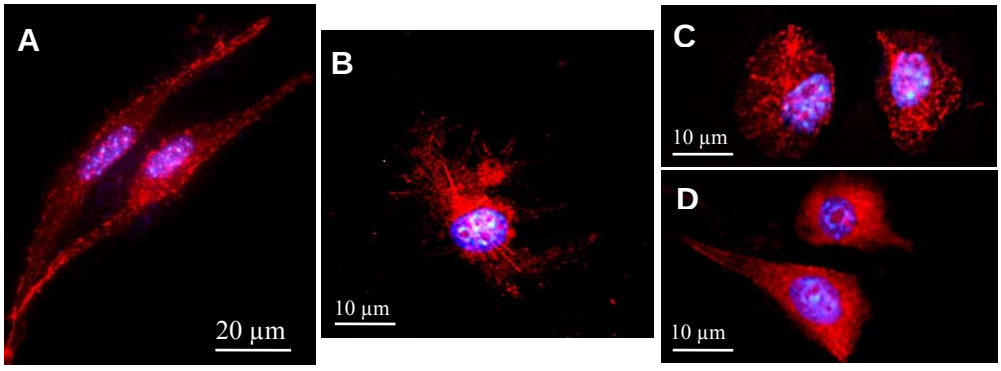

Figure 2.5 *Confocal images of L929 cells on polymer microarrays. Cells were imaged under ex/em 578/603 nm and ex/em 360/40 nm using a DeltaVision RT microscope (×63 objective) and then merged: A) PU87; B) PU133; C) PU161; and D) PU107.*

2.3 Conclusion

A fluorescence-based high-throughput microarray approach facilitated the rapid screening of libraries of potential biomaterials and was used for the study of L929 cellular adhesion. This screening allowed the identification of a group of fourteen biocompatible polyurethanes which enabled a good adhesion of L929cells.

Thirteen out of the fourteen best polyurethanes contained the diol, PTMG, underlining the important role of this monomer in the adhesion of L929 fibroblasts cells. Further analysis emphasizes the significant role of the polymer's physical properties on cell adhesion and indicates that L929 cells require a relatively hydrophobic substrate for adherence. The method also allowed the study of polyurethane on the typical L929's morphology. In spots showing low density cell binding a rounded morphology was typically observed.

Chapter 3

The Molecular Basis of Cell-Biomaterial Interactions: Transcriptomic Studies

3.1 Introduction

Various studies have been reported on gene expression analysis of cell-biomaterial investigations *via* reverse transcriptase polymerase chain reaction (RT-PCR)[110, 111] and Northern blotting.[112] However, these methods look at only limited numbers of genes and are insufficient for conducting large-scale transcriptomic analysis. Over the last few years, there have been tremendous advances in high-throughput gene expression analysis *via* the application of DNA microarray technology, which has emerged as a valuable tool in providing important insights into the molecular basis of cellular responses to various physiological stimuli and toxic insults.[113] Various studies have used microarray technology to understand the complex nature of cell–biomaterial interactions.

Xynos analysed the gene expression profile of human osteoblasts on Bioglass 45S5.[114] This biomaterial is an osteoproductive material which is resorbed by releasing its constitutive ions into solution. Using DNA microarray technology, they found that the expression of a potent osteoblast mitogenic growth factor, insulin-like growth factor II (IGF-II), was increased. There was also a large increase in the concentration of IGF-II protein in the conditioned media of treated osteoblasts. Expression levels of IGFBP-3, an IGF-II carrier protein, metalloproteinase-2 and cathepsin-D were also strikingly up-regulated. Metalloproteinase-2 and cathepsin-D are proteases that cleave IGF-II from its carrier proteins, resulting in the release of biologically active IGF-II. The authors concluded, therefore, that the stimulatory

effect of the ionic products of Bioglass 45S5 dissolution on osteoblast proliferation may be mediated by IGF-II.

Ku tested a new thermal surface treatment which allowed an increase in the oxide layer thickness of a Titanium alloy (Ti–6Al–4V) used in orthopaedic implants.[115] In this study the reaction of osteoblasts to this new surface treatment was tested and compared to other surface treatments currently used in implant surgery. Twenty-eight genes were selected in order to compare the effects of these surfaces on osteoblasts. Based on the genes studied, a general pathway for the cells' reaction according to the surface treatments was proposed. Metal ion release affected the time course of gene expression in the FAK pathway; over a certain threshold value metal ions release from the newly developed surface treatment diminished cell growth and apoptosis could occur. The release of metal ions stimulate PTK up-regulation; and the over-expression of the Bcl-2 family and Bax suggest that metal ions provoke apoptosis. The new surface treatment tested in this study seemed to increase the Ti–6Al–4V biocompatibility compared to that of the other treatments currently available, as indicated by the reduced inflammatory reaction and reduced chance of apoptosis.

Carinci used expression profiling to study the osteoblast-like cell line (MG-63) on zirconium oxide discs.[116] The expression of several of the genes was significantly up or down-regulated and covered a broad range of functional activities, including immunity, vesicular transport and cell cycle regulation. The data reported allowed a better understanding of the molecular mechanism of biocompatibility and could be used as a model for comparing other materials.

Allen used transcriptomic DNA microarray-based analysis to study the interaction of cells with a homologous series of copolymer films that had slightly different levels of surface hydrophobicity.[117] They used various combinations of *N*-isopropylacrylamide, which is currently used as an adaptive cell culture substrate, and the more hydrophobic, yet structurally similar, monomer *N*-*tert*-butylacrylamide. They examined the connection between phenotypic responses to cell–biomaterial interaction and global gene expression profile alterations. Their research showed that high-throughput analysis of gene expression enhances understanding of cell–biomaterial interaction, and offers refinement of biocompatibility assessment.

3.2 Erythroleukaemia cells (K562)

K562 cells are a suspension cell line derived from a chronic myelogenous leukaemia patient.[118] These non-adherent, suspension cells do not need to be attached to ECM proteins in order to survive and grow.[118, 119] This cell line does not normally undergo the same adhesion process as anchorage-dependent cells (see Chapter 2.1),[120] and, therefore, is especially appropriate for the study of cell adhesion over long periods of time. Understanding why cells like K562 convert from suspension to adherent cells could be of enormous benefit in refining our understanding of metastasis.[121] Using suspension cells, which have significantly fewer surface receptor proteins (integrins) than adherent cells,[122] it is possible to separate out the effect of protein adsorption from adhesion phenomena, including the role of non-specific surface charge in cell binding.[123] K562 cells are important as they lack the major histocompatibility complex (MHC) required to inhibit natural killer (NK) activity.[124] If they can be successfully immobilised, as has been attempted in this study, it could be possible to develop a NK cell-cell killing assay, in an attempt to understand better how NK cells attach in order to destroy leukaemia cells, and, consequently, to develop new strategies for combating leukaemia.[125, 126]

3.3 A polymer DNA-microarray approach to biomaterials

The aim of the study undertaken in this Chapter was, first, to apply polymer microarrays to identify polymers which allow the immobilisation of K562, and secondly, use DNA-microarray analysis for the rapid transcriptomic examination of specific cell-biomaterial interaction arising as a result of the immobilisation (**Figure 3.1**), which would allow better understanding of the links between phenotypic responses and global gene expression. Adhered cells, which usually grow in suspension, demonstrate a change in their gene expression profile. The importance of this research, therefore, lies not only in the identification of polymers which bind K562 (with all the possible applications already described) (**Figure 3.1 A**), but also potentially improved understanding of the changes in gene expression caused by forcing suspension cells to grow when bound to a surface (**Figure 3.1 B**).

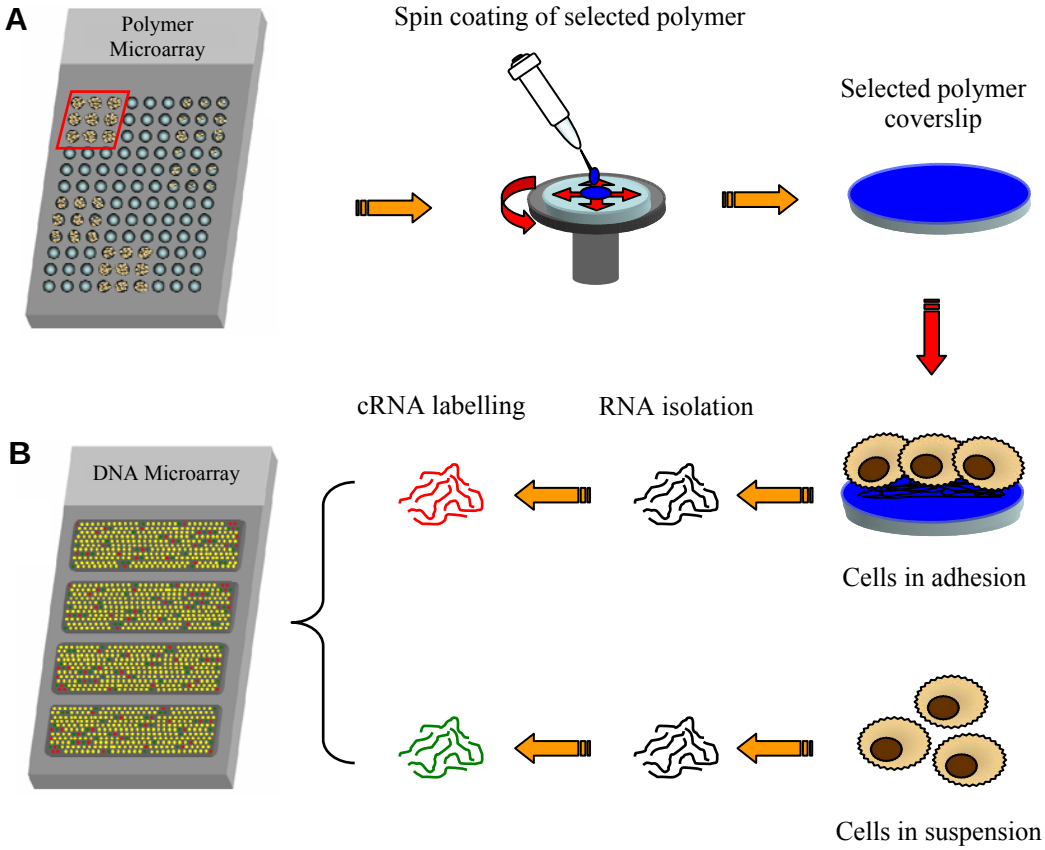

Figure 3.1 *Dual polymer–microarray-co-DNA-microarray strategies for the assessment of cell-biomaterial interactions. A) Polymer libraries screening; B) transcriptomic analysis.*

3.3.1 Analysis of cell attachment and proliferation

In the first instance, cellular binding of suspension cells onto polymer microarrays of 271 polymers were explored. The identification of polymers that immobilised K562 cells was achieved *via* the analysis of polymer microarrays that not only measured polymer-binding capacities but also cellular proliferation.[127] In order to quantify both cellular adhesion and proliferation, the average number of cells and the standard deviation across the replicates were determined at three different incubation times (24 h, 48 h and 72 h) on six separate polymer microarrays. Each polymer microarray was washed at each time-point in order to remove the cells which had not adhered to the polymer. Consequently, *via* analysis of the arrays it was possible to profile the polymer libraries in terms both of binding and proliferation, through the analysis of fluorescence images coming from the nuclei stained (**Figure 3.2**).

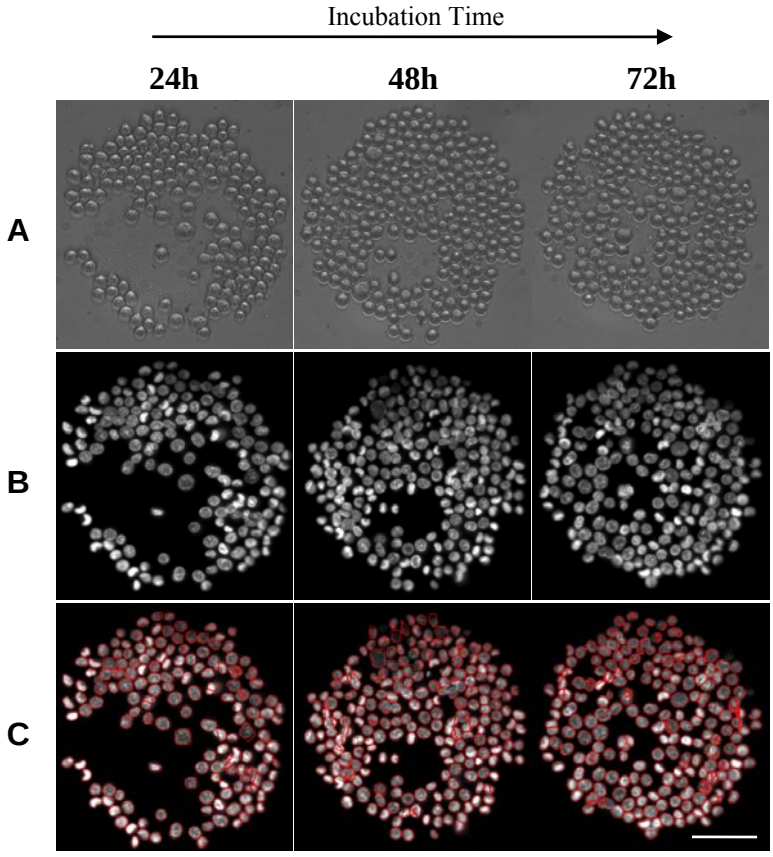

Figure 3.2 *Parallel analyses of polymer cellular binding and proliferation on a representative spot (PA374): A) brightfield images; B) DAPI channel; C) cell nuclei automatically recognised and quantified by the pathfinder™ (Chapter 2.2.1). Scale bar 100 µm.*

3.3.1.1 Polyurethanes[99]

Analysis revealed a set of polyurethanes with high cell binding (**Figure 3.3**). Fourteen polyurethanes showed more than 1000 cells/mm^2 after 72 h. The diols PTMG and PPG, were a common component of all the hit polymers, whereas more than half of the chain extender components were either DEAPD or DMAPD, both of which contained a tertiary amino group, which may be a factor in cellular adhesion activity, underlining that the positive surface charge of biomaterials plays a major role in cellular immobilization (**Table 3.1**).

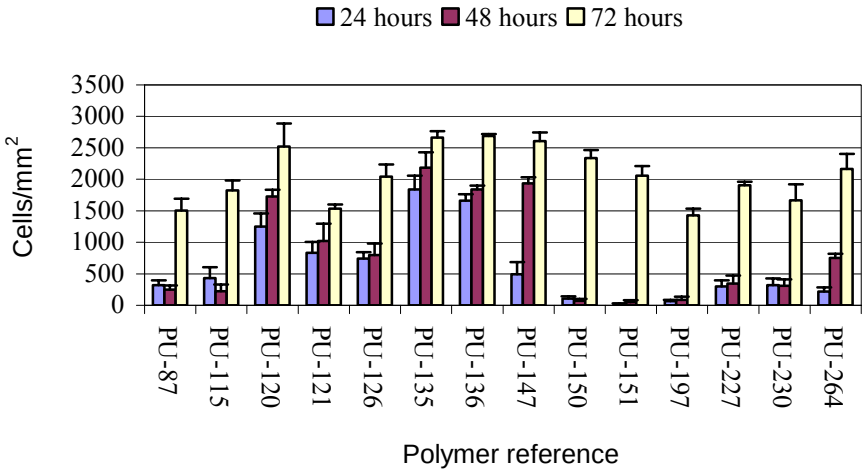

Figure 3.3 *Polyurethanes cell binding after 24, 48 and 72 h (average from 4 spots of same polymer). The number of cells/mm^2 was calculated assuming a spot diameter of 300 µm. The error bars represent the standard error of the average. Complete K562 cell-polyurethane binding analysis is reported on CD (Supplementary Information, excel folder named "Chapter 3").*

PU	Polymer structure			
	Diol	Mn	Diisocyanate	Chain Extender
87	PPG	200	HMDI	BD
115	PPG	100	HDI	BD
120	PPG	425	BICH	DEAPD
121	PPG	100	BICH	DEAPD
126	PPG	425	TDI	DMAPD
135	PTMG	250	BICH	DMAPD
136	PTMG	250	BICH	DEAPD
147	PTMG	250	HDI	DEAPD
150	PTMG	650	HDI	EG
151	PTMG	100	HDI	EG
197	PTMG	650	BICH	DHM
227	PPG	190	HDI	none
230	PPG	190	HDI	BD
264	PTMG	100	HDI	DMAPD

Table 3.1 *K562 cell binding polymers with polymer composition: Diol/Diisocyanate/Chain Extender (1:2:1), except PU115 and PU227 which are: Diol/Diisocyanate (1:1), and PU264 which is: Diol/Diisocyanate/Chain Extender (2:5:3).*

Monomers abbreviations:

Diol:
PPG: poly(propylene glycol)
PTMG: poly(butylene glycol)
Diisocyanate:
BICH: 1,3-bis(isocyananatomethyl)cyclohexane
HDI: 1,6-diisocyanohexane
HMDI: 4,4'-methylenebis(cyclohexylisocyanate)
MDI: 4,4'-methylenebis(phenylisocyanate)
TDI: 4-methyl-1,3-phenylene diisocyanate
Chain Extender:
BD: 1,4-butanediol
DEAPD: 3-diethylamino-1,2-propanediol
DMAPD: 3-dimethylamino-1,2-propanediol
ED: ethylene diamine
EG: ethylene glycol

The three hit polyurethanes (PU135, 136 and 147) had a similar structure, demonstrating correlation between polymer structure and cell binding. Moreover, data analysis revealed the unique proliferation behaviour for different sets of polymers (**Figure 3.3**).

Some polymers showed consistent proliferation through each period of 24 h. Others, meanwhile, showed poor cell binding for the first 24 h and 48 h, but then underwent a burst of growth over the following 24 h.

For example, PU150 and 151, which have the same type of monomers (**Table 3.1**) (differing only in the molecular weight of the diol used – PTMG 650 and 1000 respectively), showed similar cell-attachment trends. Low cell binding was observed during the first 48 h followed by a vigorous growth in the remaining 24 h. Other polyurethanes lacking the tertiary amino group (PA197, 227 and 230) (**Table 3.1**) showed a modest cell binding during the first 48 h followed by a vigorous growth only in the remaining 24 h. This suggested the importance of the positive surface charge in initiating an early process (first 24 h) during immobilisation of suspension cells. In fact, only polymers containing a tertiary amino group, showed both a rapid immobilisation at the beginning and than a further constant cell-binding trend for the following 48 h (**Figure 3.3**).

The polymers without a positive charge, probably allow the cell adhesion only involving: firstly the abortion of ECM proteins in the given media with the polyurethane surfaces, and then the covalent connection of ECM proteins to cell surface receptors.

PU87 has already been shown (Chapter 2) to be one of the best polymer for binding L929 cells, and it confirms its status as a polymer with high cellular affinity by promoting strong adhesion and growth with K562 cells (**Figure 3.3**).

3.3.1.2 Polyacrylates[40]

A library of polyacrylates was also evaluated (**Figure 3.4**). Fifteen polyacrylates (co-polymers with amino groups within monomer 2) showed significant cellular attachment (**Figure 3.4, darker grey squares)**, possibly due to the overall positive surface charge. The four best polymers, which provided a binding higher than 3500 cells/mm^2 after 72 h, were PA365, 368, 371 and 374 (**Figure 3.4, in red** and **Figure 5**). Those polymers are composed of HBMA (**Table 3.2)**. The proliferation behaviour of K562 cells on these polymers showed steady proliferation with time (**Figure 3.5**).

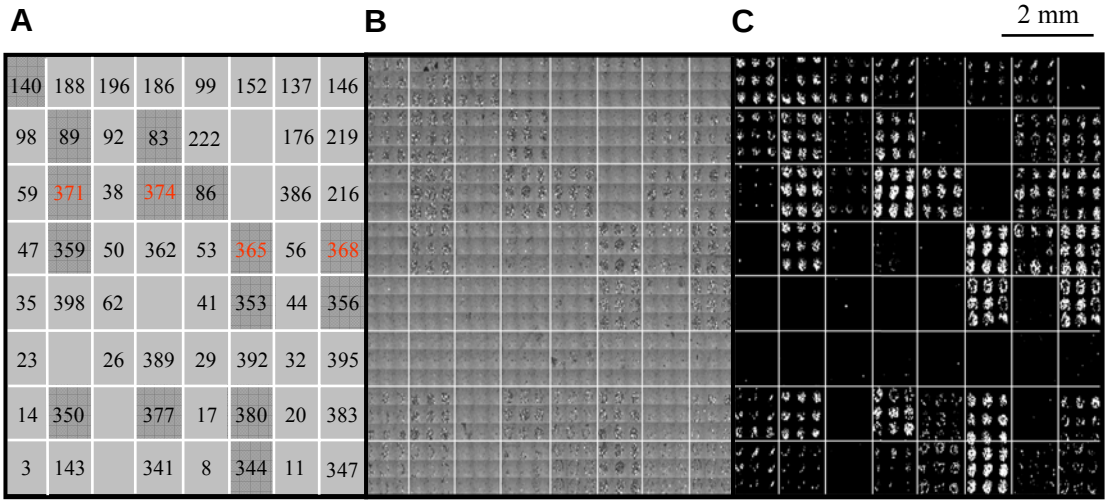

Figure 3.4 *Polyacrylates cell binding after 72 h. A) Array design with 58 polyacrylates and 6 "empty" areas, each square represents 9 replications of the same polymer spot. In darker grey squares: the 15 polyacrylates which showed more than 2000 cells/mm^2. In red: the 4 polyacrylates which showed more than 3500 cells/mm^2; B) brightfield mosaic image; C) DAPI mosaic image.*

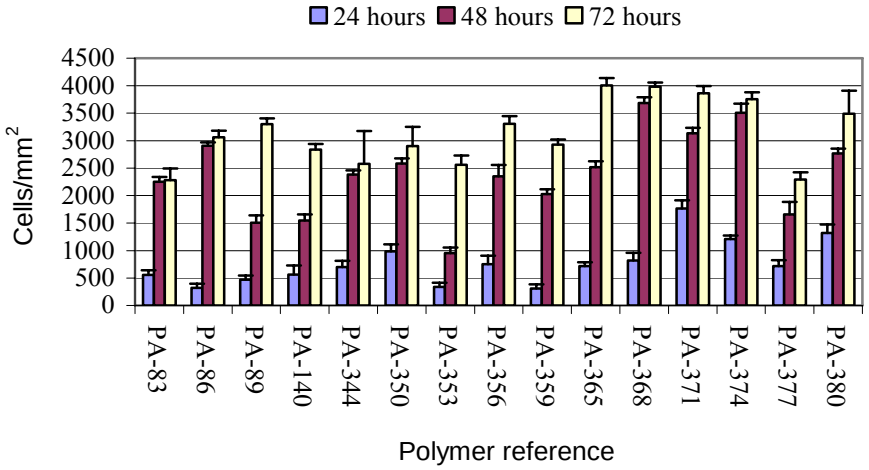

Figure 3.5 *Polyacrylates cell binding after 24, 48 and 72 h (average from 9 spots of same polymer). The number of cells/mm^2 was calculated assuming a spot diameter of 300 µm. The error bars represent the standard error of the average. Complete K562 cell-polyacrylate binding analysis is reported on CD (Supplementary Information, excel folder named "Chapter 3").*

PA	Polymer structre	
	Monomer 1	Monomer 2
83	MEMA	DEAEMA
86	MEMA	DMAEMA
89	MEMA	DEAEA
140	HEMA	DMAEMA
344	MMA	DMAEMA
350	MMA	DMAEA
353	HPMA	DEAEMA
356	HPMA	DMAEMA
359	HPMA	DEAEA
365	HBMA	DEAEMA
368	HBMA	DMAEMA
371	HBMA	DEAEA
374	HBMA	DMAEA
377	EMA	DEAEMA
380	EMA	DMAEMA

Table 3.2 *K562 cell binding polymer with polymer composition: Monomers 1/Monomers 2 (7:3).*

Monomers abbreviations:

Monomer 1

EMA: ethyl methacrylate
HBMA: hydroxybutylmethacrylate
HEMA: 2-hydroxyethylmethacrylate
HPMA: hydroxypropylmethacrylate
MEMA: 2-methoxyethylmethacrylate

MMA: methyl methacrylate
Monomer 2
DEAEA: 2-(diethylamino)ethyl acrylate
DEAEMA: 2-(diethylamino)ethyl methacrylate
DMAEA: 2-(diethylamino)ethyl acrylate
DMAEMA: 2-(diethylamino)ethyl methacrylate

3.3.2 SEM analysis

SEM studies were undertaken so that the effect of the different polymers on the cells could be assessed in relation to the nature of the cells on the polymer surface. Analysis suggested that cell morphology had changed. Control cells (**Figure 3.6 A-B**), appeared well rounded with numerous microvilli on their surfaces. Meanwhile, the surfaces of cells grown on the 4 polyacrylates (PA365, 368, 371 and 374) for 24 h (**Figure 3.6 C-F**) appeared different with numerous contact points with the substratum. This forced them to take a slightly flatter morphology, presumably as a consequence of the positive charge on the surface. This was particularly evident after 72 h with cells grown on PA368 (**Figure 3.6 G**) and PA365 (**Figure 3.6 H**).

3.3.3 Gene expression profiling

Following the adhesion of K562 cells onto coverslips coated with the selected polymers, total RNA was isolated and used for transcriptomic analysis. Gene expression analysis was carried out to study the result of interactions between polyacrylates PA368 and PA365 and K562 cells after 72 h using an Agilent 4 x 44 K Whole Human Genome microarray. Analysis gave 709 genes with a p-value < 0.01, which were then subjected to a fold change analysis to determine which genes were up- and down-regulated using a 2-fold increase or decrease as a cut-off value.

3.3.3.1 Analysis

The general effect of polyacrylates on transcriptomic response was studied irrespective of whether PA368 or PA365 was used. The entire dataset across the four arrays was grouped and analysed as a single entity. 34 genes appeared to be up-regulated, while 135 were down-regulated.

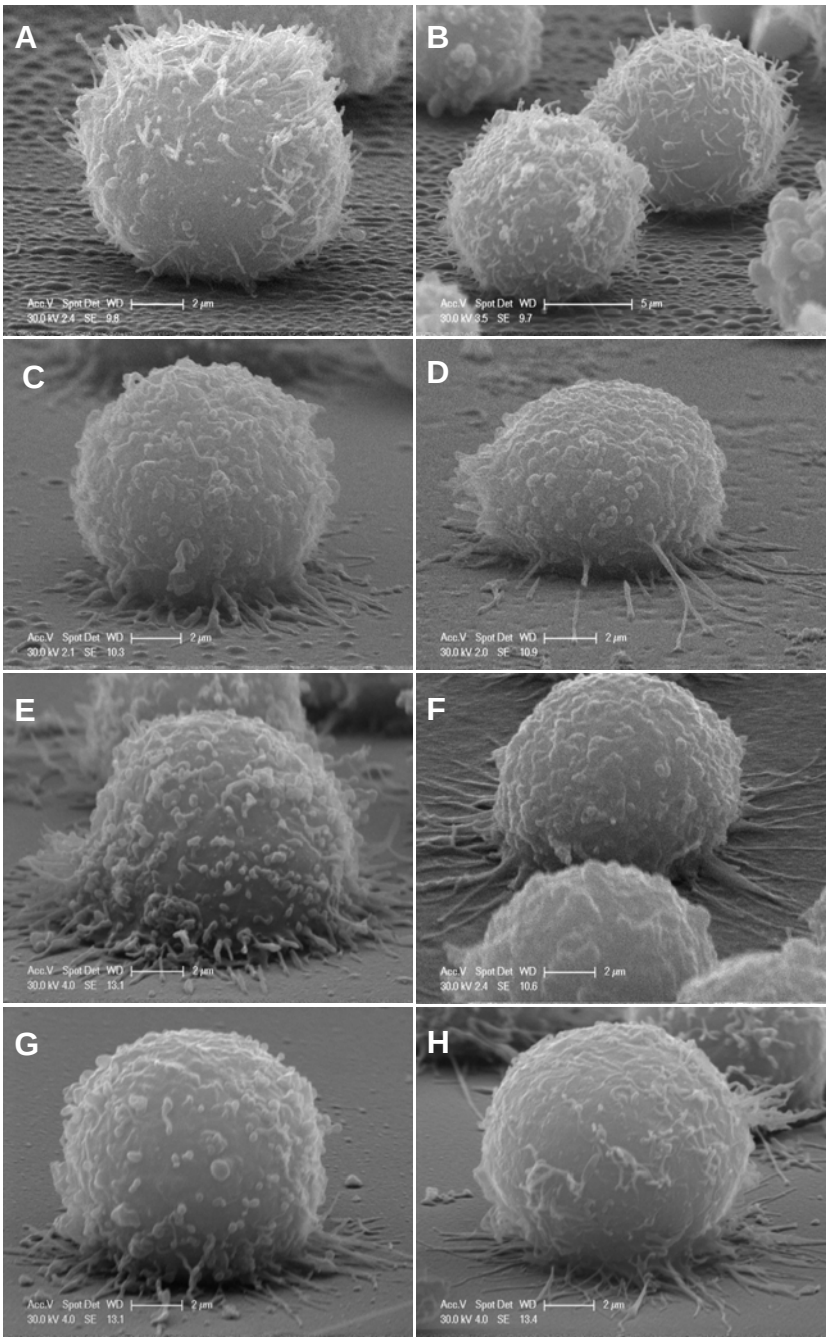

Figure 3.6 *Scanning electron micrographs. A-B) Control K562 cells after 24 h. C-F) Cells grown on PA365, 368, 371, 374 after 24 h, respectively. G and H) Cells grown on PA368 and PA365 after 72 h, respectively.*

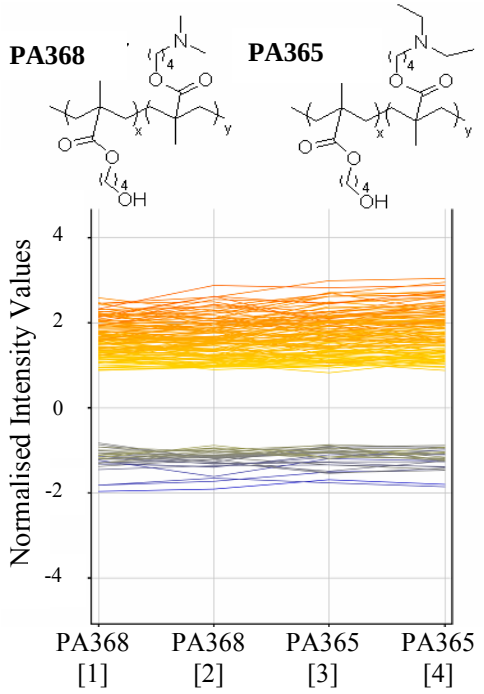

Figure 3.7 *Structures of polymer PA368 (top left) and polymer PA365 (top right) and profile plot of up- and down-regulated genes across the 4 polymer samples (normalized values in log_2 scale). [1]–[4] represent analysis on the four different subarrays. [1] and [2] represent subarrays hybridised with total RNA obtained from cells grown on PA368 and [3] and [4] from cells grown on PA365 compared to the "suspension cell control". Up-regulated genes have a negative value as the control genes were labelled with Cy5. (GeneSpring GX 9.0.2 software assumed that control genes are labelled with Cy3).*

The expression of the up- and down-regulated genes on each array is shown in **Figure 3.7** with the profile plots of these genes. Further refinement was carried out by increasing the cut-off value to identify genes which showed the largest changes in expression. Using a 3-fold change as a cut-off value[128] just three genes were identified as being up-regulated and 74 as down-regulated (**Table 7.1** in Chapter 7). This showed that when K562 cells become immobilised on polyacrylates, a chain of cellular changes is triggered, most notably resulting in gene down-regulation.

The 3 up-regulated genes were mediator complex subunit 18 (MED18), xenotropic and polytropic retrovirus receptor 1 (XPR1) and 3-hydroxy-3-methylglutaryl-coenzyme A synthase 1 (HMGCS1), and they were individually analysed in order to ascertain their function.

MED18 is a component of the Mediator complex, which is a co-activator for DNA-binding factors that activate transcription *via* RNA polymerase II.[129] Mediator

functions act as a bridge to convey information from gene-specific regulatory proteins to the basal RNA polymerase II transcription machinery. Mediator is recruited to promoters by direct interactions with regulatory proteins and serves as a scaffold for the assembly of a functional pre-initiation complex with RNA polymerase II and the general transcription factors.[130]

XPR1 may function in G-protein coupled signal transduction, and may act as a receptor for xenotropic and polytropic murine leukaemia retroviruses. Polytropic leukaemia viruses use this receptor to enter into cells, and, interestingly, adhesion on surfaces PA-368 and PA-365 induces over-expression of this receptor.[131] As a result, G proteins maybe were altered to deal with this new forced adhesion arena in which K562 cells were constricted and consequently act to ensure that only the appropriate response is triggered.

HMGCS1 is known to stimulate lipid synthesis and uptake and is part of the sterol-regulatory element binding proteins (SREBPs),[132] which are essential in cholesterol metabolism regulation and show the need for the cells to increase membrane lipid content when binding onto the polyacrylates.

3.3.3.1.1 Pathway analysis

The 74 down-regulated genes were analysed using KEGG (Kyoto Encyclopedia of Genes and Genomes) database,[133] allowing the identification of gene products which form part of six known biological pathways. As shown in **Table 3.3**, some identified pathways were found to be involved in intracellular pathways including: mitogen-activated protein kinase (MAPK) signalling; cytokine-cytokine receptor interaction; adipocytokine signalling; calcium signalling pathway; neuroactive ligand-receptor interaction pathway; and the focal adhesion pathway.

Many of the pathways were found to be involved in the process of cell adhesion and proliferation control, as well as in cell membrane modification. The MAPK pathway is involved in various cellular functions, including cell proliferation, differentiation and migration. Mammals express at least four distinctly regulated groups of MAPKs.[134] The cytokine-cytokine receptor interaction pathway is involved in the control of cytokines, which are crucial intercellular regulators and mobilises of cells engaged in innate as well as adaptive inflammatory host defences, cell growth,

differentiation, cell death, angiogenesis, and development and repair processes aimed at the restoration of homeostasis.[135] The calcium signalling pathway is involved in the control of calcium concentration. Ca^{2+} that enters the cell from the outside is driven by the presence of a large electrochemical gradient across the plasma membrane. Cells use this external source of Ca^{2+} signal by activating various entry channels with widely different properties. The influx of Ca^{2+} from the environment or release from internal stores causes a very rapid and dramatic increase in cytoplasmic calcium concentration, which has been widely exploited for signal transduction.[136] The focal adhesion pathway plays an essential role in biological processes such as cell motility, cell proliferation, cell differentiation and cell survival.[137] These results suggest that the process, by which K562 cells adhere alters the cellular membrane, produces a significant down-regulation of membrane receptors and ligands. Furthermore, this down-regulation interferes with cell-cell communication through the control of cytokines. It seems also that the electrochemical gradient across the plasma membrane is highly modified by an alteration of calcium exchange between cells and environment.

Kegg ID	Name	Class	Total genes	Genes found
hsa04010	MAPK signalling	Environmental Information Processing; Signal Transduction	357	TNFRSF1A CACNA1B CACNA1E
hsa04060	Cytokine-cytokine receptor interaction	Environmental Information Processing; Signaling Molecules and Interaction	260	CXCR3 CXCL3 TNFRSF1A
hsa04920	Adipocytokine signaling	Cellular Processes; Endocrine System	72	CAMKK2 TNFRSF1A IRS2
hsa04020	Calcium signaling	Environmental Information Processing; Signal Transduction	174	CACNA1B CACNA1E
hsa04080	Neuroactive ligand-receptor interaction	Environmental Information Processing; Signaling Molecules and Interaction	254	GPR156 NPBWR1
hsa04510	Focal adhesion	Cellular Processes; Cell Communication	200	COL6A1 PIP5K1C

Table 3.3 *Down-regulated pathways of genes identified in the microarray screening.*

Gene abbreviations:

TNFRSF1A: tumor necrosis factor receptor superfamily, member 1A
CACNA1B: calcium channel, voltage-dependent, N type, alpha 1B subunit
CACNA1E: calcium channel, voltage-dependent, R type, alpha 1E subunit
CXCR3: chemokine (C-X-C motif) receptor 3
CXCL3: chemokine (C-X-C motif) ligand 3
IRS2: insulin receptor substrate 2
CAMKK2: calcium/calmodulin-dependent protein kinase kinase 2, beta
GPR156: G protein-coupled receptor 156
NPBWR1: neuropeptides B/W receptor 1
COL6A1: collagen, type VI, alpha 1
PIP5K1C: phosphatidylinositol-4-phosphate 5-kinase, type I, gamma

3.3.3.1.2 Gene ontology analysis

The 3 up-regulated and 74 down-regulated genes identified in the first investigation were subjected to a gene ontology (GO) enrichment study performed using the GeneSpring GX 9.0.2 GO browser[138] to analyse their roles in biological processes. This analysis showed an over-representation of one molecular function category, "cadmium ion binding" (GO:0046870, p=0.0000838, 10 genes were found on the 4 x 44 K Whole Human microarray belonging to this GO term), with five of them (MT1X, MT1B, MT1H, MT2A, MT1E),[139] which belong to the metallothionein family, down-regulated when K562 cells adhered onto the "hit" PA368 and 365.

3.3.4 Data validation

One of the disadvantages of high throughput methods, such as DNA microarrays, is the sheer quantity of data, and the consequent risk of data error. Therefore, in order to validate the DNA microarray approach, the expression profiles of three down-regulated genes (MT1E, MT2A and MT1X) were analysed by real-time PCR. These three genes were selected because they were involved in a particularly striking result the over-representation of one molecular function category "cadmium ion binding" (Chapter 3.3.3.1.2). In order to validate the results for these three genes, quantitative real-time PCR was performed on K562 cells grown for 72 h on PA368, PA365 and in suspension as a control. The gene expression was normalised with respect to the expression of a human ring finger protein 7 (hRNF7) housekeeping gene.

The relative mRNA level for each gene (as the fold change) is shown in **Figure 3.8**. The mRNA levels obtained clearly confirmed the data obtained *via* DNA microarray analysis providing proof of the effect of polyacrylate-cell interactions on gene expression.

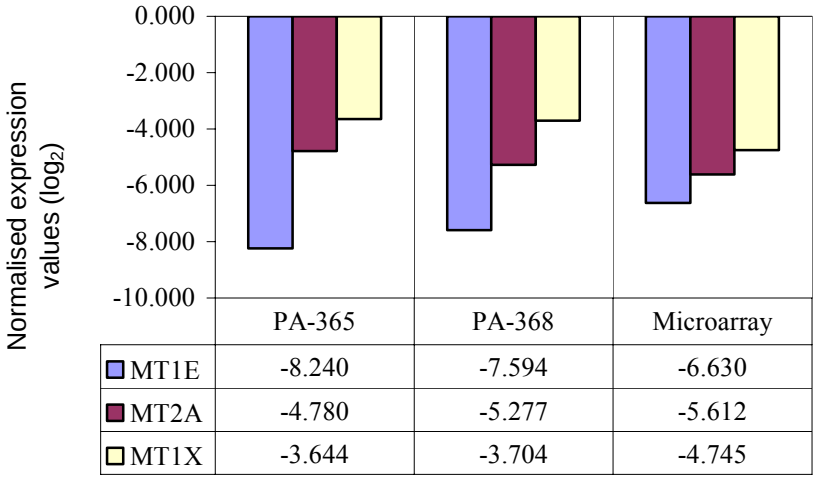

	PA-365	PA-368	Microarray
MT1E	-8.240	-7.594	-6.630
MT2A	-4.780	-5.277	-5.612
MT1X	-3.644	-3.704	-4.745

Figure 3.8 *Real-time PCR for three members of the metallothionein family (MT1E, MT2A, and MT1X) on the two polyacrylates (368 and 365). Fold change (in log_2) of the genes expression levels is reported compared to samples grown in suspension. All values are normalised hRNF7 expression levels.*

3.4 Conclusions

Polymer microarrays were successfully used for the identification of a family or group of polyurethanes that enabled adhesion and proliferation of a suspension cell line. Half of these PUs contained a tertiary amino group on their chain-extender, underlining the important role that positive surface charge plays in immobilising suspension cells on polyurethanes. To further emphasise the importance of positive surface charge, a group of polyacrylates containing the tertiary amino group was analysed by means of live cell scanning. Four polyacrylates PA365, 368, 371 and 374 showed particularly strong cell immobilisation, and these were composed of HBMA. Further analysis of the interaction between the four hit polyacrylates and K562 cells, by means of SEM, showed cells with numerous contact points with the

substratum, as a consequence of adhesive growth onto the positively charged surface. This demonstrates that K562 cells not only interact with the polymer electrostatically but also by means of the involvement of membrane receptors.

DNA microarrays were successfully used for gene expression profiling analysis, demonstrating that interactions between cells and some polyacrylates induce a number of changes in the transcriptom. When K562 cells become immobilised on polyacrylates, a chain of cellular changes is triggered, most notably resulting in down-regulation of the altered genes. The results of pathway analysis suggest that the process by which K562 cells adhere alters the cellular membrane, producing a significant down-regulation of membrane receptors and ligands. Furthermore, this down-regulation interferes with cell-cell communication through the control of cytokines. It seems also that the electrochemical gradient across the plasma membrane is modified by an alteration of calcium exchange between cells and environment. Validation by quantitative real-time PCR confirmed the gene expression analysis.

Chapter 4

Promotion and Stabilisation of hESC-Derived Cells by New Polymer Matrix

4.1 Human embryonic stem cells

hESCs are pluripotent cells which are isolated from the inner cells of blastocysts approximately four to five days post fertilization.[140, 141]

hESCs can differentiate into any of the three germ layers (ectoderm, endoderm and mesoderm) or they can, through self-renewal, maintain their undifferentiated state.[142] Theoretically, they can develop into each of the more than 200 primary cell types of the body when given the necessary stimulation (**Figure 4.1**).[143]

The therapeutic use of stem cells began in the 1970s with bone marrow transplants (containing human stem cells) into patients with diseased blood or bone marrow.[144] Following many advances in the field, stem cells have become the subject of extensive research and are now being investigated in many areas of cell-based therapy, such as: (a) the development of new treatments for nervous system diseases by surgical implantation of fetal cells;[145] (b) in tissue engineering for producing 'spare parts' of the body for replacement of damaged or lost organs;[146] and (c) in the field of drug and toxicity studies by monitoring the behaviour of embryonic stem cells exposed to a drug-candidate compounds.[147, 148] However, it is necessary to reduce or obviate the current dependence that all stem cell types and their derivatives have on vertebrate animal cell and tissue derived biological reagents (ie. ECM preparations, blood serum/serum fractions) for their growth, differentiation and storage.[149] These reagents can contribute to variations in stem cell behaviour through their own variability in purity and bioactivity. They also pose serious risks to

transplant recipients and through them, the general population, for transmission of known and unknown adventitious pathogens.[150]

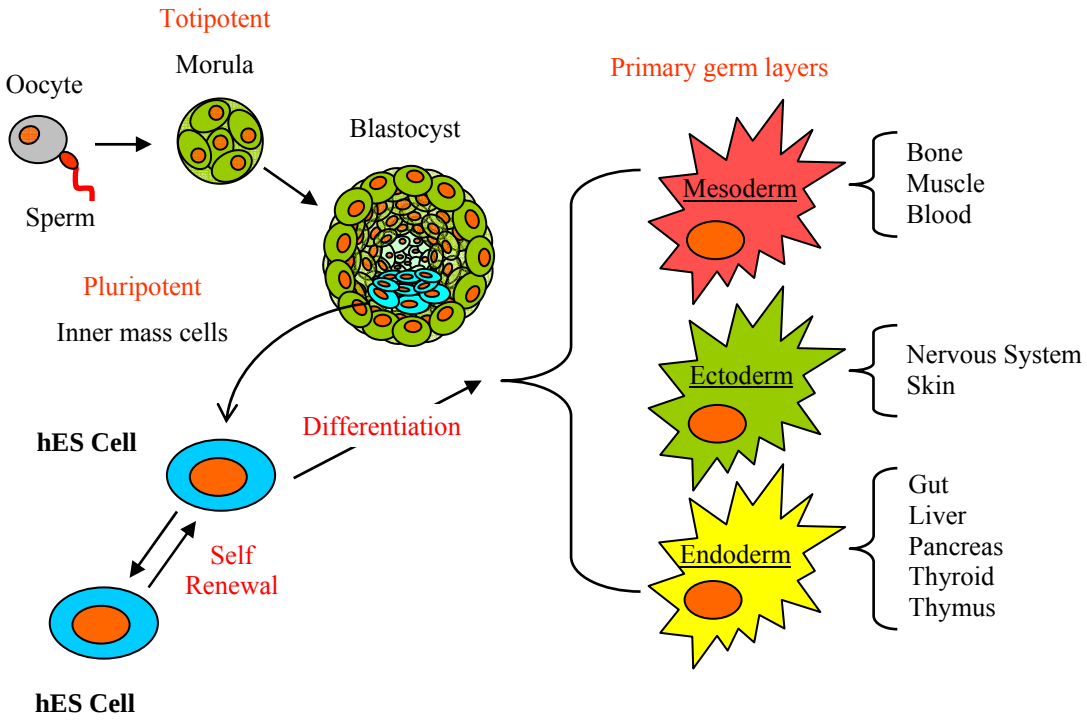

Figure 4.1 *General scheme of embryonic stem cell origins and differentiation into the three primary germ layers.*

4.2 Introduction to the Chapter

Hepatocytes are the primary cells of the liver, and have been the particular focus of many studies, because the liver plays a central role in many functions of the human body.[151] The ability to derive hepatocyte-like cells (HLCs) from hESCs constitutes an attractive scalable resource which holds great potential to develop a detailed understanding of human liver disease and metabolism. In particular, any strategies which might streamline and standardize the process of drug and toxicology testing would represent a significant development.[152] Presently, primary human hepatocytes (PHHs) are the "gold standard" cell type used in predictive drug toxicology. Unfortunately PHHs are scarce, heterogeneous and expensive resources which

function only short term *in vitro*. The generation of HLCs from hESCs has the potential to address the major challenge to acquire a reliable and clonal source of functional human hepatocyte cells for this purpose.[153]

Over the last few years, several studies have reported the differentiation of HLCs from hESCs.[154-156] Although there have been improvements in efficiencies, current strategies still yield relatively heterogeneous populations. Recently Hay developed an efficient model of deriving HLCs from hESCs.[157, 158] The generation of hepatic endoderm from hESCs for the first time provides a reliable and stable source of primary HLCs. As with hepatocytes freshly isolated from the liver,[159] however, a technique has not yet been found for maintaining the phenotype and function of these HLCs *in vitro*. Long-term HLC culture would permit the in-depth study of human liver development and create novel opportunities to model hepatic disease *in vitro*.

The investigation reported in this chapter relates to the search for polymers to which HLCs derived from hESCs are able to attach and maintain long term hepatocyte function. This may provide not only alternatives to current dependence on crude biological reagent (Matrigel (MG)), but a new generation of better extra-cellular support which significantly improves both HLCs function and lifespan. Once a suitable polymer was found, able to maintain and cultivate HLCs to such an extent that it might potentially allow the generation of a bio-artificial liver, tests to assess drug inducibility were also carried out.

4.3 Polymer microarray screening

Polymer libraries were screened in order to identify new supports for attachment, stabilisation and promotion of hepatocyte function. Hay cultivated hESC-derived HLCs using the *in vitro* model given in **Figure 4.2**.[158, 160] At day 9 in the differentiation process the cells were removed from their substrate. Following this, HLCs were re-plated onto the polymer microarray and cultured in maturation medium (Chapter 7.4.3). The medium was changed every second day during maturation up to day 16 (**Figure 4.2**). The polymer microarray onto which the HLCs were re-plated at day 9 consisted of 337 polymers printed in quadruplicate onto an

agarose-coated glass microscope slide. At day 16, cells were fixed and stained with a nuclear stain (Hoechst 33342), and a monoclonal antibody against albumin followed by incubation with a fluorescein-conjugated secondary antibody. Cell attachment was recorded by using the HCS systems and Pathfinder™ software. Hepatic phenotype and function was assessed by albumin production, which is an efficient marker for hepatic cells.

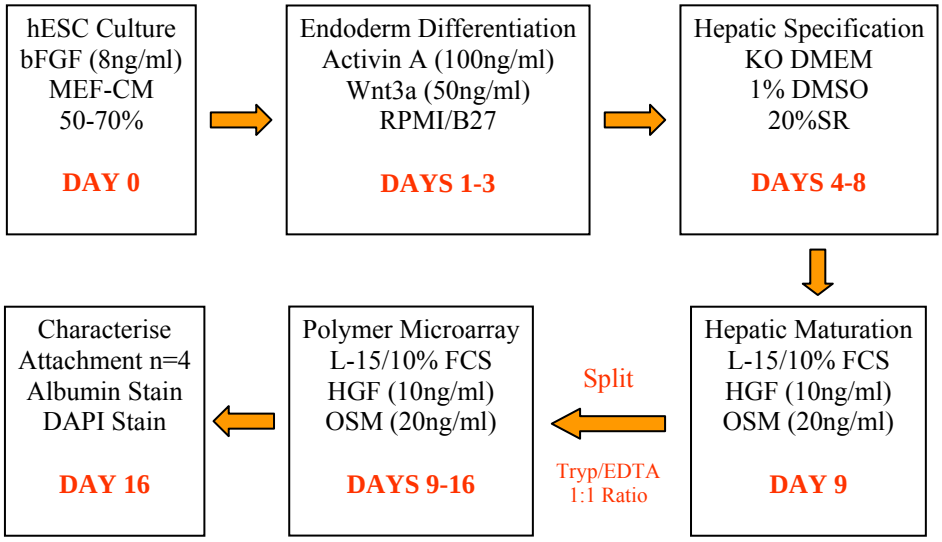

Figure 4.2 *The Hay model. hESCs were differentiated into HLCs using an efficient differentiation protocol (Chapter 7.4.2). Abbreviations – bFGF – basic fibroblast growth factor; MEF-CM – mouse embryonic fibroblast conditioned medium; KO DMEM – knock out Dulbecco's Modified Eagle Medium; DMSO - Dimethyl sulfoxide ; SR- serum replacement ; L-15 - Leibovitz's L-15 ; FCS – Fetal Calf Serum ; HGF – Hepatocyte growth factor ; OSM – oncostatin M ; DAPI - 4',6-diamidino-2-phenylindole.*[158, 160]

4.3.1 Analysis

Primary screening identified eight polyurethanes and eleven polyacrylates that supported HLCs attachment, providing (over the 4 identical polymer spots) over 250 cells/mm^2 (**Figure 4.3**). It was observed that all the polyurethane surfaces formed from diol PHNGAD, MDI as the diisocyanate and an extender (see **Table 4.1** for structure), as well as enabling high cell adhesion, displayed hepatic function for 8 days after re-plating (**Table 4.1**).

The success of this family of polyurethanes may be due to the fact that PHNGAD

and the extender all serve to modulate physical parameters, such as elasticity, wettability, surface topography, and that MDI helps to absorb ECM proteins. Polyurethanes which did not comprise an extender did not bind HLCs (**Table 4.1**). PU134 was found to be the most successful member of this family of polyurethanes in terms of binding and promoting the function of hepatocytes, although other related polyurethanes (PU103, 104 and 247) also displayed suitable properties (**Figure 4.4**).

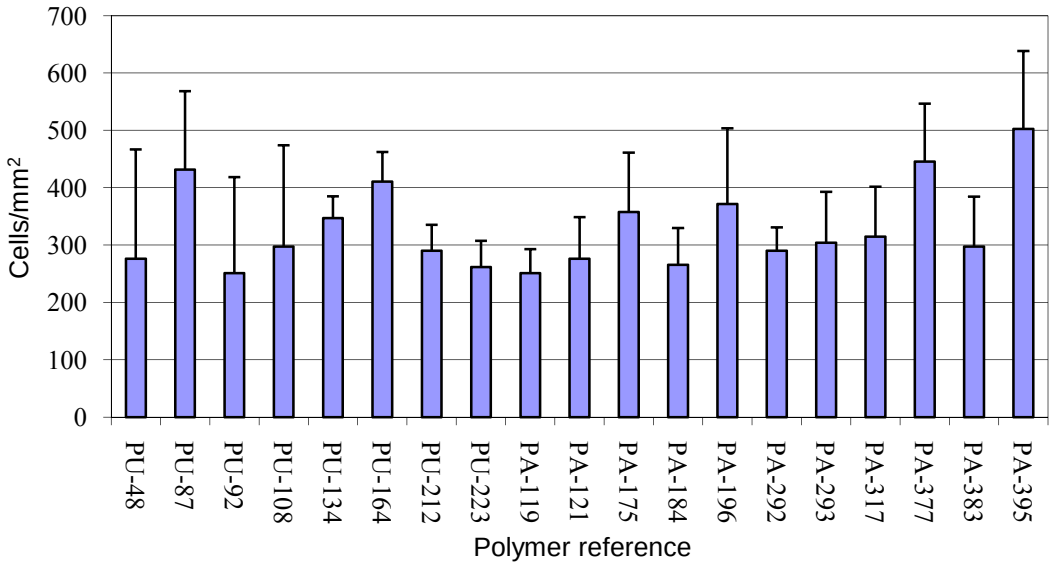

Figure 4.3 *Polymers HLC binding after 8 days of cultivation on polymer microarray (day 16). The number of cells/mm^2 (average from 4 spots) was calculated assuming a spot diameter of 300 µm. The error bars represent the standard error of the average. Complete HLC-polyacrylate binding analysis is reported on CD (Supplementary Information, excel folder named "Chapter 4").*

PU	Polymer structure			Microarray screening	
	Diol	Diisocyanate	Chain Extender	Adhesion	Hepatic Functions
103	PHNGAD	MDI	DMAPD	✓	✓
104	PHNGAD	MDI	DEAPD	✓	✓
134	PHNGAD	MDI	BD	✓	✓
247	PHNGAD	MDI	OFHD	✓	✓
248	PHNGAD	MDI	none	×	×

Table 4.1 *The polyurethanes which promote HLC adhesion and hepatocyte phenotype. Only PU248 which lacks a chain extender does not allow adhesion.*

Monomers abbreviations:

Diol:
PHNGAD: diols poly[1,6-hexanediol/neopentyl glycol/diethylene glycol-*alt*-(adiptic acid)]diol
Diisocyanate:
MDI: 4,4'-methylenebis(phenylisocyanate)
Chain Extender:
DMAPD: 3-dimethylamino-1,2-propanediol
DEAPD: 3-diethylamino-1,2-propanediol
BD: 1,4-butanediol
OFHD: 2,2,3,3,4,4,5,5-octafluoro-1,6-hexanediol

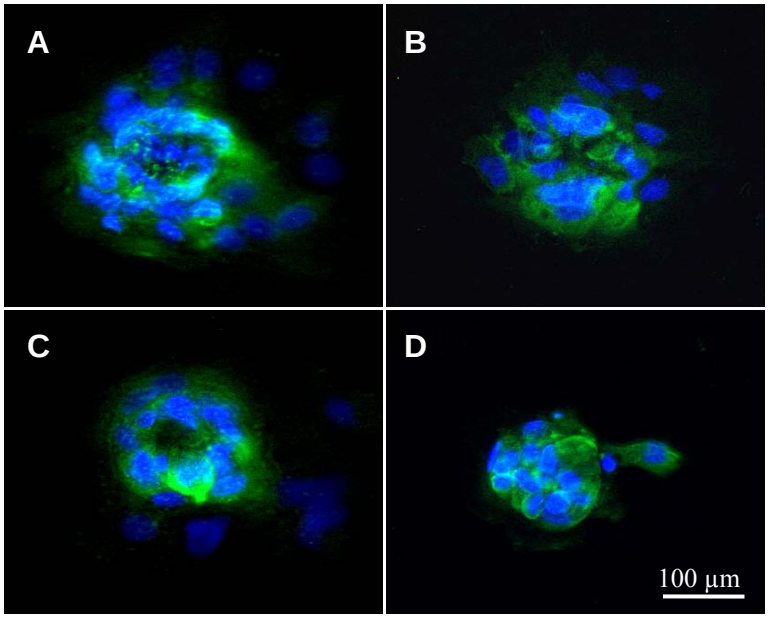

Figure 4.4 *Fluorescent microscopy of HLCs re-plated for 8 days on the polyurethane spots which promote adhesion and hepatocyte function (DAPI channel shows the cell nucleus stained with (Hoechst 33342). FITC channel shows the hepatocyte phenotype via albumin staining using a monoclonal antibody followed by incubation with a fluorescein-conjugated secondary antibody. A) PU134; B) PU103; C) PU104; D) PU247.*

4.4 Coverslip experiments

In order to study hepatic function in further detail and confirm the results of these experiments, six hit selected polymers (PU134, 212, 223 and PA119, 196, 395) (**Figure 4.3**) were scaled-up, spin-coated onto glass coverslips (Chapter 7.4.4.1).

4.4.1 Serum protein production analysis

After re-plating at day 9 as above, cells were cultured for a further 15 days onto the six polymer coverslips in conditions that support hepatic function and differentiation *in vitro* (Chapter 7.4.3),[158, 160] with hepatocyte function defined by the expression of a panel of hepatocyte-specific export proteins (fibronectin,[119] fibrinogen[161] and transthyretin (TTR)[162]).Using an enzyme-linked immunoabsorbant assay (Chapter 7.4.4.2),[163, 164] PU134 was identified as the most effective bio-active support, associated with ~2-fold enhanced expression of fibronectin, fibrinogen and TTR (**Figure 4.5**).

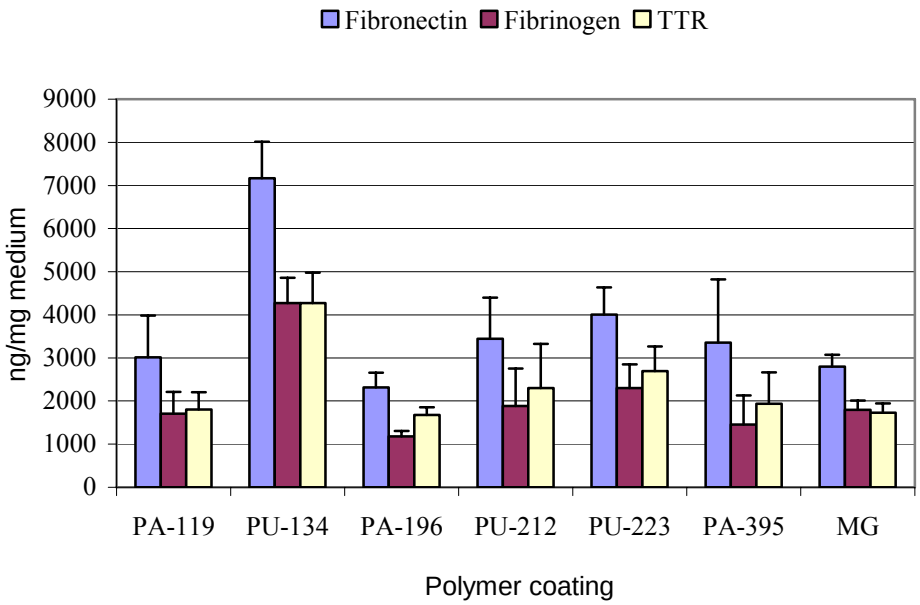

Figure 4.5 *HLCs serum export protein production. HLCs were plated and maintained in 1 mL of hepatocyte culture medium on MG, PU134, 212, 223 and PA119, 196, 395. After 24 h, culture supernatants were harvested and serum protein production was measured by ELISA and quoted as nanograms per milligram of tissue culture medium. In all lines, the serum protein tested was detected: fibrinogen, fibronectin and TTR (n = 3).*

4.4.2 Morphology analysis

MG was used as the control as it has previously been shown to improve hepatocyte performance *in vitro* and is currently considered the "gold standard".[165]

A significant change in HLCs morphology was observed by day 24, with HLCs passaged and maintained on MG or PU196, 212 and PA119, 196, 395, having become granular. In contrast, HLCs passaged on PU134 maintained a clear hepatic morphology (**Figure 4.6**).

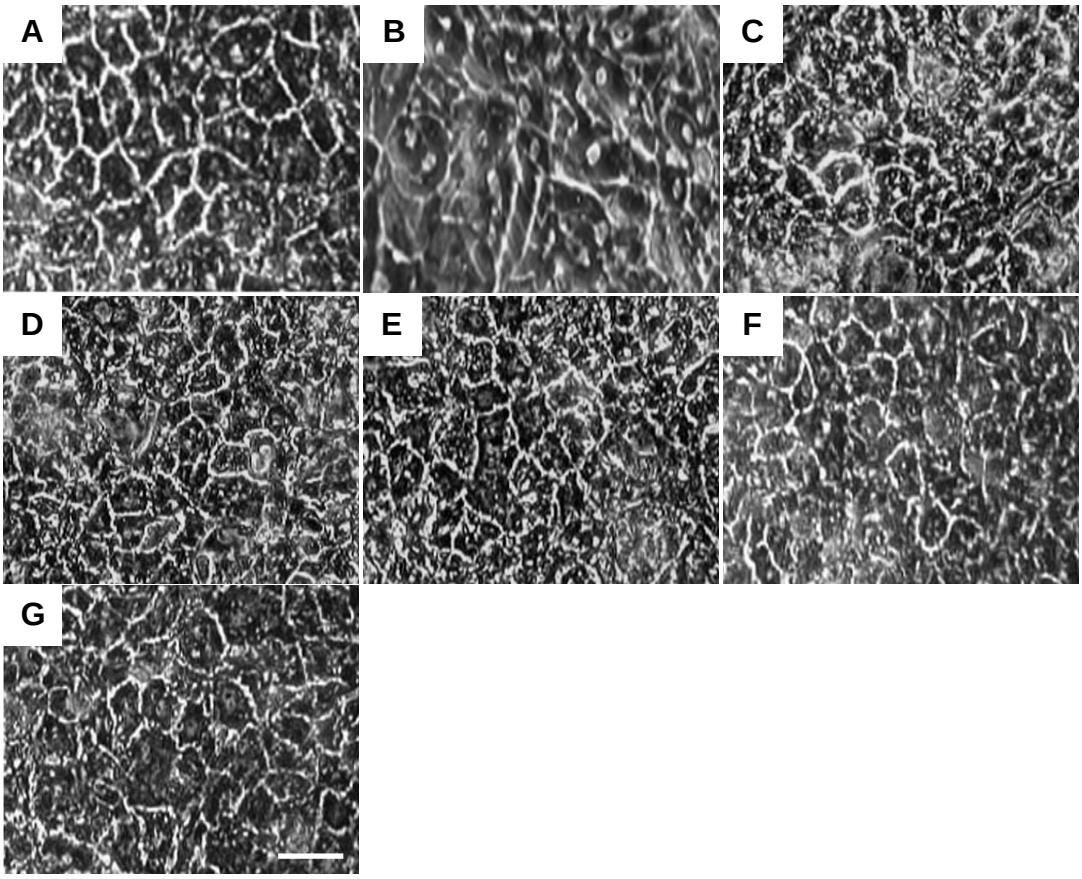

Figure 4.6 *Contrast microscopy (x10) of HLC morphology plated on: A) MG; B-D) PU134, 212, 223 respectively and (E-G) PA119, 196, 395 respectively. Scale bar 50 µm.*

4.5 Polyfibre core experiments (bio-artificial liver)

A subsidiary branch of this research concerns hepatocyte transplantations, whose aim is to increase the number of functional hepatocytes, and could be employed as an alternative therapeutic approach to whole organ transplantation for liver failure.[166]

Stem cell-derived hepatocytes could also be used to develop extra-corporeal support devices for acute liver failure.[167] In order to explore the potential for generating a bio-artificial liver, a polyfibre core (PFC) was prepared by dip-coating it with PU134.

4.5.1 SEM analysis

In order to generate a bio-artificial liver, a PFC (**Figure 4.7 A**) was dip-coated in PU134 (**Figure 4.7 B**). The control was PFC in its native form. Upon adopting a hepatic fate (day 9), HLCs were detached from the biological ECM and re-plated onto native or PU134-coated PFC and cultured for a further 15 days under conditions that supported hepatic identity (Chapter 7.4.3).[158, 160] At day 24 HLCs had attached to the uncoated and PU134-coated PFC matrix, and the cells were fixed for scanning by electron microscopic examination of cell structure. HLCs maintained on uncoated PFC demonstrated cell attachment and cell processes resembling stress fibres (**Figure 4.7 C**), suggesting that a particular arrangement of the microfilament system may be necessary for their adhesion. In contrast, HLCs maintained on PU134-coated PFC exhibited a smooth tissue-like appearance (**Figure 4.7 D**), which may limit the effects of fluid shear stress (the drag exerted by liquid flowing over cells in culture). The tissue-like substance, formed by HLCs and PU134, might limit this stress when compared to HLCs plated on the uncoated PFC but this hypothesis remains to be investigated.

4.5.2 Bio-artificial liver drug inducibility analysis

At day 9 in the differentiation process the cells were removed from their biological ECM. HLCs were cultured on the two PFCs (one native, one dip-coated in PU134) for 13 days, changing media every second day. At day 22 HLCs were induced with 0.4mM phenobarbital and maintained in control media for 48 h, changing the media daily. At day 24 the HLCs maintained on both the PFC support matrices was assessed for CYP3A4 drug induction. CYP3A4 was chosen because it has been estimated to play a role in the metabolism of approximately 50% of therapeutic drugs and is, therefore, essential to predictive drug toxicity and extra-corporeal support.[168] The uncoated PFC supported hepatocyte attachment and function (**Figure 4.8, -**

PU134, **violet bar**), but however did not support phenobarbital drug induction of CYP3A4 (**Figure 4.8, - PU134**, **purple bar**). In contrast HLCs re-plated onto PU134-coated PFC supported both HLC attachment (**Figure 4.8, + PU134**, **violet bar**) and phenobarbital inducible CYP3A4 drug metabolism (**Figure 4.8, + PU134**, **purple bar**). These data exemplify the value of PU134 and HLCs in both a bio-artificial liver setting, and as a tool in drug metabolism studies.

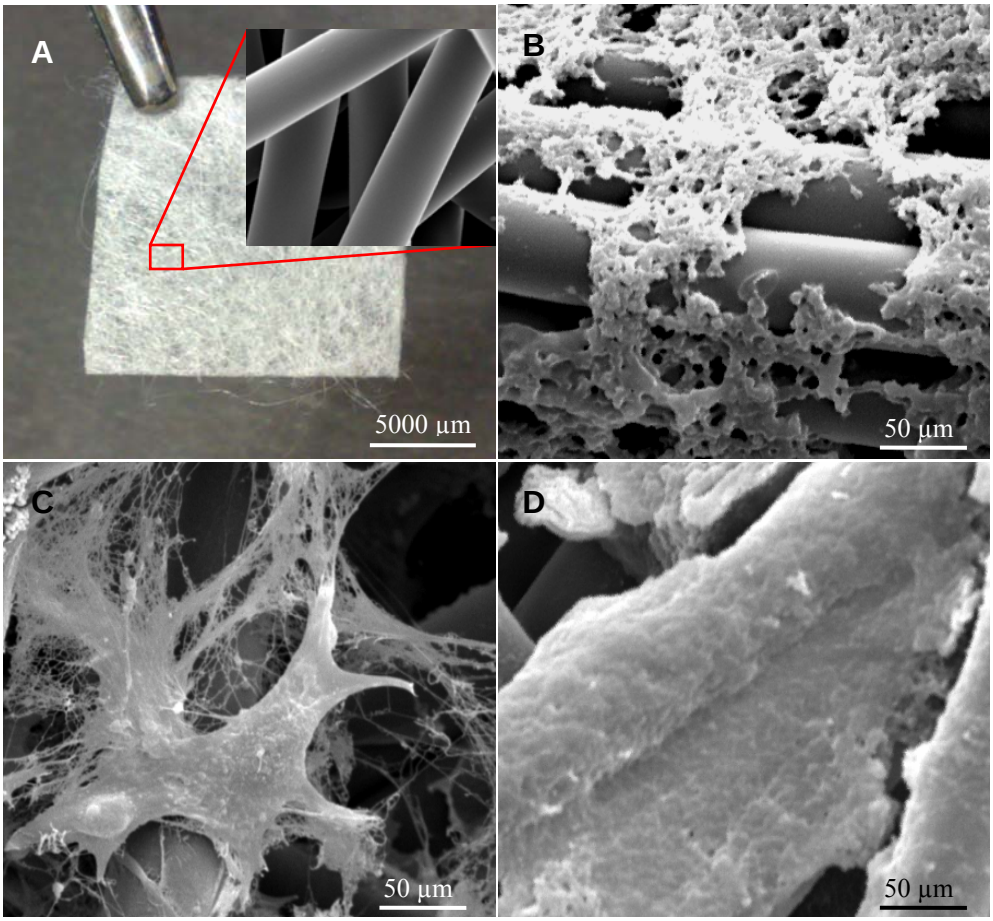

Figure 4.7 *HLCs were either plated on an uncoated or PU134 coated polyfibre. At day 24 in culture the cells were fixed and examined by electron microscopy. A) PFC with SEM image of uncoated (native) PFC; B) SEM image of PU134 coated PFC; D) SEM image of uncoated PFC with cells attached; E) SEM image of PU134 coated PFC with cells.*

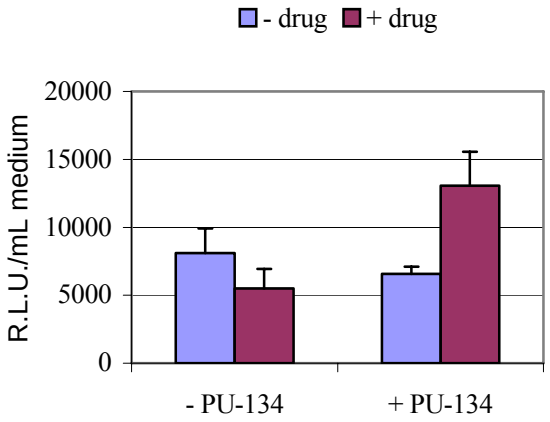

Figure 4.8 *HLCs cytochrome P450 metabolism. HLCs were either plated in an uncoated or coated PFC of the bio-artificial liver. The cultures were incubated in the presence (purple bars) or absence (violet bars) of phenobarbital in order to measurement of CYP3A4 activity (Chapter 7.4.5.3). At 48 h after treatment, 50 µL of culture medium was removed and read on a luminometer (POLARstar optima). CYP3A4 activity is expressed as relative light units (R.L.U.) per milliliter of tissue culture medium (n = 4).*

4.6 Conclusions

By fusing cutting-edge hESC models and high throughput polymer screening technologies we have developed a novel system which identifies ECM supporting cell specific function and viability. Using this approach a generic polyurethane extra-cellular support (PU134) has been pinpointed which significantly improves both hESC-HLC function and lifespan.

Before the advent of scalable hESC-HLC models, a number of strategies were focused on improving primary human hepatocyte lifespan and function by means of immortilisation. Cells established using these methods exhibited, however, phenotypic changes, poor hepatic specific gene function and karyotypic abnormalities over prolonged culture. By contrast, the method reported in this chapter maintains long-term hESC-HLC function of high fidelity in a scalable model synthesizable to GMP standards, which contains no xenobiotic material.

In conclusion, a system has been created in which we observe improved hESC-HLC performance. More importantly, proof-of-concept has been provided that high throughput polymer screening is a viable approach for identifying simple and

scalable culture matrices which may “hold” or regulate specific cell phenotypes. This technology is likely to have wider applications in the field of biotechnology in the future.

Chapter 5

Biopolymer Matrices as Defined Environments for Edothelial Progenitor Cells

5.1 Adult stem cells

The primary role of adult stem cells in a living organism is to maintain and repair the tissue in which they are found. [169-172] Adult stem cells are rare: they are found in so-called niches, surrounded by millions of ordinary cells, which differ according to the tissue in which they are located. Although adult stem cells are rare they are more abundant in organs which have the constant requirement for cell regeneration such as blood and skin. Bone marrow (BM) and umbilical cord blood (UCB) are particularly rich tissues for adult stem cells.[173] There are three type of adult stem cells contained in the bone marrow: hematopoietic stem cells (HSCs), which give rise to the three classes of blood cells that are found in the circulation – white blood cells (leukocytes), red blood cells (erythrocytes), and platelets (thrombocytes);[174-176] mesenchymal stem cells (MSCs), which are found arrayed around the central sinus in the bone marrow and have the capability to differentiate into osteoblasts, chondrocytes, myocytes, and many other types of cells, while also functioning as 'gatekeeper' cells of the bonemarrow;[171, 177] and endothelial progenitor cells (EPCs).[178, 179]

Typically, once removed from the body, the capacity of adult stem cells to divide without differentiating is limited, making generation of large quantities of stem cells difficult.[180, 181] There are many efforts to find better ways to grow large quantities of undifferentiated adult stem cells in cell culture and to manipulate them to generate

specific cell types so they can be used to treat injury or disease.[180] An example of potential treatments includes repairing damaged heart muscle following a heart attack with cardiac muscle cells.[182] Importantly, it must be demonstrated that a single adult stem cell can generate a line of genetically identical cells that then gives rise to all the appropriate differentiated cell types of the tissue.[183] To confirm experimentally that a putative adult stem cell is indeed a stem cell, scientists tend to show either that the cell can give rise to these genetically identical cells in culture, and/or that a purified population of these candidate stem cells can repopulate or reform the tissue after transplant into an animal.[184, 185]

5.1.1 Endothelial progenitor cells

Traditionally, vascular repair in adults was thought only to occur through the proliferation and migration of pre-existing mature endothelial cells (ECs) from the adjacent vasculature.[186] Evidence now confirms the existence of bone-marrow-derived EPCs which play an important role in *de novo* vascularisation.[187-190] In response to injury, EPCs are mobilised and recruited to the ischaemic sites where they contribute to new-vessel formation.[179, 186, 187, 190, 191] EPCs not only directly incorporate into blood vessels, replacing the defective or injured mature endothelial cells, but also secrete a variety of cytoprotective or proangiogenic factors in a paracrine manner to promote the survival and proliferation of endothelial cells.[192]

EPCs can be isolated from adult peripheral and umbilical cord blood (UCB). Robust proliferative activity is an important property of EPCs that distinguishes them from monocyte/macrophage-derived endothelial-like cells.[193] EPCs are identified according to the expression of both hematopoietic stem cell markers and endothelial cell markers.[191] However, their characterisation remains controversial,[189] partly because researchers have used EPCs from a variety of sources and employed substantially different isolation procedures.[189, 191, 192] Initially, two antigens shared by EPCs and haematopoietic stem cells, vascular endothelial growth factor (VEGF) receptor 2 (also referred to as Flk-1 or KDR) and CD34, were used to isolate EPCs from the leukocyte fraction of peripheral blood,[189] and subsequent studies have identified EPCs on the basis of co-expression of CD133 with CD34 expression.[179, 189, 191] More recently the co-expression of CD34, CD133 and CD146 has been used to

identify a representative population of human EPCs, which can be isolated by flow cytometry sorting based on co-expression of these markers.[194, 195] In spite of the existence of numerous clinical studies based on localised implantation of autologous cells to revascularise ischaemic tissue, particularly in myocardial and critical limb ischaemias, a precise definition of EPCs remains elusive. *In vitro* phenotypic studies have demonstrated that cells defined as EPCs by different groups consist of a heterogeneous population, containing cells with differential phenotype and outgrowth potential.[196, 197] EPC definitions include cells which contribute to angiogenesis directly by incorporation into new vessels (true EPCs), also referred to as endothelial outgrowth cells (EOCs) and, indirectly, by positively regulating the angiogenic process (myeloid-derived EPCs or also referred to as CFU-Hill colony forming cells).[198]

5.2 Introduction to the study

Since the discovery of circulating endothelial cells in peripheral blood a decade ago,[179] regenerative stem-cell-based therapeutic strategies aimed at developing novel therapies or improving current treatments to restore the ischaemic tissue have been under investigation.[199] Traditional methods of direct cell infusion or injection (which represent the most commonly utilised cell delivery strategy in the clinic – for example, bone marrow transplants) often lead to: a) massive cell death of the transplanted cells due to mass transport limitations of oxygen and nutrients in case of local injection;[200] b) extremely poor (typically less than 3%) homing/engraftment efficiency to the target tissue (in the case of systemically infused cells);[201] and c) the loss of control over the fate of the transplanted cells.[202]

The introduction of biomaterial scaffolds as a cell carrier provides a potential solution to these problems, because they can be a template for guiding the formation of new tissue and for promoting engraftment with the host.[200] An emerging area of bioengineering research is the development of synthetic biopolymer matrices as defined environments for EPC growth, providing sites of adhesion together with signals that control EPC propagation and synchronise their differentiation.[203] Peripheral blood-derived EPCs have been explored for the generation of blood

vessels *in vitro* and for the endothelialisation of artificial vessel prostheses and endoluminal vessel prostheses.[204, 205]

This study aims to develop, *via* high throughput screening of a polymer microarray, the identification of new polymer matrices which contain the necessary signals that not only promote adhesion and propagation of EPCs but also, synchronise their endothelial specialisation.[206] If these could be manufactured to GMP standards they could potentially provide a resource for the construction of extra-corporeal devices (artificial vessel prostheses)[207] and facilitate novel studies in modern vascular surgery.

5.3 Polymer microarray screening

Polymer libraries were screened in order to identify new supports for attachment, promotion, propagation, and to synchronise endothelial cells function.[204]

Cord blood (CB) products (50 mL) were aspirated from the umbilical placental veins from normal caesarean deliveries and collected into heparin.[208] Mononuclear cells (MNCs) were isolated by buoyant density centrifugation and cultured over 3 weeks in endothelial basal medium (EBM-2). By that time, spindle-shaped endothelial cells now called EOCs started to emerge.[195] These cells express a number of endothelial markers (Chapter 5.4.1) comparable to a mature endothelial cell and human umbilical vein endothelial cells (HUVECs) are able to form new blood vessels in MG (**Figure 5.1 A** and **B**).[209] Thereafter cells were passaged until incubation with the polymer microarrays. As a control HUVECs,[210] which are specialised endothelial cells, were maintained in culture. At this point EOCs and HUVECs were removed from their substrate.[211] Following this, cells were re-plated onto two identical polymer microarrays containing 345 polyurethanes and polyacrylates each printed in quadruplicate. After 3 days, cells were fixed and stained with a nuclear stain (Hoechst 33342), and directly conjugated monoclonal mouse anti-human CD31-PE antibody. CD31 (Anti-PECAM-1) recognizes the platelet/endothelial cell adhesion molecule-1 (PECAM-1), a 130 to 140-kdalton single-chain integral membrane glycoprotein that is a member of the immunoglobulin gene superfamily.[212] The CD31 antigen is expressed on endothelial cells, functions as a vascular cell adhesion

molecule and is involved in the process of leukocyte migration through the intercellular junctions of vascular endothelial cells[213] (**Figure 5.2**).

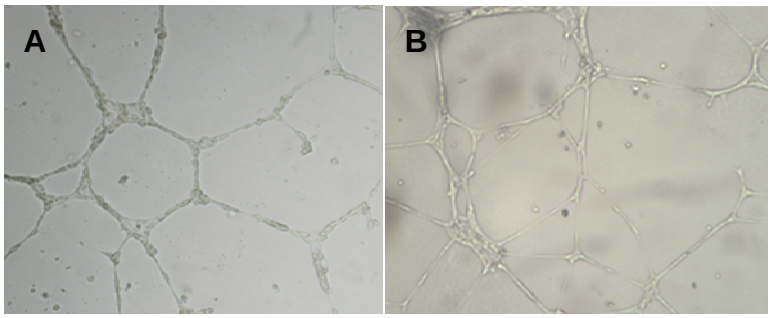

Figure 5.1 *Contrast microscopy using an inverted microscope (Nikon Eclipse TS100-F) equipped with an integrated digital camera (x40). Images were taken at 22 h. Both A) HUVECs and B) EOCs are able to form tubular structures in MG.*[196]

5.3.1 Polymers analysis

At this point analysis was carried out as described previously (Chapter 2.2.1), using the HCS platform, to assess EOCs binding and endothelial specialisation (**Figure 5.2)**.

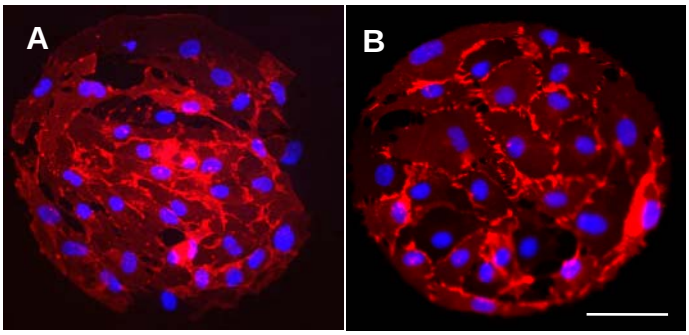

Figura 5.2 *Fluorescent microscopy: A) EOCs; and B) HUVECs on PA383 which promote adhesion and endothelial phenotype. DAPI channel shows the cell nucleus stained with (Hoechst 33342); rhodamine channel shows the endothelial phenotype via CD31 antigen staining using a directly conjugated monoclonal mouse anti-human CD31-PE antibody. Scale bar 100 µm.*

Primary screening identified six polyurethanes and twelve polyacrylates that supported attachment of EOCs providing over 150 cells/mm^2 (**Figure 5.3**). PU139 and 140 have an almost identical chemical structure, composed of diol PTMG and diisocyanate 1,3-Bis(isocyanatomethyl) cyclohaxane (BICH) and chain extender ethylene glycol (EG) and differing only in the molecular weight of the diol (650 and 1000 respectively). PU134, which was the most successful for binding HLCs (Chapter 4), was shown to have high affinity also for EOCs and HUVECs.

A few polyacrylates have almost identical chemical structures, differing only in their molar ratios, for example polyacrylates 395 and 398 and polyacrylates 175 and 177 (for polymer structures, see Appendix II). PA119, 383 and 395 (**Figure 5.4**) were found to be the most successful polymers for both cell lines (EOCs and HUVECs), providing over 200 cells/mm^2 (**Figure 5.3**). This result is consistent with the hypothesis that PA119, 383 and 395, as well as enabling high cell adhesion, displayed endothelial specialisation of EOCs after re-plating (rendering them as specialised cells such HUVECs).

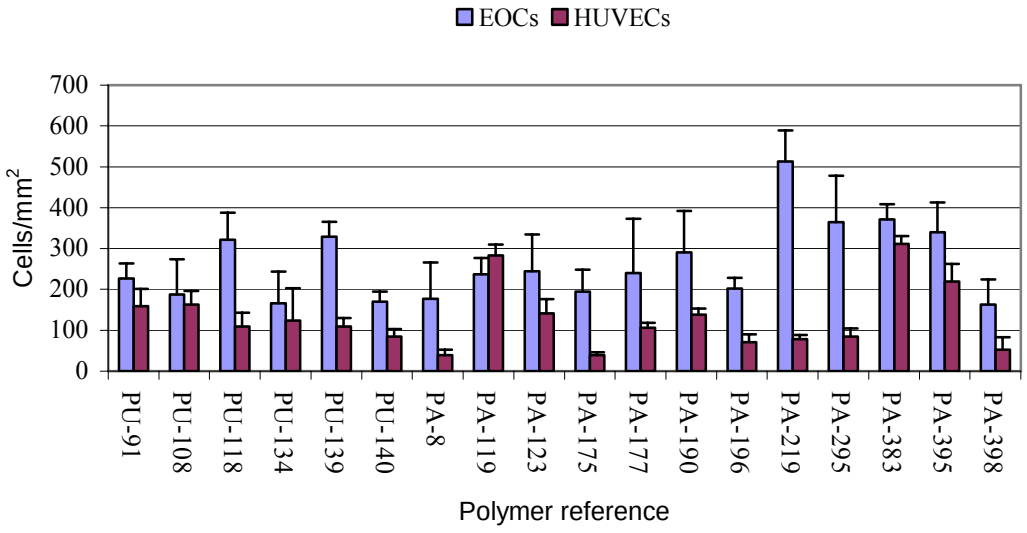

Figura 5.3 *Polyurethanes and polyacrylates which provide a high EOC binding, compared to the HUVEC, after 3 days of cultivation on polymer microarray. The number of cells/mm^2 (average from 4 spots) was calculated assuming a spot diameter of 300 µm. The error bars represent the standard error of the average. Complete EOC and HUVEC-polymer binding analysis is reported on CD (Supplementary Information, excel folder named "Chapter 5").*

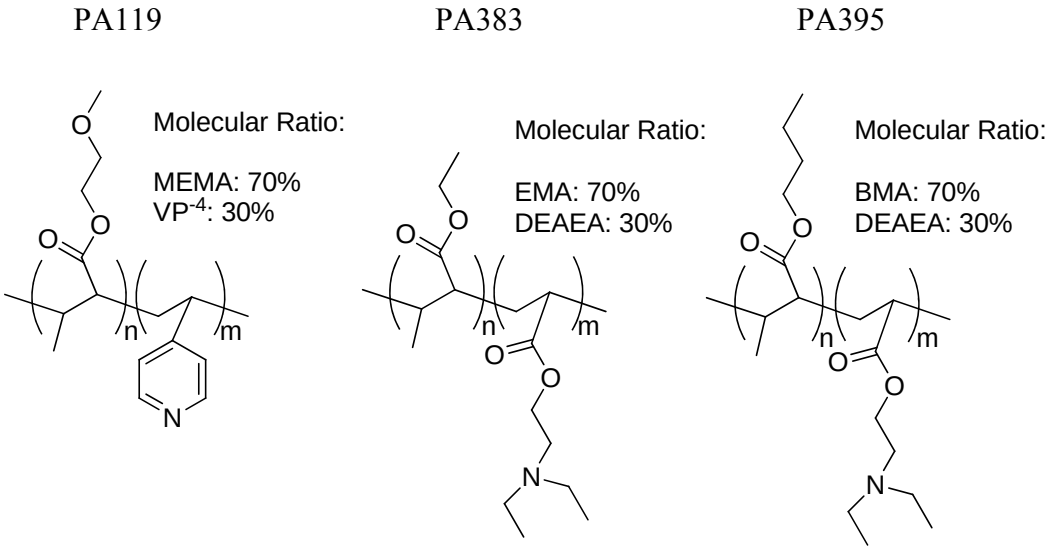

Figure 5.4 *Chemical compositions of PA119, 383 and 395. Abbreviations: MEMA – 2-methoxyethylmethacrylate; VP-4 – 4-vinylpyridine; EMA – ethyl methacrylate; DEAEA – 2-(diethylamino)ethyl acrylate; BMA – butyl methacrylate.*

5.4 Coverslip experiments

In order to study the endothelial function in further detail and confirm the results of these experiments, the three selected polymers (PA119, 383 and 395), with excellent binding for EOCs and HUVECs (**Figure 5.4**), were scaled-up and spin-coated onto glass coverslips for flow cytometry analysis.

5.4.1 Flow cytometry analysis

EOCs and HUVECs were cultivated as previously described (Chapter 5.3) on the glass coverslips (Chapter 7.5.4.1), then directly stained and analysed for immunophenotyping expression of surface endothelial markers using anti-human monoclonal antibodies (MAbs) conjugated to phycoerythrin (PE), fluorescein isothiocynate (FITC), Peridin Chlorophylla protein (PerCP) or Allophycocyanin (APC) as described.[196] Harvested cells were resuspended and analysed by flow cytometry (**Figure 5.5 A** and **B**). Phenotype analysis revealed that all 3 polymers promote endothelial cellular growth and endothelial specialisation comparable to cells grown in their gold-standard conditions (collagen and bare plastic for EOCs and

HUVECs, respectively). PA119, 383 and 395 confirmed the result from the high throughput analysis (**Figure 5.3**). EOCs and HUVECs expressed endothelial cells surface markers von Willebrand factor (vWF), vascular endothelial growth factor (VEGF) receptor 2 (also referred to as Flk-1 or KDR), endothelial nitric oxide synthase (eNOS), CD31, CD34, CD105 and CD146 but not the haematopoietic cell surface antigens CD45 (**Figure 5.5 A** and **B**).

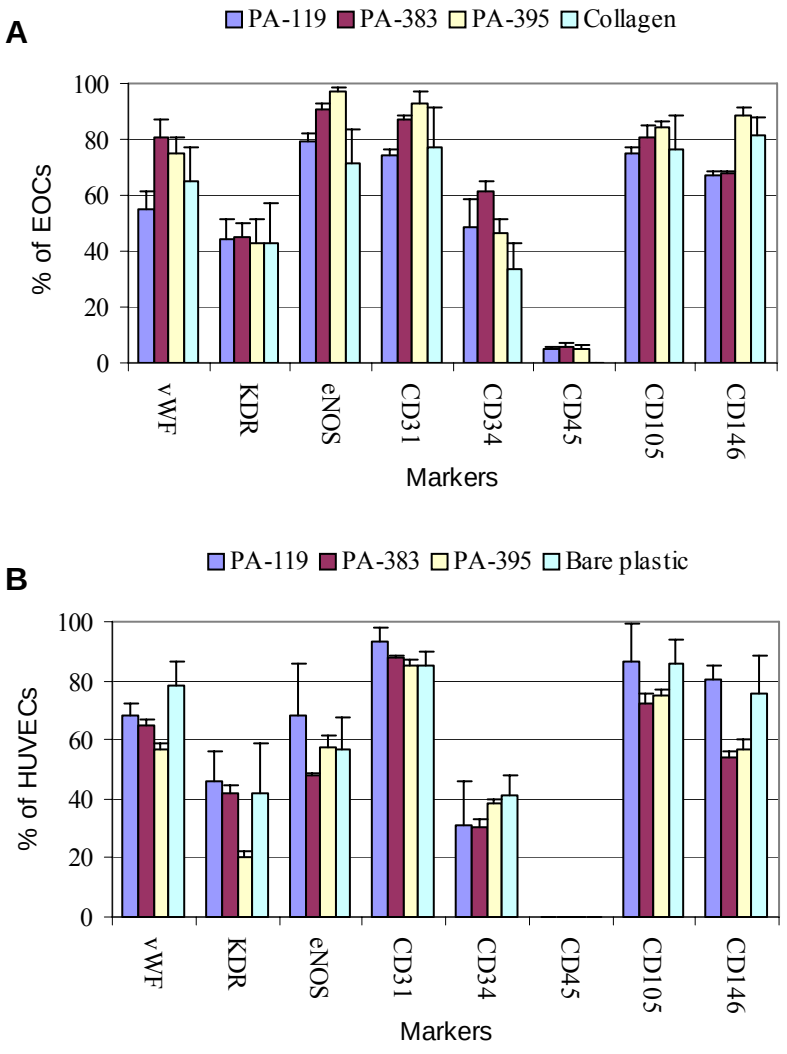

Figure 5.5 *Flow cytometry analysis: A) EOCs grown on PA119, 383, 395 and, as a control, collagen; B) HUVECs grown on PA119, 383, 395 and, as a control, bare plastic. Shown are representative data from 5 independent experiments using 5 different coverslips for each coated sample.*

5.5 Sponge experiments

Further studies were undertaken by cultivating EOCs and HUVECs on pieces of polyether sponges dipped in a solution of PA383. The ultimate aim of studying sponge as a cell scaffold was to generate functional 3-D tissues outside of the organism, which might then be implanted into the organism. In an ideal scenario PA383 would have the ability to adhere EOCs from *in vitro* cultivation, and once implanted, either promote the growth and the specialisation of cells anchored to the sponge previously or recruit distant bone marrow-derived progenitor cells for restoring vascularisation at the implanted scaffold/host tissue interface.

5.5.1 *In vitro*

Two 1 cm^3 polyether sponges were dip-coated in a 1% solution of PA383 and a further two 1 cm^3 sponges were dip-coated in the gold standard matrix support (growth factor reduced (GFR)-MG). Polymer coated sponge showed a smoother uniformly coated layer allowing a friendlier environment for cells to grow (**Figure 5.6**). The coated sponge was impregnated with either EOCs or HUVECs in complete EBM-2 medium that supports endothelial cultivation.[193] After overnight incubation cells in both sponges were fixed and SEM analysed, **Figure 5.7 A** and **C** clearly showed only sponges pre-coated with polymer allowed tube formation.

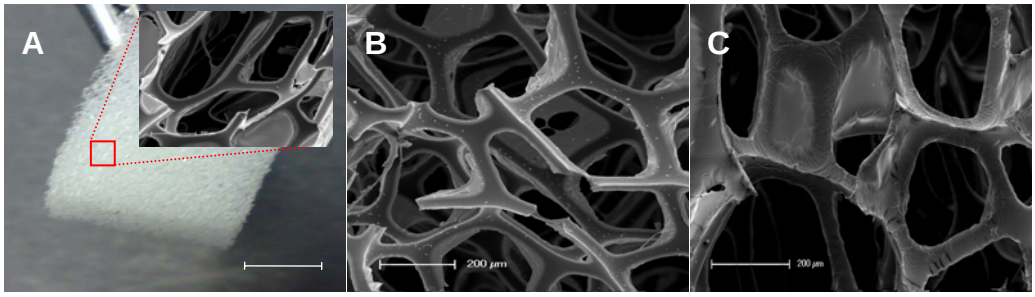

Figure 5.6 *Sponge pre-treated with either GFR-MG or PA385. A) 1 cm^3 polyether sponge, scale bar 5 mm; B) SEM image of GFR-MG pre-treated sponge, scale bar 200 µm; C) SEM image of PA385 coated sponge.*

The other two sponges pre-treated with GFR-MG lacked tube formation (**Figure 5.7 B** and **D**). It is evident that on increased number of EOCs adhered to the PA383 sponge, allowed a major release of cytoprotective or proangiogenic factors in a paracrine manner to promote the survival and proliferation of endothelial cells.[214]

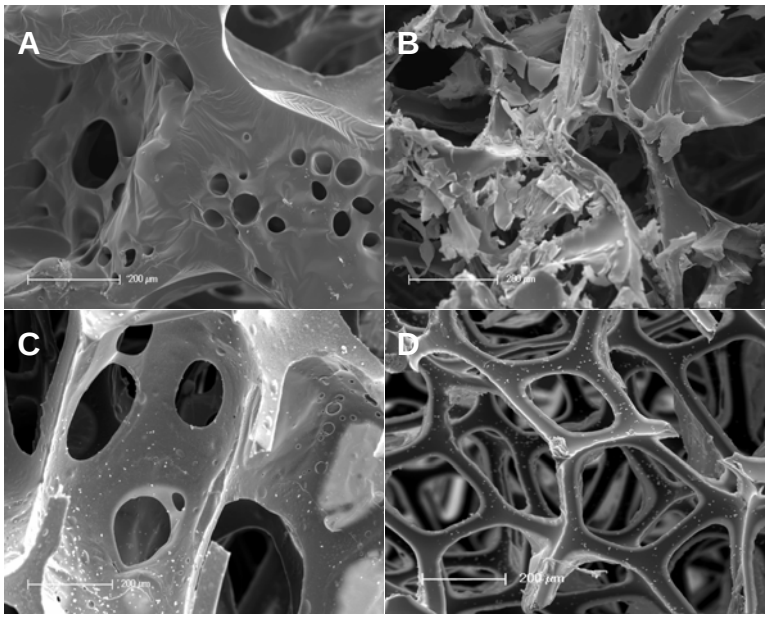

Figure 5.7 *EOCs and HUVECs were either loaded on an uncoated or PA383 coated sponge. After 12 h incubation the cells were fixed and examined by electron microscopy. A) PA383 coated sponge with HUVECs; B) GFR-MG pre-treated sponge with HUVECs; C) PA385 coated sponge with EOCs; D) GFR-MG pre-treated sponge with EOCs.*

5.5.2 *In vivo*

The functional 3-D tissue generated (*in vitro*) was tested for its ability to promote cell growth and recruit distant bone marrow-derived progenitor cells for promoting engraftment with the host, after implantation. Mice were anaesthetised and a sterilised polymer-coated sponge cylinder (0.5 cm/1 cm) was implanted subcutaneously on each flank. Sponges were impregnated with PA383 and loaded with EOCs. Each animal had a EOCs-loaded PA383 impregnated sponges on one side and a control EOCs loaded native sponge on the other.

Twenty days after implantation, mice were sacrificed and sponges were excised and analysed for vessel formation. Sponges were divided into 3 pieces and analysed as follows: SEM imaging; Chalkley count[215] and haemoglobin assay.[216]

5.5.2.1 SEM analysis

After implantation in mice, the sponges impregnated with PA383 promoted better engraftment within the host. **Figure 5.8 B** shows clearly the formation of a vascular network in contrast with the blank (uncoated) sponge (**Figure 5.8 A, red arrows)**. Notably, uncoated sponge resulted in a poor and incomplete engraftment within the host, showing the native sponge without cells at several points (**Figure 5.8 A, red arrows)**. It seems evident that the large number of EOCs adhered to the PA383 sponge, allowed not only a large quantity of local cell growth but also made possible a major release of cytokines which recruited distant bone marrow-derived progenitor cells that effectively mediated vascularisation at the implanted scaffold/host tissue interface.

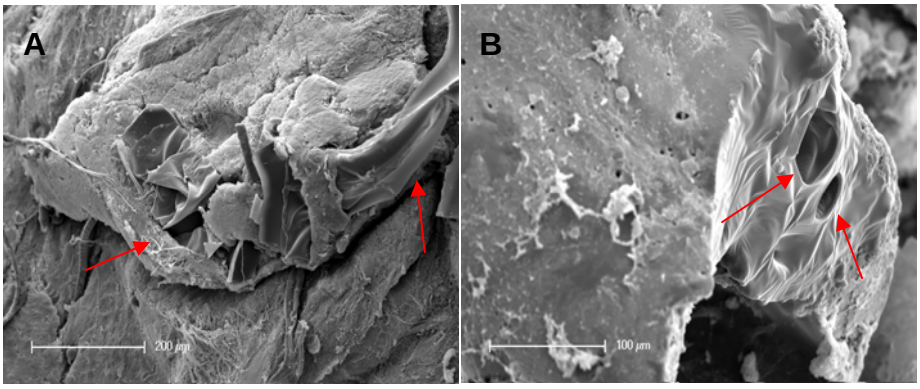

Figure 5.8 *Electron microscopy analysis: A) sponge uncoated (native); B) sponge pre-coated with PA383. Both sponges were pre-incubated with EOCs overnight.*

5.5.2.2 Blood vessels formation analysis

Histological analysis revealed that significantly increased numbers of vessels formed on the polymer coated sponge compared with the control (sponge uncoated).

One part of the sponge was fixed in 10% formalin and embedded in paraffin wax.

Sections (5 µm) were stained with haematoxylin/eosin for identification of blood vessels, as described.[217] Sponge vessel density was determined by using the mean of triplicate Chalkley counts on two sections per sponge (**Figure 5.9 left**).[215, 218] Histology showed vascularisation by a number of blood vessels but in polymer coated sponges had significantly more blood vessels compared to non polymer coated sponges (**Figure 5.9 left**).

5.5.2.3 Haemoglobin assay

A further study focused on measuring the concentration of haemoglobin in the sample. It is an excellent method of determining the frequency of blood vessels, which are proportional to the blood haemoglobin.[216] One part of the sponge was weighed, homogenized in 1 ml sterile PBS, centrifuged and the amount of haemoglobin present in the sample measured (**Figure 5.9 right**). Polymer coated sponges had significantly more haemoglobin, displaying ~2-fold increase compared to uncoated polymer sponges (**Figure 5.9 right**).

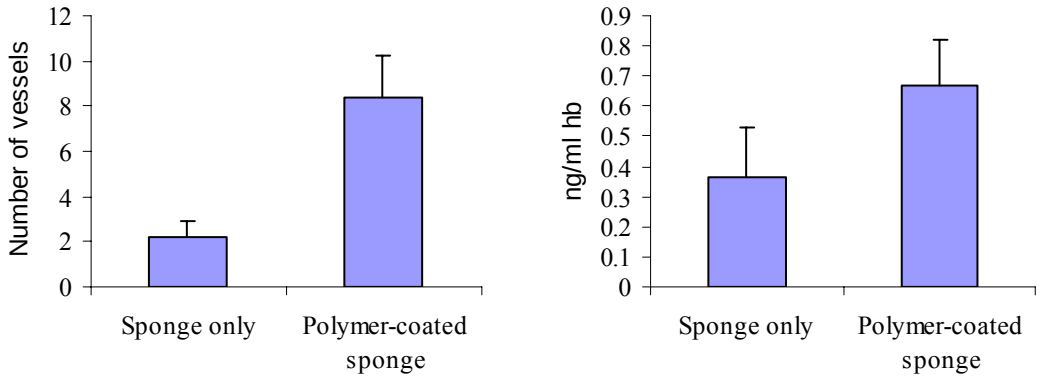

Figure 5.9 *Left) Sponge vessel density determination by the Chalkley method on two sections per sponge (n=4); right) haemoglobin assay: measure of the amount of haemoglobin present in the samples (n=2).*

5.6 Stent experiments

5.6.1 Stenosis

Stenosis is one of the most common pathological conditions connected to the cardiovascular system: it is a restriction of the blood vessels caused by an atherosclerotic plaque which is deposited on the arterial wall reducing or arresting the flow of blood to the heart.[219, 220] Coronary angioplasty is an interventional strategy which consists of pressing the stenotic plaque against the arterial wall through the introduction and expansion, at the site of the obstruction, of a catheter with balloon.[221] This treatment was introduced in 1979 and rapidly became the principal method of coronary revascularisation as well as the most common therapeutic procedure used in cardiology.[222, 223] Nonetheless, in the long term angioplasty often ends in reblockage of the treated vessel, that is, restenosis.[224] Restenosis is the response of the blood vessel to the tissue damage caused by angioplasty and is linked mainly to huge proliferation of neointima and the elastic recoil of the vessel walls.[225] Elastic recoil is the collapse of the vessel wall into the lumen, caused by loss of elasticity, at the position of plaque pressed on the vessel walls.[226]

5.6.2 Stents and scope of the study

A notable step forward in the treatment of such pathological ischemia occurred in the 1990s with the introduction of metal scaffolds, stents, capable of giving the stenotic vessel the necessary mechanical support to avoid collapse.[227] The introduction into medical practice of such devices revolutionised the field of interventional cardiology, bringing notable improvements in prevention of restenosis.[228] In spite of the fact that stents are capable of eliminating elastic recoil of the stenotic vessel, however, their implantation and the consequent trauma to the vessel walls initiates an excessive proliferation of neointima and, therefore, an in-stent restenosis.[229]

An initial negative reaction following implant of the stent is due to the raised thrombogenicity of the metal link of which it is made. Therefore, a first intuitive approach is aimed at improving the biocompatibility of the implant through the recoating of the stent with polymer film.[230]

Although such modification brings substantial improvements in clinical intervention, through the use of hybrid devices capable of combining the supportive properties of metal with the biocompatibility of polymers, in a certain percentage of cases in-stent restenosis still occurs. In light of this, researchers in engineering, biology, biomaterials and cardiology have, through an interdisciplinary approach, developed a new device combining the supportive properties and biocompatibility previously described with pharmacological therapy. Stents have been developed which release drugs – Drug-Eluting Stent (DES) – which use the metal structure of the stent as a platform for local release of drugs capable of preventing and avoiding restenosis.[231, 232]. More recently, other techniques, including impregnating stents with either antibodies or integrin-binding cyclic Arg-Gly-Asp (cRGD) peptides, were analysed *in vitro* and *in vivo*. These functionalised stents display molecules that are directed toward proteins on the cell surface of endothelial progenitor cells, thereby attracting the EPCs to migrate to the surface of the stent and limit coronary neointimal formation.[233]

The project reported in this chapter describes a possible alternative which involves the use of polymers which promote the adhesion of endothelial progenitor cells.

5.6.3 Stent cell coating

In order to study adhesion of endothelial outgrowth cell to the polymer-coated stent, PA383 was used. A coronary stent was dip-coated in the PA383 (**Figure 5.10 A-C**).

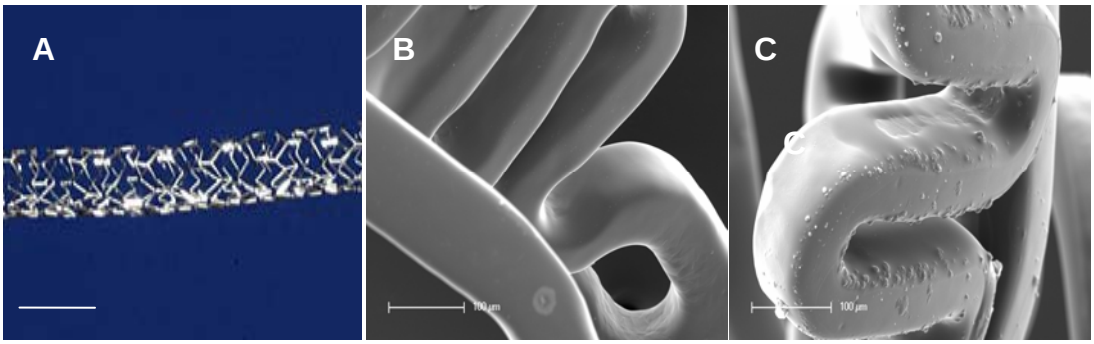

Figure 5.10 *A) Coronary stent, scale bar 1cm. B) SEM image of uncoated stent; C) SEM image of PA383 coated stent.*

The control was a coronary stent in its native form. EOCs were removed from their substrate and re-incubated onto both, a PA383-coated stent or native stent and culture ed over-night in conditions that support endothelial cell survival.[193]

In order to assess cellular adhesion and the utility of PA383, following incubation cells on both stents were fixed and SEM analysed (**Figure 5.11**). EOCs maintained on the uncoated stent showed poor cell attachment (**Figure 5.11 A, B**), whereas EOCs maintained on the PA383-coated stent exhibited a consistent adhesion with around 80% of confluence (**Figure 5.11 C, D**).These data exemplify the value of PA383 and EOCs in an alternative setting for improvement in angioplasty therapy.

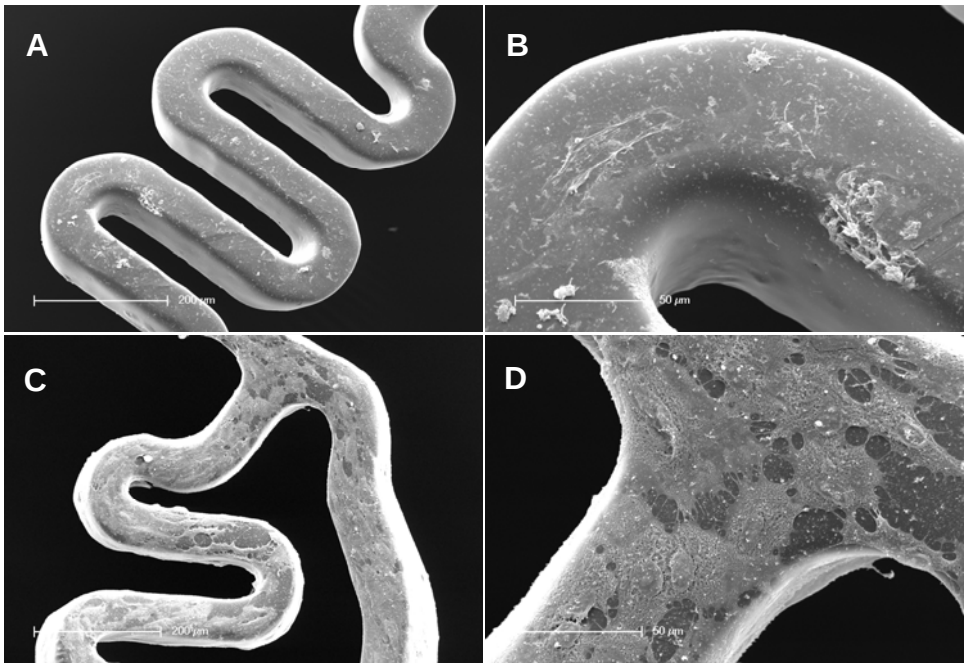

Figure 5.11 *EOCs were either plated on uncoated or PA383-coated coronary stent. After overnight incubation in vitro the cells were fixed and examined by electron microscopy. A and B) Uncoated stent with EOCs; C and D) PA383 coated stent with EOCs attached.*

5.7 Conclusions

Thanks to polymer microarray a library of 345 polyacrylates and polyurethanes were screened to identify new synthetic biopolymer matrices as defined environments for endothelial progenitor cell adhesion, cell propagation and synchronise their endothelialisation. Six polyurethanes and thirteen polyacrylates supported attachment of EOCs. Three polymers (PA119, 383 and 395) showed strong binding both for EOCs and HUVECs. This suggests that those three polymers might allow specialisation of EOCs, a hypothesis supported by the expression of endothelial surface markers when EOCs were cultivated on the scaled up coverslips in contrast with the gold standard supports.

PA383 was used to coat a sponge for the generation of blood vessels *in vitro* and for the endothelialisation of artificial vessel prostheses. The results showed a notable difference in the process of vascularisation between the sponge coated with PA383 and that coated with the gold standard matrix support GFR-MG.

This result suggested a possible application *in vivo* as a potential method for remedying ischaemic injury. The artificial vessel prostheses generated *in vitro* coated with PA383 was implanted in mice with a notable difference in the re-endothelialisation in contrast to the native sponge. The reason for this is unclear but might have been due to the fact that there was already a large quantity of cells growing on the sponge. Alternatively, it might have been caused by the fact that those cells attracted bone marrow-derived progenitor cells through the release of cytokines. The capacity of PA383 to bind endothelial progenitor cell suggests the possibility of using this polymer for coating stents. These cells might be isolated from blood from the patient and used to adhere and cover the stent pre-coated with the selected polymer *in vitro*. At this point the stent could be reintroduced into the patient avoiding the problems mentioned above. It was demonstrated that a stent can easily be coated with PA383, and, as a consequence of cell adhesion, an EOCs layer was generated *in vitro*. This method might, therefore, offer a future means of reducing the process of thrombogenesis and in-stent restenosis and improving angioplasty therapy.

Chapter 6

Discovery of New Microbial-Modulating Materials

Polymer microarrays were used to identify a number of polymers that would selectively capture *Salmonella* or *E. coli* (prokaryotic cells), or prevent microbial binding. The approach offers tools for the identification of new biomaterials for either selective bacterial enrichment or preventing surface contamination, with polymers identified that allowed discrimination between bacterial genera.

6.1 Introduction to the study

Salmonella is a serious pathogen of medical and veterinary importance in both developing and developed nations.[234, 235] For humans, infection occurs mainly *via* contaminated food and water, with disease largely manifesting itself as gastroenteritis with fever and other associated symptoms, such as occasional reactive arthritis or meningitis,[236] but in the case of serovars Typhi and Paratyphi, infection can result in typhoid fever. Worldwide, around 1.3 billion cases of salmonellosis are reported per year with 3 million fatalities,[237] while there are approximately 20 million cases of typhoid fever per annum, with 200,000 deaths.[238] Where drug intervention is required, fluoroquinolones are the primary drugs of choice for treating systemic infections, however, many patient isolates now exhibit multi-drug resistance, complicating clinical management and resulting in enhanced mortality rates.[239]

It is well known that bacterial surface charge, cell density, and the presence of microbially-produced compounds, such as exopolysaccharides, pili or flagella, are determinant factors in the adhesion process, but other physicochemical features such as pH, temperature, composition of growth media are also known to affect surface attachment.[240, 241]

In order to control bacterial attachment, there is a need for materials which result in specific bacterial sequestration or repulsion. Such materials would offer a means for the rapid isolation of organisms from hospital, industrial or domestic environments, or for minimising surface contamination through the development of microbe repelling/killing surfaces, as well as innovative intervention approaches for reducing bacterial loads *via* human, animal or poultry feeds.

In this chapter polymer microarrays were used to explore: (i) the identification of polymers that allowed rapid and specific/selective attachment (sequestration) of bacteria; (ii) materials that are capable of limiting or preventing bacterial adhesion.

These studies focused on the adhesion of the food-borne pathogenic bacterium *Salmonella enterica* serovar *typhimurium* (*S. typhimurium*), strain SL1344,[242] and the commensal bacterium *Escherichia coli*, strain W3110.[243]

6.2 Analysis of bacteria attachment

S. typhimurium was evaluated in comparison with a commensal strain of *E. coli*, both expressing Green Fluorescent Protein (GFP).[244] Fluorescence was used to profile bacterial binding on a library of 372 polyurethanes and polyacrylates. *S. typhimurium*-GFP or *E. coli*-GFP were added to duplicate polymer microarrays, each containing 1480 spots (four per polymer), and incubated at room temperature (RT). Subsequently the polymer microarrays were washed and analysed using a FITC filter with a BioAnalyzer 4F/4S LaVition BioTech scanner, with bacterial adhesion evaluated *via* the integrated fluorescence intensity for each spot after background correction (**Figure 6.1**).

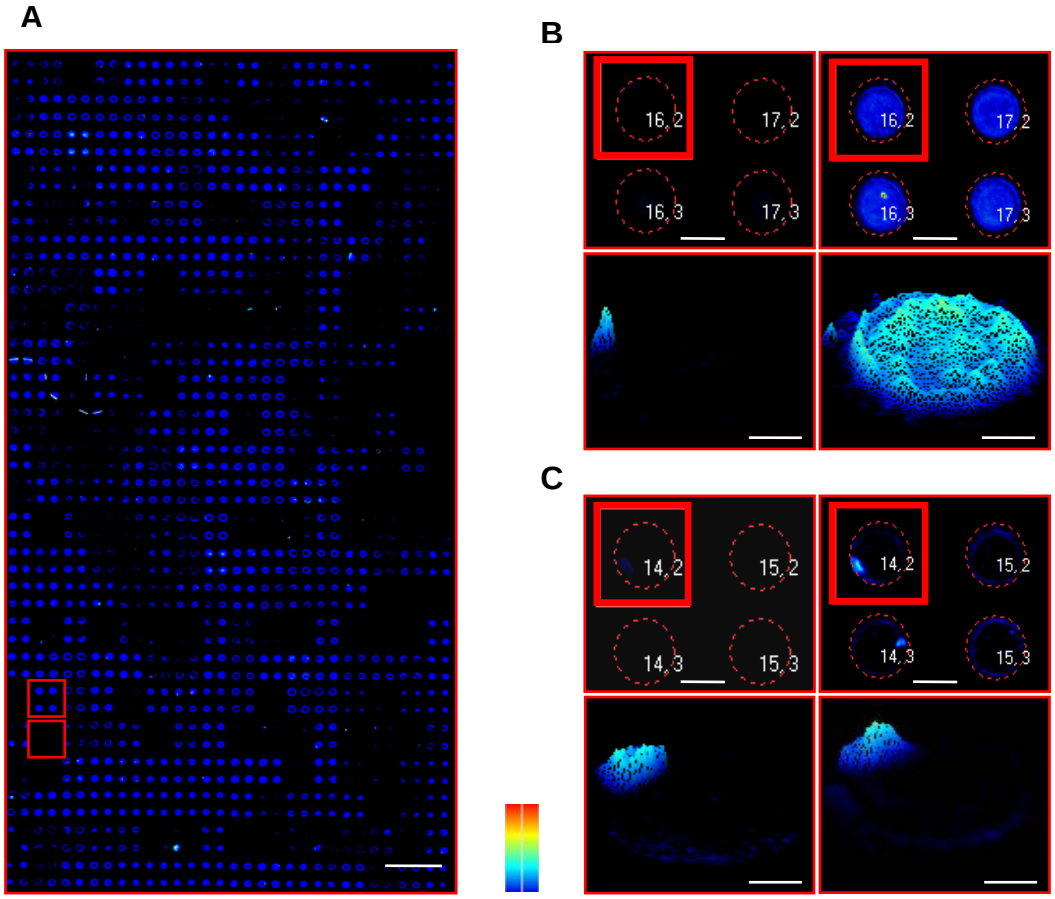

Figure 6.1 *La Vition BioTech software automatic quantification. A) Fluorescence associated with the expression of GFP on a library of 372 polyurethanes and polyacrylates (scale bare 3.5mm). Areas in the square are hit polymers, shown in B and C (scale bare 300 µm). B) Background of the polymer auto fluorescence (left) is shown prior to adding bacteria and fluorescence intensity detection in presence of bacteria (right) after background correction on representative strong binding PA141. C) Poor binding PA311. In A and B: 3D image of the spot in the selected area is shown in lower panel (scale bare 100µm). In B and C: the number in the square is the position of the polymer spot in the array, allocated automatically by the software. An intensity scale bar is shown (botton right).*

Analysis revealed six polyacrylates and thirteen polyurethanes which showed strong binding of *Salmonella* (polymer microarray slides were washed vigorously with shaken three times with PBS, and then rinsed in deionised water) (**Figure 6.2**). Binding of *E. coli* on these polymers was weaker in general but varied with the particular polymer. For example, PU222 showed good binding of *Salmonella* and *E. coli*, whereas there was a substantial difference between the binding of *Salmonella* and *E. coli* on PU178. Analysis of the polyurethanes revealed that the diols, PTMG and PPG were found in ten of the thirteen hit polyurethanes (**Table 6.1**).

Four of the six hit polyacrylates (141, 158, 167 and 168) contained the monomer HEMA and of those four, two contained the monomer VI (**Table 6.2**).

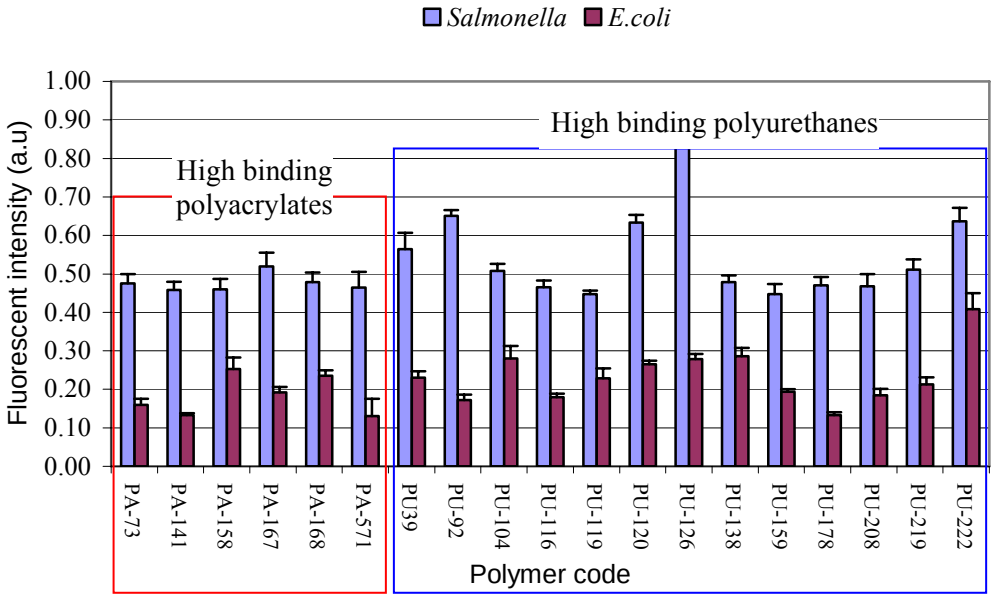

Figure 6.2 *Polymers which mediate high Salmonella binding for two gram-negative bacteria linegies (Salmonella and E. coli). Bacteria binding expressed as background corrected mean fluorescent intensity (a.u = arbitrary units) with error bars representing the standard deviation. Complete Salmonella and E. coli-polymer binding analysis is reported on CD (Supplementary Information, excel folder named "Chapter 6")*

PU	Polymer Structure			
	Diol	Mn	Diisocyanate	Chain Extender
39	PTMG	1000	HDI	BD
92	PHNAD	900	BICH	OFHD
104	PPG	425	BICH	DEAPD
116	PTMG	2000	HDI	BD
119	PHNAD	900	BICH	DMAPD
120	PHNGAD	1800	MDI	DEAPD
126	PPG	425	TDI	DMAPD
138	PTMG	2000	MDI	EG
159	PTMG	250	BICH	EG
178	PPG	1000	MDI	OFHD
208	PPG	425	BICH	BD
219	PTMG	250	MDI	BD
222	PPG	1000	MDI	DMAPD

Table 6.1 *Salmonella binding polyurethanes with polymer composition. Diol/Diisocyanate/Chain Extender (1:2:1), except PU39 and PU208 which are: Diol/Diisocyanate (1:1).*

Monomers abbreviations:

Diol:
PPG: poly(propylene glycol)
PTMG: poly(butylene glycol)
Diisocyanate:
BICH: 1,3-bis(isocyananatomethyl)cyclohexane
HDI: 1,6-diisocyanohexane
HMDI: 4,4'-methylenebis(cyclohexylisocyanate)
MDI: 4,4'-methylenebis(phenylisocyanate)
TDI: 4-methyl-1,3-phenylene diisocyanate
Chain Extender:
BD: 1,4-butanediol
DEAPD: 3-diethylamino-1,2-propanediol
DMAPD: 3-dimethylamino-1,2-propanediol
ED: ethylene diamine
EG: ethylene glycol

PA	Polymer structure					
	Monomer 1	Monomer 2	Monomer 3	Ratio (mol)		
				mon (1)	mon (2)	mon (3)
73	HBMA	DEAAm	-	90	10	-
141	HEMA	DMAEMA	-	50	50	-
158	HEMA	BACOEA	-	70	30	-
167	HEMA	VI	-	70	30	-
168	HEMA	VI	-	50	50	-
571	MEMA	A-H	DEAEA	50	15	35

Table 6.2 *Symbol definition of Salmonella binding polyacrylates.*

Monomers abbreviations:

Monomer 1
HBMA: hydroxybutylmethacrylate
HEMA: 2-hydroxyethylmethacrylate
MEMA: 2-methoxyethylmethacrylate
Monomer 2
DEAAm: diethylacrylamide
DMAEMA: 2-(diethylamino)ethyl methacrylate
BACOEA: 2-[[(butylamino)carbonyl]oxy]ethyl acrylate
VI: 1-vinylimidazol
A-H: acrylic acid
Monomer 3
DEAEA: 2-(diethylamino)ethyl acrylate

Sixteen polyacrylates showed substantial inhibition of *Salmonella* adhesion, with thirteen containing the monomer MMA. Eleven of these also contained the monomer glycidyl methacrylate GMA (**Figure 6.3**). PA221 and PA222 which were composed of both MMA and MA-H were highly successful in preventing adhesion of both *Salmonella* and *E. coli*. PA317, PA323 and PA324 selectively bound *E. coli*, but did not bind *Salmonella*, with PA323 and PA324 differing only in the molar ratios of the monomers. MMA and GMA, the related polymer PA322 showed a similar trend (**Figure 6.3**), but with slightly less selectivity (see Appendix II for monomer structures and abbreviations).

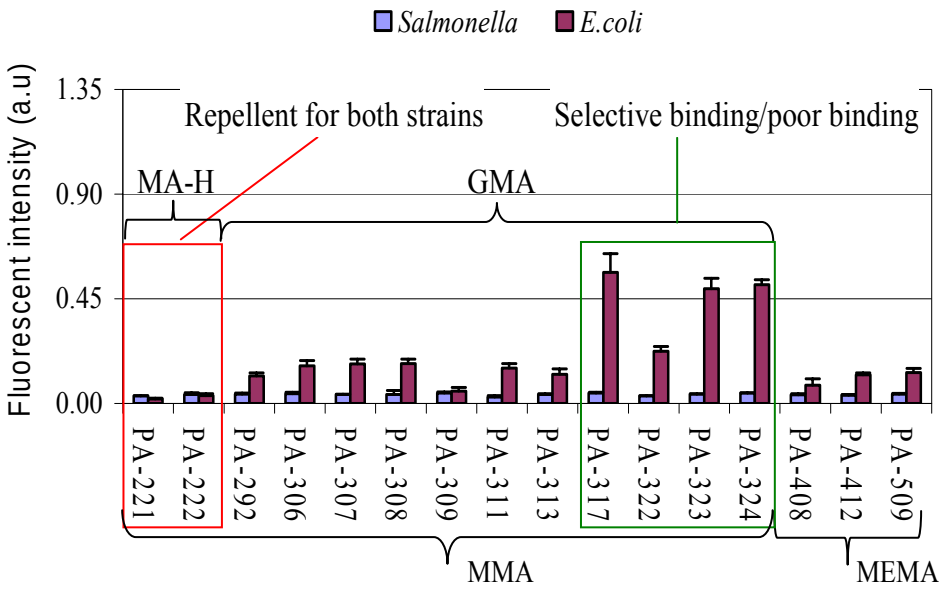

Figure 6.3 *Polyacrylates showing Salmonella binding and both poor and strong E .coli binding (a.u = arbitrary units). X-axis: polymer references. Complete Salmonella and E. coli-polymer binding analysis is reported on CD (Supplementary Information, excel folder named "Chapter 6").*

6.2.1 Reprinting

Following the analysis of the entire library, several polymers which resulted in the strongest or weakest binding of *Salmonella* were printed onto another microarray slide and examined. Each polymer was printed in a 5 x 5 pattern and incubated overnight with bacteria.

PU104, 120, 126 and 141 showed consistent cellular attachment, whilst the four poor binding polymers PA221, 311, 408 and 412 confirmed their anti-bacterial binding properties (**Figure 6.4**).

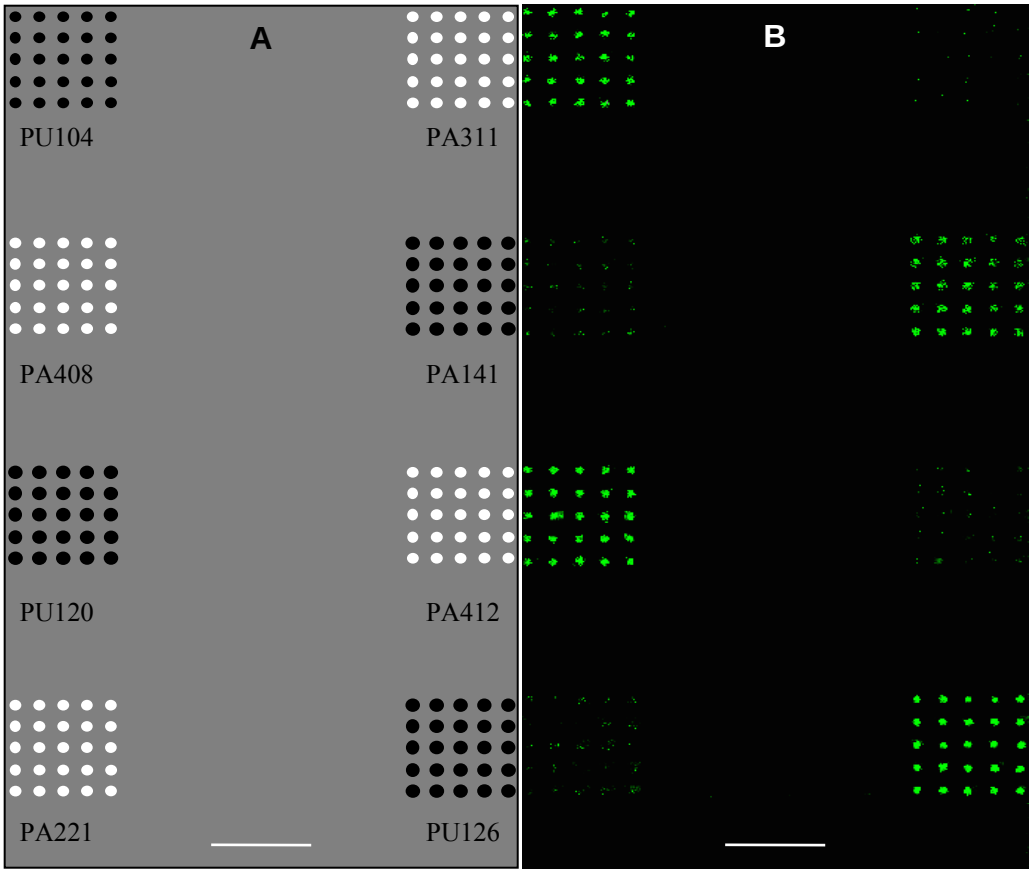

Figure 6.4 *A) Slide template with 8 fields of 25 spots pattern (PU104, PU120, PU126, PA141, PA221, PA311, PA408 and PA412 respectively); B) fluorescent microscopy imaging of Salmonella-GFP (Fluorescein channel). Scale bar 3.5 mm.*

6.2.2 Impact of time on attachment

It would clearly be advantageous for a polymer to be able to bind bacteria in a rapid time frame. Therefore, to test the rapidity of *Salmonella* binding, an array with the letters 'UK' was fabricated using high and low binding polymers (PU104 and PA311, respectively) and *Salmonella* were incubated on the array for four hours (instead of 24 h, as previously). As can be seen (**Figure 6.5**), a uniform binding pattern was observed when printed with PU104, while little binding was observed with PA311.

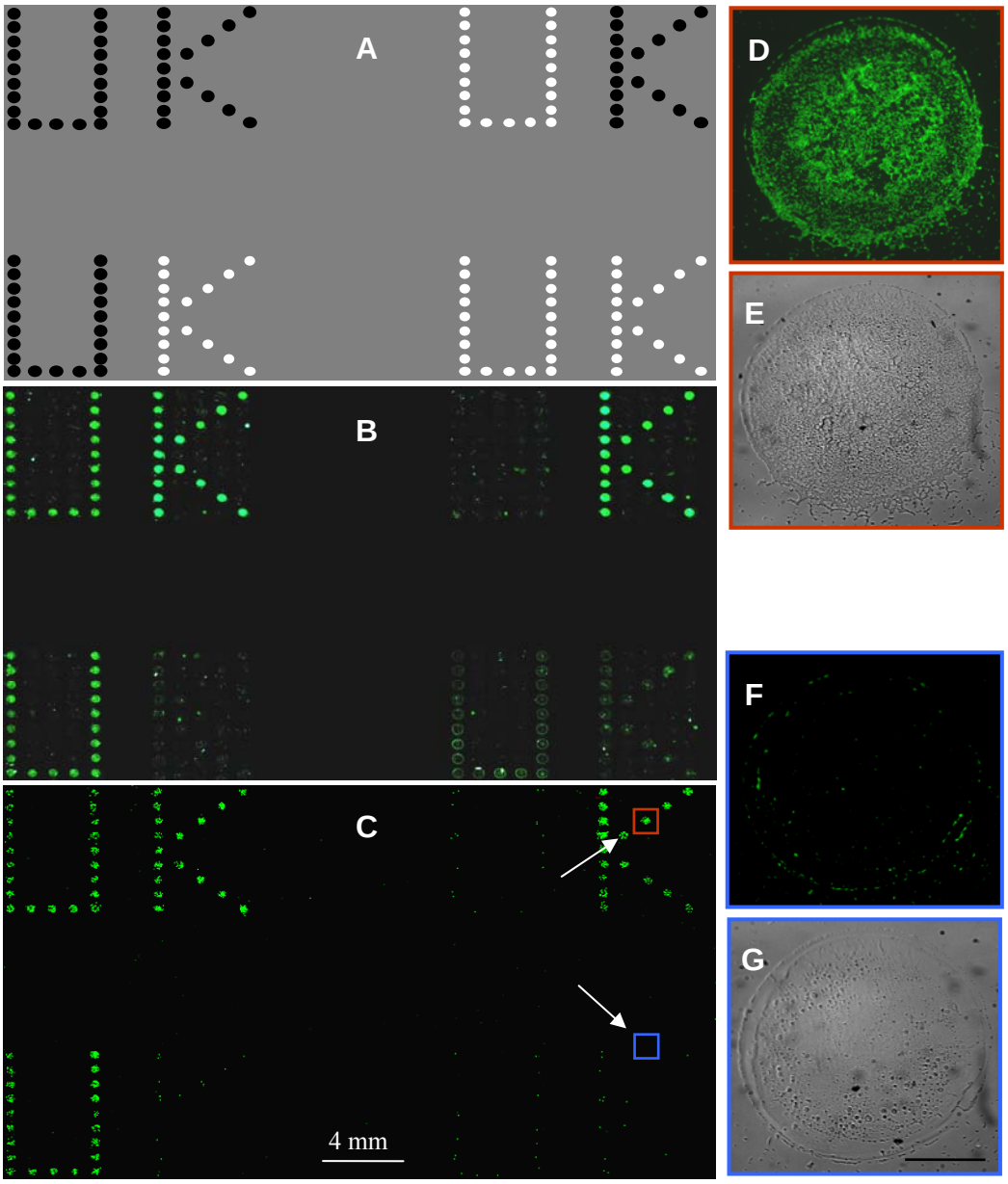

Figure 6.5 *Salmonella attachment/repulsion: A) Array design with the good-binding polymer PU104 (in black) and the non-binding polymer PA325 (in white); B) BioAnalyzer scanning of the array using a Fluorescein filter; C) Fluorescent microscopy imaging (x20 objective); D-G) fluorescent and brightfield microscopy images of Salmonella attached to representative polymer spots; D) fluorescein channel and (E) brightfield of PU104; F) fluorescein channel and (G) brightfield of PA325*

6.3 SEM Analysis

6.3.1 Polymer analysis

A SEM study was undertaken of *Salmonella* binding on some of the selected high binding PU104, 120, 126 and PA141 (**Figure 6.6 A-D**), as well as low binding PA221, 311, 408 and 412 (**Figure 6.6 E-H**). Particular attention was paid to the binding characteristics and polymer spot topography.

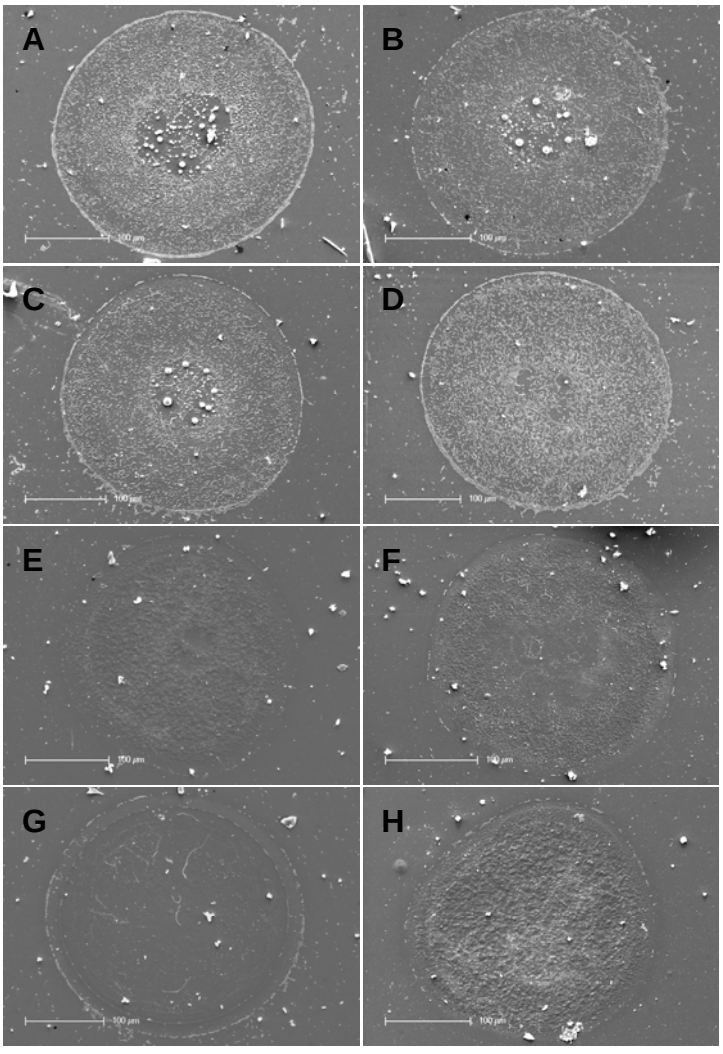

Figure 6.6 *SEM images of Salmonella binding on selected polymers. Single spots: A-D) PU104, 120, 126 and PA141, respectively (strong binding); E-H) PA-221, 311, 408 and 412, respectively (poor binding).*

Bacteria appeared firmly attached and closely packed on PA141, aligning along their longitudinal axis. Small micro-colonies were observed on the strong-binding polymer surface (**Figure 6.7 A**). In contrast, non-binding polymers (PA331) showed little attachment and no evidence for early biofilm formation, implicating these polymers as potential new materials for antibacterial surface coatings (**Figure 6.6 B**).

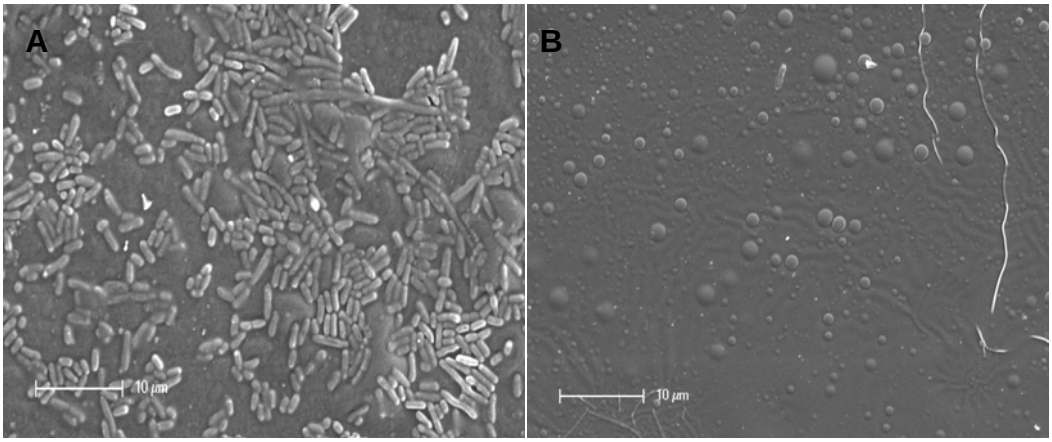

Figure 6.7 *SEM images of Salmonella binding on selected polymers. High magnification: A) PA141 and B) PA311.*

6.3.2 Coverslip analysis

In order to see if the selected polymers could be scaled-up and, to find whether those polymers could be used in practical applications, PA141 and 311 were spin-coated onto glass coverslips, which were formed of a central square (1 x 1 mm) subdivided in one hundred squares (100 x 100 µm). These coated coverslips, and uncoated coverslips (as a control), were incubated with *Salmonella*-GFP as previously reported (Chapter 6.2) and imaged *via* SEM (**Figure 6.8**). The number of bacteria on randomly selected subsquares on the coverslips were counted in give the number of bacteria per mm^2 (**Figure 6.9**).

The analysis of binding on both coated and uncoated coverslips confirmed the expected results. *Salmonella* maintained on PA141 displayed ~7-fold increase in binding function over an uncoated coverslip, whereas the number of *Salmonella* on the non-binding PA311 was twenty times less than the glass control (**Figure 6.9**).

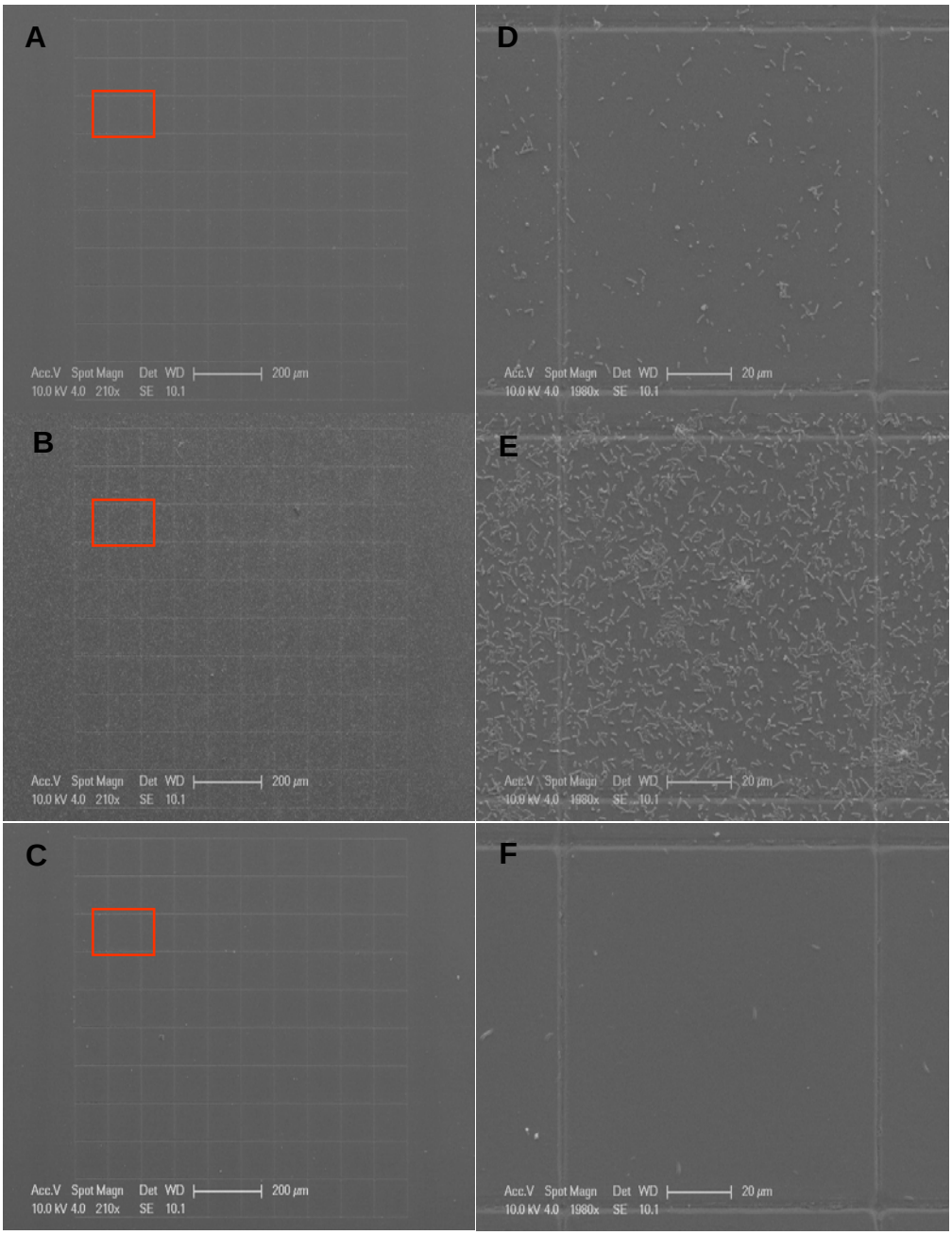

Figure 6.8 *SEM of Salmonella binding on coverslips. A, D) Control (no-polymer coating); B, E) PA141 (strong binding); C, F) PA311 (poor binding).*

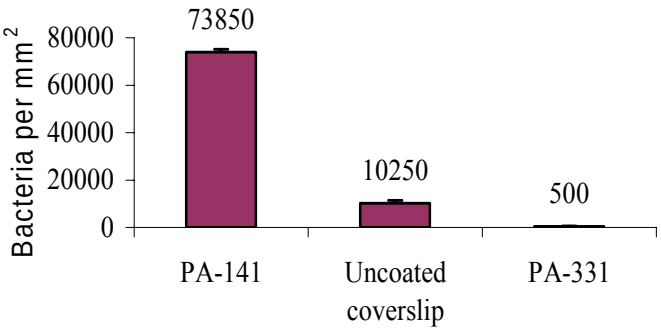

Figure 6.9 *The average number of bacteria per millimeter square on PA141 (binding), PA311 (non-binding) coated coverslips (n=4).*

6.4 Conclusion

Polymer microarrays were successfully used for the high throughput screening of *Salmonella* typhimurium and *E.* coli for binding or repultion. A fluorescence imaging detection analysis allowed rapid, parallel, and comprehensive evaluation of bacteria adhesion on 372 polymers. Immobilisation of bacteria was shown to be highly dependent on both the chemical structures and properties of the polymers and their ability to discriminate between different bacterial genera was observed. Bacteria generally exhibited similar binding characteristics for the same polymers over long (24 h) and short (4 h) periods. For strong binding polymers, SEM revealed the formation of early biofilm-like microcolonies, where cells were longtitudinally aligned and closely packed. A number of polymers were also identified which clearly prevented bacterial attachment, even at these high cell densities and over a long time period (24 h).

Chapter 7

Experimental

7.1 General information

7.1.1 Equipment

Q-Array Mini microarrayer (Genetix).

BioAnalyzer 4F/4S white light scanner and FIPS software (LaVision BioTech).

HCS platform and Pathfinder™ software (IMSTAR).

Biosafety cabinet: HERAsafe KS 18 class II (Heraeus).

Incubator: HERAsafe KS 18 class II (Heraeus).

Vacuum oven: Vacutherm VT6025 (Heraeus).

P6708 spin coater (Speedlines Technologies).

2100 Electrophoresis Bioanalyzer (Agilent).

DNA Microarray hybridization oven (Agilent).

DNA Microarray hybridization Chamber – SureHyb (Agilent).

G2565AA DNA microarray scanner (Agilent).

NanoDrop® ND-3300 fluorospectrometer (Agilent).

Eppendorf biophotometer plus (Eppendorf).

7.1.2 Polymers

The polymer libraries (poly(urethane) and poly(acrylate) libraries, respectively, Appendices I and II) were synthesised by Jean-Francois Thaburet, Hitoshi Mizomoto and Ann Jasmine Jose as part of a previous project. [40, 79, 245]

Each polymer had been previously characterised in terms of molecular weight by GPC, wettability[245] and glass transition temperature (DSC).[83]

7.1.3 Chemicals and solvents

Chemicals and solvents used in all the experiments were obtained from Sigma-Aldrich. Phosphate Buffer Saline (10 mM phosphate, 27 mM KCl, 137 mM NaCl, pH 7.4) is referred to as PBS.

7.1.4 Microscope slides and coverslips

Aminoalkylsilane microscope slides were obtained from Sigma-Aldrich and the coverslips from VWR International Ltd.

7.1.5 Cell culture media and supplements

All cell culture media were from Sigma-Aldrich and all supplements added to the culture medium were supplied by Gibco and Invitrogen, except where stated in the text.

7.2 Experimental for Chapter 2

7.2.1 Polymer microarray fabrication

214 polyurethanes were "spotted" on aminoalkylsilane-treated glass slides, previously coated with agarose to impede unspecific cell adhesion. Coating with agarose was achieved by manually dip-coating the slide in agarose Type I-B (1 % w/v in deionised water at 65 ºC), followed by removal of the coating on the bottom of the side by wiping with a clean piece of tissue. Subsequently, the slides were dried overnight at room temerature in a dust free environment. Polyurethanes were prepared by dissolving 10 mg of polymer in 1mL (10 $mg.mL^{-1}$) of NMP. Polymer microarrays were then fabricated by contact printing (Q-Array Mini microarrayer) with 32 aQu solid pins (K2785, Genetix) using the polymer solutions placed in polypropylene 384-well microplates (X7020, Genetix). The 214 members of the PU library were printed following a four-replicate pattern with 1 single field of 32 x 32 spots containing 42 control (emptied) areas. Printing conditions were as follows: 5 stampings per spot, 200 ms inking time and 10 ms stamping time. The typical spot size was 300-320 μm in diameter with a pitch distance of 1120 μm (y-axis) and 560 μm (x-axis), allowing up to 1024 features to be printed on a standard 25 x 75 mm slide. Once printed, the slides were dried under vacuum (12 h at 42 ºC/200 mbar) and sterilised in a bio-safety cabinet by exposure to UV irradiation for 20 min prior to use.

7.2.2 Polymer microarray screening

Mouse fibroblast cells (L929) (kindly provided by Prof. Timothy Elliott, School of Medicine, University of Southampton) were grown in Dubelcco's Modified Eagle's Medium (DMEM) supplemented with heat inactivated fetal bovine serum (FBS) (10% v/v), penicillin (100 $units.mL^{-1}$), streptomycin (100 $mg.mL^{-1}$) and L-glutamine (4 mM) at 37 °C with 5% CO_2.

Prior to seeding onto the polymer microarray, L929 cells were washed with PBS, detached with trypsin (0.050% w/v), EDTA (0.20% w/v) in PBS and, counted and diluted with media to a final concentration of (1 x 10^5 cells/slide in 5 mL). This

dilution was gently added onto the polymer microarray contained in a sterile four well-plate (Nunc) and incubated for different periods of time (48 h and 72 h). Cell performed was done as follows: (i) incubation with CTG-CMFDA (5 μM in PBS, Molecular Probes Inc, Invitrogen) at 37 °C and 5% CO_2 for 15 min; (ii) slides were then gently washed in PBS and fixed with 4% w/v p-formaldehyde in PBS at RT for 15 min; (iii) incubation with Hoechst-33342 (1 μg/mL in PBS) (Sigma-Aldrich) for 15 min at RT; and subsequently, (iv) incubation with AlexaFluor 568 phalloidin (0.2 μM in 1% in PBS containing 1% v/v FBS, Molecular Probes Inc, Invitrogen) for 15 min at RT. The polymer microarray slides were then rinsed in deionized water and air-dried before scanning.

7.2.2.1 Image capture and analyses

Image capture and analyses were carried out using a high content screening (HCS) platform (Nikon 50i fluorescence microscope (x20 objective) with an X-Y-Z stage), equipped with Pathfinder™ software package. Cell number (Hoechst-33342: ex/em 355/465 nm), biocompatibility (CellTracker Green: ex/em 492/516 nm), and morphology (AlexaFluor 568: ex/em 578/603 nm, Invitrogen) for each polyurethane member was determined using fluorescent (DAPI, FITC, and rhodamine-like band-pass filters) and bright field channels by automated scanning of polymer spots. Complete L929 cell-polyurethane binding analysis is reported on CD (Supplementary Information, excel folder named “Chapter 2”).

7.2.3 Analysis of cell morphology

Cell morphology was analysed by confocal microscopy after 72 h of culture. Image capture was performed by a DeltaVision Real-Time Microscope (x63 objective) using DAPI and rhodamine channels.

7.3 Experimental for Chapter 3

7.3.1 Polymer microarray printing

Polymer microarrays were prepared using the same conditions as described in Chapter 7.2.1. However, the 213 members of the polyurethane library were printed following a four-replicate pattern with 1 single field of 32 x 32 spots containing 45 control (empty) areas. The 58 members of the polyacrylate library were printed following a nine-replicate pattern within 1 single field of 24 x 24 spots containing 6 control (empty) areas.

7.3.2 Cell cultures

Human erythroleukemic cells (K562) (kindly provided by Salim Khakoo, Department of Hepatology, Division of Medicine, Imperial College, London, UK) were grown in RPMI 1640 growth medium supplemented with heat inactivated FBS (10% v/v), penicillin (100 unit.mL^{-1}), streptomycin (100 µg mL^{-1}) and L-glutamine (4 mM) at 37 °C with 5% CO_2.

7.3.3 Scanning for cell binding

K562 were centrifugated at 250 x g for 5 min. The resulting cell pellet was resuspended in PBS and centrifugated again at 250 x g 5 min. The pellet was resuspended in 2 mL of RPMI 1640. K562 were counted and diluted with media to a final concentration of 1 x 10^5 per mL. An aliquot of 6 mL of this dilution was gently added to each of the six polymer microarrays contained in two four well-plate (Nunc) and incubated for 24, 48 and 72 h. Thirty minutes before screening, slides were washed with PBS and then incubated for 30 min with fresh RPMI 1640 media and Hoechst 33342 (1 µg/mL) for nuclei staining. The polymer microarray slides were then rinsed in an isotonic solution (8.1 g/L NaCl, 0.2 g/L KCl) and immersed in this solution to facilitate K562 live cell analysis. Cell binding with the different polymers was carried out, using DAPI and brightfield channels, as described in Chapter 7.2.2.1. Complete K562 cell-polyurethane and polyacrylate binding analysis is reported on CD (Supplementary Information, excel folder named “Chapter 3”).

7.3.4 Polymer coating of coverslips

50 mm diameter glass coverslips (CB00500RA1, Menzel-Gläser) were cleaned with tetrahydrofuran (THF). 500 µL of each of the polyacrylate (PA365, 368, 371 and 374) solution (2.0% w/v in THF) was placed onto the coverslips and spin coated for 10s at 2000 rpm. Coverslips were dried under vacuum (12 h at 45 °C/200 mbar) and irradiated with UV light for 20 min before using.

7.3.5 SEM

As controls, K562 cells were collected, centrifuged for 5 min at 250 x g. The resulting cell pellet was resuspended in 10 mL of (0.1 M cacodylate buffer, and centrifugated again at 250 x g for 5 min. The pellet was fixed in 2 mL of 2.5% v/v glutaraldehyde in 0.1 M cacodylate buffer at RT for 2 h. After washing twice (0.1 M cacodylate buffer), the cells were seeded on coverslips coated with PA365. For polymer treated samples, cells were then grown for 24 h and 72 h directly on glass coverslips coated with the selected polyacrylates (365, 368, 371 and 374) and were fixed with 2 mL of 2.5% v/v glutaraldehyde for 2 h at RT and washed as above. All samples were fixed with 1% w/v osmium tetroxide for 1 h at RT, dehydrated through graded ethanol (50, 70, 90 and 100%), critical point dried in CO_2 (EMS 850 Critical Point Drier) and gold coated by sputtering (Edwards S150B Sputter Coater). The samples were examined with a Philips XL30CP Scanning Electron Microscope.

7.3.6 Gene expression analysis

7.3.6.1 RNA isolation

Total RNA was isolated from both K562 cells grown adhesively on coated coverslips (Chapter 7.3.4) and in suspension. RNA extraction was performed using a SV total isolation kit according to the manufacturer's protocol (Promega). The integrity and concentration of total RNA was determined using a RNA 6000 Nano Assay Kit and a Bioanalyzer 2100 supported with RNA integrity number (RIN) software according to the manufacturer's protocols (Agilent). The RIN software algorithm allowed the determination of critical features (peak markers,

18 S and 28 S) extracted from three electrophoretic traces (**Figures 7.1**) using appropriate integrators.[246] This allowed the categorization of total RNA, with a numbering system from 1 to 10 (with 1 being the most degraded profile and 10 being the most intact). The RIN software also calculated total RNA concentration (**right Figures 7.1**).

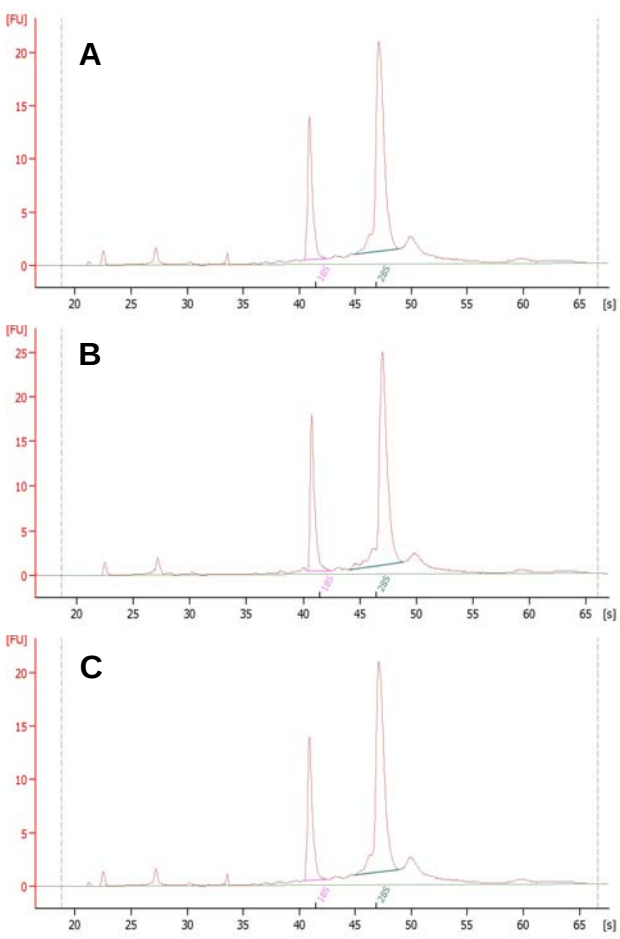

Total RNA concentration: 310 ng/µl
Ratio [28 S/18 S]: 2.2
RIN: 10.0

Total RNA concentration: 272 ng/µl
Ratio [28 S/18 S]: 2.2
RIN: 10.0

Total RNA concentration: 298 ng/µl
Ratio [28 S/18 S]: 2.2
RIN: 10.0

Figure 7.1 *Agilent 2100 Bioanalyzer data electropherogram used to measure the quality and quantity of total RNA. A) Total RNA isolated from K562 cells grown in suspension (control); B) total RNA isolated from K562 cells grown adhesively on coated coverslips (PA368); C) total RNA isolated from K562 cells grown adhesively on coated coverslips (PA365). X-axis: time [s]; Y-axis: arbitrary fluorescence units [FU].*

7.3.6.2 cRNA labelling

cRNA synthesis and labelling reactions (fluorophores Cy3 and Cy5 both from PerkinElmer/NEN Life Sciences) were performed using a Low RNA Input Linear Amplification Kit according to the manufacturer's protocol (Agilent). Labelled cRNA was assessed using a NanoDrop® ND-3300 Fluorospectrometer (Agilent) (**Figures 7.2**).

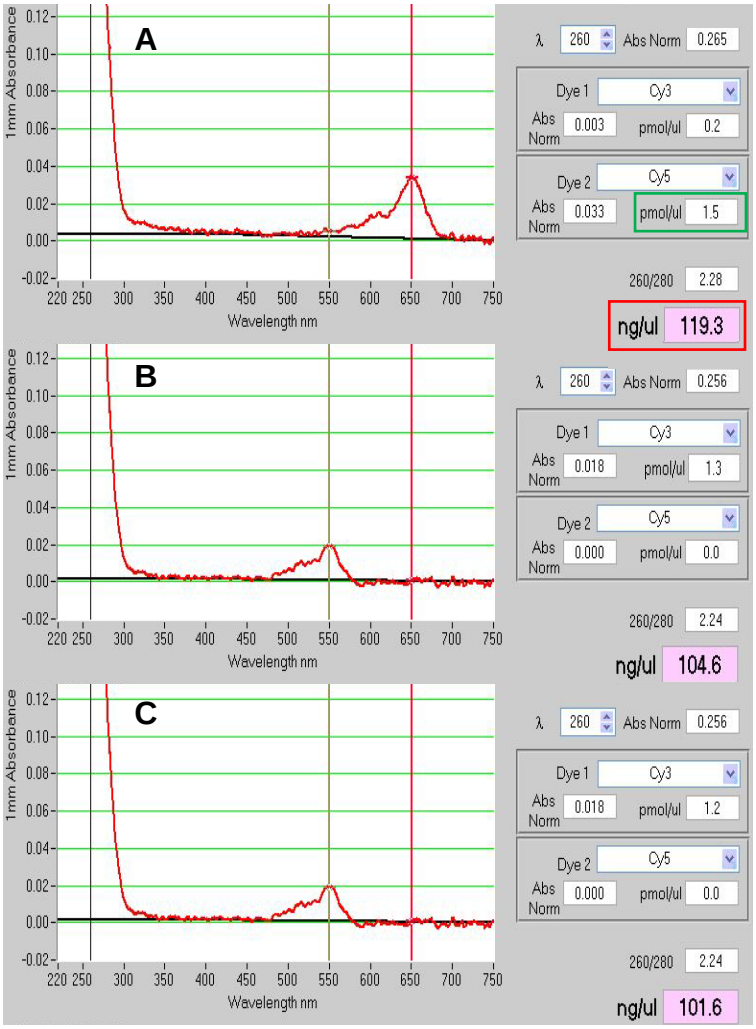

Figure 7.2 *NanoDrop 3300 data viewer software displays a full UV-Vis absorbance spectrum as well as the calculated concentrations of both the nucleic acid (red rectangle) and the fluorescent labelled cRNA (green rectangle). Peaks for cRNA, and incorporated Cy3 and Cy5 are found at 260, 550 and 650 nm, respectively. 1 uL absorbance measurement of: A) Cy5-labelled cRNA from K562 cells grown in suspension (control); B) Cy3-labelled cRNA from K562 cells grown adhesively on coated coverslips (PA368); C) Cy3-labelled cRNA from K562 cells grown adhesively on coated coverslips (PA365).*

7.3.6.3 Hybridisation and scanning

Array hybridisation was carried out using 4 x 44 K Whole Human Genome microarray (design 014850 Agilent).

Array hybridisation was performed using a Gene Expression Hybridization Kit (Agilent). Briefly, 850 ng of each CyDye™-labeled cRNA (Chapter 7.3.6.2**)** were added with a 2X Hi-RPM Hybridization Buffer (Agilent) up to a final volume of 500 µL. The hybridization was carried out using a DNA microarray hybridization oven with a constant temperature of 65 ºC for 17 h at 10 rpm. The hybridized array was washed following the post-hybridization washing step according to the manufacturer's Gene Expression Wash Buffer Kit protocol (Agilent). The dried slide was scanned with Agilent DNA microarray scanner (**Figures 7.3**).

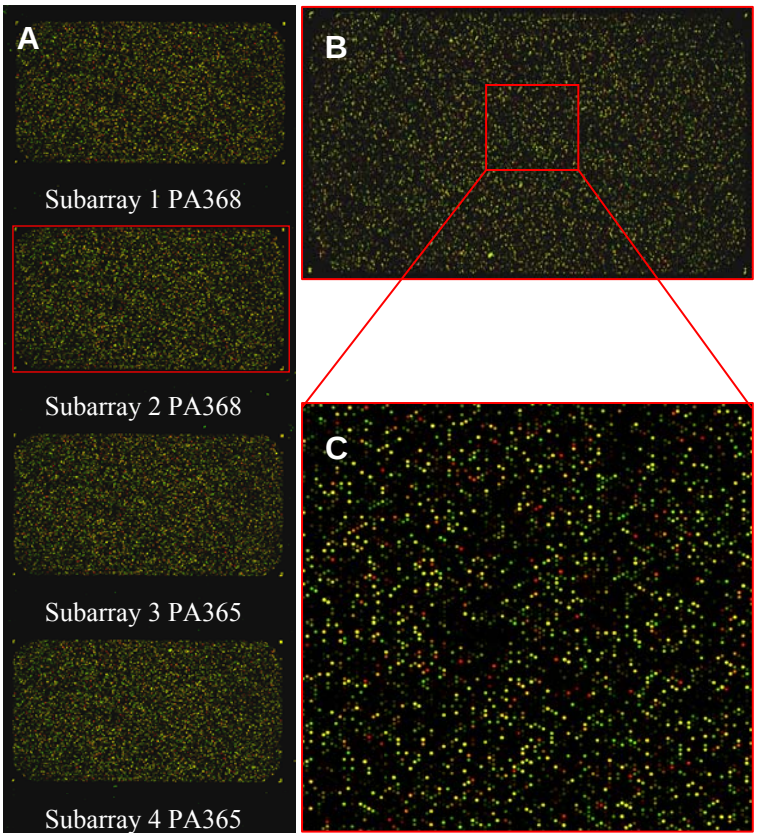

Figure 7.3 *Agilent DNA microarray scanning (2 micron resolution). A) 4 x 44 K Whole Human Genome microarray; B) subarray 2; C) magnification of subarray 2.*

7.3.6.4 Data analysis

Datasets pre-processed by Agilent's Feature Extraction 9.1, were analysed by Genespring GX 9.0.2. Datasets were filtered by flags given by the FE software (present, marginal and absent), only samples detected as present were used for the statistical analysis. The four datasets were grouped together and assigned as a unique condition to analyse the more general interaction between polymers and K562 cells, irrespective of the polyacrylates (PA365 or 368), against the control (suspension cells). T Test statistical analyses were carried out (T Test against zero) and p-values were computed asymptotically, where p-values < 0.01 were considered significant, meaning a probability of real changes in expression of 99.9%. Gene expression data has been deposited in ArrayExpress EBI (www.ebi.ac.uk/arrayexpress) under accession number E-MEXP-1570. Results are presented in **Table 7.1**.

Gene Symbol	UniGene	Gene Description	Regulation	Fold change
MED18	Hs.479911	mediator of RNA polymerase II transcription	up	3.60
XPR1	Hs.227656	xenotropic and polytropic retrovirus receptor (XPR1)	up	3.43
HMGCS1	Hs.397729	3-hydroxy-3-methylglutaryl-Coenzyme A synthase 1 (soluble) (HMGCS1)	up	3.10
A_24_P110101			down	6.86
MT1E	Hs.534330	metallothionein 1E (MT1E)	down	6.63
GDNF	Hs.248114	Glial cell line-derived neurotrophic factor precursor (Astrocyte- derived trophic factor 1) (ATF-1).	down	5.93
MT2A	Hs.647371	metallothionein 2A (MT2A)	down	5.61
PIP5K1C	Hs.282177	phosphatidylinositol-4-phosphate 5-kinase	down	5.48
OTUD7A	Hs.355236	OTU domain containing 7A (OTUD7A)	down	5.40
MT1L	Hs.647358	mRNA for metallothionein isoform 1R. [X97261]	down	5.35
NPBWR1	Hs.248117	neuropeptides B/W receptor 1 (NPBWR1)	down	5.28
BX089650	Hs.520524	BX089650 Soares_senescent_fibroblasts_NbHSF	down	5.23
PPP1R11	Hs.82887	protein phosphatase 1	down	5.13
SCRT2	Hs.355284	scratch homolog 2	down	5.12
MT1G	Hs.433391	metallothionein 1G (MT1G)	down	5.10
ENAH	Hs.497893	enabled homolog (Drosophila) (ENAH)	down	4.95
FOXC1		FOXD4a mRNA	down	4.90
KRT80	Hs.140978	keratin 80 (KRT80)	down	4.81
SLC26A1	Hs.658244	solute carrier family 26 (sulfate transporter)	down	4.80

Gene Symbol	UniGene	Gene Description	Regulation	Fold change
SLC26A1	Hs.658244	solute carrier family 26 (sulfate transporter)	down	4.80
AVP	Hs.89648	arginine vasopressin (neurophysin II	down	4.77
MT1X	Hs.374950	metallothionein 1X (MT1X)	down	4.74
MT1H	Hs.438462	metallothionein 1H (MT1H)	down	4.63
BG182941	Hs.635280	RST1823 Athersys RAGE Library cDNA	down	4.60
AF100640		metastasis related protein (MB2) mRNA	down	4.57
IFITM5	Hs.443469	interferon induced transmembrane protein 5 (IFITM5)	down	4.48
LOC146325	Hs.632220	similar to hypothetical protein FLJ13841 (LOC146325)	down	4.47
GPX1	Hs.76686	glutathione peroxidase 1 (GPX1)	down	4.45
MT1X	Hs.374950	metallothionein 1X (MT1X)	down	4.43
THC2724451			down	4.43
DEAF1	Hs.243994	deformed epidermal autoregulatory factor 1 (Drosophila) (DEAF1)	down	4.34
CACNA1E	Hs.437444	calcium channel	down	4.21
GPR78	Hs.350588	G protein-coupled receptor 78 (GPR78)	down	4.21
BX427435	Hs.625249	BX427435 FETAL LIVER cDNA clone CS0DM010YK16 3-PRIME	down	4.16
LBH	Hs.567598	limb bud and heart development homolog (mouse) (LBH)	down	4.13
PRR15	Hs.91109	proline rich 15 (PRR15)	down	4.12
BM913108	Hs.675862	AGENCOURT_6614092 NIH_MGC_41 cDNA clone IMAGE:5475119 5'	down	4.09
FOXE1		HFKH4 mRNA for fork head like protein.	down	4.08
LOC728864		PREDICTED: similar to Mucin-2 precursor (Intestinal mucin 2) (LOC728864)	down	4.06
A_32_P105865			down	4.02
LCE2D	Hs.490225	late cornified envelope 2D (LCE2D)	down	4.00
AY227436		drug-sensitive protein 1 mRNA	down	3.96
NP511100		GB|AB065467.1|BAC05726.1 seven transmembrane helix	down	3.92
AF264621		uncharacterized gastric protein YA42P mRNA	down	3.82
C6orf85	Hs.132340	chromosome 6 open reading frame 85 (C6orf85)	down	3.80
NKX2-8	Hs.234763	NK2 transcription factor related	down	3.76
MPHOSPH9	Hs.577404	M-phase phosphoprotein 9 (MPHOSPH9)	down	3.75
BU191598	Hs.657999	AGENCOURT_8099541 NIH_MGC_102 cDNA clone IMAGE:6254414 5'	down	3.74
AA420998	Hs.178095	AA420998 zu08f10.s1 Soares_testis_NHT	down	3.69
ZNF771	Hs.148584	zinc finger protein 771 (ZNF771)	down	3.69
A_32_P101195			down	3.68
ALDH7A1	Hs.483239	aldehyde dehydrogenase 7 family	down	3.65
NKD2	Hs.240951	naked cuticle homolog 2 (Drosophila) (NKD2)	down	3.62
AT_ssH_RR_5			down	3.61

Gene Symbol	UniGene	Gene Description	Regulation	Fold change
MT1B	Hs.656629	metallothionein 1B (MT1B)	down	3.61
GLIS2	Hs.592087	GLIS family zinc finger 2 (GLIS2)	down	3.56
CDH24	Hs.155912	cadherin-like 24 (CDH24)	down	3.55
GPSM3	Hs.520046	G-protein signalling modulator 3 (AGS3-like	down	3.51
LOC441204	Hs.587432	cDNA FLJ31922 fis	down	3.48
A_24_P932958			down	3.47
BC080624	Hs.661522	cDNA clone MGC:99790 IMAGE:6304510	down	3.46
RHBDL1	Hs.137572	rhomboid	down	3.41
THC2545510		ALU1_HUMAN (P39188) Alu subfamily J sequence contamination warning entry	down	3.33
THC2625851			down	3.32
C19orf31	Hs.620488	chromosome 19 open reading frame 31 (C19orf31)	down	3.30
ARTN	Hs.632404	artemin (ARTN)	down	3.25
MT1H	Hs.438462	metallothionein 1H (MT1H)	down	3.15
LOC651746	Hs.680828	PREDICTED: similar to ankyrin repeat domain 33 (LOC651746)	down	3.14
CXorf57	Hs.274267	chromosome X open reading frame 57 (CXorf57)	down	3.12
AK095945	Hs.134857	cDNA FLJ38626 fis	down	3.12
PYY2	Hs.157195	peptide YY	down	3.11
LIPE	Hs.656980	lipase	down	3.07
BC009749	Hs.611748	cDNA clone IMAGE:3689276	down	3.07
CTSL2	Hs.660866	cathepsin L2 (CTSL2)	down	3.05
SYNGR4	Hs.408333	synaptogyrin 4 (SYNGR4)	down	3.04
MAFA	Hs.670866	v-maf musculoaponeurotic fibrosarcoma oncogene homolog A (avian) (MAFA)	down	3.01
A_24_P928250			down	3.01

Table. 7.1 *A list of genes either up- or down-regulated when K562 cells were adhered onto PA368 and 365. The data was processed with a cut-off value of 3 fold increase or decrease in expression when compared to the "suspension cell control".* [a]*Genes Symbol starting by A_ are still unknown.* [b]*Normalised absolute values.*

7.3.6.5 Quantitative real-time PCR analysis

Quantitative real-time PCR was used to validate the effect of the cell-polymer interactions on the gene expression profile.

7.3.6.5.1 RNA isolation

Total RNA was isolated from both K562 cells grown adhesively on coated coverslips (PA368 and 365) and K562 grown in suspension (Chapter 7.3.6.1).

RNA extraction was performed using a RNeasy Mini Kit according to the manufacturer's protocol (QIAGEN). The integrity and concentration of total RNA were determined as described in Chapter 7.3.6.1 (**Figure 7.4**).

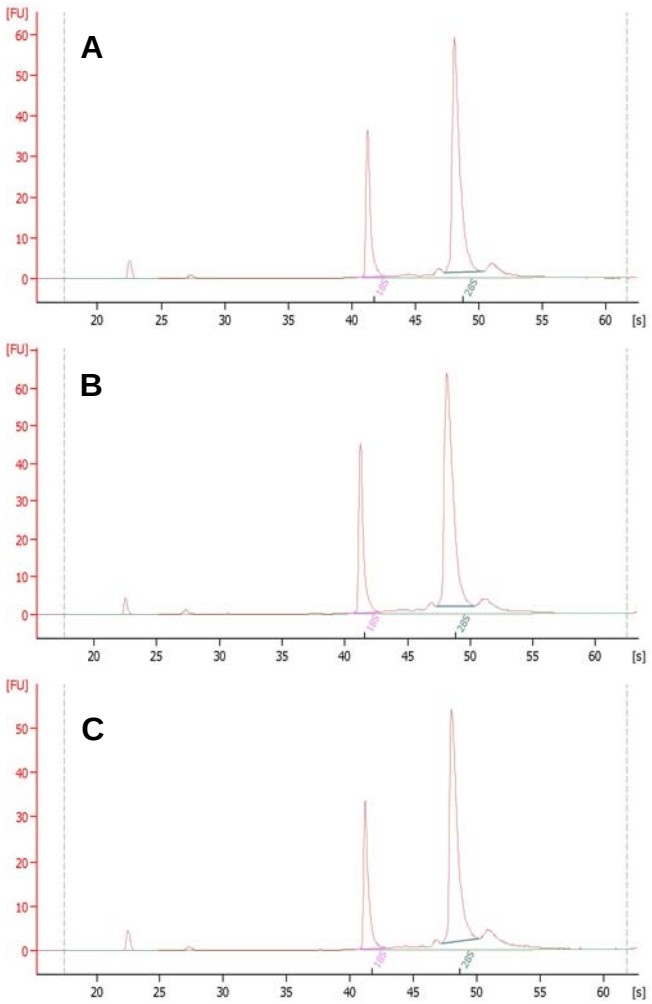

Total RNA concentration: 461 ng/µl
Ratio [28 S/18 S]: 2.3
RIN: 10.0

Total RNA concentration: 368 ng/µl
Ratio [28 S/18 S]: 2.2
RIN: 10.0

Total RNA concentration: 367 ng/µl
Ratio [28 S/18 S]: 2.2
RIN: 10.0

Figure 7.4 *Agilent 2100 Bioanalyzer data electropherogram used to measure the quality of total RNA for dat validation. A) Total RNA isolated from K562 cells grown adhesively on coated coverslips (PA365); B) total RNA isolated from K562 cells grown adhesively on coated coverslips (PA368); C) total RNA isolated from K562 cells grown in suspension (control). X-axis: time [s]; Y-axis: arbitray fluorescence units [FU].*

7.3.6.5.2 Real-time PCR

RNA (500 ng) was used for cDNA synthesis using Superscript III (Invitrogen), according to the manufacturer's instructions. Real-time RT-PCR was performed

using a LightCycler 480 (Roche) and a LightCycler 480 SYBR Green 1 Master (Roche). PCR primers and annealing temperature (Ta) for RNF7, MT1E, MT2A, MT1X genes were those available the in literature.[247, 248] 0.04 µmol HPLC purified primers were purchased from Microsynth AG (Switzerland). The following cycling conditions were used: denaturation: 95 °C 5 min, amplification: 95 °C 5 s, 58 °C 10 s, 72 °C 20 s (45 cycles), acquisition: 81 °C 1 s, melting curve: 95 °C 1 s, 65 °C 10 s, 95 °C – ramp 5 °C/s continuous, cool: -40 °C 10 s. Standard curves were generated from cDNA dilutions. Data were normalised relative to hRNF7 expression levels. PCR primers are shown in **Table 7.2**.

Gene	Forward primer*	Revers primer*
RNF7	5'-CTCCCTCAAGAAGTGGAACG-3'	5'-TTGACATCTAAGACAGGCATCC-3'
MT1E	5'-GCTTGTTCGTCTCACTGGTG-3'	5'-CAGGTTGTGCAGGTTGTTCTA-3'
MT2A	5'-CCGACTCTAGCCGCCTCTT-3'	5'-GTGGAAGTCGCGTTCTTTACA-3'
MT1X	5'-TCTCCTTGCCTCGAAATGGAC-3'	5'-GGGCACACTTGGCACAGC-3'

Table 7.2 *Sequences of PCR primers. *Primers are writer 5'* →

7.4 Experimental for Chapter 4

The preparation of HLCs, incubation with the polymer microarray, fixing and staining were carried out by Dr David Hay in the Centre for Regenerative Medicine (University of Edinburgh).

7.4.1 Polymer microarray preparation

Polymer microarrays were prepared using the same conditions as described in Chapter 7.2.1. However, the 337 members of the polyurethane (161) and polyacrylate (176) libraries were printed following a four-replicate pattern with 1 single field of 32 x 48 spots containing 47 control (empty) areas with a pitch distance of 560 μm (y-axis) and 750 μm (x-axis).

7.4.2 Cell culture and differentiation – David Hay Method –

Human embryonic stem cells (H9) were cultured and propagated in MG coated plates with mouse embryonic fibroblast conditioned medium (MEF-CM) supplemented with basic fibroblast growth factor in feeder-free, serum-free conditions as previously described.[158, 160] Differentiation was initiated at 60-70% confluence, by replacing the MEF-CM with differentiation medium (RPMI1640 with 1 x B27 (Invitrogen), 100 ng/mL activin A (Peprotech) and 50 ng/ml Wnt3a (R&D Systems)). After 72 h (changing medium every day) differentiating cells were cultured in differentiation medium (SR/DMSO medium: knockout-DMEM containing 20% v/v serum replacement (SR), 1 mM glutamine, 1% v/v non-essential amino acids, 0.1 mM β-mercaptoethanol and 1% v/v dimethyl sulfoxide (DMSO)) for 6 days. At day 9 in the differentiation process the HLCs were removed from their substrate using 5 min 37 ^{o}C incubation with trypsin (0.050 % w/v), EDTA (0.20 % w/v) in PBS.

7.4.3 Scanning for cell binding

HLCs were counted and diluted with L15 medium supplemented with 8.3% v/v FCS, 8.3% v/v tryptose phosphate broth, 10 μM Hydrocortisone 21-hemisuccinate, 1 μM insulin and 2 mM glutamine containing 10 ng/mL

hepatocyte growth factor (Peprotech) and 20 ng/mL oncostatin M (R&D Systems). An aliquot of 10 mL (0.5 x 10^6 per mL) of this dilution was gently added to the polymer microarrays contained in a 100 x 25 petri dish (Nunc) and incubated for a further 8 days changing the medium every 2 days.[158, 160] At this point cells were fixed in ice-cold methanol for 10 min at RT. After blocking with PBS containing 10% v/v FBS, cells were incubated with primary antibody (human serum albumin 1:500, SIGMA or human IgG2a, DAKO) at 4 °C overnight, followed by 30 min incubation with appropriate secondary antibody at RT.[160] Cell compatibilitity with the different polymers was carried out, using DAPI and FITC channels as described in Chapter 7.2.2.1. Complete HLC-polymer binding analysis is reported on CD (Supplementary Information, excel folder named "Chapter 4").

7.4.4 Coverslip experiments

The preparation of HLCs (see Chapter 7.4.2), incubation with the coverslips, and measurement of hepatocyte export proteins were carried out by Dr David Hay in the Centre for Regenerative Medicine (University of Edinburgh).

7.4.4.1 Polymer coating of coverslips

19 mm diameter glass coverslips (CB00190RA1, Menzel-Gläser) were prepared using the conditions described in Chapter 7.3.4 with the following samples: 200 μL of three polyurethanes (PU134, 212 and 223) and three polyacrylates (PA119, 196 and 395).

7.4.4.2 Measurement of hepatocyte export proteins on coverslips

Human embryonic stem cells (H9) were differentiated to HLCs and cultured using an established method (David Hay's method, Chapter 7.4.2). At day 23, 1 mL of HLCs culture medium (0.5 x 10^6 per mL) was incubated with either each of six polymer spin-coated coverslips (PU134, 212 and 223) and (PA119, 196 and 395) or pre-coated MG well (as control) for 24 h.

After 12 h culture supernatants were harvested and serum protein production (fibrinogen, transthyretin and fibronectin) measured by ELISA as previously described,[163, 164] and quoted as nonogram of cellular protein per milligram of tissue culture medium.

7.4.4.3 Morphology analysis

HLCs were detached from their biological ECM (Chapter 7.4.2) and replated onto the six polymers coated coverslips and MG as described above (Chapter 7.4.4.2). HLCs morphology plated on MG or both PA119, 196 and 395 and PU134, 212 and 223 were evaluated visually with Zeiss Axiovert 200 fluorescence microscope (magnification x10).

7.4.5 Bio-artificial liver experiments

The preparation of HLCs, incubation with the coated and uncoted PFCs, fixing and induction experiments were carried out by Dr David Hay in the Centre for Regenerative Medicine (University of Edinburgh).

7.4.5.1 Dip-coating of PFC

PFCs were placed onto 2 mL of polyurethane 134 solution (2.0% w/v in THF) for 2 min. PFCs were dried under vacuum (12 h at 45 °C/200 mbar) and irradiated with UV light for 20 min before use.

7.4.5.2 SEM

HLCs were plated and maintained on uncoated and PU134 coated PFCs for 15 days. At day 16, HLCs maintained on both matrices were fixed and visualised as described in Chapter 7.3.5.

7.4.5.3 Drug inducibility

HLCs were incubated with PFC in its native form or coated with PU134. HLCs were cultured on these different substrates for 13 days as described in Chapter 7.4.3, changing media every second day, before assessing HLCs drug inducibility. At day 14 the cultures were incubated in the presence or absence of a known CYP3A4

inducer, phenobarbital (0.4 mM), for 48 h prior to measurement of CYP3A4 activity. On day 16, HLCs were incubated with hepatocyte culture media supplemented with 50 μM of CYP3A4 pGlo ™ substrate as per the manufactureris instructions. 4 h post-treatment a 50 μL sample of the supernatant was removed and read on a luminometer (POLARstar optima). CYP3A4 activity was expressed as relative light units (R.L.U.)/mg protein. * $p < 0.05$ by the Student's t-test. ($n = 3$).

7.5 Experimental for Chapter 5

HUVECs were purchases from Lonza, UK. The isolation and cultivation of EOCs, incubation with the polymer microarray, fixing and staining were carried out by Dr Olga Tura in the Centre for Regenerative Medicine (University of Edinburgh).

7.5.1 Polymer microarray manufacture

Polymer microarrays were prepared using the same conditions as described in Chapter 7.4.1.

7.5.2 Cell isolation and culture

7.5.2.1 Cell source and sampling

Cord blood (CB) products (20-50 mL) were aspirated from the umbilical placental veins from normal caesarean deliveries and collected into heparin. Appropriate ethics committee approval was obtained and written informed consent from each patient.

7.5.2.2 Mononuclear cell isolation

MNCs were separated by buoyant density centrifugation of blood samples over Histopaque (1.077 g/ml; Sigma Diagnostics, UK). Once isolated, EOCs culture was performed as described.[193] Briefly, a minimum of 10-30 x 10^6 MNCs were resuspended in endothelial growth medium (EGM)-2 medium (Cambrex) and plated onto type 1 collagen six-well tissue culture wells (BD Bioscience). The cells were incubated at 37 °C with 5% CO_2 for 3-4 weeks. Medium was changed every 2 days for 7 days and then twice a week until first passage. Thereafter cells were passaged until the incubation with the polymer microarrays.

7.5.3 Scanning for cell binding

EOCs and HUVECs were harvested using 1 mL trypsin (0.050 % w/v)-EDTA (0.20 % w/v) in PBS. After 10 min at 37 ^oC, 5 mL of IMDM with 10% v/v FBS was added and cells were recovered by vigorous aspiration. Cells were counted and re-plated at 0.5 x 10^6 for 3 days on two identical polymer microarrays

(Chapter 7.5.1). The cells were fixed in 100% methanol for 10 min and blocked in 10% goat serum for 1 h after washing with PBS. 20 μL of directly conjugated monoclonal mouse anti-human CD31-PE antibody (BD, UK) was applied overnight at 4 °C. The cells were washed with PBS and finally mounted with DAPI-containing Vectashield hardest mounting medium (Vector Lab Ltd, UK). Image capture and cell binding quantification with the different polymers were carried out using DAPI and rhodamine channels as described in section 7.2.2.1. Complete EOC and HUVEC–polymer binding analysis is reported on CD (Supplementary Information, excel folder named "Chapter 5").

7.5.4 Polymer coating of coverslips

Flow cytometry analysis reported below was undertaken by Dr Olga Tura at the Centre for Regenerative Medicine, University of Edinburgh.

7.5.4.1 Coverslips preparation

Polymer-coated coverslips (19 mm diameter, CB00190RA1, Menzel-Gläser) were prepared using the conditions described previously in Chapter 7.4.4.1. Polymer coating of coverslips used 200 μL of the following three polyacrylates (119, 383 and 395) samples.

7.5.4.2 Flow cytometry analysis

EOCs and HUVECs were cultivated as previously described (Chapter 7.5.2.2) on the glass coverslips (Chapter 7.5.4.1), then directly stained and analysed for phenotypic expression of surface markers using anti-human monoclonal antibodies (MAbs) conjugated to phycoerythrin (PE), fluorescein isothiocynate (FITC), Peridin Chlorophylla protein (PerCP) or Allophycocyanin (APC) as described.[196] Harvested cells were resuspended in FACS-PBS (PBS supplemented with 0.1% v/v FBS and 0.1% w/v sodium azide), at 1 x 10^7 cells/mL for use. Aliquots of up to 1 x 10^6 cells were incubated for 30 min in RT at the dark with 5 μL of untouched antibody (determined by titration), of directly conjugated antibody (below listed**,** Chapter 7.5.4.2.1). Cells were washed twice to remove unbound antibody and resuspended in 300 μL FACS-PBS solution. Unstained cells were included as controls. Dead and

apoptotic cells and debris were excluded from analysis using an electronic 'live' gate on forward scatter and side scatter parameters. Data for 5, 000 - 100,000 'live' events were acquired for each sample using a FACSCaliber cytometer equipped with a 488 nm and 633 nm lasers and analysed using CellQuest software (Becton Dickinson).[249]

7.5.4.2.1 Antibodies

The anti-human monoclonal antibodies (MAbs) used for flow cytometry included anti-CD34-FITC, anti-CD45-PerCP, anti-CD49d-FITC, anti-CD49e-APC (Becton Dickinson, UK); anti-CD133-APC (Myltenyi Biotec, UK); anti-CD29-FITC, anti-CD54 (ICAM-1) and anti-CD50 (ICAM-3) (Caltag, UK).

7.5.5 Sponge experiments

The isolation and culture of EOCs (see Chapter 7.5.2) and incubation with the sponges were carried out by Dr Olga Tura in the Centre for Regenerative Medicine (University of Edinburgh). The animal experiments, Chalkley count and haemoglobin assays reported below were undertaken by Dr Olga Tura and Mrs Kay Samuel in the Centre for Regenerative Medicine (University of Edinburgh). All animal experiments were undertaken with an approved licence from the Animal Scientific Procedure Division of the Home Office, London, UK.

7.5.5.1 *In vitro*

Two 1 cm^3 sponges were dip coated in 2 mL of PA383 solution (2.0% w/v in THF) and GFR-MG respectively. Sponges were dried under vacuum (12 h at 45 °C/200 mbar) and irradiated with UV light for 20 min. One of each type of coated sponge was impregnated with 1 x 10^7/mL of EOCs and the other one using the same concentration of HUVECs in complete EBM-2 medium (Lonza, UK).[196] After overnight incubation, cells in both sponges were fixed and SEM analysed as described in Chapter 7.3.5.

7.5.5.2 *In vivo* (subcutaneous sponge implantation)

Male C57B6J mice aged 10-12 weeks were purchased from Charles River Laboratories (UK). Experimental procedures were approved by the University of

Edinburgh ethics committee and were authorized by the Home Office under the Animals (Scientific Procedures) Act 1986.

Mice were anesthetized with halothane two sterilized sponges (0.5 cm/1cm) were implanted subcutaneously on each flank. EOCs were incubated for overnight with native sponges or sponges impregnated with PA383 (Chapter 7.5.5.1). Each animal had an intervention-no-impregnated sponge (EOCs + native sponge) on one side and a placebo-impregnated sponge (EOCs + PA383) on the other. Twenty days after implantation, mice were killed by asphyxiation in CO_2 and sponges excised were trisected and analysed as follows:

SEM analysis

The first section was fixed and analysed *via* SEM microscopy as previously described (Chapter 7.3.5).

Chalkley count

A second frozen section was fixed in 10% v/v neutral buffered formalin, embedded in paraffin. Sections (5 μm) were mounted on poly-L-lysine-coated slides and stained with hematoxylin/eosin for identification of blood vessels density within Chalkley counts by using the mean of the triplicate values as described.[215]

Haemoglobin assay

The third frozen section was weighed, homogenized in 1 mL of sterile PBS, and centrifuged (2,000 g for 10 min) to measure the amount of haemoglobin present in the sample. Following the manufacturer's instructions (Bioassay systems, QuantiChrom) haemoglobin was converted into a uniform colored end product which its intensity was measured at 400 nm. The colour intensity is directly proportional to the amount of haemoglobin concentration in the sample.[217, 218]

7.5.6 Stent experiment

Two coronary stents (Abbott Laboratorieas) were cleaned with THF. One stent was placed into 2 mL of PA383 solution (2.0% w/v in THF) for 5 min. This stent was dried under vacuum (12 h at 45 ºC/200 mbar) and together with the uncoated stent

was irradiated with UV light for 20 min before using. Both coated and uncoated stents impregnated with 1 x 10^7/mL of EOCs in complete EBM-2 medium (Lonza, UK). After overnight incubation, cells in both stents were fixed and SEM analysed as described in Chapter 7.3.5.

7.6 Experimental for Chapter 6

The work reported in this Chapter was undertaken at the Bradley Group, School of Chemistry, University of Edinburgh by Mei Wu and myself.

7.6.1 Polymer microarray fabrication and growth of bacteria

Polymer microarrays were prepared using 372 members of the polyurethane and polyacrylate libraries previously described (Chapter 7.4.1).

Salmonella SL1344 and *E. coli* W3110 transformed with pHC60 (to be referred to as *Salmonella*-GFP and *E. coli*-GFP) constitutively express GFP and were grown overnight with aeration at 37 °C or 30 °C respectively in Luria-Bertani (LB) broth containing tetracycline (10 $\mu g.mL^{-1}$). Cultures were collected by centrifugation at 15,000 rpm for 5 min, washed with fresh LB broth and diluted tenfold to a final concentration of approximately (2×10^8 CFU mL^{-1}) for microarray binding studies.

7.6.2 Bacteria binding analysis

6 mL (12×10^8 CFU mL^{-1}) of either *Salmonella*-GFP or *E. coli*-GFP were added to duplicate polymer microarrays in a four-well plate (Nunc) and incubated 12 h (except where stated) at RT. Subsequently, the polymer microarray slides were washed vigorously three times with PBS, rinsed in deionised water, and dried with a stream of air. A GeneFrame and coverslip (1.9 x 6.0 cm, AB-0630, Thermo Scientific) was then applied to each slide. Polymer microarrays were analysed using a BioAnalyzer 4F/4S scanner with a FITC filter. Bacterial adhesion was evaluated *via* integration of the fluorescence intensity of a spot (300 μm in diameter) after background correction. The average and the standard deviation for sets of four identical polymer features were determined, with the reproducibility between two identical microarrays evaluated by a student t-test. Polymers with p-values < 0.001 and 6 degrees of freedom were considered statistically significant. Results for *E. coli*-GFP and *Salmonella*-GFP-polymer binding analysis are reported on CD (Supplementary Information, excel folder named “Chapter 6”).

7.6.2.1 SEM

Bacteria on the polymer samples were washed twice with 0.1 M cacodylate buffer and then fixed and visualised as described in Chapter 7.3.5.

7.6.2.2 Polymer microarray for reproducibility binding studies

Polymer microarrays were prepared using the same conditions as described in Chapter 7.2.1. However, the 8 members of the polyurethane and polyacrylate libraries were printed using 8 aQu solid pins (K2785, Genetix), following a four-replicate pattern with 8 single fields of 5 x 5 spots with a pitch distance of 900 µm (y-axis) and 900 µm (x-axis). *Salmonella* imaging was carried out using a HCS platform with Pathfinder^{TM} software package (IMSTAR) as described in Chapter 7.2.2.1.

7.6.2.3 Polymer microarrays for time-dependent binding

Polymer microarrays with letters U and K were fabricated with PU104 and PA311 using 1 aQu solid pins (K2785, Genetix) in accordance with the same conditions as described in Chapter 7.6.2.2. *Salmonella*-GFP, prepared as in Chapter 7.6.2, were incubated for 4 h at RT on this array and scanned and imaged as described in Chapters 7.2.2.1and 7.6.2 respectively.

7.6.3 Coverslip scale-up

PA141 and PA331 were spin-coated onto grided glass coverslips (CELL-VU DRM 800) and incubated overnight with *Salmonella*-GFP at RT and imaged *via* SEM as described in Chapter 7.3.5. The number of bacteria in randomly selected sub-squares (100 µm x 100 µm), four for each coverslip, was counted with Image-Pro Plus 4.5 (Media Cybernetics, Silver Spring, MD)[250] on the coated and non-polymer coated as a control (**Figure 7.5**). The software was instructed to count the number of "objects" in the image, in this case the number of bacteria. The data were then exported to excel and reproducibility was determined by calculating the average and the standard deviation for the four identical sub-squares.

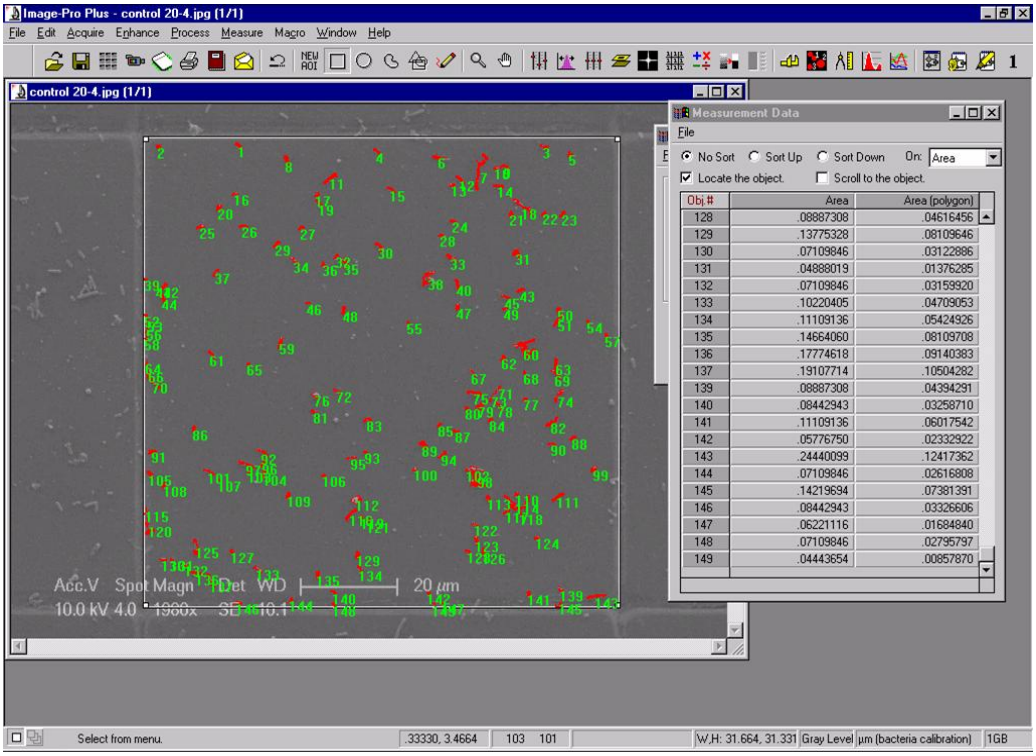

Figure 7.5 *Automated counting of Salmonella binding. The picture files were transferred to Image-Pro Plus for processing. In this example, the number of bacteria on one single square of the uncoated coverslip (control) was counted. Salmonella identified by Image-Pro Plus are in red with an associated number in green.*

Reference List

1. Clare, A. G., Materials science vs. ceramic engineering - Parasitic or symbiotic? *American Ceramic Society Bulletin* **2001,** 80, (9), 61-61.

2. Grainger, D. W., The Williams dictionary of biomaterials. *Materials Today* **1999,** 2, (3), 29-29.

3. Langer, R.; Tirrell, D. A., Designing materials for biology and medicine. *Nature* **2004,** 428, (6982), 487-492.

4. Dobrzanski, L. A., Significance of materials science for the future development of societies. *Journal of Materials Processing Technology* **2006,** 175, (1-3), 133-148.

5. Putti, V., Historical Prostheses. *The Journal of Hand Surgery: Journal of the British Society for Surgery of the Hand* **2005,** 30, (3), 310-325.

6. Drucker Charles, B., Ambroise Pare and the birth of the gentle art of surgery. *The Yale Journal of Biology and Medicine* **2008,** 81, (4), 199-202.

7. Carter, K. C., Toward a rational history of medical science. *Studies In History and Philosophy of Science Part A* **1995,** 26, (3), 493-502.

8. Arunakul, N. R., Dr. Joseph Lister: the founder of antiseptic surgery. *Giants in the Field of Microbiology Serie* **2003,** 10, (2), 71-72.

9. Refior, H. J.; Parhofer, R.; Ungethüm, M.; Biömer, W., Special problems of cementless fixation of total hip-joint endoprostheses with reference to the PM type. *Archives of Orthopaedic and Trauma Surgery* **1988,** 107, (3), 158-171.

10. Moukwa, M., The development of polymer-based biomaterials since the 1920s. *Jom-Journal of the Minerals Metals & Materials Society* **1997,** 49, (2), 46-50.

11. Hyman, W., Book reviews. *Annals of Biomedical Engineering* **1987,** 15, (5), 525-532.

12. Binyamin, G.; Shafi, B. M.; Mery, C. M., Biomaterials: A primer for surgeons. *Seminars in Pediatric Surgery* **2006,** 15, (4), 276-283.

13. Seal, B. L.; Otero, T. C.; Panitch, A., Polymeric biomaterials for tissue and organ regeneration. *Materials Science and Engineering: R: Reports* **2001,** 34, (4-5), 147-230.

14. Pizzoferrato, A.; Ciapetti, G.; Stea, S.; Cenni, E.; Arciola, C. R.; Granchi, D.; Savarino, L., Cell culture methods for testing biocompatibility. *Clinical Materials* **1994,** 15, (3), 173-190.

15. Kirkpatrick, C. J.; Bittinger, F.; Wagner, M.; Kohler, H.; van Kooten, T. G.; Klein, C. L.; Otto, M., Current trends in biocompatibility testing. *Proceedings of the Institution of Mechanical Engineers Part H-Journal of Engineering in Medicine* **1998,** 212, (H2), 75-84.

16. Langer, R., The evolution of biomaterials. *Nature Materials* **2009,** 8, (6), 444-445.

17. Williams, D. F., On the nature of biomaterials. *Biomaterials* **2009,** 30, (30), 5897-5909.

18. Scott A. Guelcher, H. J. O., *An Introduction to Biomaterials*. Hardcover ed.; CRC Press: New York, **2006**; p 553.

19. Piskin, E., Biodegradable Polymers as Biomaterials. *Journal of Biomaterials Science-Polymer Edition* **1995,** 6, (9), 775-795.

20. Geetha, M.; Singh, A. K.; Asokamani, R.; Gogia, A. K., Ti based biomaterials, the ultimate choice for orthopaedic implants - A review. *Progress in Materials Science* **2009,** 54, (3), 397-425.

21. Lee, J. H.; Ryu, H. S.; Lee, D. S.; Hong, K. S.; Chang, B. S.; Lee, C. K., Biomechanical and histomorphometric study on the bone-screw interface of bioactive ceramic-coated titanium screws. *Biomaterials* **2005,** 26, (16), 3249-3257.

22. Best, S. M.; Porter, A. E.; Thian, E. S.; Huang, J., Bioceramics: Past, present and for the future. *Journal of the European Ceramic Society* **2008,** 28, (7), 1319-1327.

23. Suchanek, W.; Yashima, M.; Kakihana, M.; Yoshimura, M., Hydroxyapatite ceramics with selected sintering additives. *Biomaterials* **1997,** 18, (13), 923-933.

24. Vallet-Regí, M., Evolution of bioceramics within the field of biomaterials. *Comptes Rendus Chimie* **in Press**, doi:10.1016/j.crci.2009.03.004.

25. Nair, L. S.; Laurencin, C. T., Biodegradable polymers as biomaterials. *Progress in Polymer Science* **2007,** 32, (8-9), 762-798.

26. Quatela, V. C.; Chow, J., Synthetic Facial Implants. *Facial Plastic Surgery Clinics of North America* **2008,** 16, (1), 1-10.

27. Attmann, T.; Steinseifer, U.; Cremer, J.; Lutter, G., Percutaneous valve replacement: a novel low-profile polyurethane valved stent. *European Journal of Cardio-Thoracic Surgery* **2006,** 30, (2), 379-379.

28. Andrew, F. H., Use of organ cultures to evaluate biodegradation of polymer implant materials. *Journal of Biomedical Materials Research* **1973,** 7, (2), 205-214.

29. Gogolewski, S., Selected topics in biomedical polyurethanes. A review. *Colloid & Polymer Science* **1989,** 267, (9), 757-785.

30. Santerre, J. P.; Woodhouse, K.; Laroche, G.; Labow, R. S., Understanding the biodegradation of polyurethanes: From classical implants to tissue engineering materials. *Biomaterials* **2005,** 26, (35), 7457-7470.

31. German Patent 728.981 (**1937**) I.G. Farben.

32. Mirkovitch, V.; Akutsu, T.; Kolff, W. J., Intracardiac thrombosis on plastics in relation to construction of artificial valves. *Jounal of Applied Physiology* **1961,** 16, (2), 381-384.

33. Andreas, E.; Ze, Z.; Robert, G.; Gaétan, L.; Louis, G.; Dominique De La, F.; Michel, B.; Martin, W. K., A new generation of polyurethane vascular prostheses: Rara Avis or Ignis Fatuus? *Journal of Biomedical Materials Research* **1999,** 48, (4), 546-558.

34. Santerre, J. P.; Labow, R. S., The effect of hard segment size on the hydrolytic stability of polyether-urea-urethanes when exposed to cholesterol esterase. *Journal of Biomedical Materials Research* **1997,** 36, (2), 223-232.

35. Goto, A.; Fukuda, T., Kinetics of living radical polymerization. *Progress in Polymer Science* **2004,** 29, (4), 329-385.

36. Zeng, W. R.; Li, S. F.; Chow, W. K., Preliminary studies on burning behavior of polymethylmethacrylate (PMMA). *Journal of Fire Sciences* **2002,** 20, (4), 297-317.

37. Cui, L. L.; Jiang, J.; Xia, Z. G.; Chen, G. J.; Wang, Z. Z., Charge storage and transport in polymethylmethacrylate (PMMA) film. *Journal of Electrostatics* **1998,** 44, (1-2), 61-65.

38. Park, J. B., Acrylic bone cement: in vitro and in vivo property-structure relationship--a selective review. *Annals of Biomedical Engineering* **1983,** 11, (3-4), 297-312.

39. Langer, R., Biomaterials and biomedical engineering. *Chemical Engineering Science* **1995,** 50, (24), 4109-4121.

40. Mizomoto, H. The synthesis and screening of polymer libraries using a high throughput approach (**2004**). PhD thesis, University of Southampton,

Southampton, UK.

41. Heikkilä, J. T.; Aho, A. J.; Kangasniemi, I.; Yli-Urpo, A., Polymethylmethacrylate composites: disturbed bone formation at the surface of bioactive glass and hydroxyapatite. *Biomaterials* **1996,** 17, (18), 1755-1760.

42. Santin, M.; Huang, S. J.; Iannace, S.; Ambrosio, L.; Nicolais, L.; Peluso, G., Synthesis and characterization of a new interpenetrated poly(2-hydroxyethylmethacrylate)-gelatin composite polymer. *Biomaterials* **1996,** 17, (15), 1459-1467.

43. Yañez, F.; Concheiro, A.; Alvarez-Lorenzo, C., Macromolecule release and smoothness of semi-interpenetrating PVP-pHEMA networks for comfortable soft contact lenses. *European Journal of Pharmaceutics and Biopharmaceutics* **2008,** 69, (3), 1094-1103.

44. Commission, E., Medical device directive (93/42/CEE). In Official Journal of the European Communities EC N L169, p. 1, Ed. *Official Journal of the European Communities*: **1993**.

45. Ramakrishna, S.; Mayer, J.; Wintermantel, E.; Leong, K. W., Biomedical applications of polymer-composite materials: a review. *Composites Science and Technology* **2001,** 61, (9), 1189-1224.

46. Carlson, M. D. A. N.; Stewart, M. D. W. C.; Tso, M. D. P. C., Intraocular Lens Complications Requiring Removal or Exchange. *Survey of Opthalmology* **1998,** 42, (5), 417-440.

47. Basmadjian, D.; Sefton, M. V.; Baldwin, S. A., Coagulation on biomaterials in flowing blood: some theoretical considerations. *Biomaterials* **1997,** 18, (23), 1511-1522.

48. Dhruv, H. D. Controlling nonspecific adsorption of proteins at bio-Interfaces for biosensor and biomedical applications (**2009**). PhD thesis, Utah State University Logan, Utah, USA.

49. Anderson, J. M.; Rodriguez, A.; Chang, D. T., Foreign body reaction to biomaterials. *Seminars in Immunology* **2008,** 20, (2), 86-100.

50. Ratner, B. D.; Bryant, S. J., Biomaterials: Where we have been and where we are going. *Annual Review of Biomedical Engineering* **2004,** 6, 41-75.

51. Teruo, O.; Shoji, N.; Isao, S.; Toshihiro, A.; Yasuhisa, S.; Kazunori, K.; Teiji, T., Effect of hydrophilic and hydrophobic microdomains on mode of interaction between block polymer and blood platelets. *Journal of Biomedical Materials Research* **1981,** 15, (3), 393-402.

52. Tzu-Wen, C.; Dong-Tsamn, L.; Feng-Huei, L., Immobilization of NaIO4-treated heparin on PEG-modified 316L SS surface for high anti-thrombin-III

binding *Journal of Biomedical Materials Research Part A* **2008,** 86A, (3), 648-661.

53. Zhang, F.; Kang, E. T.; Neoh, K. G.; Wang, P.; Tan, K. L., Surface modification of stainless steel by grafting of poly(ethylene glycol) for reduction in protein adsorption. *Biomaterials* **2001,** 22, (12), 1541-1548.

54. Langer, R.; Peppas, N. A., Advances in biomaterials, drug delivery, and bionanotechnology. *Aiche Journal* **2003,** 49, (12), 2990-3006.

55. Sawhney, A. S.; Pathak, C. P.; Hubbell, J. A., Bioerodible hydrogels based on photopolymerized poly(ethylene glycol)-co-poly(.alpha.-hydroxy acid) diacrylate macromers. *Macromolecules* **2002,** 26, (4), 581-587.

56. Behravesh, E.; Shung, A. K.; Jo, S.; Mikos, A. G., Synthesis and characterization of triblock copolymers of methoxy poly(ethylene glycol) and poly(propylene fumarate). *Biomacromolecules* **2001,** 3, (1), 153-158.

57. Gray, J. E.; Norton, P. R.; Griffiths, K., Surface modification of a biomedical poly(ether)urethane by a remote air plasma. *Applied Surface Science* **2003,** 217, (1-4), 210-222.

58. Fodor, S. P.; Read, J. L.; Pirrung, M. C.; Stryer, L.; Lu, A. T.; Solas, D., Light-directed, spatially addressable parallel chemical synthesis. *Science* **1991,** 251, (4995), 767-773.

59. Pease, A. C.; Solas, D.; Sullivan, E. J.; Cronin, M. T.; Holmes, C. P.; Fodor, S. P., Light-generated oligonucleotide arrays for rapid DNA sequence analysis. *Proceedings of the National Academy of Sciences of the United States of America* **1994,** 91, (11), 5022-5026.

60. Kulesh, D. A.; Clive, D. R.; Zarlenga, D. S.; Greene, J. J., Identification of interferon-modulated proliferation-related cDNA sequences. *Proceedings of the National Academy of Sciences of the United States of America* **1987,** 84, (23), 8453-8457.

61. Schena, M.; Shalon, D.; Davis, R. W.; Brown, P. O., Quantitative monitoring of gene-expression patterns with a complementary-DNA microarray. *Science* **1995,** 270, (5235), 467-470.

62. Lashkari, D. A.; DeRisi, J. L.; McCusker, J. H.; Namath, A. F.; Gentile, C.; Hwang, S. Y.; Brown, P. O.; Davis, R. W., Yeast microarrays for genome wide parallel genetic and gene expression analysis. *Proceedings of the National Academy of Sciences of the United States of America* **1997,** 94, (24), 13057-13062.

63. Adomas, A.; Heller, G.; Olson, A.; Osborne, J.; Karlsson, M.; Nahalkova, J.; Van Zyl, L.; Sederoff, R.; Stenlid, J.; Finlay, R.; Asiegbu, F. O., Comparative analysis of transcript abundance in Pinus sylvestris after challenge with a

saprotrophic, pathogenic or mutualistic fungus. *Tree Physiol* **2008,** 28, (6), 885-897.

64. Hacia, J. G.; Fan, J. B.; Ryder, O.; Jin, L.; Edgemon, K.; Ghandour, G.; Mayer, R. A.; Sun, B.; Hsie, L.; Robbins, C. M.; Brody, L. C.; Wang, D.; Lander, E. S.; Lipshutz, R.; Fodor, S. P. A.; Collins, F. S., Determination of ancestral alleles for human single-nucleotide polymorphisms using high-density oligonucleotide arrays. *Nature Genetics* **1999,** 22, (2), 164-167.

65. Thomas, P. D.; Ernest, V. C.; Richard, L. D.; Paola, G.; Edward, S. R.; Teresa, W. W., DNA microarrays and likelihood ratio bioinformatic methods: discovery of human melanocyte biomarkers. *Pigment Cell Research* **2003,** 16, (3), 245-253.

66. Crowther, D. J., Applications of microarrays in the pharmaceutical industry. *Current Opinion in Pharmacology* **2002,** 2, (5), 551-554.

67. Zhu, H.; Snyder, M., Protein chip technology. *Current Opinion in Chemical Biology* **2003,** 7, (1), 55-63.

68. Uttamchandani, M.; Wang, J.; Yao, S. Q., Protein and small molecule microarrays: powerful tools for high-throughput proteomics. *Molecular Biosystems* **2006,** 2, (1), 58-68.

69. Feizi, T.; Fazio, F.; Chai, W.; Wong, C.-H., Carbohydrate microarrays - a new set of technologies at the frontiers of glycomics. *Current Opinion in Structural Biology* **2003,** 13, (5), 637-645.

70. Kononen, J.; Bubendorf, L.; Kallioniemi, A.; Barlund, M.; Schraml, P.; Leighton, S.; Torhorst, J.; Mihatsch, M. J.; Sauter, G.; Kallioniemi, O. P., Tissue microarrays for high-throughput molecular profiling of tumor specimens. *Nature Medicine* **1998,** 4, (7), 844-847.

71. Fernandes, T. G.; Kwon, S.-J.; Lee, M.-Y.; Clark, D. S.; Cabral, J. M. S.; Dordick, J. S., On-chip, cell-based microarray immunofluorescence assay for high-throughput analysis of target proteins. *Analytical Chemistry* **2008,** 80, (17), 6633-6639.

72. Lecuit, T.; Lenne, P.-F., Cell surface mechanics and the control of cell shape, tissue patterns and morphogenesis. *Nature Reviews Molecular Cell Biology* **2007,** 8, (8), 633-644.

73. Smith, J. R.; Knight, D.; Kohn, J.; Rasheed, K.; Weber, N.; Kholodovych, V.; Welsh, W. J., Using surrogate modeling in the prediction of fibrinogen adsorption onto polymer surfaces. *Journal of Chemical Information and Computer Sciences* **2004,** 44, (3), 1088-1097.

74. Michael, A. R. M.; Richard, H.; Ulrich, S. S., Combinatorial methods, automated synthesis and high-throughput screening in polymer research: The

evolution continues. *Macromolecular Rapid Communications* **2004,** 25, (1), 21-33.

75. Hook, A. L.; Anderson, D. G.; Langer, R.; Williams, P.; Davies, M. C.; Alexander, M. R., High throughput methods applied in biomaterial development and discovery. *Biomaterials* **2010,** 31, (2), 187-198.

76. Anderson, D. G.; Levenberg, S.; Langer, R., Nanoliter-scale synthesis of arrayed biomaterials and application to human embryonic stem cells. *Nature Biotechnology* **2004,** 22, (7), 863-866.

77. Anderson, D. G.; Putnam, D.; Lavik, E. B.; Mahmood, T. A.; Langer, R., Biomaterial microarrays: rapid, microscale screening of polymer-cell interaction. *Biomaterials* **2005,** 26, (23), 4892-4897.

78. Tourniaire, G.; Collins, J.; Campbell, S.; Mizomoto, H.; Ogawa, S.; Thaburet, J.-F.; Bradley, M., Polymer microarrays for cellular adhesion. *Chemical Communications* **2006**, (20), 2118-2120.

79. Jose, A. J. Synthesis and Screening of biocompatible polymer using a multiparallel approach (**2005**). PhD Thesis, University of Southampton, Southampton, UK.

80. Tourniaire, G. Polymer microarray-development and applications (**2006**). PhD Thesis, University of Edinburgh, Edinburgh, UK.

81. Zhang, R.; Liberski, A.; Khan, F.; Diaz-Mochon, J. J.; Bradley, M., Inkjet fabrication of hydrogel microarrays using in situ nanolitre-scale polymerisation. *Chemical Communications* **2008,** 21, (11), 1317-1319.

82. Liberski, A.; Zhang, R.; Bradley, M., Inkjet fabrication of polymer microarrays and grids-solving the evaporation problem. *Chemical Communications* **2009**, (3), 334-336.

83. Tourniaire, G.; Diaz-Mochon, J. J.; Bradley, M., Fingerprinting polymer microarrays. *Combinatorial Chemistry & High Throughput Screening* **2009,** 12, (7), 690-696.

84. Khomyakova, E. B.; Dreval, E. V.; Papin, A. A.; Soussaline, F. P., OSA microarray reader instrumentation and its applications for registration of on-chip real-time reactions. *IRBM* 28, (5-6), 230-234.

85. Chen, G.; Liu, D.; Maruyama, N.; Ohgushi, H.; Tanaka, J.; Tateishi, T., Cell adhesion of bone marrow cells, chondrocytes, ligament cells and synovial cells on a PLGA-collagen hybrid mesh. *Materials Science and Engineering: C* **2004,** 24, (6-8), 867-873.

86. Rimpelova, S.; Kasalkova, N.; Svorcik, V.; Ruml, T., Cell adhesion on artificial materials modified for tissue engineering. *The Febs Journal* **2009,** 276, 339-

339.

87. Stevens, M. M.; George, J. H., Exploring and engineering the cell surface interface. *Science* **2005,** 310, (5751), 1135-1138.

88. Sundelacruz, S.; Kaplan, D. L., Stem cell- and scaffold-based tissue engineering approaches to osteochondral regenerative medicine. *Seminars in Cell & Developmental Biology* **2009,** 20, (6), 646-655.

89. Wozniak, M. A.; Modzelewska, K.; Kwong, L.; Keely, P. J., Focal adhesion regulation of cell behavior. *Biochimica et Biophysica Acta - Molecular Cell Research* **2004,** 1692, (2-3), 103-119.

90. Furong, T.; Hossein, H.; Mohsen, H.; Ali, K.; Yoshiro, Y.; Giovani Gomez, E.; Hisatoshi, K., Quantitative analysis of cell adhesion on aligned micro- and nanofibers. *Journal of Biomedical Materials Research Part A* **2008,** 84A, (2), 291-299.

91. Garcia, A. J.; Vega, M. D.; Boettiger, D., Modulation of cell proliferation and differentiation through substrate-dependent changes in fibronectin conformation. *Molecular Biology of the Cell* **1999,** 10, (3), 785-798.

92. Sivakumar, R., On the relevance and requirements of biomaterials. *Bulletin of Materials Science* **1999,** 22, (3), 647-655.

93. Courtney, T.; Sacks, M. S.; Stankus, J.; Guan, J.; Wagner, W. R., Design and analysis of tissue engineering scaffolds that mimic soft tissue mechanical anisotropy. *Biomaterials* **2006,** 27, (19), 3631-3638.

94. Geiger, B.; Bershadsky, A.; Pankov, R.; Yamada, K. M., Transmembrane crosstalk between the extracellular matrix and the cytoskeleton. *Nature Reviews Molecular Cell Biology* **2001,** 2, (11), 793-805.

95. Humphries, M. J., Integrin structure. *Biochemical Society Transactions* **2000,** 28, (4), 311-339.

96. Löster, K.; Horstkorte, R., Enzymatic quantification of cell-matrix and cell-cell adhesion. *Micron* **2000,** 31, (1), 41-53.

97. Geiger, B.; Spatz, J. P.; Bershadsky, A. D., Environmental sensing through focal adhesions. *Nature Reviews Molecular Cell Biology* **2009,** 10, (1), 21-33.

98. Magie, C. R.; Martindale, M. Q., Cell-cell adhesion in the Cnidaria: insights into the evolution of tissue morphogenesis. *The Biological Bulletin* **2008,** 214, (3), 218-232.

99. Jean-François, T.; Hitoshi, M.; Mark, B., High-Throughput Evaluation of the Wettability of Polymer Libraries. *Macromolecular Rapid Communications* **2004,** 25, (1), 366-370.

100. Chang, H. Y.; Chi, J.-T.; Dudoit, S.; Bondre, C.; van de Rijn, M.; Botstein, D.; Brown, P. O., Diversity, topographic differentiation, and positional memory in human fibroblasts. *Proceedings of the National Academy of Sciences of the United States of America* **2002,** 99, (20), 12877-12882.

101. Lamme, E. N.; van Leeuwen, R. T. J.; Jonker, A.; van Marle, J.; Middelkoop, E., Living skin substitutes: survival and function of fibroblasts seeded in a dermal substitute in experimental wounds. *Journal of Investigative Dermatology* **1998,** 111, (6), 989-995.

102. Sakiyama-Elbert, S. E.; Hubbell, J. A., Functional biomaterials: design of novel biomaterials. *Annual Review of Materials Research* **2001,** 31, (1), 183-201.

103. Gallagher, W. M.; Lynch, I.; Allen, L. T.; Miller, I.; Penney, S. C.; O'Connor, D. P.; Pennington, S.; Keenan, A. K.; Dawson, K. A., Molecular basis of cell-biomaterial interaction: Insights gained from transcriptomic and proteomic studies. *Biomaterials* **2006,** 27, (35), 5871-5882.

104. Sherratt, M. J.; Baldock, C.; Morgan, A.; Kielty, C. M., The morphology of adsorbed extracellular matrix assemblies is critically dependent on solution calcium concentration. *Matrix Biology* **2007,** 26, (3), 156-166.

105. Ferdous, K.; Rahul, S. T.; Richard. , O. C. O.; Mark, B., Versatile Biocompatible Polymer Hydrogels: Scaffolds for Cell Growth13. *Angewandte Chemie International Edition* **2009,** 48, (5), 978-982.

106. Pucci, F.; Geslin, E.; Barras, C.; Morigi, C.; Sabbatini, A.; Negri, A.; Jorissen, F. J., Survival of benthic foraminifera under hypoxic conditions: Results of an experimental study using the CellTracker Green method. *Marine Pollution Bulletin* **2009,** 59, (8-12), 336-351.

107. Singh, S.; Dwarakanath, B. S.; Mathew, T. L., DNA ligand Hoechst-33342 enhances UV induced cytotoxicity in human glioma cell lines. *Journal of Photochemistry and Photobiology B: Biology* **2004,** 77, (1-3), 45-54.

108. Cooper, J. A., Effects of cytochalasin and phalloidin on actin. *The Journal of Cell Biology* **1987,** 105, (4), 1473-1478.

109. Landim-Alvarenga, F.; Lima-Neto, J.; Dores, C.; Golim, M.; Silva, V., Analysis of cell viability and cellular cycle in equine fibroblasts cultured in vitro. *Biology of Reproduction* **2007**, 177-177.

110. Kato, S.; Akagi, T.; Sugimura, K.; Kishida, A.; Akashi, M., Evaluation of biological responses to polymeric biomaterials by RT-PCR analysis IV: study of c-myc, c-fos and p53 mRNA expression. *Biomaterials* **2000,** 21, (5), 521-527.

111. Kato, S.; Akagi, T.; Sugimura, K.; Kishida, A.; Akashi, M., Evaluation of biological responses to polymeric biomaterials by RT-PCR analysis III: Study

of HSP 70, 90 and 47 mRNA expression. *Biomaterials* **1998,** 19, (7-9), 821-827.

112. Gao, T.; Aro, H. T.; Ylänen, H.; Vuorio, E., Silica-based bioactive glasses modulate expression of bone morphogenetic protein-2 mRNA in Saos-2 osteoblasts in vitro. *Biomaterials* **2001,** 22, (12), 1475-1483.

113. Korke, R.; Rink, A.; Seow, T. K.; Chung, M. C. M.; Beattie, C. W.; Hu, W.-S., Genomic and proteomic perspectives in cell culture engineering. *Journal of Biotechnology* **2002,** 94, (1), 73-92.

114. Xynos, I. D.; Edgar, A. J.; Buttery, L. D. K.; Hench, L. L.; Polak, J. M., Ionic products of bioactive glass dissolution increase proliferation of human osteoblasts and induce insulin-like growth factor II mRNA expression and protein synthesis. *Biochemical and Biophysical Research Communications* **2000,** 276, (2), 461-465.

115. Ku, C.-H.; Browne, M.; Gregson, P. J.; Corbeil, J.; Pioletti, D. P., Large-scale gene expression analysis of osteoblasts cultured on three different Ti-6Al-4V surface treatments. *Biomaterials* **2002,** 23, (21), 4193-4202.

116. Carinci, F.; Volinia, S.; Pezzetti, F.; Francioso, F.; Tosi, L.; Piattelli, A., Titanium-cell interaction: analysis of gene expression profiling. *Journal of Biomedical Materials Research Part B: Applied Biomaterials* **2003,** 66B, (1), 341-346.

117. Allen, L. T.; Fox, E. J. P.; Blute, I.; Kelly, Z. D.; Rochev, Y.; Keenan, A. K.; Dawson, K. A.; Gallagher, W. M., Interaction of soft condensed materials with living cells: phenotype/transcriptome correlations for the hydrophobic effect. *Proceedings of the National Academy of Sciences of the United States of America* **2003,** 100, (11), 6331-6336.

118. Leif, C. A.; Kenneth, N.; Carl, G. G., K562 - A human erythroleukemic cell line. *International Journal of Cancer* **1979,** 23, (2), 143-147.

119. Pankov, R.; Yamada, K. M., Fibronectin at a glance. *Journal of Cell Science* **2002,** 115, (20), 3861-3863.

120. Mefti, N.; Haussy, B.; Ganghoffer, J. F., Mechanical modeling of the rolling phenomenon at the cell scale. *International Journal of Solids and Structures* **2006,** 43, (24), 7378-7392.

121. Podsypanina, K.; Du, Y.-C. N.; Jechlinger, M.; Beverly, L. J.; Hambardzumyan, D.; Varmus, H., Seeding and propagation of untransformed mouse mammary cells in the lung. *Science* **2008,** 321, (5897), 1841-1844.

122. Li, S. S.; Liu, Z.; Uzunel, M.; Sundqvist, K.-G., Endogenous thrombospondin-1 is a cell-surface ligand for regulation of integrin-dependent T-lymphocyte adhesion. *Blood* **2006,** 108, (9), 3112-3120.

123. Gabriella, R.; Perla, F.; Antonella, F.; Pietro, L. I.; Maria, T. S., Fibronectin facilitates adhesion of K562 leukemic cells normally growing in suspension to cationic surfaces. *Journal of Biomedical Materials Research* **2001,** 55, (1), 104-113.

124. Lozzio, B. B.; Lozzio, C. B., Properties and usefulness of the original K-562 human myelogenous leukemia cell line. *Leukemia Research* **1979,** 3, (6), 363-370.

125. Gilman-Sachs, A.; DuChateau, B. K.; Aslakson, C. J.; Wohlgemuth, G. P.; Kwak, J. Y.; Beer, A. E.; Beaman, K. D., Natural killer (NK) cell subsets and NK cell cytotoxicity in women with histories of recurrent spontaneous abortions. *American Journal of Reproductive Immunology* **1999,** 41, (1), 99-105.

126. Sandra, E. S.; Helena, C. K.; Eric, N.; Daniel, P. S.; Inka, W.; David, S., Improving methods of assessing natural killer cell cytotoxicity. *International Journal of Methods in Psychiatric Research* **2006,** 15, (1), 12-21.

127. Wang, J.-H.; Hung, C.-H.; Young, T.-H., Proliferation and differentiation of neural stem cells on lysine-alanine sequential polymer substrates. *Biomaterials* **2006,** 27, (18), 3441-3450.

128. Reid, R.; Fodor, A., Determining gene expression on a single pair of microarrays. *BMC Bioinformatics* **2008,** 9, (1), 489.

129. Sato, S.; Tomomori-Sato, C.; Banks, C. A. S.; Sorokina, I.; Parmely, T. J.; Kong, S. E.; Jin, J.; Cai, Y.; Lane, W. S.; Brower, C. S.; Conaway, R. C.; Conaway, J. W., Identification of Mammalian Mediator Subunits with Similarities to Yeast Mediator Subunits Srb5, Srb6, Med11, and Rox3. *The Journal of Biological Chemistry* **2003,** 278, (17), 15123-15127.

130. Lariviere, L.; Geiger, S.; Hoeppner, S.; Rother, S.; Straszer, K.; Cramer, P., Structure and TBP binding of the Mediator head subcomplex Med8-Med18-Med20. *Nature Structural & Molecular Biology* **2006,** 13, (10), 895-901.

131. Hartley, J. W.; Wolford, N. K.; Old, L. J.; Rowe, W. P., A new class of murine leukemia virus associated with development of spontaneous lymphomas. *Proceedings of the National Academy of Sciences of the United States of America* **1977,** 74, (2), 789-792.

132. Demoulin, J.-B.; Ericsson, J.; Kallin, A.; Rorsman, C.; Ronnstrand, L.; Heldin, C.-H., Platelet-derived Growth Factor Stimulates Membrane Lipid Synthesis Through Activation of Phosphatidylinositol 3-Kinase and Sterol Regulatory Element-binding Proteins. *The Journal of Biological Chemistry* **2004,** 279, (34), 35392-35402.

133. Ogata, H.; Goto, S.; Fujibuchi, W.; Kanehisa, M., Computation with the KEGG pathway database. *Biosystems* **1998,** 47, (1-2), 119-128.

134. Orton, R. J.; Sturm, O. E.; Vyshemirsky, V.; Calder, M.; Gilbert, D. R.; Kolch, W., Computational modelling of the receptor-tyrosine-kinase-activated MAR pathway. *Biochemical Journal* **2005,** 392, 249-261.

135. Leonard, W. J.; Lin, J.-X., Cytokine receptor signaling pathways. *Journal of Allergy and Clinical Immunology* **2000,** 105, (5), 877-888.

136. Sloan-Lancaster, J.; Steinberg, T. H.; Allen, P. M., Selective activation of the calcium signaling pathway by altered peptide ligands. *The Journal of Experimental Medicine* **1996,** 184, (4), 1525-1530.

137. Berman, A. E.; Kozova, N. I.; Morozevich, G. E., Integrins: Structure and signaling. *Biochemistry-Moscow* **2003,** 68, (12), 1284-1299.

138. Hallock, N., World News. *Journal of the Association for Laboratory Automation* **2006,** 11, (4), 19-44.

139. Karin, M.; Imbra, R. J.; Heguy, A.; Wong, G., Interleukin-1 Regulates Human Metallothionein Gene-Expression. *Molecular and Cellular Biology* **1985,** 5, (10), 2866-2869.

140. Thomson, J. A.; Kalishman, J.; Golos, T. G.; Durning, M.; Harris, C. P.; Becker, R. A.; Hearn, J. P., Isolation of a primate embryonic stem cell line. *Proceedings of the National Academy of Sciences of the United States of America* **1995,** 92, (17), 7844-7848.

141. Thomson, J. A.; Itskovitz-Eldor, J.; Shapiro, S. S.; Waknitz, M. A.; Swiergiel, J. J.; Marshall, V. S.; Jones, J. M., Embryonic Stem Cell Lines Derived from Human Blastocysts. *Science* **1998,** 282, (5391), 1145-1147.

142. Thomson, J. A.; Marshall, V. S., Primate embryonic stem cells. In *Current Topics in Developmental Biology*, Academic Press Inc: San Diego, 1998; Vol. 38, pp 133-165.

143. Reubinoff, B. E.; Pera, M. F.; Fong, C. Y.; Trounson, A.; Bongso, A., Embryonic stem cell lines from human blastocysts: somatic differentiation in vitro. *Nature Biotechnology* **2000,** 18, (4), 399-404.

144. Bo, D., Immunology of hematopoietic stem cell transplantation: a brief review of its history. *Immunological Reviews* **1997,** 157, (1), 5-12.

145. Langston, J. W., The promise of stem cells in Parkinson disease. *Journal of Clinical Investigation* **2005,** 115, (1), 23-25.

146. Bianco, P.; Robey, P. G., Stem cells in tissue engineering. *Nature* **2001,** 414, (6859), 118-121.

147. Allen, D. D.; Caviedes, R.; Caedenas, A. M.; Shimahara, T.; Segura-Aguilar, J.; Caviedes, P. A., Cell lines as in vitro models for drug screening and toxicity studies. *Drug Development and Industrial Pharmacy* **2008,** 34, (2), 234-234.

148. McNeish, J., Embryonic stem cells in drug discovery. *Nature Reviews Drug Discovery* **2004,** 3, (1), 70-80.

149. Chase, L. G.; Firpo, M. T., Development of serum-free culture systems for human embryonic stem cells. *Current Opinion in Chemical Biology* **2007,** 11, (4), 367-372.

150. Hoffman, L. M.; Carpenter, M. K., Characterization and culture of human embryonic stem cells. *Nature Biotechnology* **2005,** 23, (6), 699-708.

151. Jay, C. L.; Butt, Z.; Ladner, D. P.; Skaro, A. I.; Abecassis, M. M., A review of quality of life instruments used in liver transplantation. *Journal of Hepatology* **2009,** 51, (5), 949-959.

152. Hughes, B., Drug metabolism: Production line for hepatocytes. *Nature Reviews Drug Discovery* **2007,** 6, (10), 781-781.

153. Ballet, F., Hepatotoxicity in drug development: detection, significance and solutions. *Journal of Hepatology* **1997,** 26, (2), 26-36.

154. Rambhatla, L.; Chiu, C. P.; Kundu, P.; Peng, Y.; Carpenter, M. K., Generation of hepatocyte-like cells from human embryonic stem cells. *Cell Transplantation* **2003,** 12, (1), 1-11.

155. Lavon, N.; Yanuka, O.; Benvenisty, N., Differentiation and isolation of hepatic-like cells from human embryonic stem cells. *Differentiation* **2004,** 72, (5), 230-238.

156. Schwartz, R. E.; Linehan, J. L.; Painschab, M. S.; Hu, W.-S.; Verfaillie, C. M.; Kaufman, D. S., Defined conditions for development of functional hepatic cells from human embryonic stem cells. *Stem Cells and Development* **2005,** 14, (6), 643-655.

157. David, C. H.; Debiao, Z.; Judy, F.; Zoë, A. H.; Doris, M.; Alai, U.-U.; James, R. B.; Cliff, E.; James, A. R.; Roland, W.; Wei, C., Efficient differentiation of hepatocytes from human embryonic stem cells exhibiting markers recapitulating liver development *in vivo*. *Stem Cells* **2008,** 26, (4), 894-902.

158. Hay, D. C.; Fletcher, J.; Payne, C.; Terrace, J. D.; Gallagher, R. C. J.; Snoeys, J.; Black, J. R.; Wojtacha, D.; Samuel, K.; Hannoun, Z.; Pryde, A.; Filippi, C.; Currie, I. S.; Forbes, S. J.; Ross, J. A.; Newsome, P. N.; Iredale, J. P., Highly efficient differentiation of hESCs to functional hepatic endoderm requires ActivinA and Wnt3a signaling. *Proceedings of the National Academy of Sciences* **2008,** 105, (34), 12301-12306.

159. Li, J.; Li, L.-J.; Chao, H.-C.; Yang, Q.; Liu, X.-L.; Sheng, J.-F.; Yu, H.-Y.; Huang, J.-R., Isolation and short term cultivation of swine hepatocytes for bioartificial liver support system. *Hepatobiliary & Pancreatic Diseases International* **2005,** 4, (2), 249-53.

160. Hay, D. C.; Zhao, D.; Fletcher, J.; Hewitt, Z. A.; McLean, D.; Urruticoechea-Uriguen, A.; Black, J. R.; Elcombe, C.; Ross, J. A.; Wolf, R.; Cui, W., Efficient differentiation of hepatocytes from human embryonic stem cells exhibiting markers recapitulating liver development *in vivo*. *Stem Cells* **2008,** 26, (4), 894-902.

161. Tennent, G. A.; Brennan, S. O.; Stangou, A. J.; O'Grady, J.; Hawkins, P. N.; Pepys, M. B., Human plasma fibrinogen is synthesized in the liver. *Blood* **2007,** 109, (5), 1971-1974.

162. Ingenbleek, Y.; Young, V., Transthyretin (prealbumin) in health and disease: nutritional implications. *Annual Review of Nutrition* **1994,** 14, (1), 495-533.

163. O'Riordain, M. G.; Ross, J. A.; Fearon, K. C.; Maingay, J.; Farouk, M.; Garden, O. J.; Carter, D. C., Insulin and counterregulatory hormones influence acute-phase protein production in human hepatocytes. *American Journal of Physiology-Endocrinology and Metabolism* **1995,** 269, (2), 323-330.

164. Wheelhouse, N. M.; Dowidar, N.; Dejong, C. H. C.; Garden, O. J.; Powell, J. J.; Barber, M. D.; Sangster, K.; Maingay, J. P.; Ross, J. A., The effects of macrophage migratory inhibitory factor on acute-phase protein production in primary human hepatocytes. *International Journal of Molecular Medicine* **2006,** 18, (5), 957-961.

165. Bissell, D. M.; Arenson, D. M.; Maher, J. J.; Roll, F. J., Support of cultured-hepatocytes by a laminin-rich gel - evidence for a functionally significant subendothelial matrix in normal rat-liver. *Journal of Clinical Investigation* **1987,** 79, (3), 801-812.

166. Muraca, M., Cell therapy as support or alternative to liver transplantation. *Transplantation Proceedings* **2003,** 35, (3), 1047-1048.

167. Christina, C.; François, B.; Bharath, D. N.; Arno, W. T.; Mehmet, T.; Martin, L. Y., Hepatic tissue engineering for adjunct and temporary liver support: Critical technologies. *Liver Transplantation* **2004,** 10, (11), 1331-1342.

168. Keshava, C.; McCanlies, E. C.; Weston, A., CYP3A4 polymorphisms - potential risk factors for breast and prostate cancer: a HuGE review. *American Journal of Epidemiology* **2004,** 160, (9), 825-841.

169. Jiang, Y.; Jahagirdar, B. N.; Reinhardt, R. L.; Schwartz, R. E.; Keene, C. D.; Ortiz-Gonzalez, X. R.; Reyes, M.; Lenvik, T.; Lund, T.; Blackstad, M.; Du, J.; Aldrich, S.; Lisberg, A.; Low, W. C.; Largaespada, D. A.; Verfaillie, C. M., Pluripotency of mesenchymal stem cells derived from adult marrow. *Nature* **2002,** 418, (6893), 41-49.

170. Clarke, D.; Frisén, J., Differentiation potential of adult stem cells. *Current Opinion in Genetics & Development* **2001,** 11, (5), 575-580.

171. Pittenger, M. F.; Mackay, A. M.; Beck, S. C.; Jaiswal, R. K.; Douglas, R.; Mosca, J. D.; Moorman, M. A.; Simonetti, D. W.; Craig, S.; Marshak, D. R., Multilineage Potential of Adult Human Mesenchymal Stem Cells. *Science* **1999,** 284, (5411), 143-147.

172. Potten, C. S., Stem cells in gastrointestinal epithelium: numbers, characteristics and death. *Philosophical Transactions of the Royal Society of London. Series B: Biological Sciences* **1998,** 353, (1370), 821-830.

173. Toma, J. G.; Akhavan, M.; Fernandes, K. J. L.; Barnabe-Heider, F.; Sadikot, A.; Kaplan, D. R.; Miller, F. D., Isolation of multipotent adult stem cells from the dermis of mammalian skin. *Nature Cell Biology* **2001,** 3, (9), 778-784.

174. Muller-Sieburg, C. E.; Cho, R. H.; Thoman, M.; Adkins, B.; Sieburg, H. B., Deterministic regulation of hematopoietic stem cell self-renewal and differentiation. *Blood* **2002,** 100, (4), 1302-1309.

175. Muller-Sieburg, C. E.; Cho, R. H.; Karlsson, L.; Huang, J.-F.; Sieburg, H. B., Myeloid-biased hematopoietic stem cells have extensive self-renewal capacity but generate diminished lymphoid progeny with impaired IL-7 responsiveness. *Blood* **2004,** 103, (11), 4111-4118.

176. Sieburg, H. B.; Cho, R. H.; Dykstra, B.; Uchida, N.; Eaves, C. J.; Muller-Sieburg, C. E., The hematopoietic stem compartment consists of a limited number of discrete stem cell subsets. *Blood* **2006,** 107, (6), 2311-2316.

177. Okumura, T.; Wang, S. S. W.; Takaishi, S.; Tu, S. P.; Ng, V.; E Ericksen, R.; Rustgi, A. K.; Wang, T. C., Identification of a bone marrow-derived mesenchymal progenitor cell subset that can contribute to the gastric epithelium. *Lab Invest* **2009**, 89, (12),1410-22.

178. Jackson, K. A.; Majka, S. M.; Wang, H.; Pocius, J.; Hartley, C. J.; Majesky, M. W.; Entman, M. L.; Michael, L. H.; Hirschi, K. K.; Goodell, M. A., Regeneration of ischemic cardiac muscle and vascular endothelium by adult stem cells. *The Journal of Clinical Investigation* **2001,** 107, (11), 1395-1402.

179. Asahara, T.; Masuda, H.; Takahashi, T.; Kalka, C.; Pastore, C.; Silver, M.; Kearne, M.; Magner, M.; Isner, J. M., Bone Marrow Origin of Endothelial Progenitor Cells Responsible for Postnatal Vasculogenesis in Physiological and Pathological Neovascularization. *Circulation Research* **1999,** 85, (3), 221-228.

180. Kallos, M.; Sen, A.; Behie, L., Large-scale expansion of mammalian neural stem cells: a review. *Medical and Biological Engineering and Computing* **2003,** 41, (3), 271-282.

181. Cheshier, S. H.; Morrison, S. J.; Liao, X.; Weissman, I. L., In vivo proliferation and cell cycle kinetics of long-term self-renewing hematopoietic stem cells. *Proceedings of the National Academy of Sciences of the United States of America* **1999,** 96, (6), 3120-3125.

182. Orlic, D.; Kajstura, J.; Chimenti, S.; Jakoniuk, I.; Anderson, S. M.; Li, B.; Pickel, J.; McKay, R.; Nadal-Ginard, B.; Bodine, D. M.; Leri, A.; Anversa, P., Bone marrow cells regenerate infarcted myocardium. *Nature* **2001,** 410, (6829), 701-705.

183. Yamada, Y.; Sakurada, K.; Takeda, Y.; Gojo, S.; Umezawa, A., Single-cell-derived mesenchymal stem cells overexpressing Csx/Nkx2.5 and GATA4 undergo the stochastic cardiomyogenic fate and behave like transient amplifying cells. *Experimental Cell Research* **2007,** 313, (4), 698-706.

184. Gojo, S.; Gojo, N.; Takeda, Y.; Mori, T.; Abe, H.; Kyo, S.; Hata, J.-i.; Umezawa, A., In vivo cardiovasculogenesis by direct injection of isolated adult mesenchymal stem cells. *Experimental Cell Research* **2003,** 288, (1), 51-59.

185. Hakuno, D.; Fukuda, K.; Makino, S.; Konishi, F.; Tomita, Y.; Manabe, T.; Suzuki, Y.; Umezawa, A.; Ogawa, S., Bone Marrow-Derived Regenerated Cardiomyocytes (CMG Cells) Express Functional Adrenergic and Muscarinic Receptors. *Circulation* **2002,** 105, (3), 380-386.

186. Sata, M., Circulating Vascular Progenitor Cells Contribute to Vascular Repair, Remodeling, and Lesion Formation. *Trends in Cardiovascular Medicine* **2003,** 13, (6), 249-253.

187. Shintani, S.; Murohara, T.; Ikeda, H.; Ueno, T.; Honma, T.; Katoh, A.; Sasaki, K.-i.; Shimada, T.; Oike, Y.; Imaizumi, T., Mobilization of Endothelial Progenitor Cells in Patients With Acute Myocardial Infarction. *Circulation* **2001,** 103, (23), 2776-2779.

188. Kalka, C.; Masuda, H.; Takahashi, T.; Kalka-Moll, W. M.; Silver, M.; Kearney, M.; Li, T.; Isner, J. M.; Asahara, T., Transplantation of ex vivo expanded endothelial progenitor cells for therapeutic neovascularization. *Proceedings of the National Academy of Sciences of the United States of America* **2000,** 97, (7), 3422-3427.

189. Asahara, T.; Murohara, T.; Sullivan, A.; Silver, M.; van der Zee, R.; Li, T.; Witzenbichler, B.; Schatteman, G.; Isner, J. M., Isolation of Putative Progenitor Endothelial Cells for Angiogenesis. *Science* **1997,** 275, (5302), 964-966.

190. Shi, Q.; Rafii, S.; Wu, M. H.-D.; Wijelath, E. S.; Yu, C.; Ishida, A.; Fujita, Y.; Kothari, S.; Mohle, R.; Sauvage, L. R.; Moore, M. A. S.; Storb, R. F.; Hammond, W. P., Evidence for Circulating Bone Marrow-Derived Endothelial Cells. *Blood* **1998,** 92, (2), 362-367.

191. Zisch, A. H., Tissue engineering of angiogenesis with autologous endothelial progenitor cells. *Current Opinion in Biotechnology* **2004,** 15, (5), 424-429.

192. Yu, Y.; Gao, Y.; Wang, H.; Huang, L.; Qin, J.; Guo, R.; Song, M.; Yu, S.; Chen, J.; Cui, B.; Gao, P., The matrix protein CCN1 (CYR61) promotes proliferation, migration and tube formation of endothelial progenitor cells.

Experimental Cell Research **2008,** 314, (17), 3198-3208.

193. Ingram, D. A.; Mead, L. E.; Tanaka, H.; Meade, V.; Fenoglio, A.; Mortell, K.; Pollok, K.; Ferkowicz, M. J.; Gilley, D.; Yoder, M. C., Identification of a novel hierarchy of endothelial progenitor cells using human peripheral and umbilical cord blood. *Blood* **2004,** 104, (9), 2752-2760.

194. Mead, L. E.; Prater, D.; Yoder, M. C.; Ingram, D. A., Isolation and characterization of endothelial progenitor cells from human blood. *Current Protocols in Stem Cell Biology* **2008,** Chapter 2.

195. Yoder, M. C., Defining human endothelial progenitor cells. *Journal of Thrombosis and Haemostasis* **2009,** 7, 49-52.

196. Tura, O.; Barclay, G. R.; Roddie, H.; Davies, J.; Turner, M. L., Optimal ex vivo expansion of neutrophils from PBSCCD34(+) cells by a combination of SCF, Flt3-L and G-CSF and its inhibition by further addition of TPO. *Journal of Translational Medicine* **2007,** 5.

197. Rehman, J.; Li, J.; Orschell, C. M.; March, K. L., Peripheral Blood "Endothelial Progenitor Cells" Are Derived From Monocyte/Macrophages and Secrete Angiogenic Growth Factors. *Circulation* **2003,** 107, (8), 1164-1169.

198. Caballero, S.; Sengupta, N.; Shaw, L. C.; Grant, M. B., Circulating endothelial progenitor cells and adult vasculogenesis. *Retinal and Choroidal Angiogenesis* **2008**, 339-362.

199. Chan, G.; Mooney, D. J., New materials for tissue engineering: towards greater control over the biological response. *Trends in Biotechnology* **2008,** 26, (7), 382-392.

200. Hench, L. L.; Polak, J. M., Third-Generation Biomedical Materials. *Science* **2002,** 295, (5557), 1014-1017.

201. Muschler, G. F.; Boehm, C.; Easley, K., Aspiration to Obtain Osteoblast Progenitor Cells from Human Bone Marrow: The Influence of Aspiration Volume. *The Journal of Bone and Joint Surgery* **1997,** 79, (11), 1699-1709.

202. Karp, J. M.; Teol, G. S. L., Mesenchymal Stem Cell Homing: The Devil Is in the Details. *Cell Stem Cell* **2009,** 4, (3), 206-216.

203. Mooney, D. J.; Vandenburgh, H., Cell delivery mechanisms for tissue repair. *Cell Stem Cell* **2008,** 2, (3), 205-213.

204. Roncalli, J. G.; Tongers, J.; Renault, M.-A.; Losordo, D. W., Endothelial progenitor cells in regenerative medicine and cancer: a decade of research. *Trends in Biotechnology* **2008,** 26, (5), 276-283.

205. Carmeliet, P.; Jain, R. K., Angiogenesis in cancer and other diseases. *Nature* **2000,** 407, 249-257.

206. Fischbach, C.; Kong, H. J.; Hsiong, S. X.; Evangelista, M. B.; Yuen, W.; Mooney, D. J., Cancer cell angiogenic capability is regulated by 3D culture and integrin engagement. *Proceedings of the National Academy of Sciences of the United States of America* **2009,** 106, (2), 399-404.

207. Sato, T.; Araki, M.; Nakajima, N.; Omori, K.; Nakamura, T., Biodegradable polymer coating promotes the epithelization of tissue-engineered airway prostheses. *The Journal of Thoracic and Cardiovascular Surgery* **2010,** 139, (1), 26-31.

208. Padfield, G.; Mills, N. L.; Tura, O.; Millar, C.; Lang, N.; Stirling, D.; Ludlam, C.; Turner, M. L.; Barclay, G. R.; Newby, D. E., Dissociation of phenotypic and functional endothelial progenitor cells in patients undergoing percutaneous coronary intervention. *Scottish Medical Journal* **2007,** 52, (2), 51-51.

209. Skovseth, D. K.; Küchler, A. M.; Haraldsen, G., The HUVEC/Matrigel Assay. In *Target Discovery and Validation Reviews and Protocols*, 2007; pp 253-268.

210. Simoncini, T.; Apa, R.; Reis, F. M.; Miceli, F.; Stomati, M.; Driul, L.; Lanzone, A.; Genazzani, A. R.; Petraglia, F., Human Umbilical Vein Endothelial Cells: A New Source and Potential Target for Corticotropin-Releasing Factor. *The Journal of Clinical Endocrinology & Metabolism* **1999,** 84, (8), 2802-2806.

211. Montesano, R.; Orci, L.; Vassalli, P., In vitro rapid organization of endothelial cells into capillary-like networks is promoted by collagen matrices. *The Journal of Cell Biology* **1983,** 97, (5), 1648-1652.

212. Pinter, E.; Barreuther, M.; Lu, T.; Imhof, B. A.; Madri, J. A., Platelet-endothelial cell adhesion molecule-1 (PECAM-1/CD31) tyrosine phosphorylation state changes during vasculogenesis in the murine conceptus. *American Journal of Pathology* **1997,** 150, (5), 1523-1530.

213. DeLisser, H. M.; Baldwin, H. S.; Albelda, S. M., Platelet Endothelial Cell Adhesion Molecule 1 (PECAM-1/CD31): A Multifunctional Vascular Cell Adhesion Molecule. *Trends in Cardiovascular Medicine* **1997,** 7, (6), 203-210.

214. Gnecchi, M.; Zhang, Z. P.; Ni, A. G.; Dzau, V. J., Paracrine Mechanisms in Adult Stem Cell Signaling and Therapy. *Circulation Research* **2008,** 103, (11), 1204-1219.

215. Fox, S. B.; Leek, R. D.; Weekes, M. P.; Whitehouse, R. M.; Gatter, K. C.; Harris, A. L., Quantitation and Prognostic Value of Breast-Cancer Angiogenesis - Comparison of Microvessel Density, Chalkley Count, and Computer Image-Analysis. *Journal of Pathology* **1995,** 177, (3), 275-283.

216. Adamczyk, M.; Chen, Y.-Y.; Johnson, D. D.; Mattingly, P. G.; Moore, J. A.; Pan, Y.; Reddy, R. E., Chemiluminescent acridinium-9-carboxamide boronic acid probes: Application to a homogeneous glycated hemoglobin assay. *Bioorganic & Medicinal Chemistry Letters* **2006,** 16, (5), 1324-1328.

217. Andrade, S. P.; Fan, T. P. D.; Lewis, G. P., Quantitative Invivo Studies on Angiogenesis in a Rat Sponge Model. *British Journal of Experimental Pathology* **1987,** 68, (6), 755-766.

218. Hague, S.; MacKenzie, I. Z.; Bicknell, R.; Rees, M. C. P., In-vivo angiogenesis and progestogens. *Human Reproduction* **2002,** 17, (3), 786-793.

219. Yap, S.-C.; Kouwenhoven, G. C.; Takkenberg, J. J. M.; Galema, T. W.; Meijboom, F. J.; van Domburg, R.; Simoons, M. L.; Roos-Hesselink, J. W., Congenital aortic stenosis in adults: Rate of progression and predictors of clinical outcome. *International Journal of Cardiology* **2007,** 122, (3), 224-231.

220. Yang, F.; Patterson, R. P., A novel impedance-based tomography approach for stenotic plaque detection: A simulation study. *International Journal of Cardiology* **in Press**, doi:10.1016/j.ijcard.2009.01.059.

221. Boden, W. E.; O'Rourke, R. A.; Teo, K. K.; Hartigan, P. M.; Maron, D. J.; Kostuk, W. J.; Knudtson, M.; Dada, M.; Casperson, P.; Harris, C. L.; Chaitman, B. R.; Shaw, L.; Gosselin, G.; Nawaz, S.; Title, L. M.; Gau, G.; Blaustein, A. S.; Booth, D. C.; Bates, E. R.; Spertus, J. A.; Berman, D. S.; Mancini, G. B. J.; Weintraub, W. S.; the, C. T. R. G., Optimal Medical Therapy with or without PCI for Stable Coronary Disease. *The New England Journal of Medicine* **2007,** 356, (15), 1503-1516.

222. Braunwald, E., Cardiology: the past, the present, and the future. *Journal of the American College of Cardiology* **2003,** 42, (12), 2031-2041.

223. Mabin, T. A.; Holmes, D. R., Jr.; Smith, H. C.; Vlietstra, R. E.; Reeder, G. S.; Bresnahan, J. F.; Bove, A. A.; Hammes, L. N.; Elveback, L. R.; Orszulak, T. A., Follow-up clinical results in patients undergoing percutaneous transluminal coronary angioplasty. *Circulation* **1985,** 71, (4), 754-760.

224. Hamon, M.; Bauters, C.; McFadden, E. P.; Wernert, N.; LaBlanche, J. M.; Dupuis, B.; Bertrand, M. E., Restenosis after coronary angioplasty. *European Heart Journal* **1995,** 16, (1), 33-48.

225. Rud Andersen, H.; Mæng, M.; Thorwest, M.; Falk, E., Remodeling Rather Than Neointimal Formation Explains Luminal Narrowing After Deep Vessel Wall Injury : Insights From a Porcine Coronary (Re)stenosis Model. *Circulation* **1996,** 93, (9), 1716-1724.

226. Liu, M. W.; Roubin, G. S.; King, S. B., Restenosis after Coronary Angioplasty - Potential Biologic Determinants and Role of Intimal Hyperplasia. *Circulation* **1989,** 79, (6), 1374-1387.

227. Fanelli, C.; Aronoff, R., Restenosis following coronary angioplasty. *American Heart Journal* **1990,** 119, (2, Part 1), 357-368.

228. Goy, J. J.; Sigwart, U., Twenty-two years angiographic and clinical follow-up

of the first patient treated with intracoronary stent placement for acute vessel closure following percutaneous transluminal coronary angioplasty. *European Heart Journal* **2009,** 30, (15), 1926-1926.

229. Scheller, B.; Hehrlein, C.; Bocksch, W.; Rutsch, W.; Haghi, D.; Dietz, U.; Bohm, M.; Speck, U., Treatment of Coronary In-Stent Restenosis with a Paclitaxel-Coated Balloon Catheter. *The New England Journal of Medicine* **2006,** 355, (20), 2113-2124.

230. Tepe, G.; Schmehl, J.; P Wendel, H.; Schaffner, S.; Heller, S.; Gianotti, M.; D Claussen, C.; H Duda, S., Reduced thrombogenicity of nitinol stents--In vitro evaluation of different surface modifications and coatings. *Biomaterials* **2006,** 27, (4), 643-650.

231. Ajani, A. E.; Yan, B. P.; Clark, D. J.; Eccleston, D.; Walton, A.; Lew, R.; Meehan, A.; Brennan, A.; Reid, C.; Duffy, S. J., Contemporary Treatment of In-Stent Restenosis and the Incidence of Recurrent In-Stent Restenosis in the Era of Drug-Eluting Stents. *Heart, Lung and Circulation* **2007,** 16, (4), 269-273.

232. Brodie, B. R.; Stuckey, T.; Downey, W.; Humphrey, A.; Bradshaw, B.; Metzger, C.; Hermiller, J.; Krainin, F.; Juk, S.; Cheek, B.; Duffy, P.; Smith, H.; Edmunds, J.; Varanasi, J.; Simonton, C. A., Outcomes and Complications With Off-Label Use of Drug-Eluting Stents: Results From the STENT (Strategic Transcatheter Evaluation of New Therapies) Group. *Journal of the American College of Cardiology: Cardiovascular Interventions* **2008,** 1, (4), 405-414.

233. Avci-Adali, M.; Paul, A.; Ziemer, G.; Wendel, H. P., New strategies for in vivo tissue engineering by mimicry of homing factors for self-endothelialisation of blood contacting materials. *Biomaterials* **2008,** 29, (29), 3936-3945.

234. Stephen, J.; Wallis, T. S.; Starkey, W. G.; Candy, D. C. A.; Osborne, M. P.; Haddon, S., Salmonellosis - in Retrospect and Prospect. *Ciba Foundation Symposia* **1985,** 112, 175-192.

235. Coburn, B.; Grassl, G. A.; Finlay, B. B., Salmonella, the host and disease: a brief review. *Immunology and Cell Biology* **2007,** 85, (2), 112-118.

236. Maskey, A. P.; Day, J. N.; Tuan, P. Q.; Thwaites, G. E.; Campbell, J. I.; Zimmerman, M.; Farrar, J. J.; Basnyat, B., Salmonella enterica serovar Paratyphi A and S-enterica serovar Typhi cause indistinguishable clinical syndromes in Kathmandu, Nepal. *Clinical Infectious Diseases* **2006,** 42, (9), 1247-1253.

237. Coburn, B.; Grassl, G. A.; Finlay, B. B., Salmonella, the host and disease: a brief review. *Immunology and Cell Biology* **2006,** 85, (2), 112-118.

238. Boyle, E. C.; Bishop, J. L.; Grassl, G. A.; Finlay, B. B., Salmonella: from pathogenesis to therapeutics. *Journal of Bacteriology* **2007,** 189, 1489-1495.

239. Glynn, M. K.; Bopp, C.; Dewitt, W.; Dabney, P.; Mokhtar, M.; Angulo, F. J., Emergence of Multidrug-Resistant Salmonella enterica SerotypeTyphimurium DT104 Infections in the United States. *The New England Journal of Medicine* **1998,** 338, (19), 1333-1339.

240. Carballo, J.; Ferreiros, C. M.; Criado, M. T., Factor Analysis in the Evaluation of the Relationship between Bacterial Adherence to Biomaterials and Changes in Free Energy. *Journal of Biomaterials Applications* **1992,** 7, (2), 130-141.

241. Lee Wong, A. C., Biofilms in Food Processing Environments. *Journal of Dairy Science* **1998,** 81, (10), 2765-2770.

242. Hoiseth, S.; Stocker, B., Aromatic-dependent Salmonella typhimurium are non-virulent and effective as live vaccines. *Nature* **1981,** 291, 238-239.

243. Riley, M.; Abe, T.; Arnaud, M.; Berlyn, M.; Blattner, F.; Chaudhuri, R.; Glasner, J. D., Escherichia coli K-12: a cooperatively developed annotation snapshot--2005. *Nucleic Acids Research* **2006,** 34, 1-9.

244. Valdivia, R. H.; Hromockyj, A. E.; Monack, D.; Ramakrishnan, L.; Falkow, S., Applications for green fluorescent protein (GFP) in the study of hostpathogen interactions. *Gene* **1996,** 173, (1), 47-52.

245. Thaburet, J. F. O.; Mizomoto, H.; Bradley, M., High-throughput evaluation of the wettability of polymer libraries. *Macromolecular Rapid Communications* **2004,** 25, (1), 366-370.

246. Imbeaud, S.; Graudens, E.; Boulanger, V.; Barlet, X.; Zaborski, P.; Eveno, E.; Mueller, O.; Schroeder, A.; Auffray, C., Towards standardization of RNA quality assessment using user-independent classifiers of microcapillary electrophoresis traces. *Nucleic Acids Research* **2005,** 33, (6), e56-.

247. Jane, S.; Theresa, L. G.; Sudeshna, A.; Reeti, T.; Karin, N.; Anders, L.; Patric, N.; Deirdre, N.; Björn, O.; Mikael, C. O. E.; Stewart, A.; Peter, S., Differentiating Human Embryonic Stem Cells Express a Unique Housekeeping Gene Signature. *Stem Cells* **2007,** 25, (2), 473-480.

248. Hasumi, M.; Suzuki, K.; Matsui, H.; Koike, H.; Ito, K.; Yamanaka, H., Regulation of metallothionein and zinc transporter expression in human prostate cancer cells and tissues. *Cancer Letters* **2003,** 200, (2), 187-195.

249. Gareth, J. S.; David, C. H.; In-Hyun, P.; Judy, F.; Zara, H.; Catherine, M. P.; Donna, D.; James, R. B.; James, A. R.; Kay, S.; Gang, W.; George, Q. D.; Je-Hyuk, L.; George, M. C.; Stuart, J. F.; John, P. I.; Ian, W., Generation of functional human hepatic endoderm from human induced pluripotent stem cells. *Hepatology* 51, (1), 329-335.

250. Jose, A. J.; Wong, L. S.; Merrington, J.; Bradley, M., Automated image analysis of polymer beads and size distribution. *Industrial and Engineering Chemistry Research* **2005,** 44, (23), 8659-8662.

Appendices

Appendix I: polyurethane library[245]

Synthesis of the polyurethanes

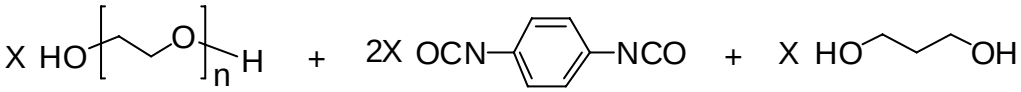

Diol **Diisocyanate** **Chain Extender**

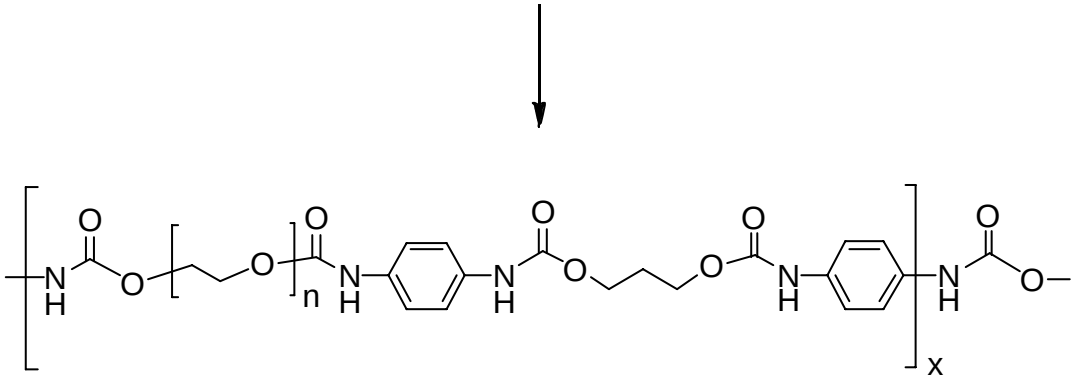

List of monomers used in the synthesis of the polyurethanes

Diol:

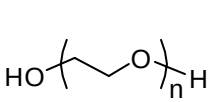

PEG400,900,2000

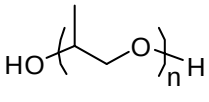

PPG450,1000,2000

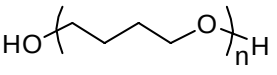

PTMG250,650,1000,2000

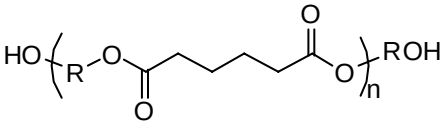

R= -CH2$(CH_2)_4$$CH_2$- PHAD1800
-CH2C$(CH_3)_2$$CH_2$- PNAD1800
-CH2CH_2O$CH_2$$CH_2$- PGAD1800

Diisocyanate:

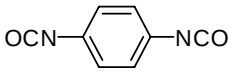

PDI

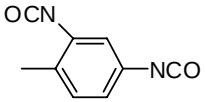

TDI

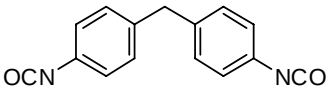

MDI

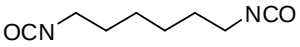

HDI

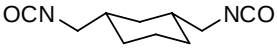

BICH

HMDI

Chain Extender:

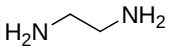

ED

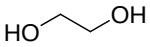

EG

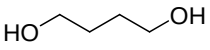

BD

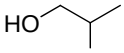

PG

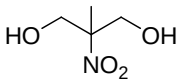

NMPD

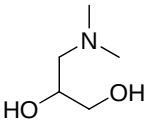

DMAPD

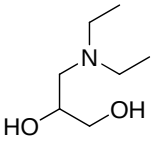

DEAPD

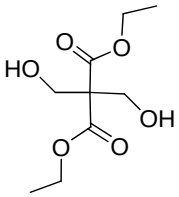

DHM

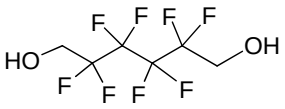

OFHD

Monomer abbreviations:

Diol:

PEG: poly(ethylene glycol)

PPG: poly(propylene glycol)

PTMG: poly(butylene glycol)

PHNAD: poly[1,6-hexanediol/neopentyl glycol-*alt*-(adiptic acid)]diol

PHNGAD: poly[1,6-hexanediol/neopentyl glycol/diethylene glycol-*alt*-(adiptic acid)]diol

Diisocyanate:

PDI:	1,4-diisocyanobenzene
TDI:	4-methyl-1,3-phenylene diisocyanate
MDI:	4,4’-methylenebis(phenylisocyanate)
HDI:	1,6-diisocyanohexane
BICH:	1,3-bis(isocyananatomethyl)cyclohexane
HMDI:	4,4’-methylenebis(cyclohexylisocyanate)

Chain Extender:

ED:	ethylene diamine
EG:	ethylene glycol
BD:	1,4-butanediol
PG:	propylene glycol
NMPD:	2-nitro-2-methyl-1,3-propanediol
DMAPD:	3-dimethylamino-1,2-propanediol
DEAPD:	3-diethylamino-1,2-propanediol
DHM:	diethyl bis(hydroxymethyl)malonate
OFHD:	2,2,3,3,4,4,5,5-octafluoro-1,6-hexanediol

List of polyurethanes used in the thesis with their corresponding monomers and monomer molecular ratio used in the synthesis

Polymer reference	Diol		Diisocyanate	Chain Extender	Ratio (% mol.)		
	Nature	MW (Da)			Monomer (Diol)	Monomer (Diisocyanate)	Monomer (Extender)
1	PEG	2000	HDI	none	48.5	51.5	0
2	PEG	900	HDI	none	48.5	51.5	0
3	PEG	400	HDI	none	48.5	51.5	0
4	PPG	2000	HDI	none	48.5	51.5	0
5	PTMG	2000	HDI	none	48.5	51.5	0
6	PEG	2000	BICH	none	48.5	51.5	0
7	PEG	900	BICH	none	48.5	51.5	0
8	PEG	400	BICH	none	48.5	51.5	0
9	PPG	2000	BICH	none	48.5	51.5	0
10	PTMG	2000	BICH	none	48.5	51.5	0
11	PEG	2000	TDI	none	48.5	51.5	0
12	PEG	900	TDI	none	48.5	51.5	0
13	PEG	400	TDI	none	48.5	51.5	0
14	PPG	2000	TDI	none	48.5	51.5	0
15	PTMG	2000	TDI	none	48.5	51.5	0
16	PEG	2000	MDI	none	48.5	51.5	0
17	PEG	900	MDI	none	48.5	51.5	0
18	PEG	400	MDI	none	48.5	51.5	0
19	PPG	2000	MDI	none	48.5	51.5	0
20	PTMG	2000	MDI	none	48.5	51.5	0
21	PEG	2000	PDI	none	48.5	51.5	0
22	PEG	900	PDI	none	48.5	51.5	0
23	PEG	400	PDI	none	48.5	51.5	0
24	PPG	2000	PDI	none	48.5	51.5	0
25	PTMG	2000	PDI	none	48.5	51.5	0
26	PEG	2000	HMDI	none	48.5	51.5	0
27	PEG	900	HMDI	none	48.5	51.5	0
28	PEG	400	HMDI	none	48.5	51.5	0
29	PPG	2000	HMDI	none	48.5	51.5	0
33	PEG	900	HDI	BD	0.25	0.52	0.23
35	PEG	400	HDI	BD	0.25	0.52	0.23
37	PPG	2000	HDI	BD	0.25	0.52	0.23
39	PTMG	2000	HDI	BD	0.25	0.52	0.23
41	PEG	2000	BICH	BD	0.25	0.52	0.23
48	PPG	2000	BICH	ED	0.25	0.52	0.23
53	PEG	900	TDI	BD	0.25	0.52	0.23
61	PEG	2000	MDI	BD	0.25	0.52	0.23
65	PEG	400	MDI	BD	0.25	0.52	0.23
67	PPG	2000	MDI	BD	0.25	0.52	0.23
69	PTMG	2000	MDI	BD	0.25	0.52	0.23
71	PEG	2000	PDI	BD	0.25	0.52	0.23
73	PEG	900	PDI	BD	0.25	0.52	0.23
77	PPG	2000	PDI	BD	0.25	0.52	0.23
79	PTMG	2000	PDI	BD	0.25	0.52	0.23
81	PEG	2000	HMDI	BD	0.25	0.52	0.23
83	PEG	900	HMDI	BD	0.25	0.52	0.23
85	PEG	400	HMDI	BD	0.25	0.52	0.23
87	PPG	2000	HMDI	BD	0.25	0.52	0.23
39DE	PTMG	2000	HDI	DEAPD	0.25	0.52	0.23
49DE	PTMG	2000	BICH	DEAPD	0.25	0.52	0.23
91	PTMG	650	HDI	BD	0.485	0.515	0
92	PTMG	1000	HDI	BD	0.485	0.515	0
93	PTMG	650	BICH	BD	0.485	0.515	0
94	PTMG	1000	BICH	BD	0.485	0.515	0
95	PTMG	650	MDI	BD	0.485	0.515	0
96	PTMG	1000	MDI	BD	0.485	0.515	0
97	PHNGAD	1800	BICH	DMAPD	0.25	0.52	0.23
98	PHNGAD	1800	BICH	DEAPD	0.25	0.52	0.23
99	PTMG	650	HDI	DMAPD	0.25	0.52	0.23
100	PTMG	1000	HDI	DMAPD	0.25	0.52	0.23
101	PTMG	650	BICH	DMAPD	0.25	0.52	0.23
102	PTMG	1000	BICH	DMAPD	0.25	0.52	0.23

Polymer reference	Diol		Diisocyanate	Chain Extender	Ratio (% mol.)		
	Nature	MW (Da)			Monomer (Diol)	Monomer (Diisocyanate)	Monomer (Extender)
103	PHNGAD	1800	MDI	DMAPD	0.25	0.52	0.23
104	PHNGAD	1800	MDI	DEAPD	0.25	0.52	0.23
105	PHNGAD	1800	HDI	DMAPD	0.25	0.52	0.23
106	PHNGAD	1800	HDI	DEAPD	0.25	0.52	0.23
107	PTMG	650	HDI	DEAPD	0.25	0.52	0.23
108	PTMG	1000	HDI	DEAPD	0.25	0.52	0.23
110	PTMG	1000	BICH	DEAPD	0.25	0.52	0.23
111	PTMG	650	MDI	DEAPD	0.25	0.52	0.23
112	PTMG	1000	MDI	DEAPD	0.25	0.52	0.23
114	PPG	425	HDI	BD	0.485	0.515	0
115	PPG	1000	HDI	BD	0.485	0.515	0
116	PPG	425	BICH	BD	0.485	0.515	0
117	PPG	1000	BICH	BD	0.485	0.515	0
118	PPG	425	MDI	DMAPD	0.25	0.52	0.23
119	PPG	1000	MDI	DMAPD	0.25	0.52	0.23
120	PPG	425	BICH	DEAPD	0.25	0.52	0.23
121	PPG	1000	BICH	DEAPD	0.25	0.52	0.23
122	PPG	2000	BICH	DEAPD	0.25	0.52	0.23
123	PPG	2000	MDI	DMAPD	0.25	0.52	0.23
124	PPG	2000	TDI	DMAPD	0.25	0.52	0.23
125	PPG	1000	TDI	DMAPD	0.25	0.52	0.23
126	PPG	425	TDI	DMAPD	0.25	0.52	0.23
127	PPG	1000	BICH	DMAPD	0.25	0.52	0.23
128	PPG	2000	BICH	DMAPD	0.25	0.52	0.23
129	PPG	425	BICH	DMAPD	0.25	0.52	0.23
130	PTMG	650	TDI	DMAPD	0.25	0.52	0.23
131	PTMG	1000	TDI	DMAPD	0.25	0.52	0.23
132	PHNGAD	1800	BICH	BD	0.25	0.52	0.23
133	PHNGAD	1800	HDI	BD	0.25	0.52	0.23
134	PHNGAD	1800	MDI	BD	0.25	0.52	0.23
135	PTMG	250	BICH	DMAPD	0.25	0.52	0.23
136	PTMG	250	BICH	DEAPD	0.25	0.52	0.23
137	PTMG	250	BICH	BD	0.25	0.52	0.23
138	PTMG	250	BICH	EG	0.25	0.52	0.23
139	PTMG	650	BICH	EG	0.25	0.52	0.23
140	PTMG	1000	BICH	EG	0.25	0.52	0.23
141	PTMG	2000	BICH	EG	0.25	0.52	0.23
142	PTMG	250	BICH	PG	0.25	0.52	0.23
143	PTMG	650	BICH	PG	0.25	0.52	0.23
144	PTMG	1000	BICH	PG	0.25	0.52	0.23
145	PTMG	2000	BICH	PG	0.25	0.52	0.23
146	PTMG	250	HDI	DMAPD	0.25	0.52	0.23
147	PTMG	250	HDI	DEAPD	0.25	0.52	0.23
148	PTMG	250	HDI	BD	0.25	0.52	0.23
149	PTMG	250	HDI	EG	0.25	0.52	0.23
150	PTMG	650	HDI	EG	0.25	0.52	0.23
151	PTMG	1000	HDI	EG	0.25	0.52	0.23
152	PTMG	2000	HDI	EG	0.25	0.52	0.23
153	PTMG	250	HDI	PG	0.25	0.52	0.23
154	PTMG	650	HDI	PG	0.25	0.52	0.23
156	PTMG	2000	HDI	PG	0.25	0.52	0.23
157	PTMG	250	MDI	DMAPD	0.25	0.52	0.23
158	PTMG	250	MDI	OFHD	0.25	0.52	0.23
159	PTMG	250	MDI	BD	0.25	0.52	0.23
161	PTMG	650	MDI	EG	0.25	0.52	0.23
162	PTMG	1000	MDI	EG	0.25	0.52	0.23
163	PTMG	2000	MDI	EG	0.25	0.52	0.23
164	PTMG	250	MDI	PG	0.25	0.52	0.23
165	PTMG	650	MDI	PG	0.25	0.52	0.23
166	PTMG	1000	MDI	PG	0.25	0.52	0.23
167	PTMG	2000	MDI	PG	0.25	0.52	0.23
168	PTMG	250	BICH	none	48.5	51.5	0
169	PTMG	650	BICH	none	48.5	51.5	0
171	PTMG	250	HDI	none	48.5	51.5	0
172	PTMG	650	HDI	none	48.5	51.5	0
173	PTMG	1000	HDI	none	48.5	51.5	0
174	PTMG	250	MDI	none	48.5	51.5	0
175	PTMG	650	MDI	none	48.5	51.5	0
176	PTMG	1000	MDI	none	48.5	51.5	0
178	PTMG	1000	HDI	NMPD	0.25	0.52	0.23

Polymer reference	Diol		Diisocyanate	Chain Extender	Ratio (% mol.)		
	Nature	MW (Da)			Monomer (Diol)	Momomer (Diisocyanate)	Monomer (Extender)
179	PTMG	2000	HDI	NMPD	0.25	0.52	0.23
181	PTMG	2000	BICH	NMPD	0.25	0.52	0.23
183	PTMG	1000	MDI	NMPD	0.25	0.52	0.23
184	PTMG	2000	MDI	NMPD	0.25	0.52	0.23
185	PHNAD	900	MDI	OFHD	0.17	0.52	0.33
185	PHNAD	900	MDI	OFHD	0.17	0.52	0.33
186	PTMG	650	BICH	OFHD	0.25	0.52	0.23
187	PTMG	1000	BICH	OFHD	0.25	0.52	0.23
188	PTMG	2000	BICH	OFHD	0.25	0.52	0.23
189	PPG	1000	BICH	OFHD	0.17	0.52	0.33
190	PTMG	650	HDI	OFHD	0.25	0.52	0.23
191	PTMG	1000	HDI	OFHD	0.25	0.52	0.23
192	PTMG	2000	HDI	OFHD	0.25	0.52	0.23
196	PTMG	2000	MDI	OFHD	0.25	0.52	0.23
197	PTMG	650	BICH	DHM	0.25	0.52	0.23
199	PTMG	2000	BICH	DHM	0.25	0.52	0.23
201	PTMG	1000	HDI	DHM	0.25	0.52	0.23
202	PTMG	2000	HDI	DHM	0.25	0.52	0.23
203	PTMG	650	MDI	DHM	0.25	0.52	0.23
204	PTMG	1000	MDI	DHM	0.25	0.52	0.23
205	PTMG	2000	MDI	DHM	0.25	0.52	0.23
206	PPG	1000	HDI	OFHD	0.25	0.52	0.23
207	PPG	1000	BICH	OFHD	0.25	0.52	0.23
208	PPG	1000	MDI	OFHD	0.25	0.52	0.23
210	PPG	1000	BICH	PG	0.25	0.52	0.23
212	PHNAD	900	HDI	PG	0.25	0.52	0.23
213	PHNAD	900	BICH	PG	0.25	0.52	0.23
214	PHNAD	900	MDI	PG	0.25	0.52	0.23
215	PHNAD	900	HDI	BD	0.25	0.52	0.23
216	PHNAD	900	BICH	BD	0.25	0.52	0.23
217	PHNAD	900	MDI	BD	0.25	0.52	0.23
218	PHNAD	900	HDI	DMAPD	0.25	0.52	0.23
219	PHNAD	900	BICH	DMAPD	0.25	0.52	0.23
220	PHNAD	900	MDI	DMAPD	0.25	0.52	0.23
221	PHNAD	900	HDI	OFHD	0.25	0.52	0.23
222	PHNAD	900	BICH	OFHD	0.25	0.52	0.23
223	PHNAD	900	MDI	OFHD	0.25	0.52	0.23
224	PHNAD	900	HDI	none	48.5	51.5	0
225	PHNAD	900	BICH	none	48.5	51.5	0
226	PHNAD	900	MDI	none	48.5	51.5	0
227	PPG-PEG	1900	HDI	none	48.5	51.5	0
228	PPG-PEG	1900	BICH	none	48.5	51.5	0
229	PPG-PEG	1900	MDI	none	48.5	51.5	0
230	PPG-PEG	1900	HDI	BD	0.25	0.52	0.23
233	PPG-PEG	1900	HDI	OFHD	0.25	0.52	0.23
234	PPG-PEG	1900	BICH	OFHD	0.25	0.52	0.23
235	PPG-PEG	1900	MDI	OFHD	0.25	0.52	0.23
236	PPG-PEG	1900	HDI	PG	0.25	0.52	0.23
238	PPG-PEG	1900	MDI	PG	0.25	0.52	0.23
239	PPG-PEG	1900	HDI	DMAPD	0.25	0.52	0.23
241	PPG-PEG	1900	MDI	DMAPD	0.25	0.52	0.23
242	PPG-PEG	1900	HDI	EG	0.25	0.52	0.23
244	PPG-PEG	1900	MDI	EG	0.25	0.52	0.23
245	PHNGAD	1800	HDI	OFHD	0.25	0.52	0.23
246	PHNGAD	1800	BICH	OFHD	0.25	0.52	0.23
247	PHNGAD	1800	MDI	OFHD	0.25	0.52	0.23
249	PHNGAD	1800	HDI	none	48.5	51.5	0
250	PHNGAD	1800	BICH	none	48.5	51.5	0
252	PHNGAD	1800	HDI	DHM	0.25	0.52	0.33
253	PPG-PEG	1900	MDI	DMAPD	0.17	0.52	0.33
254	PHNGAD	1800	BICH	BD	0.17	0.52	0.33
255	PPG-PEG	1900	MDI	BD	0.17	0.52	0.33
256	PPG	425	MDI	none	48.5	51.5	0
257	PTMG	1000	BICH	DMAPD	0.17	0.52	0.33
259	PTMG	2000	BICH	DMAPD	0.17	0.52	0.33
260	PTMG	2000	BICH	OFHD	0.17	0.52	0.33
263	PTMG	1000	HDI	OFHD	0.17	0.52	0.33

Polymer reference	Diol		Diisocyanate	Chain Extender	Ratio (% mol.)		
	Nature	MW (Da)			Monomer (Diol)	Momomer (Diisocyanate)	Monomer (Extender)
264	PTMG	1000	HDI	DMAPD	17.0	52.0	33.0
266	PPG-PEG	1900	BICH	DMAPD	17.0	52.0	33.0
267	PPG-PEG	1900	BICH	BD	17.0	52.0	33.0
268	PTMG	1000	MDI	DMAPD	25.0	52.0	23.0
269	PPG	2000	MDI	DEAPD	25.0	52.0	23.0
270	PTMG	2000	MDI	DMAPD	25.0	52.0	23.0
271	PEG	400	MDI	DMAPD	25.0	52.0	23.0
272	PEG	400	MDI	none	58.0	42.0	0.0
273	PPG	425	MDI	DMAPD	25.0	52.0	23.0
274	PPG	425	MDI	none	48.5	51.5	0.0
275	PEG	400	MDI	none	48.5	51.5	0.0
276	PTMG	1000	MDI	OFHD	17.0	52.0	33.0
277	PTMG	2000	MDI	OFHD	17.0	52.0	33.0
278	PPG-PEG	1900	MDI	OFHD	17.0	52.0	33.0

Appendix II: polyacrylate libraries[40]

Synthesis of the polyacrylates

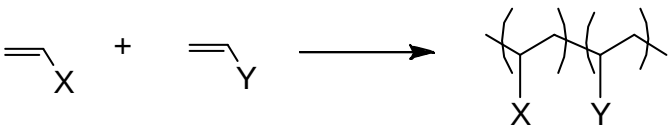

Monomer 1 **Monomer 2** **Random copolymer**

[1]/[2] = 90/10, 70/30, 50/50

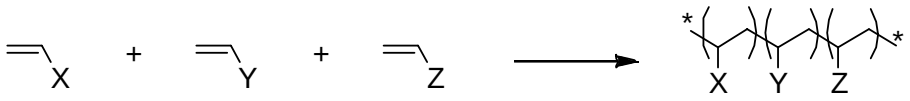

Monomer 1 **Monomer 2** **Monomer 3** **Random terpolymer**

[1]/[2]/[3] = 70/20/10, 70/15/15, 70/10/20

List of monomers used in the synthesis of the polyurethanes

List of monomer 1 used:

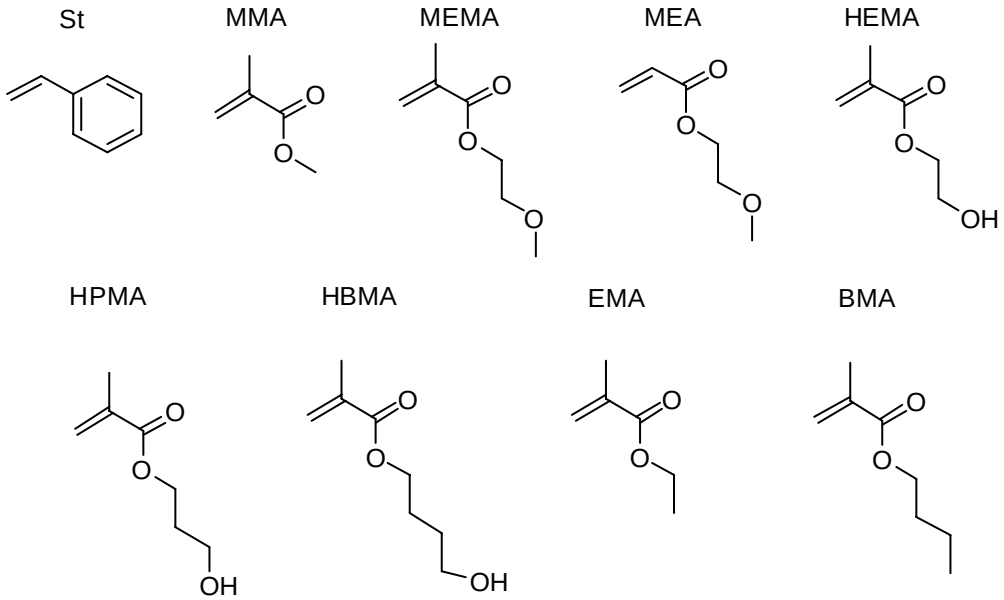

List of monomer 2 used:

DMAAm

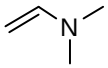

DEAAm

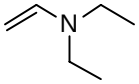

NIPAAm

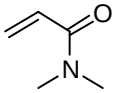

A-H

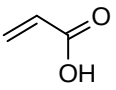

MA-H

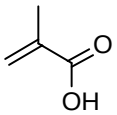

VAA

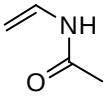

VP^{-4}

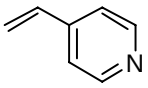

VP^{-2}

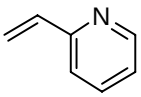

DMVBA

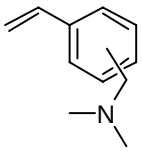

VI

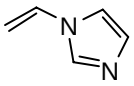

VPNO

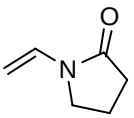

DMAEMA

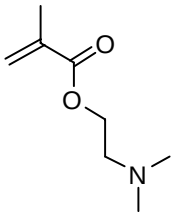

DMAEA

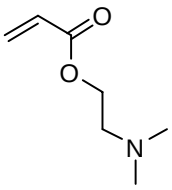

DEAEMA

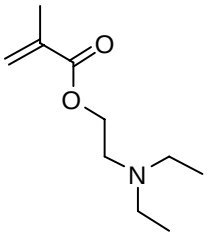

DEAEA

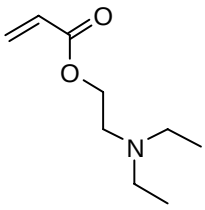

DMAPMAAm

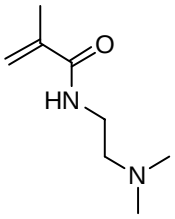

MTEMA

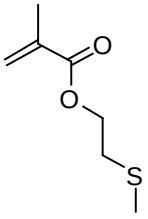

BACOEA

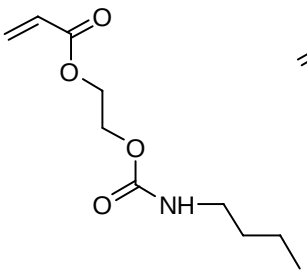

MNPMA

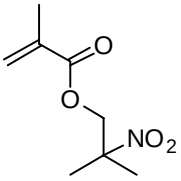

BAEMA

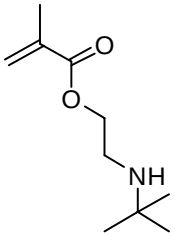

DAAAm

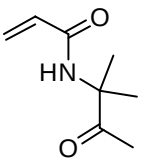

AES-H

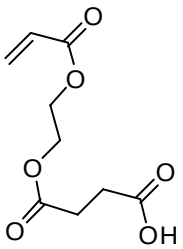

AAG-H

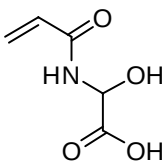

EGMP-H

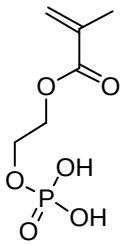

GMA

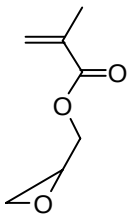

List of monomers 3 used

DEAEMA

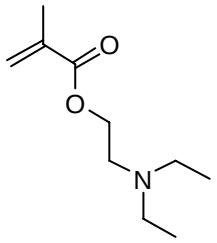

DEAEA

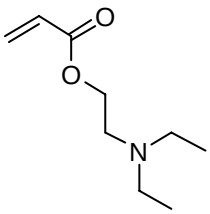

Functionalisation scheme for the copolymer of GMA

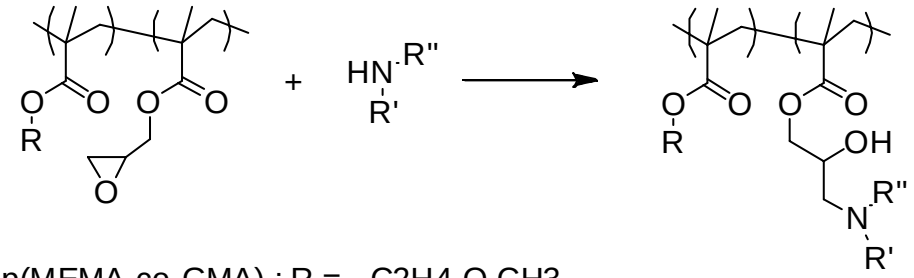

p(MEMA-co-GMA) : R = -C2H4-O-CH3
p(MMA-co-GMA) : R = -CH3

List of amines used to functionalise GMA polymers:

TMEDA

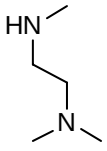

DEMEDA

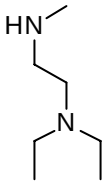

TMPDA

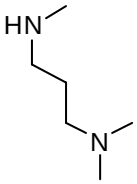

MnHA

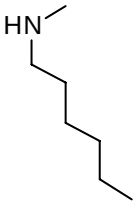

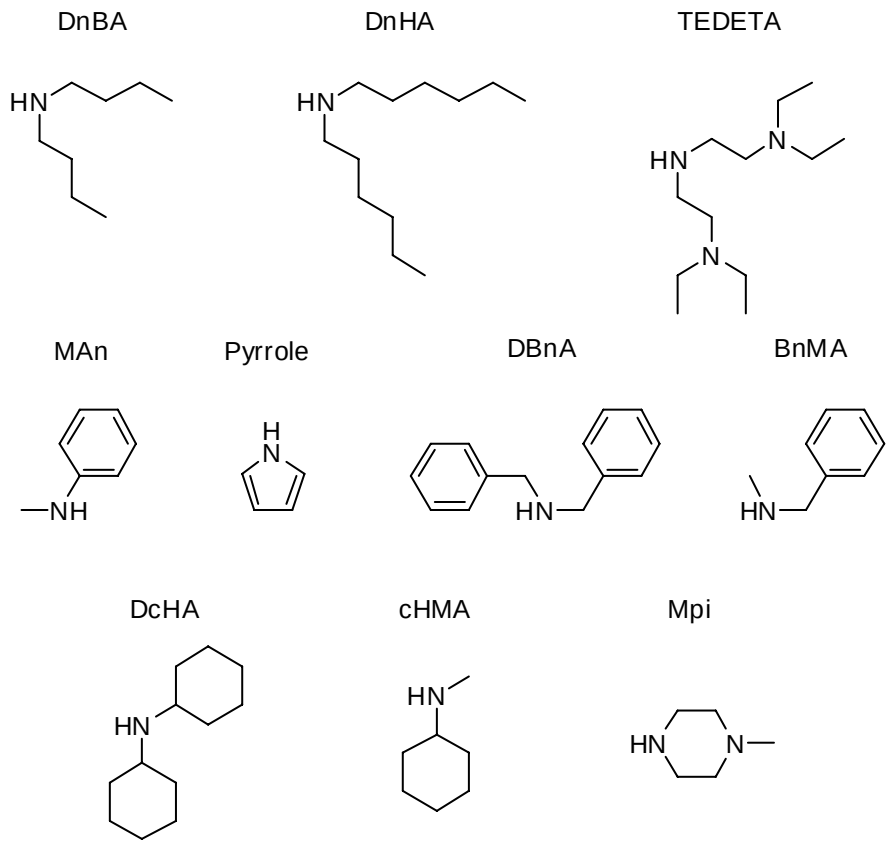

Monomers abbreviations:

Monomers 1:

St:	styrene
MMA:	methyl methacrylate
MEMA:	2-methoxyethylmethacrylate
MEA:	2-methoxyethylacrylate
HEMA:	2-hydroxyethylmethacrylate
HPMA:	hydroxypropylmethacrylate
HBMA:	hydroxybutylmethacrylate
EMA:	ethyl methacrylate
BMA:	butyl methacrylate

Monomers 2:

DEAAm:	diethylacrylamide
DMAAm:	dimethylacrylamide

NIPAAm: N-isopropylacrylamide

A-H: acrylic acid

MA-H: methacrylic acid

VAA: N-vinylacetamide

VP^{-4} 4-vinylpyridine

VP^{-2}: 2-vinylpyridine

DMVBA: N,N-dimethylvinylbenzylamine

VI: 1-vinylimidazol

VPNO: 1-vinyl-2-prrolidinone

DMAEMA: 2-(diethylamino)ethyl methacrylate

DMAEA: 2-(diethylamino)ethyl acrylate

DEAEMA: 2-(diethylamino)ethyl methacrylate

DEAEA: 2-(diethylamino)ethyl acrylate

DMAPMAAm: N-[3-(dimethylamino)propyl]acrylamide

MTEMA: 2-(methylthio)ethyl methacrylate

BACOEA: 2-[[(butylamino)carbonyl]oxy]ethyl acrylate

MNPMA: 2-methyl-2-nitropropyl methacrylate

BAEMA: 2-(tert-butylamino)ethyl methacrylate

DAAAm: diacetone acrylamide(N-(1,1-dimethyl-3-oxobutyl)-acrylamide)

AES-H: mono-2-(acryloyoxy)ethyl succinate

AAG-H: 2-acrylamidoglycolic acid

EGMP-H: ethylene glycol methacrylate phosphate

GMA glycidyl methacrylate

Monomers 3:

DEAEMA: 2-(diethylamino)ethyl methacrylate

DEAEA: 2-(diethylamino)ethyl acrylate

Amines used to functionalise GMA based co-polymers:

TMEDA N,N,N-trimethylethylenediamine

DEMEDA N,N-diethyl-N'-methylethylenediamine

TMPDA N,N,N'-trimethyl-1,3-propanediamine

MnHA	N-methylhexylamine
DnBA	di-n-Butylamine
DnHA	di-n-hexylamine
TEDETA	N,N,N',N'-tetraethyldiethylenetriamine
MAn	N-methylaniline
Pyrrole	pyrrole
DBnA	dibenzylamine
BnMA	N-benzylmethylaimne
DcHA	dicyclohexylamine
cHMA	cycloheanemethylamine
Mpi	1-methylpiperazine
MAEPy	2-(2-methylaminoethyl)pyridine

List of polyacrylates used in the thesis with their corresponding monomers and monomer molecular ratio used in the synthesis

Polymer reference	Bradley reference	Monomer (1)	Monomer (2)	Monomer (3)	Ratio (% mol.)		
					M (1)	M (2)	M (3)
1	1a9	St	DEAA	-	90	10	-
2	1a7	St	DEAA	-	70	30	-
3	1a5	St	DEAA	-	50	50	-
4	1b9	St	DMAA	-	90	10	-
5	1b7	St	DMAA	-	70	30	-
6	1b5	St	DMAA	-	50	50	-
7	1c9	St	PAA	-	90	10	-
8	1c7	St	PAA	-	70	30	-
9	1c5	St	PAA	-	50	50	-
10	2a9	MMA	DEAA	-	90	10	-
11	2a7	MMA	DEAA	-	70	30	-
12	2a5	MMA	DEAA	-	50	50	-
13	2b9	MMA	DMAA	-	90	10	-
14	2b7	MMA	DMAA	-	70	30	-
15	2b5	MMA	DMAA	-	50	50	-
16	2c9	MMA	PAA	-	90	10	-
17	2c7	MMA	PAA	-	70	30	-
18	2c5	MMA	PAA	-	50	50	-
19	3a9	MEMA	DEAA	-	90	10	-
20	3a7	MEMA	DEAA	-	70	30	-
21	3a5	MEMA	DEAA	-	50	50	-
22	3b9	MEMA	DMAA	-	90	10	-
23	3b7	MEMA	DMAA	-	70	30	-
24	3b5	MEMA	DMAA	-	50	50	-
25	3c9	MEMA	PAA	-	90	10	-
26	3c7	MEMA	PAA	-	70	30	-
27	3c5	MEMA	PAA	-	50	50	-
28	4a9	MEA	DEAA	-	90	10	-
29	4a7	MEA	DEAA	-	70	30	-
30	4a5	MEA	DEAA	-	50	50	-
31	4b9	MEA	DMAA	-	90	10	-
32	4b7	MEA	DMAA	-	70	30	-
33	4b5	MEA	DMAA	-	50	50	-
34	4c9	MEA	PAA	-	90	10	-
35	4c7	MEA	PAA	-	70	30	-
36	4c5	MEA	PAA	-	50	50	-
37	5a9	HEMA	DEAA	-	90	10	-
38	5a7	HEMA	DEAA	-	70	30	-
39	5a5	HEMA	DEAA	-	50	50	-
40	5b9	HEMA	DMAA	-	90	10	-
41	5b7	HEMA	DMAA	-	70	30	-
42	5b5	HEMA	DMAA	-	50	50	-
43	5c9	HEMA	PAA	-	90	10	-
44	5c7	HEMA	PAA	-	70	30	-
45	5c5	HEMA	PAA	-	50	50	-
46	6a9	HPMA	DEAA	-	90	10	-
47	6a7	HPMA	DEAA	-	70	30	-
48	6a5	HPMA	DEAA	-	50	50	-
49	6b9	HPMA	DMAA	-	90	10	-
50	6b7	HPMA	DMAA	-	70	30	-
51	6b5	HPMA	DMAA	-	50	50	-
52	6c9	HPMA	PAA	-	90	10	-
53	6c7	HPMA	PAA	-	70	30	-
54	6c5	HPMA	PAA	-	50	50	-
55	7a9	HBMA	DEAA	-	90	10	-
56	7a7	HBMA	DEAA	-	70	30	-
57	7a5	HBMA	DEAA	-	50	50	-
58	7b9	HBMA	DMAA	-	90	10	-
59	7b7	HBMA	DMAA	-	70	30	-
60	7b5	HBMA	DMAA	-	50	50	-
61	7c9	HBMA	PAA	-	90	10	-
62	7c7	HBMA	PAA	-	70	30	-
63	7c5	HBMA	PAA	-	50	50	-

Polymer reference	Bradley reference	Monomer (1)	Monomer (2)	Monomer (3)	Ratio (% mol.)		
					M (1)	M (2)	M (3)
64	6a9	HPMA	DEAA	-	90	10	-
65	6a7	HPMA	DEAA	-	70	30	-
66	6a5	HPMA	DEAA	-	50	50	-
67	6b9	HPMA	DMAA	-	90	10	-
68	6b7	HPMA	DMAA	-	70	30	-
69	6b5	HPMA	DMAA	-	50	50	-
70	6c9	HPMA	PAA	-	90	10	-
71	6c7	HPMA	PAA	-	70	30	-
72	6c5	HPMA	PAA	-	50	50	-
73	7a9	HBMA	DEAA	-	90	10	-
74	7a7	HBMA	DEAA	-	70	30	-
75	7a5	HBMA	DEAA	-	50	50	-
76	7b9	HBMA	DMAA	-	90	10	-
77	7b7	HBMA	DMAA	-	70	30	-
78	7b5	HBMA	DMAA	-	50	50	-
79	7c9	HBMA	PAA	-	90	10	-
80	7c7	HBMA	PAA	-	70	30	-
81	7c5	HBMA	PAA	-	50	50	-
82	3e9	MEMA	DEAEMA	-	90	10	-
83	3e7	MEMA	DEAEMA	-	70	30	-
84	3e5	MEMA	DEAEMA	-	50	50	-
85	3f9	MEMA	DMAEMA	-	90	10	-
86	3f7	MEMA	DMAEMA	-	70	30	-
87	3f5	MEMA	DMAEMA	-	50	50	-
88	3g9	MEMA	DEAEA	-	90	10	-
89	3g7	MEMA	DEAEA	-	70	30	-
90	3g5	MEMA	DEAEA	-	50	50	-
91	3h9	MEMA	DMAEA	-	90	10	-
92	3h7	MEMA	DMAEA	-	70	30	-
93	3h5	MEMA	DMAEA	-	50	50	-
94	3i9	MEMA	MTEMA	-	90	10	-
95	3i7	MEMA	MTEMA	-	70	30	-
96	3i5	MEMA	MTEMA	-	50	50	-
97	3j9	MEMA	BAEMA	-	90	10	-
98	3j7	MEMA	BAEMA	-	70	30	-
99	3j5	MEMA	BAEMA	-	50	50	-
100	3l9	MEMA	DMAPMAA	-	90	10	-
101	3l7	MEMA	DMAPMAA	-	70	30	-
102	3l5	MEMA	DMAPMAA	-	50	50	-
103	3m9	MEMA	BACOEA	-	90	10	-
104	3m7	MEMA	BACOEA	-	70	30	-
105	3m5	MEMA	BACOEA	-	50	50	-
106	3n9	MEMA	DMVBA	-	90	10	-
107	3n7	MEMA	DMVBA	-	70	30	-
108	3n5	MEMA	DMVBA	-	50	50	-
109	3v9	MEMA	VAA	-	90	10	-
110	3v7	MEMA	VAA	-	70	30	-
111	3v5	MEMA	VAA	-	50	50	-
112	3x9	MEMA	VI	-	90	10	-
113	3x7	MEMA	VI	-	70	30	-
114	3x5	MEMA	VI	-	50	50	-
115	3z9	MEMA	VPNO	-	90	10	-
116	3z7	MEMA	VPNO	-	70	30	-
117	3z5	MEMA	VPNO	-	50	50	-
118	3AA9	MEMA	VP-4	-	90	10	-
119	3AA7	MEMA	VP-4	-	70	30	-
120	3AA5	MEMA	VP-4	-	50	50	-
121	3AB9	MEMA	VP-2	-	90	10	-
122	3AB7	MEMA	VP-2	-	70	30	-
123	3AB5	MEMA	VP-2	-	50	50	-
124	3AC9	MEMA	DAAA	-	90	10	-
125	3AC7	MEMA	DAAA	-	70	30	-
126	3AC5	MEMA	DAAA	-	50	50	-
127	3AE9	MEMA	MNPMA	-	90	10	-
128	3AE7	MEMA	MNPMA	-	70	30	-
129	3AE5	MEMA	MNPMA	-	50	50	-
130	3i9	MEMA	MTEMA	-	90	10	-
131	3i7	MEMA	MTEMA	-	70	30	-

Polymer reference	Bradley reference	Monomer (1)	Monomer (2)	Monomer (3)	Ratio (% mol.)		
					M (1)	M (2)	M (3)
132	3i5	MEMA	MTEMA	-	50	50	-
133	3m9	MEMA	BACOEA	-	90	10	-
134	3m7	MEMA	BACOEA	-	70	30	-
135	3m5	MEMA	BACOEA	-	50	50	-
136	5e9	HEMA	DEAEMA	-	90	10	-
137	5e7	HEMA	DEAEMA	-	70	30	-
138	5e5	HEMA	DEAEMA	-	50	50	-
139	5f9	HEMA	DMAEMA	-	90	10	-
140	5f7	HEMA	DMAEMA	-	70	30	-
141	5f5	HEMA	DMAEMA	-	50	50	-
142	5g9	HEMA	DEAEA	-	90	10	-
143	5g7	HEMA	DEAEA	-	70	30	-
144	5g5	HEMA	DEAEA	-	50	50	-
145	5h9	HEMA	DMAEA	-	90	10	-
146	5h7	HEMA	DMAEA	-	70	30	-
147	5h5	HEMA	DMAEA	-	50	50	-
148	5i9	HEMA	MTEMA	-	90	10	-
149	5i7	HEMA	MTEMA	-	70	30	-
150	5i5	HEMA	MTEMA	-	50	50	-
151	5j9	HEMA	BAEMA	-	90	10	-
152	5j7	HEMA	BAEMA	-	70	30	-
153	5j5	HEMA	BAEMA	-	50	50	-
154	5l9	HEMA	DMAPMAA	-	90	10	-
155	5l7	HEMA	DMAPMAA	-	70	30	-
156	5l5	HEMA	DMAPMAA	-	50	50	-
157	5m9	HEMA	BACOEA	-	90	10	-
158	5m7	HEMA	BACOEA	-	70	30	-
159	5m5	HEMA	BACOEA	-	50	50	-
160	5n9	HEMA	DMVBA	-	90	10	-
161	5n7	HEMA	DMVBA	-	70	30	-
162	5n5	HEMA	DMVBA	-	50	50	-
163	5v9	HEMA	VAA	-	90	10	-
164	5v7	HEMA	VAA	-	70	30	-
165	5v5	HEMA	VAA	-	50	50	-
166	5x9	HEMA	VI	-	90	10	-
167	5x7	HEMA	VI	-	70	30	-
168	5x5	HEMA	VI	-	50	50	-
169	5z9	HEMA	VPNO	-	90	10	-
170	5z7	HEMA	VPNO	-	70	30	-
171	5z5	HEMA	VPNO	-	50	50	-
172	5AA9	HEMA	VP-4	-	90	10	-
173	5AA7	HEMA	VP-4	-	70	30	-
174	5AA5	HEMA	VP-4	-	50	50	-
175	5AB9	HEMA	VP-2	-	90	10	-
176	5AB7	HEMA	VP-2	-	70	30	-
177	5AB5	HEMA	VP-2	-	50	50	-
178	5AC9	HEMA	DAAA	-	90	10	-
179	5AC7	HEMA	DAAA	-	70	30	-
180	5AC5	HEMA	DAAA	-	50	50	-
181	5AE9	HEMA	MNPMA	-	90	10	-
182	5AE7	HEMA	MNPMA	-	70	30	-
183	5AE5	HEMA	MNPMA	-	50	50	-
184	2BA9	MMA	A-H	-	90	10	-
185	2BA7	MMA	A-H	-	70	30	-
186	2BA5	MMA	A-H	-	50	50	-
187	2BB9	MMA	AES-H	-	90	10	-
188	2BB7	MMA	AES-H	-	70	30	-
189	2BB5	MMA	AES-H	-	50	50	-
190	2BC9	MMA	MA-H	-	90	10	-
191	2BC7	MMA	MA-H	-	70	30	-
192	2BC5	MMA	MA-H	-	50	50	-
193	2BE9	MMA	AAG-H	-	90	10	-
194	2BE7	MMA	AAG-H	-	70	30	-
195	2BE5	MMA	AAG-H	-	50	50	-
196	2BG9	MMA	EGMP-H	-	90	10	-
197	2BG7	MMA	EGMP-H	-	70	30	-
198	2BG5	MMA	EGMP-H	-	50	50	-
199	3BA9	MEMA	A-H	-	90	10	-

Polymer reference	Bradley reference	Monomer (1)	Monomer (2)	Monomer (3)	Ratio (% mol.)		
					M (1)	M (2)	M (3)
200	3BA7	MEMA	A-H	-	70	30	-
201	3BA5	MEMA	A-H	-	50	50	-
202	3BB9	MEMA	AES-H	-	90	10	-
203	3BB7	MEMA	AES-H	-	70	30	-
204	3BB5	MEMA	AES-H	-	50	50	-
205	3BC9	MEMA	MA-H	-	90	10	-
206	3BC7	MEMA	MA-H	-	70	30	-
207	3BC5	MEMA	MA-H	-	50	50	-
208	3BE9	MEMA	AAG-H	-	90	10	-
209	3BE7	MEMA	AAG-H	-	70	30	-
210	3BE5	MEMA	AAG-H	-	50	50	-
211	3BG9	MEMA	EGMP-H	-	90	10	-
212	3BG7	MEMA	EGMP-H	-	70	30	-
213	3BG5	MEMA	EGMP-H	-	50	50	-
214	2BAe7-2.0	MMA	A-H	DEAEMA	70	20	10
215	2BAe7-1.5	MMA	A-H	DEAEMA	70	15	15
216	2BAe7-1.0	MMA	A-H	DEAEMA	70	10	20
217	2BAg7-2.0	MMA	A-H	DEAEA	70	20	10
218	2BAg7-1.5	MMA	A-H	DEAEA	70	15	15
219	2BAg7-1.0	MMA	A-H	DEAEA	70	10	20
220	2BCe7-2.0	MMA	MA-H	DEAEMA	70	20	10
221	2BCe7-1.5	MMA	MA-H	DEAEMA	70	15	15
222	2BCe7-1.0	MMA	MA-H	DEAEMA	70	10	20
223	2BCg7-2.0	MMA	MA-H	DEAEA	70	20	10
224	2BCg7-1.5	MMA	MA-H	DEAEA	70	15	15
225	2BCg7-1.0	MMA	MA-H	DEAEA	70	10	20
226	3BAe7-2.0	MEMA	A-H	DEAEMA	70	20	10
227	3BAe7-1.5	MEMA	A-H	DEAEMA	70	15	15
228	3BAe7-1.0	MEMA	A-H	DEAEMA	70	10	20
229	3BAg7-2.0	MEMA	A-H	DEAEA	70	20	10
230	3BAg7-1.5	MEMA	A-H	DEAEA	70	15	15
231	3BAg7-1.0	MEMA	A-H	DEAEA	70	10	20
232	3BCe7-2.0	MEMA	MA-H	DEAEMA	70	20	10
233	3BCe7-1.5	MEMA	MA-H	DEAEMA	70	15	15
234	3BCe7-1.0	MEMA	MA-H	DEAEMA	70	10	20
235	3BCg7-2.0	MEMA	MA-H	DEAEA	70	20	10
236	3BCg7-1.5	MEMA	MA-H	DEAEA	70	15	15
237	3BCg7-1.0	MEMA	MA-H	DEAEA	70	10	20
238	3GM9	MEMA	GMA	-	90	10	-
239	3GM7	MEMA	GMA	-	70	30	-
240	3GM5	MEMA	GMA	-	50	50	-
241	3GA1-9	MEMA	GMA	DnBA	90	10	-
242	3GA1-7	MEMA	GMA	DnBA	70	30	-
243	3GA1-5	MEMA	GMA	DnBA	50	50	-
244	3GA2-9	MEMA	GMA	DnHA	90	10	-
245	3GA2-7	MEMA	GMA	DnHA	70	30	-
246	3GA2-5	MEMA	GMA	DnHA	50	50	-
247	3GA3-9	MEMA	GMA	DcHA	90	10	-
248	3GA3-7	MEMA	GMA	DcHA	70	30	-
249	3GA3-5	MEMA	GMA	DcHA	50	50	-
250	3GA4-9	MEMA	GMA	DBnA	90	10	-
251	3GA4-7	MEMA	GMA	DBnA	70	30	-
252	3GA4-5	MEMA	GMA	DBnA	50	50	-
253	3GA5-9	MEMA	GMA	MnHA	90	10	-
254	3GA5-7	MEMA	GMA	MnHA	70	30	-
255	3GA5-5	MEMA	GMA	MnHA	50	50	-
256	3GA6-9	MEMA	GMA	cHMA	90	10	-
257	3GA6-7	MEMA	GMA	cHMA	70	30	-
258	3GA6-5	MEMA	GMA	cHMA	50	50	-
259	3GA7-9	MEMA	GMA	BnMA	90	10	-
260	3GA7-7	MEMA	GMA	BnMA	70	30	-
261	3GA7-5	MEMA	GMA	BnMA	50	50	-
262	3GA8-9	MEMA	GMA	MAEPy	90	10	-
263	3GA8-7	MEMA	GMA	MAEPy	70	30	-
264	3GA8-5	MEMA	GMA	MAEPy	50	50	-
265	3GA9-9	MEMA	GMA	Pyrle	90	10	-
266	3GA9-7	MEMA	GMA	Pyrle	70	30	-
267	3GA9-5	MEMA	GMA	Pyrle	50	50	-

Polymer reference	Bradley reference	Monomer (1)	Monomer (2)	Monomer (3)	Ratio (% mol.)		
					M (1)	M (2)	M (3)
268	3GA10-9	MEMA	GMA	2-MAPy	90	10	-
269	3GA10-7	MEMA	GMA	2-MAPy	70	30	-
270	3GA10-5	MEMA	GMA	2-MAPy	50	50	-
271	3GA11-9	MEMA	GMA	MAn	90	10	-
272	3GA11-7	MEMA	GMA	MAn	70	30	-
273	3GA11-5	MEMA	GMA	MAn	50	50	-
274	3GA12-9	MEMA	GMA	TMEDA	90	10	-
275	3GA12-7	MEMA	GMA	TMEDA	70	30	-
276	3GA12-5	MEMA	GMA	TMEDA	50	50	-
277	3GA13-9	MEMA	GMA	DEMEDA	90	10	-
278	3GA13-7	MEMA	GMA	DEMEDA	70	30	-
279	3GA13-5	MEMA	GMA	DEMEDA	50	50	-
280	3GA14-9	MEMA	GMA	TMPDA	90	10	-
281	3GA14-7	MEMA	GMA	TMPDA	70	30	-
282	3GA14-5	MEMA	GMA	TMPDA	50	50	-
283	3GA15-9	MEMA	GMA	Mpi	90	10	-
284	3GA15-7	MEMA	GMA	Mpi	70	30	-
285	3GA15-5	MEMA	GMA	Mpi	50	50	-
286	3GA16-9	MEMA	GMA	TEDETA	90	10	-
287	3GA16-7	MEMA	GMA	TEDETA	70	30	-
288	3GA16-5	MEMA	GMA	TEDETA	50	50	-
289	2GM9	MMA	GMA	-	90	10	-
290	2GM7	MMA	GMA	-	70	30	-
291	2GM5	MMA	GMA	-	50	50	-
292	2GA1-9	MMA	GMA	DnBA	90	10	-
293	2GA1-7	MMA	GMA	DnBA	70	30	-
294	2GA1-5	MMA	GMA	DnBA	50	50	-
295	2GA2-9	MMA	GMA	DnHA	90	10	-
296	2GA2-7	MMA	GMA	DnHA	70	30	-
297	2GA2-5	MMA	GMA	DnHA	50	50	-
298	2GA3-9	MMA	GMA	DcHA	90	10	-
299	2GA3-7	MMA	GMA	DcHA	70	30	-
300	2GA3-5	MMA	GMA	DcHA	50	50	-
301	2GA4-9	MMA	GMA	DBnA	90	10	-
302	2GA4-7	MMA	GMA	DBnA	70	30	-
303	2GA4-5	MMA	GMA	DBnA	50	50	-
304	2GA5-9	MMA	GMA	MnHA	90	10	-
305	2GA5-7	MMA	GMA	MnHA	70	30	-
306	2GA5-5	MMA	GMA	MnHA	50	50	-
307	2GA6-9	MMA	GMA	cHMA	90	10	-
308	2GA6-7	MMA	GMA	cHMA	70	30	-
309	2GA6-5	MMA	GMA	cHMA	50	50	-
310	2GA7-9	MMA	GMA	BnMA	90	10	-
311	2GA7-7	MMA	GMA	BnMA	70	30	-
312	2GA7-5	MMA	GMA	BnMA	50	50	-
313	2GA8-9	MMA	GMA	MAEPy	90	10	-
314	2GA8-7	MMA	GMA	MAEPy	70	30	-
315	2GA8-5	MMA	GMA	MAEPy	50	50	-
316	2GA9-9	MMA	GMA	Pyrle	90	10	-
317	2GA9-7	MMA	GMA	Pyrle	70	30	-
318	2GA9-5	MMA	GMA	Pyrle	50	50	-
319	2GA10-9	MMA	GMA	2-MAPy	90	10	-
320	2GA10-7	MMA	GMA	2-MAPy	70	30	-
321	2GA10-5	MMA	GMA	2-MAPy	50	50	-
322	2GA11-9	MMA	GMA	MAn	90	10	-
323	2GA11-7	MMA	GMA	MAn	70	30	-
324	2GA11-5	MMA	GMA	MAn	50	50	-
325	2GA12-9	MMA	GMA	TMEDA	90	10	-
326	2GA12-7	MMA	GMA	TMEDA	70	30	-
327	2GA12-5	MMA	GMA	TMEDA	50	50	-
328	2GA13-9	MMA	GMA	DEMEDA	90	10	-
329	2GA13-7	MMA	GMA	DEMEDA	70	30	-
330	2GA13-5	MMA	GMA	DEMEDA	50	50	-
331	2GA14-9	MMA	GMA	TMPDA	90	10	-
332	2GA14-7	MMA	GMA	TMPDA	70	30	-
333	2GA14-5	MMA	GMA	TMPDA	50	50	-
334	2GA15-9	MMA	GMA	Mpi	90	10	-
335	2GA15-7	MMA	GMA	Mpi	70	30	-

Polymer reference	Bradley reference	Monomer (1)	Monomer (2)	Monomer (3)	Ratio (% mol.)		
					M (1)	M (2)	M (3)
336	2GA15-5	MMA	GMA	Mpi	50	50	-
337	2GA16-9	MMA	GMA	TEDETA	90	10	-
338	2GA16-7	MMA	GMA	TEDETA	70	30	-
339	2GA16-5	MMA	GMA	TEDETA	50	50	-
340	2e9	MMA	DEAEMA	-	90	10	-
341	2e7	MMA	DEAEMA	-	70	30	-
342	2e5	MMA	DEAEMA	-	50	50	-
343	2f9	MMA	DMAEMA	-	90	10	-
344	2f7	MMA	DMAEMA	-	70	30	-
345	2f5	MMA	DMAEMA	-	50	50	-
346	2g9	MMA	DEAEA	-	90	10	-
347	2g7	MMA	DEAEA	-	70	30	-
348	2g5	MMA	DEAEA	-	50	50	-
349	2h9	MMA	DMAEA	-	90	10	-
350	2h7	MMA	DMAEA	-	70	30	-
351	2h5	MMA	DMAEA	-	50	50	-
352	6e9	HPMA	DEAEMA	-	90	10	-
353	6e7	HPMA	DEAEMA	-	70	30	-
354	6e5	HPMA	DEAEMA	-	50	50	-
355	6f9	HPMA	DMAEMA	-	90	10	-
356	6f7	HPMA	DMAEMA	-	70	30	-
357	6f5	HPMA	DMAEMA	-	50	50	-
358	6g9	HPMA	DEAEA	-	90	10	-
359	6g7	HPMA	DEAEA	-	70	30	-
360	6g5	HPMA	DEAEA	-	50	50	-
361	6h9	HPMA	DMAEA	-	90	10	-
362	6h7	HPMA	DMAEA	-	70	30	-
363	6h5	HPMA	DMAEA	-	50	50	-
364	7e9	HBMA	DEAEMA	-	90	10	-
365	7e7	HBMA	DEAEMA	-	70	30	-
366	7e5	HBMA	DEAEMA	-	50	50	-
367	7f9	HBMA	DMAEMA	-	90	10	-
368	7f7	HBMA	DMAEMA	-	70	30	-
369	7f5	HBMA	DMAEMA	-	50	50	-
370	7g9	HBMA	DEAEA	-	90	10	-
371	7g7	HBMA	DEAEA	-	70	30	-
372	7g5	HBMA	DEAEA	-	50	50	-
373	7h9	HBMA	DMAEA	-	90	10	-
374	7h7	HBMA	DMAEA	-	70	30	-
375	7h5	HBMA	DMAEA	-	50	50	-
376	8e9	EMA	DEAEMA	-	90	10	-
377	8e7	EMA	DEAEMA	-	70	30	-
378	8e5	EMA	DEAEMA	-	50	50	-
379	8f9	EMA	DMAEMA	-	90	10	-
380	8f7	EMA	DMAEMA	-	70	30	-
381	8f5	EMA	DMAEMA	-	50	50	-
382	8g9	EMA	DEAEA	-	90	10	-
383	8g7	EMA	DEAEA	-	70	30	-
384	8g5	EMA	DEAEA	-	50	50	-
385	8h9	EMA	DMAEA	-	90	10	-
386	8h7	EMA	DMAEA	-	70	30	-
387	8h5	EMA	DMAEA	-	50	50	-
388	9e9	BMA	DEAEMA	-	90	10	-
389	9e7	BMA	DEAEMA	-	70	30	-
390	9e5	BMA	DEAEMA	-	50	50	-
391	9f9	BMA	DMAEMA	-	90	10	-
392	9f7	BMA	DMAEMA	-	70	30	-
393	9f5	BMA	DMAEMA	-	50	50	-
394	9g9	BMA	DEAEA	-	90	10	-
395	9g7	BMA	DEAEA	-	70	30	-
396	9g5	BMA	DEAEA	-	50	50	-
397	9h9	BMA	DMAEA	-	90	10	-
398	9h7	BMA	DMAEA	-	70	30	-
399	9h5	BMA	DMAEA	-	50	50	-
400	PL6-1	MEMA	DEAEMA	MA	40	30	30
401	PL6-2	MEMA	DEAEMA	MA	60	10	30
402	PL6-3	MEMA	DEAEMA	MA	60	30	10
403	PL6-4	MEMA	DEAEMA	MA	80	10	10

Polymer reference	Bradley reference	Monomer (1)	Monomer (2)	Monomer (3)	Ratio (% mol.)		
					M (1)	M (2)	M (3)
404	PL6-5	MEMA	DEAEA	MA	40	30	30
405	PL6-6	MEMA	DEAEA	MA	60	10	30
406	PL6-7	MEMA	DEAEA	MA	60	30	10
407	PL6-8	MEMA	DEAEA	MA	80	10	10
408	PL6-9	MEMA	DEAEMA	BMA	40	30	30
409	PL6-10	MEMA	DEAEMA	BMA	60	10	30
410	PL6-11	MEMA	DEAEMA	BMA	60	30	10
411	PL6-12	MEMA	DEAEMA	BMA	80	10	10
412	PL6-13	MEMA	DEAEA	BMA	40	30	30
413	PL6-14	MEMA	DEAEA	BMA	60	10	30
414	PL6-15	MEMA	DEAEA	BMA	60	30	10
415	PL6-16	MEMA	DEAEA	BMA	80	10	10
416	PL6-17	MEMA	DEAEMA	MEA	40	30	30
417	PL6-18	MEMA	DEAEMA	MEA	60	10	30
418	PL6-19	MEMA	DEAEMA	MEA	60	30	10
419	PL6-20	MEMA	DEAEMA	MEA	80	10	10
420	PL6-21	MEMA	DEAEA	MEA	40	30	30
421	PL6-22	MEMA	DEAEA	MEA	60	10	30
422	PL6-23	MEMA	DEAEA	MEA	60	30	10
423	PL6-24	MEMA	DEAEA	MEA	80	10	10
424	PL6-25	MEMA	DEAEMA	DEGMEMA	40	30	30
425	PL6-26	MEMA	DEAEMA	DEGMEMA	60	10	30
426	PL6-27	MEMA	DEAEMA	DEGMEMA	60	30	10
427	PL6-28	MEMA	DEAEMA	DEGMEMA	80	10	10
428	PL6-29	MEMA	DEAEA	DEGMEMA	40	30	30
429	PL6-30	MEMA	DEAEA	DEGMEMA	60	10	30
430	PL6-31	MEMA	DEAEA	DEGMEMA	60	30	10
431	PL6-32	MEMA	DEAEA	DEGMEMA	80	10	10
432	PL6-33	MEMA	DEAEMA	THFFA	40	30	30
433	PL6-34	MEMA	DEAEMA	THFFA	60	10	30
434	PL6-35	MEMA	DEAEMA	THFFA	60	30	10
435	PL6-36	MEMA	DEAEMA	THFFA	80	10	10
436	PL6-37	MEMA	DEAEA	THFFA	40	30	30
437	PL6-38	MEMA	DEAEA	THFFA	60	10	30
438	PL6-39	MEMA	DEAEA	THFFA	60	30	10
439	PL6-40	MEMA	DEAEA	THFFA	80	10	10
440	PL6-41	MEMA	DEAEMA	THFFMA	40	30	30
441	PL6-42	MEMA	DEAEMA	THFFMA	60	10	30
442	PL6-43	MEMA	DEAEMA	THFFMA	60	30	10
443	PL6-44	MEMA	DEAEMA	THFFMA	80	10	10
444	PL6-45	MEMA	DEAEA	THFFMA	40	30	30
445	PL6-46	MEMA	DEAEA	THFFMA	60	10	30
446	PL6-47	MEMA	DEAEA	THFFMA	60	30	10
447	PL6-48	MEMA	DEAEA	THFFMA	80	10	10
448	PL6-49	MEMA	DEAEMA	HEA	40	30	30
449	PL6-50	MEMA	DEAEMA	HEA	60	10	30
450	PL6-51	MEMA	DEAEMA	HEA	60	30	10
451	PL6-52	MEMA	DEAEMA	HEA	80	10	10
452	PL6-53	MEMA	DEAEA	HEA	40	30	30
453	PL6-54	MEMA	DEAEA	HEA	60	10	30
454	PL6-55	MEMA	DEAEA	HEA	60	30	10
455	PL6-56	MEMA	DEAEA	HEA	80	10	10
456	PL6-57	MEMA	DEAEMA	HEMA	40	30	30
457	PL6-58	MEMA	DEAEMA	HEMA	60	10	30
458	PL6-59	MEMA	DEAEMA	HEMA	60	30	10
459	PL6-60	MEMA	DEAEMA	HEMA	80	10	10
460	PL6-61	MEMA	DEAEA	HEMA	40	30	30
461	PL6-62	MEMA	DEAEA	HEMA	60	10	30
462	PL6-63	MEMA	DEAEA	HEMA	60	30	10
463	PL6-64	MEMA	DEAEA	HEMA	80	10	10
464	PL6-65	MEMA	DEAEMA	A-H	40	30	30
465	PL6-66	MEMA	DEAEMA	A-H	60	10	30
466	PL6-67	MEMA	DEAEMA	A-H	60	30	10
467	PL6-68	MEMA	DEAEMA	A-H	80	10	10
468	PL6-69	MEMA	DEAEA	A-H	40	30	30
469	PL6-70	MEMA	DEAEA	A-H	60	10	30
470	PL6-71	MEMA	DEAEA	A-H	60	30	10
471	PL6-72	MEMA	DEAEA	A-H	80	10	10

Polymer reference	Bradley reference	Monomer (1)	Monomer (2)	Monomer (3)	Ratio (% mol.)		
					M (1)	M (2)	M (3)
472	PL6-73	MEMA	DEAEMA	MA-H	40	30	30
473	PL6-74	MEMA	DEAEMA	MA-H	60	10	30
474	PL6-75	MEMA	DEAEMA	MA-H	60	30	10
475	PL6-76	MEMA	DEAEMA	MA-H	80	10	10
476	PL6-77	MEMA	DEAEA	MA-H	40	30	30
477	PL6-78	MEMA	DEAEA	MA-H	60	10	30
478	PL6-79	MEMA	DEAEA	MA-H	60	30	10
479	PL6-80	MEMA	DEAEA	MA-H	80	10	10
480	PL6-81	MEMA	DEAEMA	DMAA	40	30	30
481	PL6-82	MEMA	DEAEMA	DMAA	60	10	30
482	PL6-83	MEMA	DEAEMA	DMAA	60	30	10
483	PL6-84	MEMA	DEAEMA	DMAA	80	10	10
484	PL6-85	MEMA	DEAEA	DMAA	40	30	30
485	PL6-86	MEMA	DEAEA	DMAA	60	10	30
486	PL6-87	MEMA	DEAEA	DMAA	60	30	10
487	PL6-88	MEMA	DEAEA	DMAA	80	10	10
488	PL6-89	MEMA	DEAEMA	DAAA	40	30	30
489	PL6-90	MEMA	DEAEMA	DAAA	60	10	30
490	PL6-91	MEMA	DEAEMA	DAAA	60	30	10
491	PL6-92	MEMA	DEAEMA	DAAA	80	10	10
492	PL6-93	MEMA	DEAEA	DAAA	40	30	30
493	PL6-94	MEMA	DEAEA	DAAA	60	10	30
494	PL6-95	MEMA	DEAEA	DAAA	60	30	10
495	PL6-96	MEMA	DEAEA	DAAA	80	10	10
496	PL6-97	MEMA	DEAEMA	MMA	40	30	30
497	PL6-98	MEMA	DEAEMA	MMA	60	10	30
498	PL6-99	MEMA	DEAEMA	MMA	60	30	10
499	PL6-100	MEMA	DEAEMA	MMA	80	10	10
500	PL6-101	MEMA	DEAEA	MMA	40	30	30
501	PL6-102	MEMA	DEAEA	MMA	60	10	30
502	PL6-103	MEMA	DEAEA	MMA	60	30	10
503	PL6-104	MEMA	DEAEA	MMA	80	10	10
504	PL6-105	MEMA	DEAEMA	St	40	30	30
505	PL6-106	MEMA	DEAEMA	St	60	10	30
506	PL6-107	MEMA	DEAEMA	St	60	30	10
507	PL6-108	MEMA	DEAEMA	St	80	10	10
508	PL6-109	MEMA	DEAEA	St	40	30	30
509	PL6-110	MEMA	DEAEA	St	60	10	30
510	PL6-111	MEMA	DEAEA	St	60	30	10
511	PL6-112	MEMA	DEAEA	St	80	10	10
512	3e8.5	MEMA	DEAEMA	-	85	15	-
513	3e8	MEMA	DEAEMA	-	80	20	-
514	3e7.5	MEMA	DEAEMA	-	75	25	-
515	3e7	MEMA	DEAEMA	-	70	30	-
516	3e6.5	MEMA	DEAEMA	-	65	35	-
517	3e6	MEMA	DEAEMA	-	60	40	-
518	3e5.5	MEMA	DEAEMA	-	55	45	-
519	P1	MEMA	A-H	DEAEMA	85	5	10
520	P2	MEMA	A-H	DEAEMA	80	5	15
521	P3	MEMA	A-H	DEAEMA	75	5	20
522	P4	MEMA	A-H	DEAEMA	70	5	25
523	P5	MEMA	A-H	DEAEMA	65	5	30
524	P6	MEMA	A-H	DEAEMA	60	5	35
525	P7	MEMA	A-H	DEAEMA	55	5	40
526	P8	MEMA	A-H	DEAEMA	50	5	45
527	P9	MEMA	A-H	DEAEMA	75	10	15
528	P10	MEMA	A-H	DEAEMA	70	10	20
529	P11	MEMA	A-H	DEAEMA	65	10	25
530	P12	MEMA	A-H	DEAEMA	55	10	35
531	P13	MEMA	A-H	DEAEMA	50	10	40
532	P14	MEMA	A-H	DEAEMA	65	15	20
533	P15	MEMA	A-H	DEAEMA	60	15	25
534	P16	MEMA	A-H	DEAEMA	55	15	30
535	P17	MEMA	A-H	DEAEMA	50	15	35
536	P18	MEMA	A-H	DEAEMA	55	20	25
537	P19	MEMA	A-H	DEAEMA	50	20	30
538	N1	MEMA	A-H	DEAEMA	90	5	5
539	N2	MEMA	A-H	DEAEMA	80	15	5

Polymer reference	Bradley reference	Monomer (1)	Monomer (2)	Monomer (3)	Ratio (% mol.)		
					M (1)	M (2)	M (3)
540	N3	MEMA	A-H	DEAEMA	70	25	5
541	N4	MEMA	A-H	DEAEMA	60	35	5
542	N5	MEMA	A-H	DEAEMA	50	45	5
543	N6	MEMA	A-H	DEAEMA	50	40	10
544	N7	MEMA	A-H	DEAEMA	60	25	15
545	N8	MEMA	A-H	DEAEMA	50	35	15
546	N9	MEMA	A-H	DEAEMA	60	20	20
547	N10	MEMA	A-H	DEAEMA	50	30	20
548	N11	MEMA	A-H	DEAEMA	50	25	25
549	Pg7	MEMA	A-H	DEAEA	55	5	40
550	Pg4	MEMA	A-H	DEAEA	70	5	25
551	Pg18	MEMA	A-H	DEAEA	55	20	25
552	3BAf 6	MEMA	A-H	DMAEMA	60	10	30
553	Pg15	MEMA	A-H	DEAEA	60	15	25
554	3BAh 6	MEMA	A-H	DMAEA	60	10	30
555	Pg3	MEMA	A-H	DEAEA	75	5	20
556	Pg5	MEMA	A-H	DEAEA	65	5	30
557	Pg1	MEMA	A-H	DEAEA	85	5	10
558	Pg10	MEMA	A-H	DEAEA	70	10	20
559	Pg11	MEMA	A-H	DEAEA	65	10	25
560	Pg16	MEMA	A-H	DEAEA	55	15	30
561	Pg8	MEMA	A-H	DEAEA	50	5	45
562	Pg2	MEMA	A-H	DEAEA	80	5	15
563	Pg14	MEMA	A-H	DEAEA	65	15	20
564	3BAf 7	MEMA	A-H	DMAEMA	70	10	20
565	Pg9	MEMA	A-H	DEAEA	75	10	15
566	Pg19	MEMA	A-H	DEAEA	50	20	30
567	Pg6	MEMA	A-H	DEAEA	60	5	35
568	Pg12	MEMA	A-H	DEAEA	55	10	35
569	3BAl 6	MEMA	A-H	DMAPMAA	60	10	30
570	Pg13	MEMA	A-H	DEAEA	50	10	40
571	Pg17	MEMA	A-H	DEAEA	50	15	35
572	3BAh 7	MEMA	A-H	DMAEA	70	10	20
573	3BAl 7	MEMA	A-H	DMAPMAA	70	10	20
576	P7	MEMA	A-H	DEAEMA	55	5	40
577	P8	MEMA	A-H	DEAEMA	50	5	45
523	P9	MEMA	A-H	DEAEMA	75	10	15
524	P10	MEMA	A-H	DEAEMA	70	10	20
525	P11	MEMA	A-H	DEAEMA	65	10	25
526	P12	MEMA	A-H	DEAEMA	55	10	35
527	P13	MEMA	A-H	DEAEMA	50	10	40
528	P14	MEMA	A-H	DEAEMA	65	15	20
529	P15	MEMA	A-H	DEAEMA	60	15	25
530	P16	MEMA	A-H	DEAEMA	55	15	30
531	P17	MEMA	A-H	DEAEMA	50	15	35
532	P18	MEMA	A-H	DEAEMA	55	20	25
533	P19	MEMA	A-H	DEAEMA	50	20	30
534	N1	MEMA	A-H	DEAEMA	90	5	5
535	N2	MEMA	A-H	DEAEMA	80	15	5
536	N3	MEMA	A-H	DEAEMA	70	25	5

Appendix III: PhD Activity

A paten, oral and poster presentations and scientific literature described in this section were carried out by the author under the supervision of Prof. Mark Bradley for the University of Edinburgh between April 2006 and April 2009.

Patent

Use of polymer for cell growth (GB 0904834.9).

Oral presentations

- Bradley group meeting presentation, 7 December 2006, Edinburgh (UK).
- Postgraduate research seminary, 27 March 2007, Edinburgh (UK).
- Bradley group meeting presentation, 29 March 2007, Edinburgh (UK).
- EUROCOMBI 4, 15-18 June 2007, Florence (Italy).
- INTERNATIONAL SCHOOL OF ADVANCED BIOMEDICINE AND BIOINFORMATICS, 1-5 September 2008, Catania (Italy).
- Istitute of stem cell research (ISCR), 25 September 2008, Edinburgh (UK).
- Bradley group meeting presentation, 8 November 2008, Edinburgh (UK).
- MATERIALS RESEARCH SOCIETY CONFERENCE, 26-30 November 2008, Boston (USA).
- Postgraduate research seminary, 15 January 2008, Edinburgh (UK).
- Bradley group meeting presentation, 8 March 2008, Edinburgh (UK).
- Postgraduate research seminary, 24 November 2008, Edinburgh (UK).
- Advances in microarray technology, 19-20 May 2009, Stockholm (Sweden).

Poster presentations

- Firbush Postgraduate Meeting, Screening of Polymer Microarrays for Suspension Cell Immobilization and Gene Expression Profiling. 4-6 April **2008**, Firbush (UK).
- 8th Would Biomaterials Congress. Polymer Microarrays - Fabrication and High-Throughput Screening for New Biomaterials. 28 May-1 June **2008**,

Amsterdam (NL).

- LabAutomation. Versatile Polymer Microarrays for Selective Cellular Control. 25-28 January 2009, Palm Springs, California (USA).
- 44th Annual Meeting of the European Association for the Study of the Liver. A Polymer Matrix Promotes and Stabilises hESC-Derived Hepatocyte Function. 22-26 April **2009**, Copenhagen (Denmark).
- BDSB Spring meeting. Identification of evolutionary and conserved Oct4 targets. 12-15 April **2010**, Warwick, England (UK).

Scientific literature

- Pernagallo, S.; Unciti-Broceta, A.; Diaz-Mochon, J. J.; Bradley, M. Deciphering cellular morphology and biocompatibility using polymer microarrays. *Biomedical Materials* **2008**, 3, 034112.
- Pernagallo, S.; Diaz-Mochon, J. J.; Bradley, M. A cooperative polymer- DNA microarray approach to biomaterial investigation. *Lab on a Chip* **2009,** 9, (3), 397-403.
- Di Pietro, V.; Amin.; Pernagallo, S.; Lazzarino, G.; Tavazzi, B.; Vagnozzi, R.; Pringle, A.; Belli, A. Transcriptomics of Traumatic Brain Injury: Gene Expression and Molecular Pathways of Different Grades of Insult in a Rat Organotypic Hippocampal Culture Model. *Journal of Neurotrauma* **2010**; 27, (2), 349-359.
- Alexander, L. M.; Pernagallo, S.; Livigni, A.; Sanchez-Martin, R. M.; Brickman, J. M.; Bradley, M. Investigation of microsphere-mediated cellular delivery by chemical, microscopic and gene expression analysis. *Molecular BioSystems* **2010**, 6, (2), 399-409.
- Hay, D. C.; Pernagallo, S.; Diaz-Mochon, J. J.; Fletcher, J.; Black, J.; Thompson, A.; Hannoun, Z.; Newsome, P.; Forbes, S.; Ross, J.; Bradley, M.; Iredale, J. P. A simple polyurethane matrix promotes hepatic endoderm viability and inducible drug metabolism. **2009,** submitted.
- Pernagallo S.; Wu M.; Gallagher M.P.; Bradley M. Colonising new frontiers - microarrays reveal novel biofilm modulating polymers. **2009**, submitted.

Edinburgh Research and Innovation
THE UNIVERSITY of EDINBURGH

Bio-active hepatocyte polymers

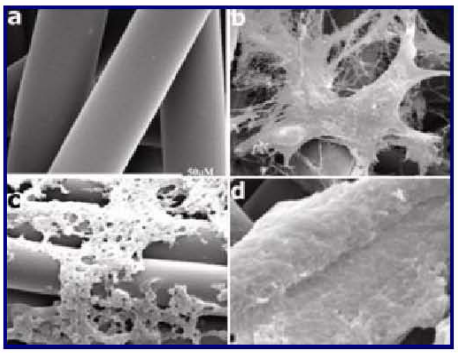

An Electron Microscope picture of (a) the bio-artificial liver (BAL) matrix, (b) hepatocytes on the BAL matrix, (c) the polymer coated BAL matrix and (d) hepatocytes on the polymer coated BAL matrix.

Generation of hepatic endoderm (HE) from human embryonic stem cells (hESCs) represents a viable route to generate a scalable resource for cell based therapy, drug and toxicology testing and for "fueling" bio-artificial liver (BAL) devices.

Researchers at the University of Edinburgh have identified a novel polymer matrix that overcomes issues of cellular phenotypic stability and viability providing a defined supporting basement matrix that significantly improves hESC-derived HE lifespan, function and inducible drug metabolism.

Ideally, drug toxicity modelling and BALs would be created using primary human hepatocytes (PHHs). However, PHHs are a scarce resource obtained from ressected liver that exhibit huge variability after isolation and exhibit diminishing function and viability following limited tissue culture. Therefore, hESC-derived HE represents a significant potential therapeutic tool.

However, like PHH, hESC-derived HE demonstrates limited viability and phenotypic stability on the current state of the art tissue culture substratum, matrigel.

This novel polymer identified by researchers at the University of Edinburgh overcomes these problems.

Key Benefits

- Combination of cutting edge hESC and polymer technologies provides a consistent source of viable and phenotypically relevant human HE
- Ideal source of human HE for in vitro drug and toxicology testing
- Scalability of HE production will drive development of humanised BAL devices
- Cost effective, consistent and reliable human HE source
- Polymer can be easily manufactured to GMP conditions

Applications

- Predictive pre-clinical toxicity testing
- Cell based therapies
- Liver support devices to aid failing detoxification as well as potential restoration of liver metabolic function

Patent Status

A UK patent (reference GB 0904834.9) has been filed, entitled, “Use of polymer for cell growth”, with a priority date of 20th March 2009.

Commercial Opportunity

The University of Edinburgh is offering this technology to commercial organisations for licensing and/or a potential research collaboration that might allow product to be developed.

Further Information

For further information on this technology transfer opportunity with the University of Edinburgh, please contact:

Dr Keith Finlayson
The University of Edinburgh
Darwin Building, King’s Buildings
Edinburgh, EH9 3JR
Scotland, UK

Telephone: +44 (0)131 650 5408
Email: Keith.Finlayson@ed.ac.uk

www.research-innovation.ed.ac.uk

Screening of Polymer Microarrays for Suspension Cell Immobilization and Gene Expression Profiling

Salvatore Pernagallo and Mark Bradley
Department of Chemistry, University of Edinburgh, EH9 3JJ, UK
E-mail: spernagallo@sms.ed.ac.uk

EPSRC Engineering and Physical Sciences Research Council

In this study, polymer microarrays were used for the rapid identification of polymer substrates/supports upon which a suspension cell line would adhere and proliferate giving a detailed and rapid understanding of cell-biomaterial interactions. Analysis demonstrated that suspension K562 human erythroleukemic cells, which normally grow in suspension, adhered and proliferated on several different polymers. Phenotypic and transcriptomic analysis techniques allowed examination of the interaction of cells with the biocompatible polymers allowing elucidation of putative links between phenotypic responses to cell-biomaterial interactions and global gene expression profiles.

-HT SCREENING OF POLYMER LIBRARIES-

Polymer Microarray Fabrication

Polymer microarrays were fabricated by contact printing (QArray^{mini},Genetix) with 32 aQu solid pins (K2785, Genetix) (Fig.1). The following printing conditions were used on aminoalkylsilane-treated glass slides (Sigma-Aldrich), previously coated with agarose Type I-B (Sigma). Two libraries were printed, a 210 member polyurethane library (PU) and a 58 member polyacrylate library (PA). The PU library was printed following a four-replicate pattern with 1 single field of 32 x 32 spots containing 46 control (empty) areas. The PA library was printed following a nine-replicate pattern within 1 single field of 24 x 24 spots containing 6 control (empty) areas. The typical spot size was 300-320 μm in diameter.

Fig.1

Qarray mini® (Genetix Ltd; UK).

Cell Binding

An aliquot of 6 mL of K562 cells (10^5 cells per mL) was added to each polymer microarrays contained in a slide well-plate (Nunc) and incubated for 24, 48 and 72 hours (Fig.2). To stain the nuclei, cells were washed in PBS and incubated for 30 min with fresh media and Hoechst 33342 (1 μg/mL). The polymer microarray were then rinsed in an isotonic solution (8.1 g/L NaCl, 0.2 g/L KCl) (Sigma-Aldrich) and immersed in this solution to facilitate K562 live cell analysis.

Fig.2

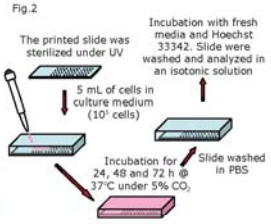

Analysis of cell attachment and proliferation

The binding of K562 cells on the polymer microarrays had two aims. Firstly to identify a polymer that would bind these suspension cells and secondly to measure cellular proliferation on the identified polymers. In order to quantify both cellular adhesion and proliferation on each polymer the average numbers of cells across the replicates were determined at three different incubation times (24, 48 and 72h) using three different polymer microarrays. Consequently, analysis of the three arrays in parallel enabled profiling of the polymer libraries in terms of cellular binding and proliferation. This was realized through the analysis of fluorescence images coming from nuclei staining using Hoechst 33342, with cell nuclei automatically recognized and quantified by the Pathfinder™ software (IMSTAR) (Fig.3).

Fig.3

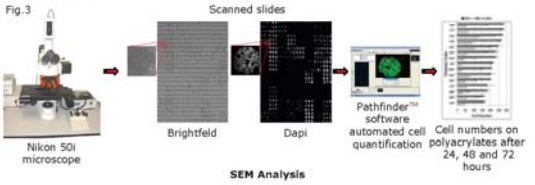

SEM Analysis

Scanning electron microscopy (SEM) studies were undertaken. The effect of the different polymers on the cells was assessed at 24 and 72 h. The surfaces of cells grown on polyacrylates for 24 h appeared to have with numerous contact with the substratum, with an evident flatter morphology at 72 h as a result.

Fig.4

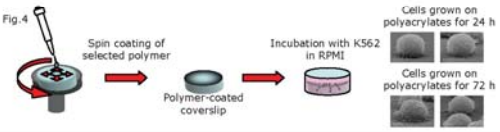

-GENE EXPRESSION PROFILE ANALYSIS-

cRNA sample preparation and hybridization

Total RNA was isolated from both K562 cells grown adhesively on coated coverslips and K562 grown in suspension. Hybridization was performed using 4 x 44 K Whole Human Genome microarray (design 014850 Agilent) (Fig.5).

Fig.5

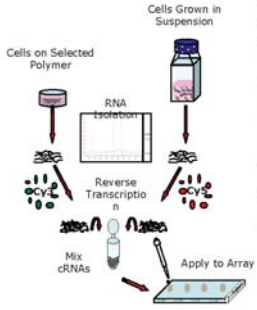

Array Scanning and Data analysis

Datasets pre-processed from Agilent Feature Extraction software (FE performs a Lowess normalization) were analysed by Genespring GX 9. The four datasets were grouped together and analysed to identify the interaction between polyacrylates (7E7 and 7F7) and K562 cells. A second analysis was performed by grouping the four datasets in a different way in order to see gene expression differences between cells grown on 7F7 (SubArray 1-2) and cells grown on 7E7 (SubArray 3-4) . *p*-values were computed asymptotically in both cases. Genes with *p*-values <0.001 were considered significant, meaning a probability of real changes in expression of 99.9% Fig.6).

Fig.6

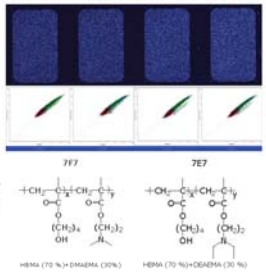

Fig.7

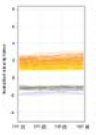

Gene Expression Profiling Analysis

Gene expression analysis gave 709 genes with a *p*-value < 0.001, which were then subjected to a fold change analysis to determine which genes were up and down-regulated using 2 fold increase or decrease as a cut-off value. 34 genes appeared to be up regulated while 135 were down-regulated. The quality of the data across each repeat is shown in the (Fig.7) with the profile plot of these genes. An ulterior refinement was done by increasing the cut-off value to identify genes which present bigger changes in expression. Thus, using a 3 fold change as cut-off value just 3 genes were identified as being up-regulated and 74 down-regulated genes (data not shown

A second analysis was performed in order to see different levels of expression when cells were grown on 7E7 and 7F7. 141 genes showed at least a 2 fold increase or decrease between the two different polymers (Fig. 8 A) . Within this dataset, 11 genes were found to have a 2 fold change versus zero, meaning that they are either up or down-regulated overall and with a 2 fold change between conditions (see heatmap in Fig.8 B).

Fig.8 A

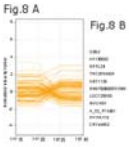

Fig.8 B

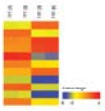

Fig.9

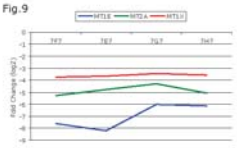

Validation of microarray results by quantitative real time RT-PCR analysis

In order to validate the observed expression profiles for the down regulated genes MT1X, MT2A and MT1E, quantitative real time (RT)-PCR on K562 cells grown on polymers 7E7, 7F7, 7G7 and 7H7 was performed (Fig.9). The results were normalised with respect to the total RNA expression of a housekeeping gene (RNF7).

-CONCLUSION-

Polymer microarrays were successfully used for the successful identification of a family/group of polymers that enabled adhesion and proliferation of a suspension cell line with scanning of live cells across the polymer microarray. A strong correlation was the importance of tertiary amino groups in promoting adhesion. These interactions were studied by SEM showing cells with numerous contact points with the substratum, as consequence of adhesive growth onto the positively charged surface. Finally gene expression profiling demonstrated that interactions between cells and materials induce a number of changes in the transcriptom. In this particular case, a remarkable down-regulation of predominantly membrane receptors, ligands and channels was observed take place. Furthermore, validation by quantitative real-time PCR, confirmed gene expression analysis.

- REFERENCES -

1. G. Tourniaire; M. Bradley; Patent number GB 2408331.
2. Pernagallo, S.; Unicit-Broceta, A; Diaz-Mochon, J.J.; Bradley Mark (2008). Deciphering cellular morphology and biocompatibility using polymer microarrays. Bio Mat. In press.
3. Pernagallo, S.; Diaz-Mochon, J.J.; Bradley Mark. Screening of Polymer Microarrays for Suspension Cell Immobilization and Gene Expression Profiling. PNAS submission.

- ACKNOWLEDGEMENTS-

We would like to thank EPSRC for a studentship.

Polymer Microarrays - Fabrication and High-Throughput Screening for New Biomaterials

Mark Bradley,[1,2] Albert Liberski,[1,2] Salvatore Pernagallo[1]
School of Chemistry, West Mains Road, Kings Buildings, University of Edinburgh, Edinburgh, UK[1] and Ilika Technologies, Chilworth Science Park, Southampton, Hants, UK[2]

Idea → 1 Microarray preparation → 2 Cellular screening → 3 Scale up → biomaterial

1 Polymer Microarray preparation

Microarray printing required extensive optimisation to ensure uniform polymer spot and shape for both inkjet and contact printing

-CONTACT PRINTING - for dispensing pre synthesised polymers

Stage 1- Solutions
Polymers(Fig 2. a,b) were dissolved at 1% w/v in a high viscosity and high boiling point solvent such as N-methyl pyrrolidinone. The solutions were placed into a 384-well polypropylene microplate prior to printing.

Stage 2- Printing
The robot used was the *Qarray mini*® (Genetix Ltd; UK).The solutions were deposited by contact printing using 150 µm solid pins. Each polymer solution was printed as 4 identical spots and each spot was formed by a minimum of 5 contact printings in order to reduce the effect of the ring stain formation[2]. The nature of the substrates were adapted to the different screenings in order to obtain the lowest background and most uniform spots. The typical spot diameter was 300 µm (±20 µm) with a volume about 7 nL which is equivalent to about 70 pg of polymer.

Stage 3- Drying
Once printed, the solvent was removed by drying under vacuum at 45°C overnight, to give a microarray with up to 2048 spots per slide.

- APPARATUS - CONTACT PRINTING

Fig. 1 Arrayer: *Qarray mini* (Genetix Ltd, UK)

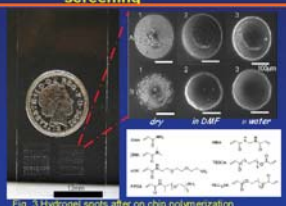

Fig. 3 Hydrogel spots after on chip polymerization

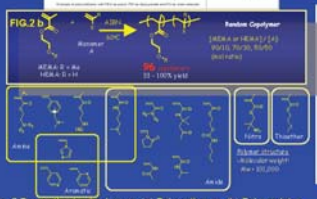

Fig. 2 Pre synthesised polymers: (a) Polyurethanes, (b) Polyacrylates

- INKJET PRINTING – for High Throughput polymer synthesis directly on chip

Fig. 5 (a) solvent, (b) monomer, (c) monomer+solvent

Stage 1- Printability
Printing parameters such voltage and impulse length either monomer concentration and solvent must be individually optimized in order to get uniform drops. FIG. 5

Stage 2- Evaporation prevention
In propose to stabilization of on chip reaction conditions the evaporation from spots was achieved by humidity control (50%) or printing on to paraffin oil layer

Stage 3- Printing
Developed software allow for automatic polymer synthesis in micro array format (minimal spot size for two monomers 100µm). Thanks surface modification (and agarose coating) polymers was immobilized on surface

Stage 4- Washing and drying
In propose to remove not reacted monomers chips was washed with water and ethanol than dried in vacuum at 45°C for 24h, to give a microarray with up to 1800 spots per slide. FIG.3

- APPARATUS - INKJET PRINTING

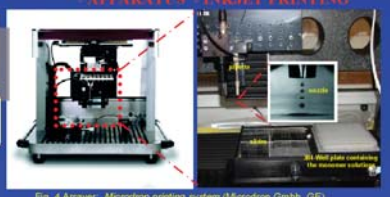

Fig. 4 Arrayer: *Microdrop printing system* (Microdrop Gmbh, GE)

2 Cellular screening

High Content screening platform:
Pathfinder™ / OSA Reader™ (IMSTAR S.A., F, www.imstar.fr)
High content, high resolution (0.3 µm) image cytometry platform allowing the determination of cell numbers, cellular coverage in the spot, all individual cell fluorescence intensities, spots fluorescence ratio & morphology characteristics.

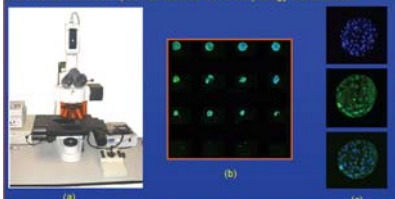

(a) (b) (c)

Fig. 6 (a) High content imaging platform; (b) Sub-array of 16 spots using composite of FITC and DAPI scan after incubation with human epithelial cells; (c) Example of scan (20X objective) obtained for each polymer spot showing from top to the bottom: the nuclei stained with Hoechst 33342 (DAPI filter), the cytoplasm stained using secondary antibody detection (FITC Filter) and merged image.

- SCREENING -

Cell compatibility:
Cells were grown on the polymeric array at 37°C under 5% CO_2. After cell staining, the array was washed and the cells immobilised with fixing solution (3.7% w/v p-formaldehyde and 4.0% w/v sucrose in H_2O).

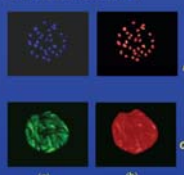

$n_{cells} = 33$

Cell Coverage ≈ 98%

(a) (b) (c)

Fig. 4 (a) Raw images; (b) Masks generated by automatic detection protocols; (c) Results obtained.

3 Scale-up

Stage 1- Scale up on cover slip
In propose to check if cell adhesion depend on polymer morphology, active polymer are solved in volatile solvent such us THF and spread on coverslip by spin coating.

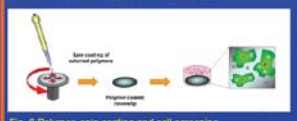

Fig. 6 Polymer spin coating and cell screening

Fig. 7 Gram scale polymer synthesis

Stage 2- Scale-up on gram scale and polymer analyze
IR, GPC, DSC, NMR, contact angle,

Biomsterials for cell patterning

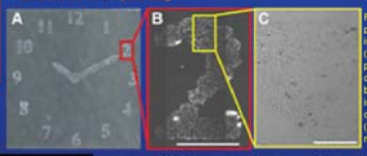

Fig. 10 Cell patterning via inkjet printing: (a) HeLa cells patterned in a clock shape on biomaterial inkjet printed onto agarose (26 mm x 26 mm);

Developed biomaterial

Substrates for suspension cells immobilization

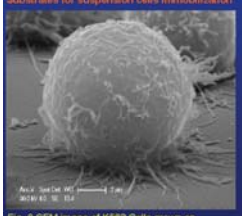

Fig. 8 SEM image of K562 Cells grown on polyacrylates for 24 h

Substrates for controlling cell morphology

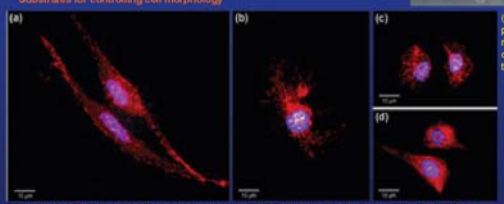

Fig. 9 Confocal images of L929 on polymer microarrays. Cells were imaged under excitation at 555/28nm and 360/40nm using a Delta Vision RT Microscope (x63 objective). (a) PU-133; (b) PU-133; (c) PU-161; (d) PU-107.

(b) Hoeshest 33342 (for nuclei staining) images of HeLa cells in a patterned "2" (Scale bar 1 mm). Images were scanned using a Nikon microscope controlled by the Pathfinder software (Imstar) using a 10x/0.30 objective and a DAPI filter; (c) Bright light image expansion showing part of the number "2" (Scale bar 0.25 mm).

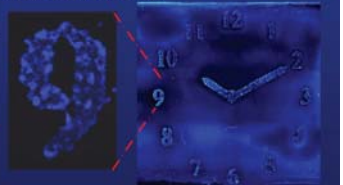

Fig. 11 Patterned mES-Oct4 cells on collagen patterns printed on agarose coated glass slide, fixed with formaldehyde (4% wt) and stained with Hoescht 33245 (nuclei stain). The image (26 mm x 26 mm) was taken with a BioAnalyzer 4F/4S with a light scanner (LaVision Bio Tech).

- CONCLUSION -

It has been shown that polymer arrays are a versatile format allowing the development of very high throughput methods for the developing of biomaterials.

- ACKNOWLEDGEMENTS -?

-REFERENCES –

Chem. Commun., 2008, 1317

Versatile Polymer Microarrays for Selective Cellular Control

Salvatore Pernagallo [1], Rong Zhang [1], David C. Hay [2], Asier Unciti-Broceta [1], Juan Jose Diaz-Mochon [1], Albert Liberski [1,3] and Mark Bradley [1,3]

Department of Chemistry, University of Edinburgh, King's Buildings, West Mains Road, Edinburgh, EH9 3JJ, U.K.[1], MRC Centre for Regenerative Medicine, University of Edinburgh, 49 Little France Crescent, Edinburgh, EH16 4SB, U.K.[2] and Ilika Technologies, Chilworth Science Park, Southampton, Hants, U.K.[3] E-mail: S.Pernagallo@sms.ed.ac.uk

Polymer microarrays are a platform that allows the high-throughput screening of polymer libraries for the purposes of finding substrates upon which a specific cell line/virus might adhere and secondarily to gain a rapid understanding of the interactions between cells and biomaterials. Polymer microarrays were fabricated using either pre-synthesised polymers printed via contact printing technologies or through more innovative inkjet printing methodologies via in situ polymerisation. These huge arrays of polymers were evaluated in a number of cell binding / release assays for cellular adhesion/manipulation studies to elucidate putative links between phenotypic responses to cell-biomaterial interactions. The polymer "chips" were successfully used to find "hit" polymers that could interrogate/manipulate numerous cell lines.

-CONTACT PRINTING-
-for dispensing pre-synthesised polymers-

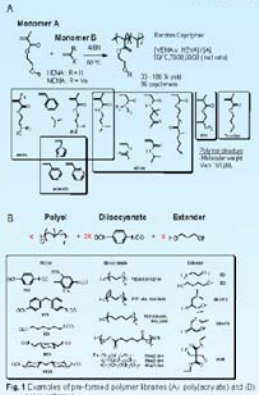

Fig. 1 Examples of pre-formed polymer libraries (A: poly(acrylate) and (B) polyurethane).

Stage 1- Solutions
Polymers (Fig.1) were dissolved at 1% w/v in *N*-methyl pyrrolidinone. The solutions were placed into 384-well microplates.

Stage 2- Printing
The solutions were deposited by contact printing using a *Q-Array mini*® (Genetix Ltd; UK) (Fig.2) with 150 µm solid pins. The nature of the substrates were adapted in order to obtain the lowest background and most uniform spots. The typical spot diameters were 300 µm (±20 µm) with a volume of approximately 7 nL, which is equivalent to about 70 pg of polymer.

Stage 3- Drying
Once printed, the solvent was removed by drying under vacuum at 45°C by-night, to give a microarray with over 2000 features per slide.

Fig.2 *Q-Array mini*® (Genetix Ltd, UK).

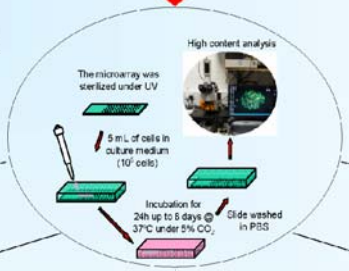

-INKJET PRINTING-
-High throughput *in situ* polymer synthesis-

Stage 1- Printability
Individual optimization of voltage, impulse length, monomer concentration and solvent volume to achieve uniform drops. The evaporation from spots was reduced by humidity control (50%) or printing through a layer of paraffin oil (Fig.3 A and B).

Stage 3- Printing
A Microdrop printing system allows automatic polymer synthesis in a microarray format (Fig.4). Thanks to prior surface modification (agarose coating) the newly synthesised polymers are immobilized on the surface.

Stage 4- Washing and drying
The non-reacted monomers were removed from the chips by a double washing with water and ethanol. Microarrays with up to 2500 spots per slide were dried under vacuum at 45°C for 24h.

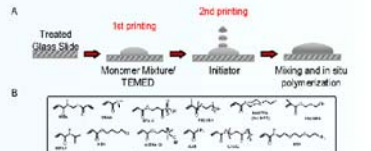

Fig. 3 A) Schematic approach of the *in situ* polymerisation. B) Monomers used for the fabrication of the hydrogel microarrays.

Fig. 4 Arrayer: Microdrop printing system (Microdrop GmbH, GE)

A Cooperative Polymer-DNA Microarray Approach to Biomaterial Investigation[1] (Fig.5)

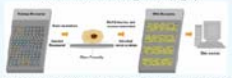

Fig. 5 Dual polymer-mouse *ex-vivo* DNA microarray strategy for the assessment of cell-biomaterial interactions.

Polymer Microarray
Identification of polymers that bound K562 suspension cells (Fig.6)
Scale-up Analysis
Phenotypic Analysis by SEM (Fig.7)
Transcriptomic analysis by DNA microarrays

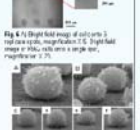

Fig. 6 A) Bright field image of cell cells 3 replicate spots, magnification 2.5). Bright field image of HeLa cells on a single spot, magnification x 20.

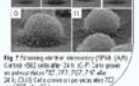

Fig. 7 Scanning electron microscopy (SEM) (A/B) Control K562 cells after 24 h. (C, D) Cells grown on polymer film n°62. (E, F) Cells grown on polymer film n°63. (G, H) Cells grown on polymer film n°67. After 24 h, (G,H) Cells grown on polymer film n°62 and 67 after 72 h.

Polymers for Controlling Cellular Morphology and Viability[2]

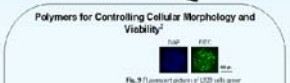

Fig. 9 Fluorescent pictures of U2OS cells grown on a representative spot on PU67

Polymer Microarray
Adhesion and viability analysis (Fig.5 and 10)
Morphological analysis (Fig.11)

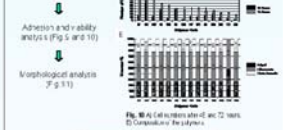

Fig. 10 A) Cell numbers after 48 and 72 hours. B) Comparison of the polymers.

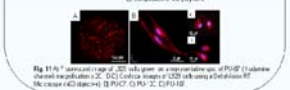

Fig. 11 A) Fluorescent image of U2OS cells grown on a representative spot of PU67 (10 solvent channels magnification x 2C. DIC) Confocal images of U2OS cells using a Definiens XD Microscope (40 objective). B) PU67. C) PU 32. D) PU 102.

Hydrogel Microarrays for Cellular Trapping and Temperature Triggered Release[3]

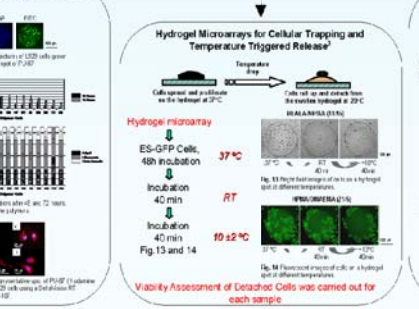

Hydrogel microarray
ES-GFP Cells, 48h incubation
37 °C
Incubation 40 min
RT
Incubation 40 min
10 ±2 °C
Fig.13 and 14

Fig. 12 Bright field images of cells on a hydrogel spot at different temperatures.

Fig. 14 Fluorescent images of cells on a hydrogel spot at different temperatures.

Viability Assessment of Detached Cells was carried out for each sample

Substrates for Mouse Bone Marrow Dendritic Cell (BMDC) Phagocytosis[4]

Polymer Microarray
Identification of materials for BMDC immobilisation (Fig. 15)
Scale-up Analysis
Cells need to be maintained in an immature state (Fig.16)
Study of intracellular processes such phagocytosis (Fig.17)

Fig. 15 Quadrilateral spots of a polymer showing good BMDC cellular adhesion. Scale bar is 100 µm.

Fig. 16 Confocal laser scanning microscopy (63x objective). Anti-LL-37 antibody (red) was used to stain BMDC that had adhered to the polymer. Nuclei (blue) were counterstained with TOPRO3. Scale bar is 30 µm.

Fig. 17 Confocal laser scanning microscopy (63x objective). The fluorescence image shows, in more detail, the internalized microspheres.

Polymer Matrix Promotes and Stabilises hESC-Derived Hepatocyte Function (HLCs)

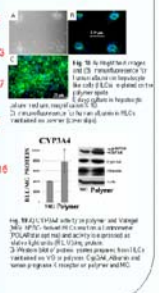

-CONCLUSION-

Polymer microarrays were successfully fabricated using either a pre-synthesised polymer approach *via* a contact printing technology or through a more innovative inkjet printing methodology (*via in situ* polymerisation). This new and powerful platform has successfully allowed the identification of a family/group of polymers that have enabled adhesion and proliferation of a suspension cell line (K562). These interactions were studied by DNA microarray analysis with the demonstration that interactions between K562 cells and materials induce a number of changes in the transcription. The method was also proficient for finding optimal polymer supports for L929 fibroblast cells.

Furthermore, *in-situ* hydrogel microarrays allowed the identification of new biomaterials for cellular trapping and temperature-sensitive release. The high multiplexing power of the polymer microarray approach has also allowed the screening of large numbers of different biomaterials to identify polymers which bound immature DCs from murine bone marrow cells. Recently, we have identified a matrix that promotes long-term hepatocellular differentiated function before and after passaging. These will play important roles in developing *in vitro* models of drug toxicology for pharma, provide a resource for the construction of extra-corporeal devices and facilitate novel studies of human liver development and disease.

-REFERENCES-

1) S. Pernagallo *et al.* Lab Chip, 2009, 9, 397–40.
2) S. Pernagallo *et al.* Biomed. Mater., 2008, 3, 034112.
3) R. Zhang *et al.* Chem. Commun., 2008, 1317-1319.
4) A. Mant et al. Biomaterials, 2006, 27, 5299-5308.

-ACKNOWLEDGEMENTS-

We would like to thank EPSRC for a studentship.

A Polymer Matrix Promotes and Stabilises hESC-Derived Hepatocyte Function

David C Hay*, Salvatore Pernagallo, Juan Jose Diaz-Mochon, Judy Fletcher, James R. Black, Alexandra I. Thompson, Zara Hannoun, Philip N. Newsome, Stuart J. Forbes, James A. Ross, Mark Bradley, John P. Iredale.
MRC Centre for Regenerative Medicine, University of Edinburgh, 49 Little France Crescent, EH16 4SB, U.K.

INTRODUCTION: The generation of functional hepatic endoderm from human embryonic stem cells (hESCs) offers a stable and inexhaustible resource vital for biotechnology, toxicology and clinical applications. Models of efficient hepatocyte differentiation have recently been developed (1), but long-term hepatocyte function following cell passaging has proven elusive. We have screened a polymer library and identified a defined extra-cellular matrix that maintains both long-term hepatocytic phenotype and high level function *in vitro*; with critical implication for biotechnology and drug testing applications.

FIGURE 1: hESC hepatocyte differentiation and polymer screening schematic.

RESULTS: hESCs were differentiated as in Figure 1 and screened using a polymer library. Screening identified 6 polymers (three polyacrylates 2BG9, 9G7, 3AA7 and three polyurethanes 134, 212, 223) that supported HLC attachment and hepatocellular identity, assessed by albumin production (Green) (Figure 2, Table (i)). We further characterised hepatocytic function in detail on these six matrices, 15 days post replating, using a panel of hepatocyte specific functions. Using this strategy, polymer 134 was identified as the most effective cellular support associated with enhanced expression of Fibrinogen, transthyretin (TTR), soluble fibronectin and function of CYP1A2 (Figure 3). Additionally, HLCs passaged and maintained on matrigel or polymers 2BG9, 212, 9G7, 3AA7 and 223 were granular. In contrast, HLCs replated on 134 exhibited hepatic morphology and improved CYP3A4 function and hPXR phosphorylation (Figure 4).

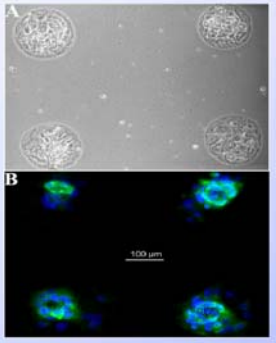

FIGURE 2: Library Screen

Polymer	Attachment
2BG9	+
2I2	+
9G7	+
3AA7	+
223	+
134	+

TABLE (i) HLC Attachment

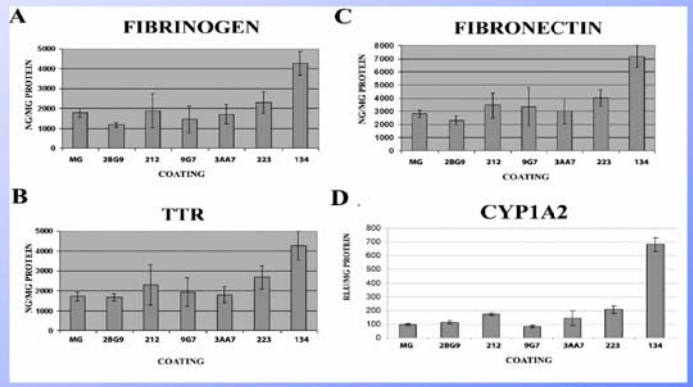

FIGURE 3: Bio-Acitve Nature of Polymer 134

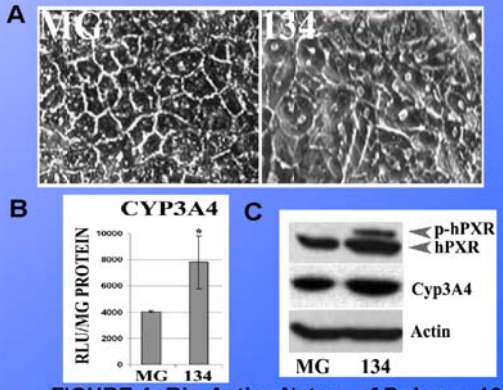

FIGURE 4: Bio-Active Nature of Polymer 134

CONCLUSION: In conclusion, high through-put screening of a polymer microarray allowed the identification of a new polymer matrix that promotes long-term hepatocellular differentiated function before and after passaging. These attributes bypass current limitations associated adult human hepatocytes, can be manufactured to GMP standards and will play important roles in developing *in vitro* models of drug toxicicology, provide a resource for the construction of extra-corporeal devices and facilitate novel studies of human liver development and disease.

REFERENCE: (1) Hay DC et al 2008 Proc Natl Acad Sci U S A. 2008 105(34):12301-6 *CONTACT: davehay@talktalk.net

Identification of evolutionarily conserved Oct4 targets

Alessandra Livigni[1], Salvatore Pernagallo[2], Alexei Sharov[3], Dawood B. Dudekula [3], Minoru Ko [3], Mark Bradley[2] and Joshua M. Brickman[1].

1. MRC Centre for Regenerative Medicine Institute for Stem Cell Research, University of Edinburgh;
2. Chemical Biology Section, School of Chemistry, University of Edinburgh; 3. National Institute on Aging, NIH, Baltimore.

The POU-V transcription factor Oct4 is a major regulator of self-renewal and pluripotency in embryonic stem (ES) cells as well as an important regulator of lineage commitment in embryonic development. Three class V POU proteins related to Oct4 (Xlpou25, Xlpou60 and Xlpou91) are expressed during Xenopus laevis embryonic development. These functional homologues maintain a pool of undifferentiated multipotent cells in the embryo. We explored the regulatory network downstream of the three amphibian Oct4 homologues by using loss of function morpholino combinations and microarray analysis. Many studies have analysed the downstream targets of mammalian Oct4 using ES cells as a model. By comparing these studies to our expression dataset we defined an evolutionarily conserved set of Oct4 targets. Further analysis in embryonic explants and in murine ES cells aims to define the mechanisms by which this conserved network regulates commitment to multiple lineages during gastrulation.

POU-V morphant phenotypes

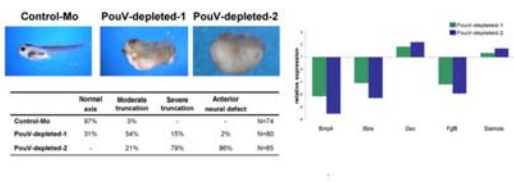

POU-V morphant embryos phenotype and scoring. PouV-depleted-1 is injected with morpholino knock-down of Xlpou91 and one pseudo-allele of Xlpou25 and Xlpou60. PouV-depleted-2 targets all three Xlpou proteins. Embryos were photographed at Stage 39. Real-time qPCR on whole embryos at stage 10. Expression normalized to Odc and relative to control-Mo.

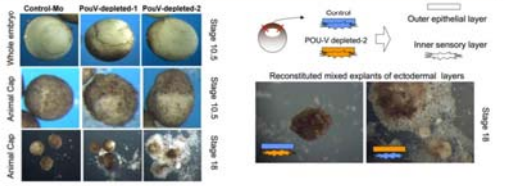

POU-V morphants were injected at 2-cell stage. Animal caps were dissected at stage 8 and cultured until sibling embryos reached Stages 10.5 and 18. Reconstituted mixed explants: animal caps dissected at stage 8 were dissociated in outer epidermal layer and inner sensorial layer. The layers were re-aggregated combining control and morphant explants to form an ectodermal sandwich.

Expression profiling of POU-V depleted embryos

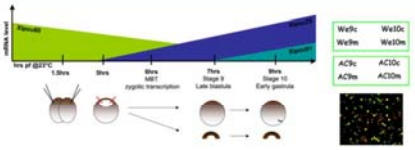

Experimental flow-chart showing sample collection for the expression profiling. Xenopus Agilent two-colors microarray was hybridised with labelled cRNA of the samples and a pooled normalization control.

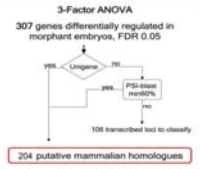

Statistical analysis was performed using NIA array online tool. Homology search was performed using Cygwin scripting for batch psi-blast (NCBI).

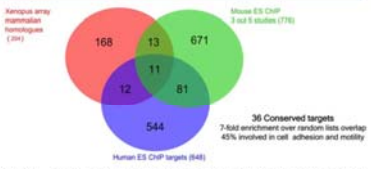

Venn diagram comparing the Xenopus mammalian homologues dataset (201) to genomewide ChIP datsets in human and murine embryonic stem (ES) cells.

Conserved targets rescue POU-V depleted embryos and respond to Oct4 during mES differentiation

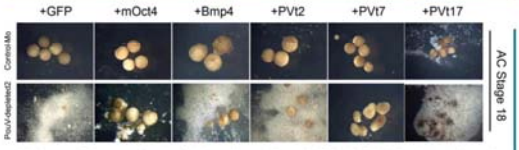

Adhesion assay. Embryos were injected at 2-cell stage with morpholino and the 500pg of mRNA (indicated on top of the panel). Animal caps were dissected at stage 8 and cultured until sibling embryos reached Stage 18. PVt is POU-V target.

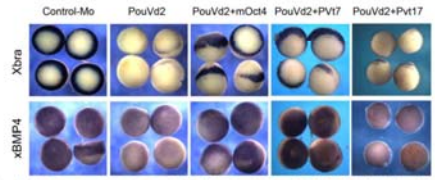

In situ hybridisation stage 10. Xbra in vegetal or lateral view. Bmp4 in vegetal view. PouVd2 is POU-V dpleted-2 morpholino.

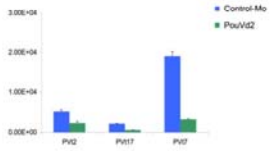

Real-time qPCR, whole embryos stage 10. Expression normalized to Odc. PVt is POU-V target.

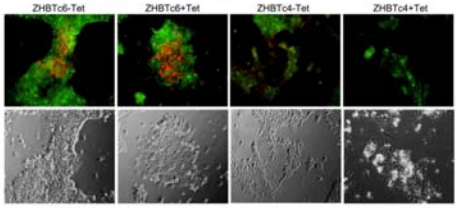

ZHBTc4/c6 cells at day 4 of differentiation. Green is E-cadherin, Red is Brachyury.

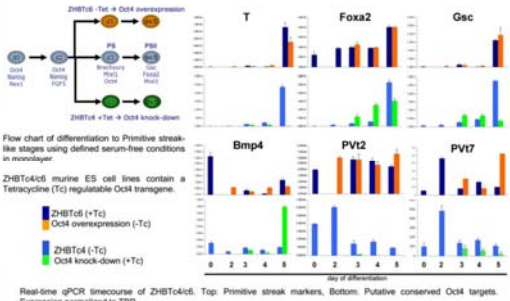

Flow chart of differentiation to Primitive streak-like stages using defined serum-free conditions in monolayer.

ZHBTc4/c6 murine ES cell lines contain a Tetracycline (Tc) regulatable Oct4 transgene.

ZHBTc6 (+Tc) Oct4 overexpression (-Tc)

ZHBTc4 (-Tc) Oct4 knock-down (+Tc)

Real-time qPCR timecourse of ZHBTc4/c6. Top: Primitive streak markers, Bottom: Putative conserved Oct4 targets. Expression normalized to TBP.

Oct4 → Cell adhesion modulators, ECM remodeling, Secreted signaling molecules → Embryonic epithelial integrity, EMT

EPSRC Engineering and Physical Sciences Research Council

wellcome trust

www.crm.ed.ac.uk

IOP PUBLISHING BIOMEDICAL MATERIALS
Biomed. Mater. 3 (2008) 034112 (6pp) doi:10.1088/1748-6041/3/3/034112

Deciphering cellular morphology and biocompatibility using polymer microarrays

Salvatore Pernagallo[1], Asier Unciti-Broceta[1], Juan José Díaz-Mochón and Mark Bradley

School of Chemistry, King's Buildings, West Mains Road, Edinburgh EH9 3JJ, UK

E-mail: Mark.Bradley@ed.ac.uk

Received 21 September 2007
Accepted for publication 1 February 2008
Published 15 August 2008
Online at stacks.iop.org/BMM/3/034112

Abstract

A quantitative and qualitative analysis of cellular adhesion, morphology and viability is essential in understanding and designing biomaterials such as those involved in implant surfaces or as tissue-engineering scaffolds. As a means to simultaneously perform these studies in a high-throughput (HT) manner, we report a normalized protocol which allows the rapid analysis of a large number of potential cell binding substrates using polymer microarrays and high-content fluorescence microscopy. The method was successfully applied to the discovery of optimal polymer substrates from a 214-member polyurethane library with mouse fibroblast cells (L929), as well as simultaneous evaluation of cell viability and cellular morphology. Analysis demonstrated high biocompatibility of the binding polymers and permitted the identification of several different cellular morphologies, showing that specific polymer interactions may provoke changes in cell shape. In addition, SAR studies showed a clear correspondence between cellular adhesion and polymer structure. The approach can be utilized to perform multiple experiments (up to 1024 single experiments per slide) in a highly reproducible manner, leading to the generation of vast amounts of data in a short time period (48–72 h) while reducing dramatically the quantities of polymers, reagents and cells used.

(Some figures in this article are in colour only in the electronic version)

1. Introduction

Intensive research efforts in biomaterial science have provided a significant number of polymers for potential applications in medicine [1, 2]. As a consequence, the clinical use of polymers has been expanded from traditional uses (catheters, syringes, etc) to other emerging areas such as drug delivery [3–5] and tissue-engineering scaffolds [6–9]. Although specific material requirements will differ according to the nature of the application, it is a universal condition that the biopolymer displays adequate so-called biocompatibility. HT technologies are gaining relevance in this field as an efficient way of screening new materials [10–13].

Due to their unique mechanical properties and their excellent tolerance in the human body, polyurethanes (PUs) have been extensively used as biomedical materials for half a century [14, 15]. This kind of material belongs to the family of urethane copolymers which are characterized by a carbamate or urethane linkage (–NH–CO–O–) in their structure. Numerous physical parameters (such as elasticity, wettability and surface topography [16]) and biochemical properties (in particular the ability to adsorb extracellular matrix (ECM) proteins [17]) are expected to play a relevant role in the cellular adhesion and biocompatibility of the polymers. In addition, the surface of the biomaterial often changes the conformation of the adsorbed ECM proteins which may partially or completely lose their bioactivity [18]. All these factors, while being dependent on the chemical structure, are not easy to predict. Consequently,

[1] These authors contributed equally to this work.

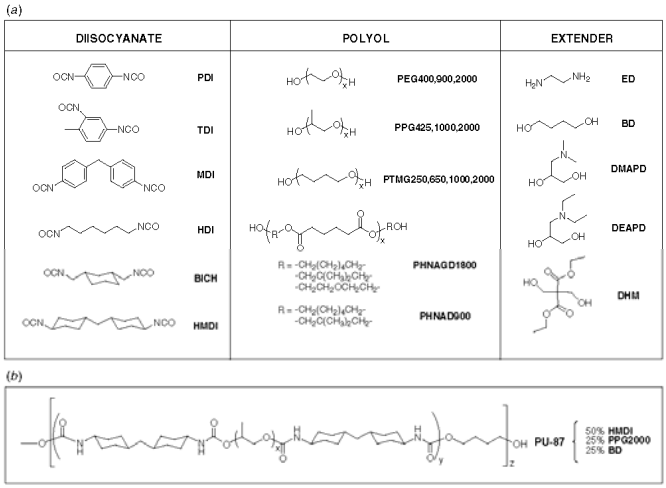

Figure 1. Chemical components of the PU library. (*a*) Monomers used in the PU library synthesis and (*b*) structure of PU-87.

the traditional studies for developing new biomaterials are highly time-consuming processes involving the rational design of biomaterials for specific needs and subsequent individual examination of the polymer properties. As a way to speed up the *modus operandi*, several research groups have recently developed high-content screening technologies for the study of cell–biomaterial interactions [11, 12, 19, 20]. These 2D micropatterned surfaces allow a variety of *in vitro* studies (cellular attachment, differentiation, phagocytosis, etc) whilst being easy to prepare, inexpensive and suitable for all kinds of adherent cell lines and importantly require only limited amounts of reagents and cells.

Herein, we describe a normalized fluorescence-based, high-throughput methodology, for the rapid screening of potential biomaterials in a microarray format. Cell binding studies were realized using a library of PUs (composed of 214 members), prepared by a combinatorial approach, and the novel microarray platform recently developed in house [12]. The presented protocol was successfully applied to find optimal polymer supports for mouse connective tissue fibroblast cells (L929), which are cells of great interest in biomedical research since fibroblasts provide a structural framework (stroma) for many tissues and play a critical role in wound healing [21]. This versatile method allowed the simultaneous study of both cellular morphology and cell viability in relation to the polymer on which the cells were adhered.

2. Materials and methods

2.1. Synthesis of PU library [22]

Twelve parallel reactions were carried out in a Stem block on a mmol scale by a typical two-stage poly-addition reaction. In brief, a pre-polymer was prepared by the reaction of 1.0 equiv of a polyol with 2.0 equiv of a diisocyanate in dry THF, followed (after titration) by the addition of 1.0 equiv of the same polyol or another chain extender (monomers used are shown in figure 1(*a*)). The library was tailored by varying the nature of the polyol (from 250 to 2000 Da and different compositions) and the diisocyanate, and substituting the polyol by a bifunctional small molecule as chain extender. Polymers were named using an identical format to that previously reported [12, 22]. A representative PU structure is shown in figure 1(*b*). The 214 polymers of the library were all characterized using high-throughput methods such as GPC (column PLgel HTS-D 150 mm × 7.5 mm ID, Polymer Laboratories, NMP 1 mL min^{-1}), Hyper DSC (Diamond, Perkin-Elmer) and FT-IR (Mattson instrument) [22].

2.2. L929 cell culture

Media, serum and antibiotics were purchased from Gibco or Sigma–Aldrich. Cultures were performed in a 5% CO_2 atmosphere at 37 °C in a SteriCult 200 (Hucoa-Erloss) incubator. L929 cells were cultured in DMEM supplemented with 10% fetal bovine serum (FBS), glutamine (4 mM) and antibiotics (penicillin and streptomycin, 100 units mL^{-1}).

2.3. Polymer microarray fabrication

Polymers were 'spotted' on aminoalkylsilane-treated glass slides (Sigma–Aldrich), previously coated with agarose to impede unspecific cell adhesion [12, 13, 23, 24]. Slides were coated by dipping once into a 1% agarose aqueous solution at 60 °C. Subsequently, polymer arrays were fabricated by contact printing (QArray^{mini}, Genetix) with 32 aQu solid

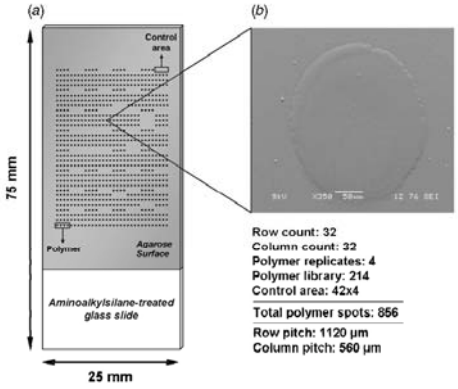

Figure 2. Polymer microarray design: (*a*) slide template and (*b*) SEM of a representative polymer spot.

pins (K2785, Genetix) using polymer solutions (1% w/v in NMP) placed in polypropylene 384-well microplates; printing conditions: 5 stamps per spot, 200 ms inking time and 100 ms stamping time. The typical spot size was 300–320 μm in diameter with a pitch distance of 1120 μm (*y*-axis) and 560 μm (*x*-axis), allowing up to 1024 features to be printed on a standard 25 mm $\times$ 75 mm slide. The 214 members of the PU library were printed following a four-replicate pattern with one single field of 32 $\times$ 32 spots containing 42 control emptied areas (see figure 2). Once printed, the slides were dried under vacuum (24 h at 42 °C/200 mbar) and sterilized in a biosafety cabinet (HERAsafe KS 18 class II Heraeus) by exposure to UV irradiation for 20 min prior to use.

2.4. Cell-based microarrays

L929 cells were washed with phosphate buffered saline (PBS), detached with trypsin/EDTA, counted and diluted with media to a final concentration of 10^5 cells per mL. 5 mL of this dilution were gently added onto the polymer microarray contained in a sterile four-well plate (Nunc) and incubated for different periods of time (48 and 72 h). Cell labeling was done as follows: (i) incubation with CellTracker Green CMFDA (5 μM in PBS, Molecular Probes Inc.) at 37 °C and 5% CO_2 for 15 min; (ii) slides were then gently washed and fixed with 4% (w/v) formaldehyde in PBS at room temperature for 15 min; (iii) incubation with Hoechst-33342 (1 μg mL^{-1} in PBS, Sigma–Aldrich) for 15 min at room temperature; and subsequently, (iv) incubation with Alexa fluor568 phalloidin (0.2 μM in 1% in PBS containing 1% FBS, Invitrogen) for 15 min at room temperature. The polymer microarray slides were then rinsed in deionized water and air dried before scanning.

2.5. Fluorescence-based HT screening

Image capture and analyses were carried out using an IMSTAR high-content screening (HCS) device equipped with the

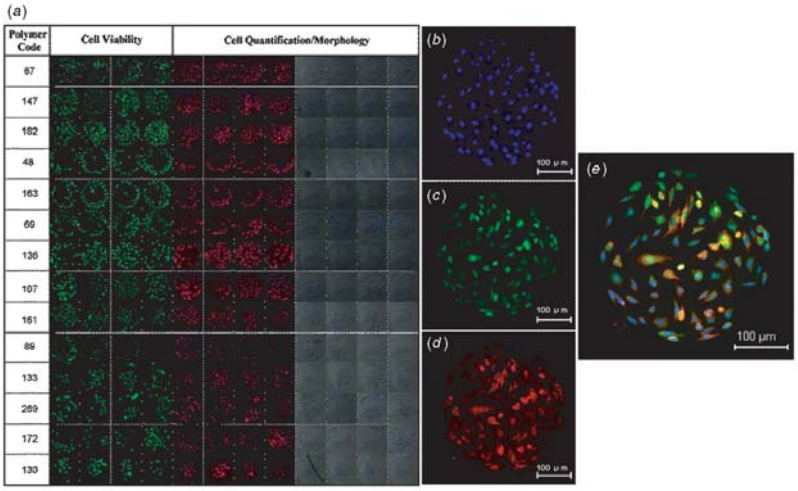

Figure 3. L929 cells grown on polymer microarrays after 72 h incubation. (*a*) Best polymer substrates for L929 cells. All polymers supported a minimum average of 20 cells. FITC channel images are shown in the *Cell viability* column. Rhodamine /DAPI merged images and brightfield/DAPI composites are shown in the *Cell Quantification/Morphology* column. (*b*)–(*e*) Fluorescent pictures of L929 cells grown on a representative spot of PU-87: (*b*) DAPI channel; (*c*) FITC channel; (*d*) rhodamine channel; (*e*) merged image.

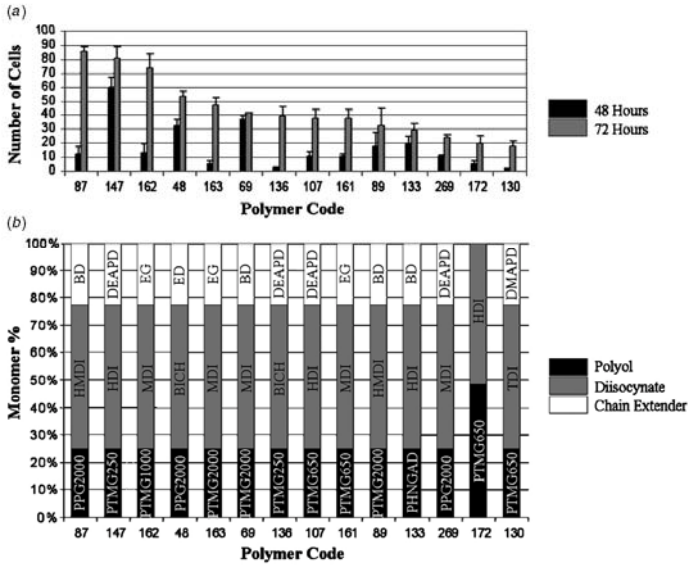

Figure 4. (*a*) Cell numbers after 48 and 72 h and (*b*) composition of the polymers.

PathfinderTM software package (IMSTAR S.A., Paris, France). Cell number (Hoechst-33342: excitation/emission 350/461 nm), biocompatibility (CellTracker Green: excitation/emission 492/516 nm) and morphology (Alexa fluor 568: excitation/emission 578/603 nm) of each PU member were determined using fluorescent (DAPI, FITC and Rhodamine-like band-pass filters) and brightfield channels by automated scanning (×20 objective) of the polymer spots.

2.6. Analysis of cell morphology

Cell morphology was analyzed by confocal microscopy after 48 and 72 h of culture. Image capture was performed by a DeltaVision RT microscope (×63 objective) using DAPI and Rhodamine channels.

3. Results and discussion

3.1. High-content screening of L929

Cell-adhesion experiments were carried out with the mouse fibrosarcoma cell line, L929, incubating the 214-member polymer microarrays for 48 h and 72 h. In order to study the biocompatibility of the polymer support, micropatterned cells were incubated with CellTracker Green CMFDA. This probe composed of 5-chloromethylfluorescein diacetate is non-fluorescent and able to freely diffuse through the membrane of live cells. Once inside the cell, intracellular esterases cleave the acetate groups to produce cells that are fluorescent, viable for at least 24 h after loading and covalent modification.

Subsequently, the micropatterned cells were fixed, and cell nuclei and cytoskeleton stained with Hoechst-33342 and Alexa fluor568, respectively. Cell permeable Hoechst-33342 is an adenine–thymine-specific dye that binds to the minor groove of DNA, and Alexa fluor568 phalloidin is a fluorescent bicyclic peptide with a high affinity for F-actin, which is an important component of the cytoskeleton. This fluorescent probe does not cross the membrane of living cells and thus requires fixation of the cells in order to increase membrane permeability. Once the cells are fixed, the staining of the cells with Hoechst-33342 is also accelerated.

The HT analysis of the fixed cells was realized using three fluorescent channels and brightfield (see figure 3).

3.2. Analysis of cell viability

Cell viability was qualitatively evaluated by the fluorescence emission of the content of each spot through the FITC-like channel (see figure 3). Generally speaking, all polymers with the ability to support L929 cells were found to have high biocompatibility with this cell line.

3.3. Analysis of cell adhesion and competitive affinity

In order to quantify cellular adhesion on each polymer, the average numbers of cells across the four spots and standard deviation were used. These values were recorded at two time points, 48 and 72 h, which allowed scoring for cellular binding of L929 cells (see figures 3(*a*) and (*b*)). This was done

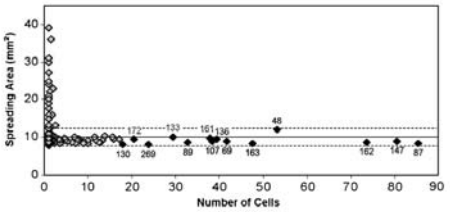

Figure 5. Analysis of polymer wettability in relation to the average number of cells found per polymer spot. Polymer wettability is expressed as the area over which a droplet of water of defined size spreads over a cover slip spin coated with the polymer (and was determined in this case after a contact time of 20 s). The hit polymers described in figure 4 are shown above the black diamonds (♦).

by fluorescence analysis of images from the DAPI channel. Pathfinder™ software package was used to automatically detect and quantify cell nuclei.

In general, significant cellular adhesion was supported by a number of the library members (figure 4(*a*)). PU-87 was the best substrate, providing an average (over the four identical polymer spots) of 82 mouse fibroblast cells. 13 out of the 14 best polymer supports were synthesized using as a chain extender, a small molecule instead of the corresponding polyol (see figure 3(*b*)). The polyol PTMG, although with different molecular weights, was a common component of ten of the hit polymers (14), thus demonstrating a certain correlation between polymer structure and cell binding.

Although two different polymers did have similar capacity for binding a specific cell line, the cell binding process could be faster on one polymer than on the other. Consequently, within a competitive assay (as the polymer microarray platform is) better polymer substrates will immobilize higher numbers of cells during the first hours. A comparative analysis of cell number per polymer over time would thus be a measure of the grade of affinity of L929 to the polymer. Data analysis revealed different behaviors for the polymers (figure 4(*a*)). For example, some polymers showed low cell binding after the first 48 h and then showed a 'burst' of growth in the following 24 h. Interestingly, the 160 series (PU-161, PU-162 and PU-163), which have the same type of monomers, only differing in the molecular weight of the polyol used (PTMG650, PTMG1000 and PTMG2000, respectively), showed similar cell attachment trends. Low cell binding was observed within the first 48 h followed by a vigorous growth in the remaining 24 h. On the other hand, polymers PU-147, PU-69 and PU-48 showed steady cell numbers over time, associated with rapid cell immobilization achieved by these polymers. Similarly, the number of cells quantified on PU-69 for both observation times showed an identical number of cells, which indicated the high grade of affinity of this polymer for L929 cells. In fact, after 48 h every single spot of PU-69 was completely covered with cells, hindering further cellular proliferation on the spot.

3.4. Correlation study between polymer wettability and cell adhesion abilities

We previously reported a HT method for evaluating the wettability of polymer libraries by measuring the spreading area of water droplets deposited onto spin-coated films of the polymer [21]. The entire polyurethane library, was, therefore characterized with spreading areas determined after a contact time of 20 s. Analysis showed that 90% of the PU library members were relatively hydrophobic, with a spreading area ranging from 8 to 12 mm^2 (equivalent to a contact angle from 90° to 70°, respectively [22]). These values were shown to be strongly correlated with the cell binding (see figure 5) with all hydrophilic polymers (having a spreading area > 15 mm^2, equivalent to contact angle <50°) found to impede cell adhesion. This analysis emphasizes the significant role of the polymer's physical properties on cell adhesion and indicates that L929 cells require a relatively hydrophobic substrate for adherence.

3.5. Analysis of cell morphology

Cells in contact with a binding surface will first attach and then spread according to the interactions created among the surface,

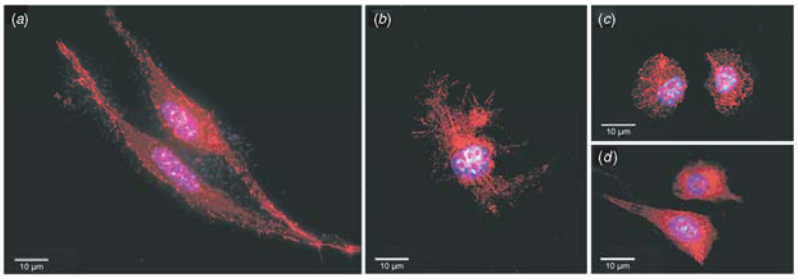

Figure 6. Confocal images of L929 cells on polymer microarrays. Cells were imaged under excitation at 555/28 nm and 360/40 nm using a DeltaVision RT microscope (×63 objective) and then merged: (*a*) PU-87; (*b*) PU-133; (*c*) PU-161; and (*d*) PU-107.

the proteins from the growth serum and the ECM proteins [25]. The nature of this adhesion will influence their morphology and their capacity for proliferation and differentiation [17]. Fibroblasts are slow-moving cells in which the cytoskeleton plays a very important role in the cell motility and shape, among others. To observe the effects of PUs on the typical morphology of this cell type, confocal microscopy studies were carried out on cultured L929 fibroblasts.

Cells cultured on the majority of the spots maintained their characteristic morphology [26] (see figure 6(*a*)). However, on some polymers there was a tendency to form highly spread-out cells (see figure 6(*b*)). Moreover, closer analysis revealed alternative cell morphologies such as those in figures 6(*c*) and (*d*). In spots containing a low density of cell binding, a rounded morphology was typically observed (figure 6(*c*)), due to the lack of a suitable attachment points needed for the development of a normal phenotype.

4. Conclusions

A fluorescence-based high-throughput microarray methodology has been developed to facilitate the rapid screening of combinatorial libraries of potential biomaterials. The normalized protocol was successfully applied to the identification of optimal polymeric supports for the L929 cells from amongst a library of 214 PUs. The application of this method simultaneously allowed the influence of polymer structure to be related to cellular binding and cellular morphology, demonstrating that specific cellular morphology and hence cellular behavior will be fundamentally altered by the substrate upon which the cell adheres. The approach presented allows hundreds of experiments to be performed in a highly reproducible and time-efficient manner, whilst both generating vast amounts of data and consuming tiny amounts of material.

Acknowledgments

We thank EPSRC (SP and JJD-M) and MRC (AU-B) for funding. We are very grateful to Prof. Tim Elliot for supplying the L929 cell line.

References

[1] Langer R and Tirrell D A 2004 Designing materials for biology and medicine *Nature* **428** 487–92
[2] Anderson D G, Burdick J A and Langer R 2004 Smart biomaterials *Science* **305** 1923–4
[3] Luo D and Saltzman W M 2000 Synthetic DNA delivery systems *Nature Biotechnol.* **18** 33–7
[4] Mathiowitz E *et al* 1997 Biologically erodable microspheres as potential oral drug delivery systems *Nature* **386** 410–14
[5] Grayson A *et al* 2003 Multi-pulse drug delivery from a resorbable polymeric microchip device *Nature Mater.* **2** 767–72
[6] Vacanti J P and Langer R 1999 Tissue engineering: the design and fabrication of living replacement devices for surgical reconstruction and transplantation *Lancet* **354** 32–4
[7] Alsberg E, Anderson K W, Albeiruti A, Rowley J A and Mooney D J 2002 Engineering growing tissues *Proc. Natl Acad. Sci. USA* **99** 12025–30
[8] Lendlein A and Langer R 2002 Biodegradable, elastic shape-memory polymers for potential biomedical applications *Science* **296** 1673–6
[9] Halstenberg S, Panitch A, Rizzi S, Hall H and Hubbell J A 2002 Biologically engineered protein-graftpoly(ethylene glycol) hydrogels: a cell adhesive and plasmin-degradable biosynthetic material for tissue repair *Biomacromolecules* **3** 710–23
[10] Pepperkok R and Ellenberg J 2006 High-throughput fluorescence microscopy for systems biology *Nat. Rev. Mol. Cell Biol.* **7** 690–6
[11] Anderson D G, Levenberg S and Langer R 2004 Nanoliter-scale synthesis of arrayed biomaterials and application to human embryonic stem cells *Nat. Biotech.* **22** 863–6
[12] Tourniaire G *et al* 2006 Polymer microarrays for cellular adhesion *Chem. Commun.* 2118–20
[13] Mant A, Tourniaire G, Diaz-Mochon J J, Elliott T J, Williams A P and Bradley M 2006 Polymer microarrays: identification of substrates for phagocytosis assays *Biomaterials* **27** 5299–306
[14] Boretos J W and Pierce W S 1967 Segmented polyurethane: a new elastomer for biomedical applications *Science* **158** 1481–2
[15] Zdrahala R J and Zdrahala I J 1999 Biomedical applications of polyurethanes: a review of past promises, present realities, and a vibrant future *J. Biomater. Appl.* **14** 67–90
[16] Shin H, Jo S and Mikos A G 2003 Biomimetic materials for tissue engineering *Biomaterials* **24** 4353–64
[17] Gallagher W M, Lynch I, Allen L T, Miller I, Penney S C, O'Connor D P, Pennington S, Keenan A K and Dawson K A 2006 Molecular basis of cell–biomaterial interaction: insights gained from transcriptomic and proteomic studies *Biomaterials* **27** 5871–82
[18] Sherratt M J, Baldock C, Morgan A and Kielty C M 2007 The morphology of adsorbed extracellular matrix assemblies is critically dependent on solution calcium concentration *Matrix Biol.* **26** 156–66 and references cited therein
[19] Derda R, Li L, Orner B P, Lewis R L, Thomson J A and Kiessling L L 2007 Defined substrates for human embryonic stem cell growth identified from surface arrays *ACS Chem. Biol.* **2** 347–55
[20] Unciti-Broceta A, Díaz-Mochón J J, Mizomoto H and Bradley M 2008 Combining nebulization-mediated transfection and polymer microarrays for the rapid determination of optimal transfection substrates *J. Comb. Chem.* **10** 179–84
[21] Chang H Y *et al* 2002 Diversity, topographic differentiation, and positional memory in human fibroblasts *Proc. Natl Acad. Sci. USA* **99** 12877–82
[22] Thaburet J-F-O, Mizomoto H and Bradley M 2004 High-throughput evaluation of the wettability of polymer libraries *Macromol. Rapid Commun.* **25** 366–70
[23] Folch A and Toner M 2000 Microengineering of cellular interactions *Ann. Rev. Biomed. Eng* **2** 227–56
[24] Roth E A, Xu T, Das M, Gregory C, Hickman J J and Boland T 2004 Inkjet printing for high-throughput cell patterning *Biomaterials* **25** 3707–15
[25] García A J 2006 Interfaces to control cell-biomaterial adhesive interactions *Advances in Polymer Science* (Berlin/ Heidelberg: Springer) pp 171–90
[26] Li P-T, Lee Y-C, Elangovan N and Chu S-T 2007 Mouse 24p3 Protein has an effect on L929 cell viability *Int. J. Biol. Sci.* **3** 100–7

A cooperative polymer-DNA microarray approach to biomaterial investigation†

Salvatore Pernagallo, Juan Jose Diaz-Mochon and Mark Bradley*

Received 19th May 2008, Accepted 6th October 2008
First published as an Advance Article on the web 14th November 2008
DOI: 10.1039/b808363k

In this study, polymer microarrays were used for the rapid identification of polymer substrates upon which a suspension cell line would both adhere and proliferate giving a detailed and rapid understanding of cell-biomaterial interactions. Analysis demonstrated that suspension K562 human erythroleukemic cells, which normally grow in suspension, adhered and proliferated on several different polymers. Phenotypic and transcriptomic analysis techniques allowed examination of the interaction between cells and polymers permitting the elucidation of putative links between phenotypic responses to cell-biomaterial interactions and global gene expression.

Introduction

Biomaterials have been defined as "materials intended to interface with biological systems to evaluate, treat, augment or replace any tissue, organ or function of the body."[1] As such, biomaterials have become an integral part of medicinal technology, with applications ranging from the implantation of devices and prostheses to the controlled delivery of drugs and as scaffolds for tissue engineering.[2–4]

Polymers are currently the material of choice for thousands of medical applications since they can be prepared in a variety of forms (solids, fibres, fabrics, films and gels) and they can be readily fabricated giving various shapes and structures. Additionally, they are easily functionalised and, depending on the polymeric building blocks, may also be degraded in the body after a desired period.[5–7]

As a consequence of the considerable success of biomedical polymers, research has begun to move from traditional methods of discovery towards high-throughput (HT) approaches[8–10] and include the polymer microarrays developed by two independent research groups, Langer[11–14] and Bradley,[15–20] which have started to play an important role in understanding these interactions and their consequential effects.

However, moves towards high-throughput approaches bring with them, not only the need to be able to rapidly analyse and access vast numbers of data, but to do so in a manner that is biologically relevant.[21,22]

Herein, we describe a highly robust fluorescence-based high-throughput methodology for studying, in a high-content manner, cellular binding on some 268 polymers using a polymer microarray format developed by our group.[15–20]

The protocol was applied to the discovery of polymer supports for the adhesion of K562 suspension cells (K562 cells do not need to be attached to Extra Cellular Matrix (ECM) proteins in order to survive and grow[23,24] and therefore do not normally undergo the same adhesion process as anchorage-dependent cells).[25,26]

Following adhesion of K562 cells onto coverslips coated with the identified polymers, total RNA was isolated and used for transcriptomic analysis, to further understand the adhesion phenomena and the complex cascade of events surrounding cell binding.

As a result, a dual polymer-microarray-co-DNA-microarray approach (Fig.1) allowed us to comprehensively map the cellular alterations in gene expression following cellular binding and interaction with the polymers,[27–31] interactions that were also characterised by Scanning Electron Microscopy (SEM).

Materials and methods

Synthesis of polymers

Polymer libraries were synthesised *via* radical polymerization on a mmol scale as previously reported[15,20,32] (see Table S1 in ESI†).

Polymer microarray fabrication

Polyurethane (PU) and polyacrylate (PA) arrays were fabricated by contact printing (QArray^{mini}, Genetix, UK) with 32 aQu solid pins (K2785, Genetix) using 1% w/v polymer solutions in N-methylpyrrolidone (NMP) placed in polypropylene 384-well microplates.

The printing conditions used were 5 stamps per spot, with a 200 ms inking time and a 100 ms stamping time on amino-alkylsilane-treated glass slides (Sigma-Aldrich, UK), previously coated with agarose Type I-B (Sigma-Aldrich, UK). Typical spot diameters were 300–320 μm.

The 210 members of the PU library were printed following a four-replicate pattern with 1 single field of 32 × 32 spots containing 46 control (empty) areas.

School of Chemistry, University of Edinburgh, Joseph Black Buildings, King's Building, West Main Road, EH9 3JJ Edinburgh, UK. E-mail: Mark.Bradley@ed.ac.uk; Fax: +44(0)1316506453; Tel: + 44 (0)131 651 3307

† Electronic supplementary information (ESI) available: Monomers details (Table S1), primer sequences (Table S2), full polymers analysis (Table S3), list of significantly genes (Table S4), and pathway analysis (Table S5). See DOI: 10.1039/b808363k. Data deposition: Gene expression data has been deposited in ArrayExpress EBI (www.ebi.ac.uk/arrayexpress) under accession number E-MEXP-1570.

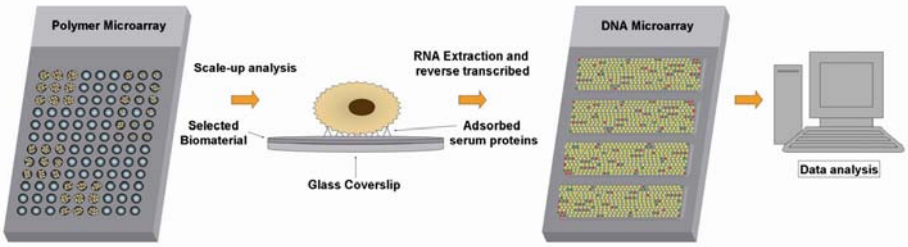

Fig. 1 Dual polymer-microarray-co-DNA-microarray strategy for the assessment of cell-biomaterial interaction.

The 58 members of the PA library were printed following a nine-replicate pattern within 1 single field of 24 × 24 spots containing 6 control (empty) areas.

K562 cell cultures

Human erythroleukemic cells were grown in RPMI 1640 growth medium supplemented with heat inactivated Fetal Bovine Serum (FBS) (10% v/v), penicillin (100 U mL^{-1}), streptomycin (100 μg mL^{-1}) and L-glutamine (4 mM) at 37 °C with 5% CO_2. Media, serum and antibiotics were purchased from (Gibco, UK) or (Sigma-Aldrich, UK).

Scanning for cell binding

K562 cells were washed with phosphate buffered saline (PBS) (Sigma-Aldrich, UK), counted and diluted with media to a final concentration of 10^5 cells per mL.

An aliquot of 6 mL of this dilution was gently added to each of the three polymer microarrays contained in a four well-plate (Nunc, Germany) and incubated for 24, 48 or 72 h.

Thirty minutes before screening, slides were washed with PBS and then incubated for 30 min with fresh media and Hoechst 33342 (1 μg/mL) nuclei stain (Invitrogen, UK).

The polymer microarray slides were then rinsed in an isotonic solution (8.1 g/L NaCl, 0.2 g/L KCl) (Sigma-Aldrich, UK) and immersed in this solution to facilitate K562 live cell analysis. Image capture was carried out *via* a Nikon 50i fluorescence microscope (×20 objective) with an automated X–Y–Z stage, using IMSTAR Pathfinder™ software package (IMSTAR S.A., Paris, France).

Polymer coating of coverslips

24 mm diameter glass coverslips (Menzel-Gläser, Germany) were cleaned with tetrahydrofuran (THF). 200 μL of the polymer solutions (2.0% w/v in THF) were placed onto the coverslips and spin coated for 2 s at 2000 rpm (P6708 spin coater, Speedlines Technologies, Indiana, USA). Coverslips were dried under vacuum (12 h at 45 °C/200 mbar) and irradiated with UV light for 20 min before

Scanning electron microscopy

As controls, K562 cells were collected, centrifuged for 5 min (300 *g* at 20 °C) and fixed in suspension with 2.5% glutaraldehyde in 0.1 M cacodylate buffer (pH 7.4) at room temperature for 2 h. After washing twice (0.1 M cacodylate buffer), the cells were seeded on coverslips coated with polyacrylate 7E7. For polymer treated samples, cells were grown for 24 h and 72 h directly on glass coverslips coated with the selected polymer (7E7, 7F7, 7G7 and 7H7) and were fixed with 2.5% glutaraldehyde for 2 h at room temperature and washed as above. All samples were post fixed with 1% osmium tetroxide for 1 h at room temperature, dehydrated through graded ethanol (50, 70, 90 and 100%), critical point dried in CO_2 and gold coated by sputtering. The samples were examined with a Philips XL30CP Scanning Electron Microscope.

RNA isolation

Total RNA was isolated from both K562 cells grown adhesively on coated coverslips and in suspension.

RNA extraction was performed using a SV Total Isolation Kit according to the manufacturer's protocol (Promega, UK). The integrity and concentration of total RNA were determined using RNA 6000 Nano Assay Kit and Bioanalyzer 2100 according to the manufacturer's protocols (Agilent, UK).

cRNA labelling

cRNA synthesis and labelling reactions (fluorophores Cy3 and Cy5 both from PerkinElmer/NEN Life Sciences, UK) were performed using a Low RNA Input Linear Amplification Kit according to the manufacturer's protocol (Agilent, UK). cRNA was assessed using a NanoDrop® ND-3300 Fluorospectrometer (Agilent, UK).

Hybridization and scanning

Array hybridization was performed using 4 × 44K Whole Human Genome microarray (design 014850 Agilent).

Array hybridization was performed using a Gene Expression Hybridization Kit (Agilent, UK). The hybridized array was washed following the post-hybridization washing step according to the manufacturer's Gene Expression Wash Buffer Kit protocol (Agilent, UK). The dried slide was scanned with an Agilent DNA microarray scanner (G2565AA).

Data analysis

Datasets pre-processed from Agilent Feature Extraction software (FE performs a lowess normalization) were analysed by Genespring GX 9. Datasets were firstly filtered by flags given by FE software (present, marginal and absent). Two different data analyses were performed.

Firstly, the four datasets were grouped together and assigned as a unique condition to analyse the interaction between polyacrylates (7E7 and 7F7) and K562.

A second analysis was performed by grouping the four datasets in a different way than before in order to see gene expression differences between cells grown on 7E7 and cells grown on 7F7. Two different T Test statistical analyses were carried out, for the first type of analysis a T Test against zero was used while for the second one a T Test unpaired, with the conditions pair being [7E7] Vs. [7F7] was performed. *p*-values were computed asymptotically in both cases. Genes with *p*-values < 0.01 were considered significant, meaning a probability of real changes in expression of 99.9%. The genes differentially altered were also subjected to a gene ontology (GO) enrichment study performed using GeneSpring GX 9 GO browser.

Gene expression data has been deposited in ArrayExpress EBI (www.ebi.ac.uk/arrayexpress) under accession number E-MEXP-1570.

Quantitative real-time PCR analysis

Quantitative real-time PCR was used to validate the effect of cell-polymer interaction on the gene expression profile. Total RNA was isolated from K562 cells grown adhesively on coated coverslips and K562 grown in suspension.

RNA extraction was performed using SV Total Isolation Kit according to the manufacturer's protocol (Promega, UK). The integrity and concentration of total RNA were determined using RNA 6000 Nano Assay Kit and Bioanalyzer 2100 (Agilent, UK). 0.5 μg of total RNA was used as a template for cDNA synthesis using Superscript III (Invitrogen, UK).

Real-time PCR was performed using LightCycler 480 (Roche, UK) and LightCycler 480 SYBR Green 1 Master (Roche, UK). The following conditions were used: an initial denaturation at 95 °C 5 min; then 45 cycles of denaturation 95 °C 5 sec, annealing 58 °C 10 sec and extension at 72 °C 20 sec during which the fluorescence produced by SYBR Green was recorded. Samples were normalized to human ring finger protein 7 (hRNF7) expression levels. Forward and reverse primer sequences were purchased from Microsynth AG (Switzerland) (0.04 μmol HPLC.purified) and are shown in Table S2 in ESI.†

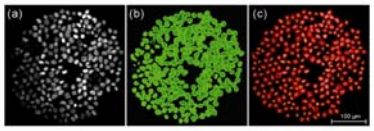

Fig. 2 Pathfinder™ software automated cell quantification. Fluorescent images of K562 cells grown on a representative polymer (PU-136): (**a**) DAPI channel; (**b** and **c**) Pathfinder™ software automatic quantification.

Results and discussion

Analysis of cell attachment and proliferation

Polymer microarrays were prepared as previously reported.[18] The identification of polymers that bound K562 cells *via* the polymer microarrays targeted not only the measurement of polymer binding capacities but also cellular proliferation.[33,34] In order to quantify both cellular adhesion and proliferation on each polymer the average number of cells and the standard deviation across the replicates were determined at three different incubation times (24, 48 and 72 h) on three different polymer microarrays with real time cellular analysis. Consequently, with parallel analysis of three arrays, it was possible to profile the polymer libraries in terms of cellular binding and proliferation, through the analysis of fluorescence images coming from nuclei stained using Hoechst 33342, with cell nuclei automatically recognized and quantified by the Pathfinder™ software (Fig. 2).

Two microarrays of polymers were studied containing either 210 different polyurethanes[32] or 58 polyacrylates[15,20] and were used to identify materials onto which K562 cells could be cultured in an adhered state.

Analysis revealed a set of polyurethanes with high cell binding (Fig. 3 a,b). The illustrated fourteen polyurethanes attached

(a)

PU	Polymer structure						
	Diol	Mn	Dis	Extender	ratio (mol)		
					Mon(1)	Mon(2)	X
136	PTMG	250	BICH	DEAPD	0.26	0.52	0.23
135	PTMG	250	BICH	DMAPD	0.25	0.52	0.23
147	PTMG	250	HDI	DEAPD	0.25	0.52	0.23
120	PPG	425	BICH	DEAPD	0.25	0.52	0.23
150	PTMG	650	HDI	EG	0.25	0.52	0.23
264	PTMG	1000	HDI	DMAPD	0.17	0.52	0.33
151	PTMG	1000	HDI	EG	0.25	0.52	0.23
126	PPG	425	TDI	DMAPD	0.25	0.52	0.23
227	PPG	1900	HDI	none	48.5	51.5	0
115	PPG	1000	HDI	BD	0.485	0.515	0
230	PPG	1900	HDI	BD	0.25	0.52	0.23
121	PPG	1000	BICH	DEAPD	0.25	0.52	0.23
87	PPG	2000	HMDI	BD	0.25	0.52	0.23
197	PTMG	650	BICH	DHM	0.25	0.52	0.23

(b)

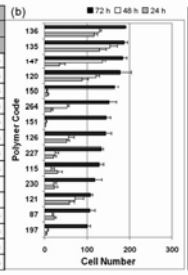

(c)

PA	Polymer structre								
	Mon(1)	Mon(2)	Mon(3)	Ratio (mol)			Monomer type		
				M(1)	M(2)	M(3)	M(2)	M(3)	
7E7	HBMA	DEAEMA	-	70	30	-	Amine	-	
7F7	HBMA	DMAEMA	-	70	30	-	Amine	-	
7G7	HBMA	DEAEA	-	70	30	-	Amine	-	
7H7	HBMA	DMAEA	-	70	30	-	Amine	-	
8F7	EMA	DMAEMA	-	70	30	-	Amine	-	
6F7	HPMA	DMAEMA	-	70	30	-	Amine	-	
3G7	MEMA	DEAEA	-	70	30	-	Amine	-	
3F7	MEMA	DMAEMA	-	70	30	-	Amine	-	
6G7	HPMA	DEAEA	-	70	30	-	Amine	-	
2H7	MMA	DMAEA	-	70	30	-	Amine	-	
5F7	HEMA	DMAEMA	-	70	30	-	Amine	-	
2F7	MMA	DMAEMA	-	70	30	-	Amine	-	
6E7	HPMA	DEAEMA	-	70	30	-	Amine	-	
8E7	EMA	DEAEMA	-	70	30	-	Amine	-	
3E7	MEMA	DEAEMA	-	70	30	-	Amine	-	

(d)

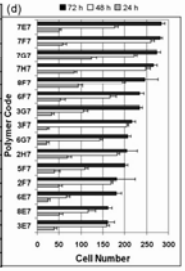

Fig. 3 Polyurethane and polyacrylate cell binding. (a) Composition of the best 14 polyurethanes; (b) Cell numbers after 24, 48 and 72 hours. (c) Composition of the best 15 polyacrylates (d) Cell numbers after 24, 48 and 72 hours. (Full polymers analysis Table S3 in ESI†.)

more than 100 cells on average (on each 300–350 μm diameter spot) after 72 h. Interestingly, the polyols poly(tetramethylene glycol) (PTMG) and poly(propylene glycol) (PPG) (see Table S1 in ESI†), were a common component of all the hit polymers, whereas more than half of the chain extender components were either 3-diethylamino-1,2-propanediol (DEAPD) or 3-dimethylamino-1,2-propanediol (DMAPD), both of which contained a tertiary amino group, which may be a factor in cellular adhesion activity, underlining that the positive surface charge of biomaterials plays a relevant role in cellular immobilization, with the best 3 polyurethanes being PU-135, 136 and 147. Moreover, data analysis revealed the unique proliferation behaviour for cells adhering on the polymers (Fig. 3b). Cells adhering on specific polymers showed a steady proliferation over the 72 h, while on others they showed only low cell binding for the first 24 and 48 hours but then underwent a 'burst' of proliferation over the following 24 hours. Cells adhering on PU-151 and 150, which have the same type of monomers, differing only in the molecular weight of the polyol used (PTMG 650 and 1000 respectively), showed similar behaviour. Low cell binding was observed during the first 48 h followed by a vigorous proliferation for the remaining 24 h. As in previous work,[18] PU-87 confirmed its high cellular affinity for K562 cells. (In all cases data were the average of the four replicates. For full polymer analysis see Table S3 in ESI†.)

A library of polyacrylates[15,20] was also evaluated (Fig. 3c,d). All the co-polymers with amino groups within monomer B induced significant cellular adhesion possibly due to the overall positive surface charge. The polyacrylates, which showed the highest number of adhered cells (more than 250 cells per spot) after 72 hours were 7E7, 7F7, 7H7 and 7G7 (Fig. 3c,d). The best binding was observed when polymers were composed of hydroxybutylmethacrylate (HBMA), which has the longest hydroxyalkyl chain when compared to methyl methacrylate (MMA), ethyl methacrylate (EMA), butyl methacrylate (BMA) and hydroxypropylmethacrylate (HPMA). The proliferation behaviour of K562 cells on these polymers (Fig. 3d) followed a uniform pattern of growth (full polymers analysis Table S3 in ESI†).

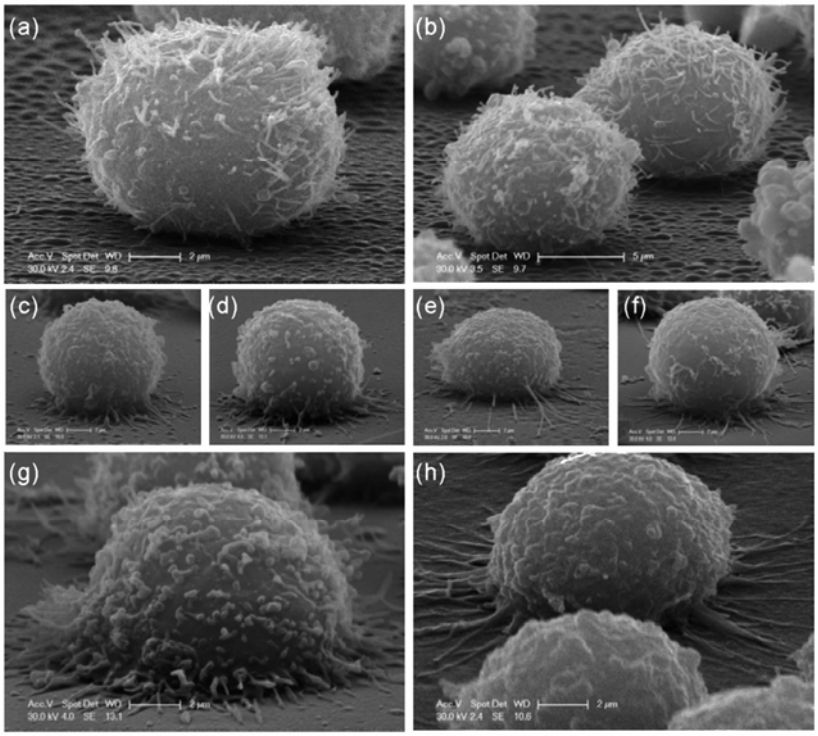

Fig. 4 Scanning electron micrographs. (a,b) Control K562 cells after 24 h; (c f) Cells grown on polyacrylates 7E7, 7F7, 7G7, 7H7 after 24 h; (g,h) Cells grown on polyacrylates 7E7 and 7F7 after 72 h.

SEM analysis

In view of the results achieved with the high-throughput analysis, scanning electron microscopy studies were undertaken so that the effect of the different polymers on the cells could be assessed in relation to the nature of the cells on the polymer surface. Analysis suggested a morphologic cellular rearrangement, with control cells (see Material and Methods for details) (Fig. 4a,b) appearing well-rounded with numerous microvilli on their surfaces. The surfaces of cells grown on the 4 polyacrylates for 24 h (Fig. 4c–f) appeared different with numerous contact points with the substratum, forcing them to take a flatter morphology, presumably as a consequence of the forced adhesive growth onto a positively charged surface.[35] This is particularly evident after 72 h with cells grown on 7E7 (Fig. 4g) and cells on 7F7 (Fig. 4h).

Gene expression profiling

Gene expression analysis was carried out to study interactions between polyacrylates and non-stained K562 cells using Agilent 4 × 44K Whole Human Genome. Analysis gave 709 genes with a p-value < 0.01, which were then subjected to a fold change analysis to determine which genes were up and down-regulated using 2 fold increase or decrease as a cut-off value. 34 genes appeared to be up-regulated while 135 were down-regulated. The quality of the data across each repeat is shown in (Fig. 5) with the profile plot of these genes.

An ulterior refinement was done by increasing the cut-off value to identify genes which show greater changes in expression. Thus, using a 3 fold change as cut-off value just 3 genes were identified as being up-regulated and 74 down-regulated genes (see Table S4 in ESI†). This shows that when K562 cells become immobilized on polyacrylates, a chain of cellular changes is triggered, most notably resulting in down- regulation.

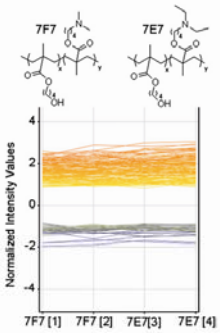

Fig. 5 Structure of polymer 7E7 (top left) and polymer 7E7 (top right) and profile plot of up and down-regulated genes across the 4 polymer samples (normalized values in $\log_2$ scale). [1] [4] represent analysis on the four different subarrays. [1] and [2] represent subarrays hybridised with total RNA obtained from cells growth on 7F7, and [3] and [4] from cells growth on 7E7. Up-regulated genes showed a negative value as the control genes were labelled with Cy5. In this case, GeneSpring GX 9.0.2 software assumed that control genes are labelled with Cy3.

This set of genes was subjected to a gene ontology enrichment study performed using GeneSpring GX 9 GO browser to analyze their roles in biological processes. This analysis showed an over-representation of one molecular function category, cadmium ion binding (GO:0046870, $p = 0.0000838$, 10 genes are found on the 4 × 44K Whole Human Genome belonging to this GO term). Five genes (MT1X, MT1B, MT1H, MT1G, MT1E), which belong to the metallothionein family, appeared to be down-regulated when K562 cells adhered onto the "hit" polyacrylate.[36]

Pathway analysis using the KEGG database was also performed, allowing the identification of gene products which form part of known biological pathways. Importantly, just down-regulated genes were identified within these relevant pathways (see Table S5 in ESI†). This suggests that the process by which K562 cells adhere alters the cellular membrane producing a significant down-regulation of membrane receptors, channels and ligands.

The 3 up-regulated genes (see Table S4 in ESI†) were individually checked.

Firstly, MED18 is a component of the mediator complex and a co-activator involved in the regulated transcription of nearly all RNA polymerase II-dependent genes. Mediator itself functions as a bridge to convey information from gene-specific regulatory proteins to the basal RNA polymerase II transcription machinery.[37]

Secondly, XPR1 xenotropic and polytropic retrovirus receptor 1 is widely expressed and is potentially involved in G/protein-coupled signal transduction. This receptor is used by polytropic leukaemia viruses to enter into cells, interestingly adhesion on surfaces induces an over-expression of this receptor.[38]

Thirdly, HMGCS1 is known to stimulate lipid synthesis and uptake and is part of the sterol-regulatory element binding proteins (SREBPs), which is essential in cholesterol metabolism regulation, showing the need for the cells to increase membrane lipid content.[39]

A second analysis was performed in order to see different levels of expression when cells were grown on 7E7 and 7F7 (Fig. 6).

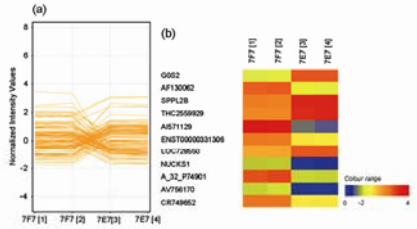

Fig. 6 (a) Profile plot of genes with different expression levels in 7E7 and 7F7. $p \leq 0.01$, 2 fold change between conditions, number of genes shown is 141. Normalized values in $\log_2$ scale. (b) Heat map of genes expressed differently in cells growth on 7E7 and 7F7. [1] and [2] represent subarrays hybridised with total RNA obtained from cells growth on 7F7 and [3] and [4] from cells growth on 7E7. Colour range represents fold change in $\log_2$ versus zero. Up-regulated gene showed a negative value as the control genes were labelled with Cy5. In this case, GeneSpring software assumed that control genes are labelled with Cy3.

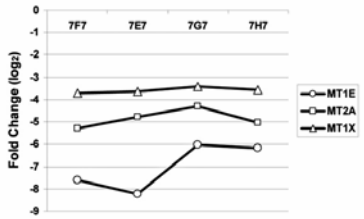

Fig. 7 Real-time PCR for three members of the metallothionein family (MT1E, MT2A, and MT1X) on the four polymers (7F7, 7E7, 7G7 and 7H7). Fold change (in $\log_2$) of the genes expression levels is reported compared to samples grown in suspension. All values are normalized against ring finger protein 7 (hRNF7) expression levels.

141 genes showed at least a 2 fold increase or decrease between the two different polymers (Fig. 6). Within this dataset, 11 genes were either up or down-regulated overall with a 2 fold change between conditions (see heat map in Fig. 6b). As shown, the gene AI571129 appears clearly to be up-regulated when K562 cells are grown on 7E7 (2.08 fold increase) and down-regulated when they are grown on 7F7 (3.40 fold decrease). This probe corresponds to a cDNA clone IMAGE: 2176344, which has no known function. The other 10 genes appear to be either up or down-regulated on one polymer and unmodified on the other.

Data validation

In order to validate the observed expression profiles for the down regulated genes MT1X, MT2A and MT1E, quantitative real time PCR on K562 cells grown on polymers 7F7, 7E7, 7G7, 7H7 and in suspension as a control was performed. The gene expression was normalised with respect to the expression of a housekeeping gene (hRNF7). The relative mRNA level for each gene (as the fold change) is showed in Fig.7.

The mRNA levels obtained clearly confirmed the data obtained *via* microarray analysis providing proof of the effect on gene expression in response to polymer-cell interactions. Moreover, an extension of real-time quantitative PCR analysis to cells grown on polymers 7G7 and 7H7 (where microarray analysis was not performed), suggested behaviour similar to 7E7 and 7F7.

Conclusions

Polymer microarrays were successfully used for the identification of a family/group of polymers that enabled adhesion and proliferation of a suspension cell line with scanning of live cells across the polymer microarray allowing elucidation of the effects of the tertiary amino groups in promoting adhesion. These interactions were studied by SEM showing cells with numerous contact points with the substratum, as consequence of adhesive growth onto the positively charged surface, a process that is undoubtedly modulated by the adhesion of extracellular proteins onto the polymeric substrate. Finally, gene expression profiling demonstrated that interactions between cells and materials induce a number of changes in the transcriptom. In this particular case, a remarkable down-regulation of predominantly membrane receptors, ligands and channels was observed to take place. Furthermore, validation by quantitative real-time PCR confirmed the gene expression analysis.

Acknowledgements

This research was supported by the EPSRC. The authors thank Dr Josh Brickman, Dr Alessandra Livigni and Dr Theodora Tzanavari from the Institute for Stem Cell Research, Edinburgh, UK, for their help in the validation of the data by real time PCR. The authors thank Dr Colin Campbell from the School of Chemistry, Edinburgh, UK and Alan Ross from the Division of Pathway Medicine, Edinburgh, UK, for their support in the use of the Agilent technology.

References

1 P. J. Doherty, R. L. Williams, D. Williams, A. J. C. Lee, editors. *Biomaterial-Tissue Interfaces: Second Consensus Conference on Definitions in Biomaterials, Chester 1991*. Amsterdam: Elsevier, 1992.
2 Q.-Z. Chen, S. E. Harding, N. N. Ali, A. R. Lyon and A. R. Boccaccini, *Mater. Sci. Eng. R.*, 2008, **59**, 1 37.
3 P. X. Ma, *Adv. Drug. Deliver. Rev.*, 2008, **60**, 184 198.
4 Z. Ma, Z. Mao and C. Gao, *Colloid Surface B.*, 2007, **60**, 137 157.
5 S. Chaterji, I. K. Kwon and K. Park, *Prog. Polym. Sci.*, 2007, **32**, 1083 1122.
6 V. Nadeau, G. Leclair, S. Sant, J.-M. Rabanel, R. Quesnel and P. Hildgen, *Polymer*, 2005, **46**, 11263 11272.
7 B. L. Seal, T. C. Otero and A. Panitch, *Mat. Sci. Eng. R.*, 2001, **34**, 147 230.
8 R. Zhang, A. Liberski, F. Khan, J. J. Diaz-Mochon and M. Bradley, *Chem. Commun.*, 2008, **11**, 1317 1319.
9 H. Zhang, M. W. M. Fijten, R. Hoogenboom, R. Reinierkens and U. S. Schubert, *Macromol. Rapid Commun.*, 2003, **24**, 81 86.
10 J. D. Hewes and L. A. Bendersky, *Appl. Surf. Sci.*, 2002, **189**, 196 204.
11 D. G. Anderson, S. Levenberg and R. Langer, *Nat. Biotechnol.*, 2004, **22**, 863 866.
12 J. A. Hubbell, *Nat. Biotechnol.*, 2004, **22**, 828 829.
13 D. G. Anderson, J. A. Burdick and R. Langer, *Science*, 2004, **305**, 1923 1924.
14 D. G. Anderson, D. Putnam, E. B. Lavik, T. A. Mahmood and R. Langer, *Biomaterials*, 2005, **26**, 4892 4897.
15 H. Mizomoto, PhD. Thesis, University of Southampton, 2004.
16 G. Tourniaire, J. Collins, S. Campbell, H. Mizomoto, S. Ogawa, J. F. Thaburet and M. Bradley, *Chem. Commun.*, 2006, **20**, 2118 2120.
17 A. Mant, G. Tourniaire, J. J. Diaz-Mochon, T. J. Elliott, A. P. Williams and M. Bradley, *Biomaterials*, 2006, **27**, 5299 5306.
18 S. Pernagallo, A. Unciti-Broceta, J. J. Diaz-Mochon and M. Bradley, *Biomed. Mater.*, 2008, **3**, 034112 (6pp).
19 J. J. Diaz-Mochon, G. Tourniaire and M. Bradley, *Chem. Soc. Rev.*, 2007, **36**, 449 457.
20 A. Unciti-Broceta, J. J. Diaz-Mochon, H. Mizomoto and M. Bradley, *J. Comb. Chem.*, 2008, **10**, 179 184.
21 J. Ziauddin and D. M. Sabatini, *Nature*, 2001, **411**, 107 110.
22 D. B. Wheeler, A. E. Carpenter and D. M. Sabatini, *Nat. Genet.*, 2005, **37**, 25 30.
23 C. B. Lozzio and B. B. Lozzio, *Blood*, 1975, **45**, 321 334.
24 E. Klein, H. Ben-Bassat, H. Neumann, P. Ralph, J. Zeuthen, A. Polliack and F. Vánky, *Int. J. Cancer*, 1976, **18**, 421 431.
25 B. Greiger, A. Bershadsky, R. Pankov and K. M. Yamada, *Nat. Rev. Mol. Cell Biol.*, 2001, **2**, 793 805.
26 N. Mefti, B. Haussy and J. F. Ganghoffer, *Int. J. Solids. Struct.*, 2006, **43**, 7378 7392.
27 C.-H. Ku, M. Browne, P. J. Gregson, J. Corbeil and D. P. Pioletti, *Biomaterials*, 2002, **23**, 4193 4202.
28 F. Carinci, S. Volinia, F. Pezzetti, F. Francioso, L. Tosi and A. Piattelli, *J. Biomed. Mater. Res. B.*, 2003, **66**, 341 346.
29 C. M. Klapperich and C. R. Bertozzi, *Biomaterials*, 2004, **25**, 5631 41.
30 L. T. Allen, E. J. P. Fox, I. Blute, Z. D. Kelly, Y. Rochev, A. K. Kenneth, K. A. Dawson and W. M. Gallagher, *Proc. Natl. Acad. Sci. USA*, 2003, **100**, 6331 6336.

31 G. E. Garrigues, D. R. Cho, H. E. Rubash, S. R. Goldring, J. H. Herndon and A. S. Shanbhag, *Biomaterials*, 2005, **26**, 2933 2945.
32 J. F. O. Thaburet, H. Mizomoto and M. Bradley, *Macromol. Rapid Commun.*, 2004, **25**, 366 370.
33 J.-H. Wang, C.-H. Hung and T.-H. Young, *Biomaterials*, 2006, **27**, 3441 3450.
34 C. Itthichaisri, M. Wiedmann-Al-Ahmad, U. Huebner, A. Al-Ahmad, R. Schoen, R. Schmelzeisen and N.-C. Gellrich, *J. Biomed. Mater. Res. A.*, 2007, **82**, 777 787.
35 A. Calcabrini, G. Rainaldi and M. T. Santini, *J. Mater. Sci-Mater. M.*, 1999, **10**, 613 620.
36 M. Karin and R. I. Richards, *Environ. Health Persp.*, 1984, **54**, 111 115.
37 L. Larivière, S. Geiger, S. Hoeppner, S. Röther, K. Sträßer and P. Cramer, *Nat. Struct. Mol. Biol.*, 2006, **13**, 895 901.
38 J. W. Hartley, N. K. Wolford, L. J. Old and W P. Rowe, *Proc. Natl. Acad. Sci. USA*, 1977, **74**, 789 792.
39 J.-B. Demoulin, J. Ericsson, A. Kallin, C. Rorsman, L. Roennstrand and C.-H. Heldin, *J. Biol. Chem.*, 2004, **279**(34), 35392 35402.

NEU-2009-1095-Di Pietro_1P
Type: Research Article

Original Article

JOURNAL OF NEUROTRAUMA 27:1–11 (February 2010)

DOI: 10.1089/neu.2009.1095

Transcriptomics of Traumatic Brain Injury: Gene Expression and Molecular Pathways of Different Grades of Insult in a Rat Organotypic Hippocampal Culture Model

Valentina Di Pietro,[1] Daven Amin,[1] Salvatore Pernagallo,[2] Giuseppe Lazzarino,[3] Barbara Tavazzi,[4] Roberto Vagnozzi,[5] Ashley Pringle,[1] and Antonio Belli[1]

Abstract

Traumatic brain injury (TBI) is the one of the most common forms of head trauma, and it remains a leading cause of death and disability. It is known that the initial mechanical axonal injury triggers a complex cascade of neuroinflammatory and metabolic events, the understanding of which is essential for clinical, translational, and pharmacological research. These can occur even in mild TBI, and are associated with several post-concussion manifestations, including transiently heightened vulnerability to a second insult. Recent studies have challenged the tenet that ischemia is the ultimate modality of tissue damage following TBI, as metabolic dysfunction can develop in the presence of normal perfusion and before intracranial hypertension. In order to elucidate the cellular and molecular changes occurring in TBI as a direct result of neuronal injury and in the absence of ischemic damage, we performed a microarray analysis of expressed genes and molecular interaction pathways for different levels of severity of trauma using an *in-vitro* model. A stretch injury, equivalent to human diffuse axonal injury, was delivered to rat organotypic hippocampal slice cultures, and mRNA levels following a 10% (mild) and 50% (severe) stretch were compared with controls at 24 h. More genes were differentially expressed following 10% stretch than 50% stretch, indicating the early activation of complex cellular mechanisms. The data revealed remarkable differential gene expression following mTBI, even in the absence of cell damage. Pathway analysis revealed that molecular interactions in both levels of injury were similar, with IL-1β playing a central role. Additional pathways of neurodegeneration involving RhoA (ras homolog gene family, member A) were found in 50% stretch.

Key words: traumatic brain injury, gene expression, IL-1, diffuse axonal injury, transcriptomics

Introduction

TRAUMATIC BRAIN INJURY (TBI) is a major public health problem, especially among young males aged 15–25 years, the elderly of both genders (those over 75 years of age), and young children under age 5 years (Jennett, 1998). TBI continues to be a leading cause of permanent disability and death in Western nations (Teasdale and Jennett, 1974). In the United States, 2% of the population is thought to suffer long-term effects of TBI, and in the United Kingdom (population 61.6 million), head injury is the presenting diagnosis for over 700,000 accident and emergency admissions each year (Kay and Teasdale, 2001).

TBI is generally subdivided into mild, moderate, or severe cases, with mild TBI (mTBI) representing the majority of all head injuries (Alexander, 1995; Vos et al., 2002). Different definitions of mTBI exist, but in general it is characterized by a shorter period of reduced consciousness and shallower coma (usually only for seconds to minutes), compared to moderate and severe injuries (Alexander, 1995; Vos et al., 2002). Common complaints of those with mTBI include headache, pain, visual and vestibular disturbances, fatigue, emotional and behavioral deficits, depression, irritability, anxiety, lack of initiative, decreased self-esteem, social difficulties, and personality changes (Comper et al., 2005; Jay et al., 1996).

[1]Division of Clinical Neurosciences, University of Southampton School of Medicine, Southampton, United Kingdom.
[2]School of Chemistry, University of Edinburgh, Edinburgh, United Kingdom.
[3]Division of Biochemistry and Molecular Biology, University of Catania, Catania, Italy.
[4]Institute of Biochemistry and Clinical Biochemistry, Catholic University of Rome "Sacro Cuore," Rome, Italy.
[5]Department of Neurosciences, University of Tor Vergata, Rome, Italy.

Mild TBI is difficult to manage properly, as those who do present for medical care are rarely admitted. Those who attend accident and emergency are often not seen by a specialist, and in many cases receive no specific advice or care at all (Comper et al., 2005; Jay et al., 1996; Teasdale and Jennett, 1974; Vagnozzi et al., 2007).

It is clear that the response of the brain to trauma is complex and involves many biochemical and molecular changes. Further, the molecular processes triggered by mTBI, in which little if any discernable cell death occurs, are likely to be, at least in part, different from those occurring after more severe injury.

Numerous researchers have examined the expression of individual genes whose products contribute to recovery or impairment of function following head injury. However as yet, a global analysis of messenger RNA (mRNA) expression in reliable models of TBI has not been carried out. The main drawback of the analysis of individual genes is that the relationships between the different pathways are extremely complex and highly variable, not only with respect to severity of injury, but also over time. An ideal approach would be to look simultaneously at a transcriptional profile at defined time points, and in response to different levels of severity of insult.

In this study, microarray technology was utilized to examine gene expression profile in an *in-vitro* model of rat hippocampal slice culture stretched at specific Lagrangian strains (10% and 50%), through the dynamic deformation of the silicone membrane to which the slices were adhered. This produces a strain field in the tissue that mimics the *in-vivo* tissue deformation experienced by brain tissue during acceleration/deceleration trauma.

This model has been amply validated and allows the study of the cellular effects of TBI without confounding systemic variables, such as hypoxia, hypotension, or sepsis. Although the latter are all powerful determinants of outcome in clinical practice, the identification of the molecular mechanisms involved in the pathophysiology of TBI is a critical step in the identification of reliable clinical biomarkers of central nervous system (CNS) injury, drug development, and stem-cell research.

Methods

Organotypic hippocampal slice cultures

Organotypic hippocampal slice cultures maintain their anatomical organization of neurons and glia, and thus provide an ideal model for studying the effects of stretch-induced brain trauma (Kumaria and Tolias, 2008).

The hippocampal cell cultures were prepared using a method initially described by B. Morrison (Morrison et al., 2006), and all procedures used were in accordance with U.K. regulations under the Animals (Scientific Procedures) Act of 1986.

Briefly, the septal portion of hippocampi from 8- to 10-day-old Wistar rats were removed and sliced using a McIlwain tissue chopper (Harvard Apparatus, Edenbridge, U.K.) to a thickness of 400 μm. These were then placed in ice-cold Geys solution supplemented with 5 mg/mL D-glucose. The slices were then placed in the center of a silicone membrane and were initially fed 1200 μL Neurobasal medium (Neurobasal-A; Invitrogen, U.K.), vitamin B_{27} (Invitrogen), 5 mg/mL D-glucose (Sigma), and 1 mmol/L glutamine (Sigma).

Prior to preparation of the slices, the wells were assembled by attaching the non-porous silicone membranes (0.25 mm; Specialty Manufacturing, Saginaw, MI) to custom-made stainless steel wells. This assembly was placed in a glass Petri dish and sterilized. Also, 48 h prior to hippocampal tissue culturing, the silicone membranes were pretreated with a coating solution of 320 μg/mL poly-D-lysine (Sigma) and 80 μg/mL of laminin (Sigma) in sterile distilled water.

After 2 days *in vitro*, the neurobasal medium bathing the slices was replaced with full serum-containing medium, consisting of 25% heat-inactivated horse serum, 25% Hanks' balanced salt solution, 50% minimum essential medium (all Invitrogen), 1 mmol/L glutamine (Sigma), and 5 mg/mL D-glucose (Sigma). This full medium was changed three times per week. To maintain an air-medium interface and provide sufficient gas exchange, the wells were rocked at 1 rev cycle/50 sec in an incubator at 37°, 100% humidity, and 5% CO_2.

Five cultures (each containing 4 slices from the same rat) were used for each experimental group.

Stretch injury device

The biomechanics of the stretch injury device have been described in detail previously (Morrison et al., 2006). Briefly, however, it is designed to stretch the organotypic hippocampal slice cultures through dynamic deformation of the silicone membrane upon which the tissue slices were grown and adhered. The strain field is produced by a mechanical loading mechanism that mimics the *in-vivo* tissue deformation thought to be experienced during TBI.

The stainless steel well and silicone membrane were held in place by a circular clamp on a heated platform (37°C). The membrane was then displaced over a fixed, hollow indenter to generate an equi-biaxial strain field, subjecting the cultures to a single stretch injury at a specified Lagrangian strain and constant strain rate. The strain was controlled by a linear actuator (BEI Kimco), and maintained under feedback control through a linear encoder (Renishaw,, U.K.), and motion control board (Precision Motion Dynamics, Canada).

Stretching the organotypic hippocampal slice cultures

After approximately 10 days *in vitro*, the viability of the organotypic hippocampal slice cultures was assessed by viewing under a light microscope to ensure the slices were adhered to the membrane, and to see if clear definition of the neuronal regions (CA1, CA3, and dentate gyrus) could be seen. Any cultures that were not completely adhered to the silicone membrane were discarded.

The cultures were placed in fresh, serum-containing full medium with 5 μg/mL of propidium iodide (PI) (Molecular Probes, Paisley, U.K.), an exclusion dye, for 2 h, and then they were imaged using a Leica DM-IRBE epifluorescence microscope (Leica Microsystems Ltd., U.K.), and any cultures expressing excessive PI fluorescence were discarded.

Images were acquired using a 5×NA 0.12 lens and a cooled Hamamatsu camera and analyzed with Volocity (Improvision, U.K.) 3-D imaging software.

The medium was removed from the healthy cultures and the wells were clamped to the stretch injury device. The membrane was then displaced to generate a strain field, and the cultures were subjected to a single stretch injury at a Lagrangian strain of 10% or 50%, at a constant strain rate of 20 sec^{-1}, or in the case of controls, no stretch at all.

Propidium iodide fluorescence

Following the stretch insult, the cultures were placed in fresh full serum-containing medium. Twenty-four hours post-injury, the organotypic hippocampal slice cultures were examined under the epifluorescence microscope to assess the percentage of cell death. Neuronal damage was expressed as a percentage of the area in which PI fluorescence was detected above threshold within a cell layer divided by the total area of that cell.

The mean percentage area of PI fluorescence for controls, 10% stretch, and 50% stretch were analyzed and compared using one-way independent group analysis of variance (ANOVA). Following one-way ANOVA, a *post-hoc* multiple comparison procedure was performed to compare pairs of group means. As one group represented control data, Dunnett's test was performed to compare 10% and 50% stretch cell damage to controls, but not to each other. All tests were two-tailed, and statistical significance was set at $p \leq 0.05$.

cDNA microarray

Total RNA was extracted from tissue cultures in a monophasic solution of phenol and guanidine isothiocyanate (Trizol; Invitrogen) as previous described (Vagnozzi et al., 2007).

The integrity and concentration of the total RNA were determined using the RNA 6000 Nano Assay Kit and a Bioanalyzer 2100 according to the manufacturer's protocols (Agilent, U.K.).

The labeling of complimentary RNA (cRNA) with the fluorophores cyanine-3 (cy-3) and cyanine-5 (cy-5) (PerkinElmer/NEN Life Sciences, U.K.) and its subsequent amplification was completed using the Low RNA Input Linear Amplification Kit (Agilent) according to the manufacturer's protocol.

Briefly, in this procedure one sample (control) is labeled with cy-3 (which was excited by a 532-nm laser), and one sample (either 10% stretch or 50% stretch) with cy-5 (which was excited by a 633-nm laser). A primer, which contains poly (oligo) dT and a T7 polymerase promoter, was annealed to the sample RNA. Next, using the T7 RNA polymerase, cRNA was synthesized and amplified, while simultaneously cy-3- or cy-5-labeled CTP is incorporated into it.

The cRNA was assessed using a NanoDrop® ND-3300 Fluorospectrometer (Agilent) to ensure that sufficient cRNA of appropriate quality had been prepared.

Once labeling was complete, equal amounts of cy-3- and cy-5-labeled probes were simultaneously applied to a 4×44 K whole rat genome microarray (Design 14879; Agilent) for a competitive hybridization reaction using a gene expression hybridization kit (Agilent), according to the manufacturer's protocol.

Following hybridization, the array was washed using the gene expression wash buffer kit (Agilent), dried, and then scanned using a DNA microarray scanner (Agilent), and the data were processed using feature extraction software (Agilent).

Data analysis

The datasets, pre-processed by Agilent Feature Extraction software, were analyzed by Genespring GX 10.0.2. Automatic flags applied by the Feature Extraction software were used to localize and exclude from the analysis any probes that were non-uniform, population outliers, saturated, absent, not positive and significant, or not above background.

The signal from each spot was calculated as the average intensity minus the average local background. Expression ratios of cy-5:cy-3 were normalized using LOESS, a method that takes into account and corrects for intensity-dependent artifacts in the measurements.

The mean $\log_2$ ratios for each probe were found across the two replicates, and the probes that revealed a >1.5-fold difference in expression (higher or lower) compared to the control sample were identified.

The gene ontology (GO) term analysis was completed using a p-value of <0.1, with Benjamini-Yekutieli false discovery rate correction.

The list of differentially expressed genes were analyzed for any gene ontologies that were statistically over-represented and assigned to functional categories (GO terms) using an enrichment analysis.

Using the GO terms and lists of differentially expressed genes produced following enrichment analysis, the European Bioinformatics Institute's (EBI) IntAct database was used to analyze molecular interaction data and generate a pathway of these molecular interactions and reactions for both 10% and 50% stretch.

Gene expression data have been deposited in ArrayExpress EBI (www.ebi.ac.uk/arrayexpress) under accession number E-MEXP-2235.

Real time-quantitative polymerase chain reaction (RT-qPCR)

RT-qPCR was used to validate the expression of several genes shown in the microarray analysis.

First, the reverse transcription of total RNA was performed for control, 10% stretch, and 50% stretch samples. From each sample, 1 μg of total RNA, 500 ng of oligo dT primers (Roche Molecular Biochemicals, U.K.), and 200 U of Superscript II Reverse Transcriptase in a total volume of 20 μL of 1× First Strand Buffer (Invitrogen) were incubated at 42°C for 60 min.

The concentration and purity of the resulting cDNA was determined with a ND-1000 UV-Vis Spectrophotometer (NanoDrop).

RT-qPCR was carried out on the single-stranded cDNA yielded from the reverse transcription using a one-step PCR kit, Rat Custom real-time PCR assay for use with SYBRgreen chemistry (PrimerDesign Ltd., Southampton, U.K.), and a Rotor-Gene 6000 real-time thermocycler (Corbett Robotics Ltd., U.K.) according to the manufacturer's protocol, for 40 cycles.

The genes selected for RT-qPCR and sequences of primers were: S100a6 (S100 calcium binding protein A6) *Rattus norvegicus* (NM_053485), forward GCACACCCTGAGCAA GAAG, reverse CCTTGTTACGGTCCAGATCATC; and interleukin-1β (IL-1β) *Rattus norvegicus* (NM_031512), forward AGCACCTTCTTTTCCTTCATCTT, reverse CAGACAGCA CGAGGCATTTT. These primers were designed by Primer Design Ltd. (Southampton, U.K.).

For accurate gene expression measurements with RT-qPCR, it is essential to normalize results to a fixed reference, and therefore the constitutively expressed housekeeping gene B2M (beta-2-microglobulin) *Rattus norvegicus* (NM_012512) was selected using the geNorm Housekeeping Gene Selection

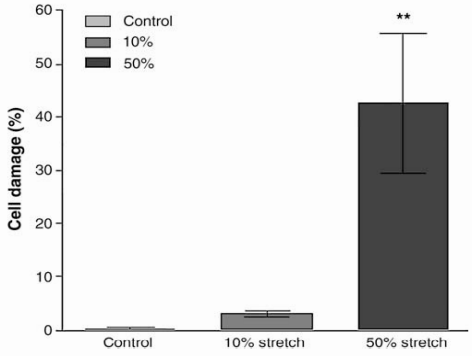

FIG. 1. Cell damage in control, 10% stretch, and 50% stretch cultures. Damage within the CA1 and CA3 regions as determined by propidium iodide fluorescence at 24 h post-injury is significantly increased following a 50% stretch injury compared to controls. No significant increase in cell damage occurred following 10% stretch compared with controls ($p = 0.44$). Data are presented as mean ± standard deviation (**$p < 0.001$ versus controls).

Kit (Primer Design Ltd.) from a list containing 12 candidate reference genes.

Results

PI fluorescence

Stretching the organotypic slice cultures resulted in cell damage, as measured by uptake of the fluorescent exclusion dye PI. Representative fluorescence images of the slice cultures were taken at 24 h after 10% stretch, 50% stretch, and of control. The percentage area of red fluorescence compared to the total area of the hippocampal slice of each image was later analyzed and compared. Analysis of percentage cell damage can be seen in Figure 1.

One-way ANOVA showed statistically significantly different cell damage between experimental sets ($p < 0.0001$). When comparing the two stretch groups with controls with Dunnett's test, the 10% stretch injury slices did not show a significantly different percentage of cell death (mean cell death 3.07%, SD ± 1.91 in 10% stretch, versus mean cell death 0.31% SD ± 0.38 in controls; $p = 0.44$), as expected in mild TBI, thus confirming the validity of this model. The damage occurring following 50% stretch, however, was significantly greater (mean 42.23%, SD ± 13.17; $p < 0.001$), again confirming this to be a valid model for this severity of injury.

cDNA microarray

Traumatic brain injury activates complex cascades of biochemical changes, and these changes alter the expression of genes, whose products contribute to the pathophysiology seen following brain trauma.

Of more than 41,000 gene probes on the microarray, 18,459 met the inclusion criteria for detectable expression.

In the 10% stretch sample, a total of 999 probes were differentially expressed, and for 50% stretch, 587 probes were differentially expressed, either increased or decreased, compared to controls, by a minimum fold change of 1.5.

After data normalization and fold change calculation, a comparison was made between genes differentially expressed in 10% stretch and 50% stretch compared with controls.

We found that in 10% stretch 210 genes were upregulated, in 50% stretch 161 genes were upregulated, and of these, 30 genes were increased in both experimental groups.

A comparison between differentially downregulated genes showed in 10% stretch 789 genes were downregulated, and in 50% stretch 426 genes were downregulated, and of these, 307 genes were decreased in both groups (Fig. 2).

The full dataset of all differentially expressed is available as a supplementary file (Supplementary Table 1) (see online supplementary material at http://www.liebertonline.com).

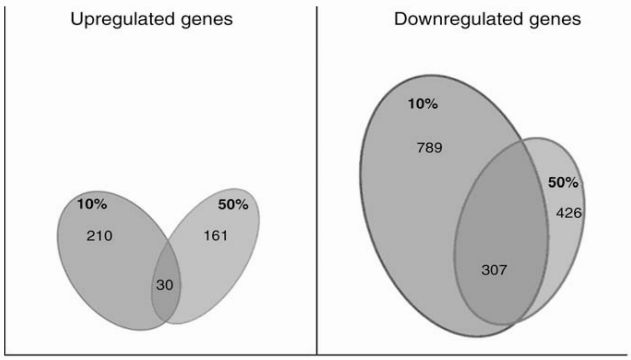

FIG. 2. Gene expression following 10% and 50% stretch injury. Venn diagram illustrating differentially expressed genes at the two different injury intensities. Overlapping areas show genes for which expression was altered in both levels of stretch injury.

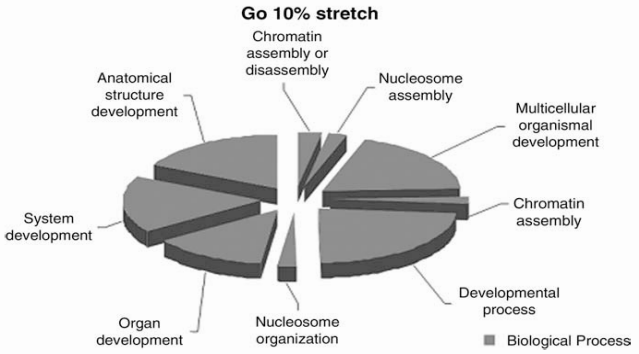

FIG. 3. Gene ontology (GO) following 10% stretch injury. Diagrammatic representation of the functional categories (GO terms) associated with differentially expressed genes following a mild (10%) stretch injury. All share the same gene ontology: Biological Process.

Gene analysis and ontology

The differentially expressed genes were assigned to functional categories using gene enrichment analysis. This process evaluates microarray data and provides categories based on genes sharing the same GO term, as defined in published information on biochemical pathways in previous experiments (Kerrien et al., 2007; Subramanian et al., 2005).

The altered genes in 10% stretched cells can be broadly classified into nine functional groups: chromatin assembly or disassembly, nucleosome organization, organ development, chromatin assembly, developmental process, nucleosome assembly, multicellular organismal development, system development, and anatomical structure development. All of these were found to be within the GO "Biological Process" (Fig. 3).

The genes found to be differentially expressed following a 50% stretch were in three different GOs: "Molecular Function," "Cellular Component," and "Biological Process," and classified within 13 functional groups. In Molecular Function the categories were G-protein coupled receptor binding, receptor binding, cytokine activity, binding, chemokine activity, and chemokine receptor binding. The categories defense response, inflammatory response, behavior, response to external stimulus, response to wounding, and neutrophil chemotaxis were found to be in Biological Process. The GO Cellular Component was represented by one functional category, extracellular region (Fig. 4).

Pathway analysis

Using the GO terms produced following gene enrichment, the EBI IntAct database was used to analyze molecular interaction data and generate a pathway of these molecular interactions and reactions for both 10% and 50% stretch. The

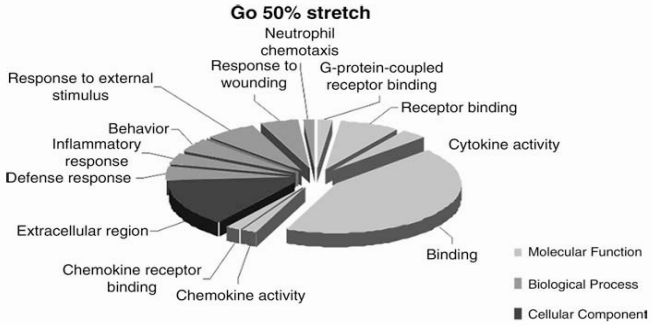

FIG. 4. Gene ontology (GO) following 50% stretch injury. Diagrammatic representation of the functional categories (GO terms) associated with differentially expressed genes following a severe (50%) stretch injury. Three gene ontologies were found to correspond with these genes: Biological Process, Molecular Function, and Cellular Component.

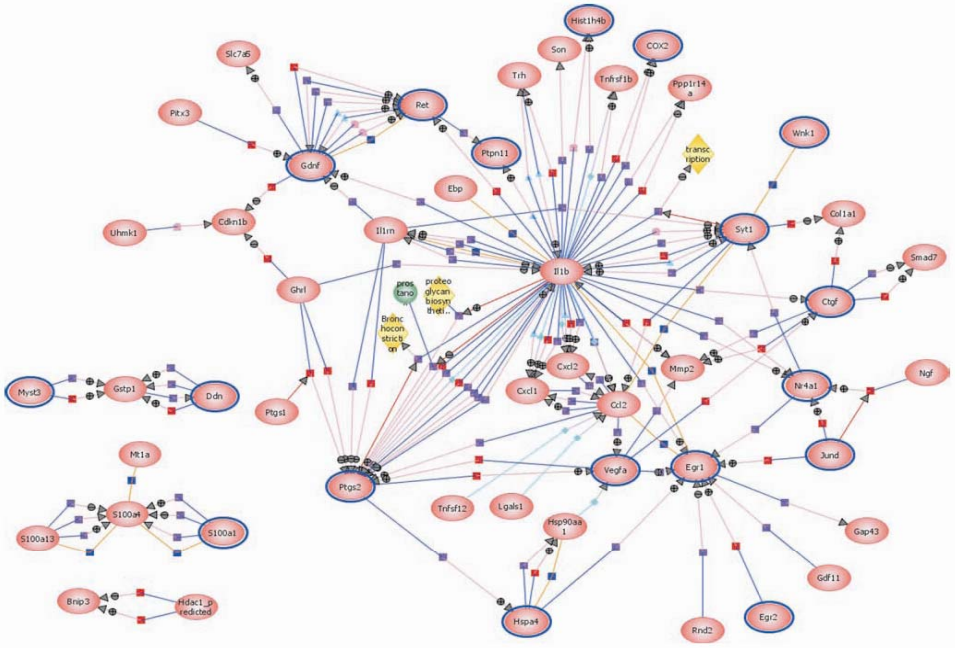

FIG. 5. Pathway analysis following 10% stretch injury. Pathway analysis diagram showing interactions between various genes with differential expression for a mild traumatic brain injury (10% stretch).

pathways produced are the extensive interactive diagrams shown in Figure 5 (for 10% stretch) and Figure 6 (for 50% stretch).

The pathway analysis for both a 10% and 50% stretch injury reveals that the pathways share many interactions, while also highlighting key differences. Proinflammatory cytokines appear to have a central role in molecular interactions following both a mild and a severe brain injury. In both pathways it can be clearly seen that IL-1β plays an important role and has numerous interactions with other genes. Prostaglandin-endoperoxide synthase 2 (PTGS2), also known as cyclooxygenase-2 (COX-2), also appears to be vital in both 10% and 50% stretch, with many regulation, expression, and metabolism interactions with IL-1β.

A crucial pathway that became evident following 50% stretch, but that was not present in the mild injury pathway analysis, involved the myelin growth inhibitor rtn4 (Nogo-A), targeting and positively regulating the GTPase RhoA (ras homolog gene family, member A), which is implicated in the neurodegenerative process.

Both pathway analysis diagrams are available as supplementary clickable files (Supplementary Figures 1 and 2) (see online supplementary material at http://www.liebertonline.com).

RT-qPCR analysis

In order to validate the expression profiles observed, RT-qPCR analysis was performed by selecting two genes with either a high or low fold change, as seen in cDNA microarray analysis results for both 10% and 50% stretch samples.

The RT-qPCR analysis confirmed the upregulation of IL-1β parallel to that seen in both 10% and 50% stretch injury following microarray analysis, and also confirmed the down-regulation of the gene S100a6, also in parallel to the microarray analysis (Fig. 7A and B).

Discussion

The results of this investigation show that the pathophysiology following TBI is complex and involves alterations in the expression of genes, whose products are involved in a variety of cellular processes that contribute to the behavioral deficits and pathological consequences of brain injury.

The identification of genes induced in response to brain injury is currently an area of intense research, particularly since the development of the microarray. The ability to use probe sequences that are complimentary to thousands of genes has allowed the study of large-scale mRNA changes

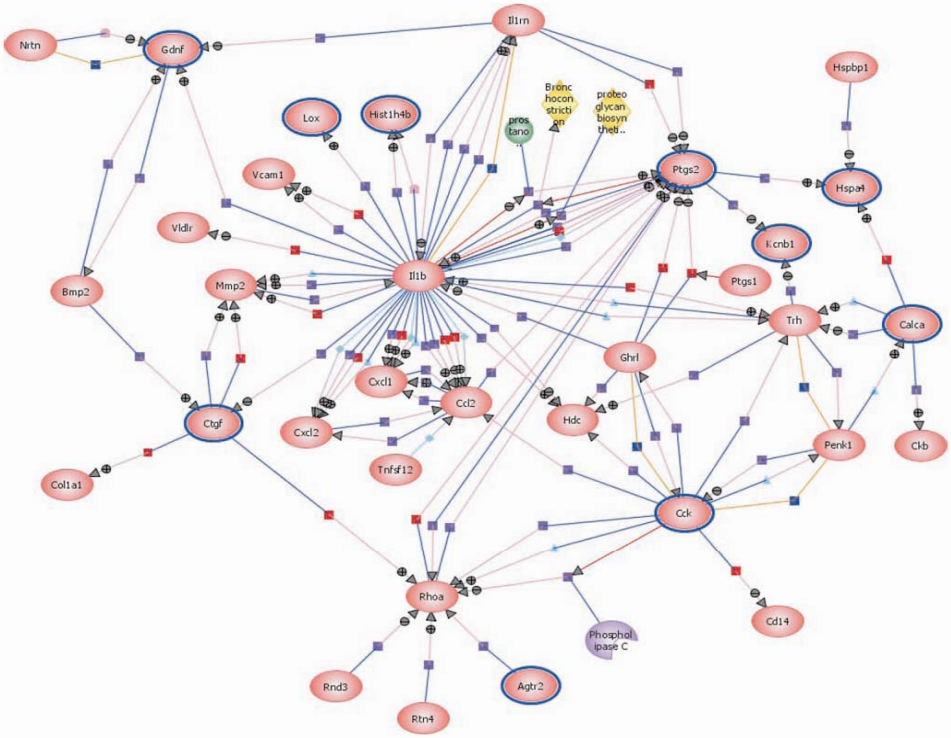

FIG. 6. Pathway analysis following 50% stretch injury. Pathway analysis diagram showing interactions between various genes with differential expression for severe traumatic brain injury (50% stretch).

associated with a variety of physiological and pathological processes (Luo and Greshwind, 2001).

Using cDNA microarray technology, we report that following stretch injury to hippocampal slice cultures, the expression of 999 genes in 10% stretch and 587 genes in 50% stretch were altered, compared with controls.

The altered genes in 10% stretched cells clustered in the "Biological Process" group, which has shown to be involved in the structural damage of cellular architecture.

Most of the genes expressed following 10% stretch are involved in signal transducer activity, regulation of transcription, and cell communication. This indicates that even after a mild injury of 10% stretch, intense activity involving transcription and signaling exchange is initiated.

Additionally, we have found that following 10% stretch, certain genes involved in the apoptotic process, such as Vdac1 (voltage-dependent anion-selective channel protein 1), Sh3glb1 (SH3-domain GRB2-like endophilin B1), Phlda1 (leckstrin homology-like domain, family A, member 1), Rock1 (Rho-associated coiled-coil containing protein kinase 1), and Eif4g2-predicted (eukaryotic translation initiation factor 4 gamma, 2) were downregulated. Further, an upregulation was seen in genes involved in the anti-apoptotic process, such as Ccl2 (chemokine [C-C motif] ligand 2), Vegfa (vascular endothelial growth factor A), BIRC3 (baculoviral IAP repeat-containing 3), Tsc22d3 (TSC22 domain family, member 3), Bnip3 (BCL2/adenovirus E1B 19-kDa interacting protein 3), and Nr4a1 (nuclear receptor subfamily 4, group A, member 1).

The majority of these expression changes were only found following 10% stretch, indicating that these hippocampal cell cultures have activated protective and repair mechanisms.

Following a severe 50% stretch, the genes were clustered in three different GOs: "Molecular Function," "Cellular Component," and "Biological Process," and the majority of genes seen to be upregulated are involved in inflammatory events, apoptosis, and necrosis, such as Casp1 (caspase 1, apoptosis-related cysteine peptidase), Nlrp3 (NLR family,

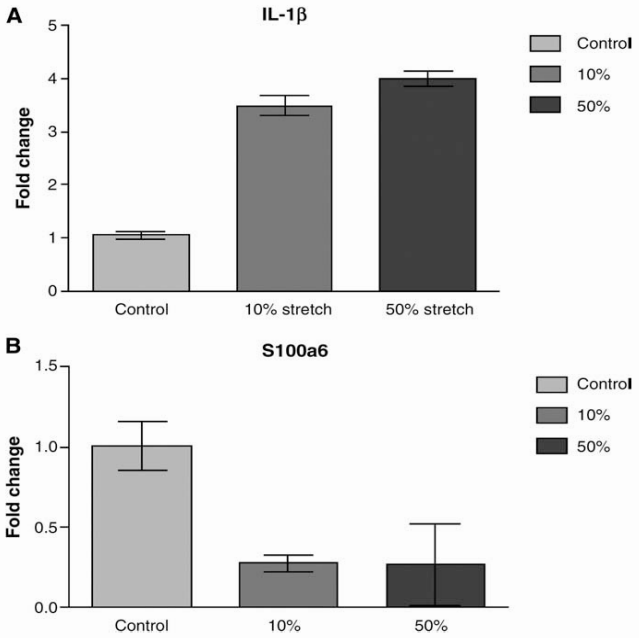

FIG. 7. RT-qPCR analysis of (**A**) IL-1β and (**B**) S100a6. Validation of microarray findings by RT-qPCR analysis. In both genes selected for validation, the RT-qPCR data are parallel to those from the microarray analysis. Data are presented as mean ± standard deviation.

pyrin domain containing 3), and as can clearly be seen in the pathway analysis, Rtn4 (reticulon 4) and RhoA.

As expected following a severe traumatic injury, in addition to the typical increase in the inflammatory process and the activation of apoptotic and necrotic events, through GO analysis we have revealed the upregulation of genes involved in the activation of oxidative and nitrosative stress, as Sod2 (superoxide dismutase 2), Rasd1 (RAS, dexamethasone-induced 1), and COX-2.

In both injury groups, the majority of genes were downregulated. Following a 10% stretch, 789 genes were downregulated, and after 50% stretch, considerably fewer, 426 genes were downregulated. Studies of hippocampal gene expression following preconditioning and tolerance to epilepsy and ischemia have also shown a similar global downregulation of gene expression following the initial mild preconditioning stimuli. In these injuries, it is thought that gene suppression is a mechanism of the reprogramming response thought to occur in tolerance (Jimenez-Mateos et al., 2008).

The suppressed expression of genes appears to be a significant feature of reprogramming that occurs after other types of CNS injury, and may explain our results following mild TBI. The mechanism of reprogramming leading toward gene suppression is largely unknown, but it appears to be a function of the preconditioning stimuli, and may involve increased transcriptional silencing (Roopra et al., 2001) or other post-transcriptional mechanisms (Saugstad et al., 2007).

Our data globally showing the large number of downregulated genes following both injury levels, and especially the increase in the number of genes differentially expressed following 10% stretch and 50% stretch, allows us to conclude that the two-dimensional stretch of organotypic hippocampal slice culture model appears comparable to mild TBI *in vivo*.

Having shown that more genes are differentially expressed following a mild brain injury than a severe injury further supports the notion that even following a mild TBI, in which an absence of radiological and clinical abnormalities is the norm, an invisible complex cellular response is initiated and distinct neuronal dysfunction occurs. This corroborates previous data obtained after *in-vivo* TBI in a rodent model (Tavazzi et al., 2007; Vagnozzi et al., 2007), but it also confirms that these are primary cellular effects that are not determined by local blood or oxygen delivery, or by systemic factors. This challenges a widely-accepted pathophysiological model of TBI that has cerebral swelling and tissue ischemia at its center. In this model, cerebral swelling caused by trauma causes a rise in intracranial pressure (ICP), which consequently produces a drop in cerebral perfusion pressure (CPP; CPP = mean arterial pressure – ICP). ICP control remains the main-

Tavazzi, B., Vagnozzi, R., Signoretti, S., Amorini, A.M., Belli, A., Cimatti, M., Delfini, R., Di Pietro, V., Finocchiaro, A., and Lazzarino, G. (2007). Temporal window of metabolic brain vulnerability to concussions: oxidative and nitrosative stresses—part II. Neurosurgery 61, 390–395; discussion 395–396.

Teasdale, G., and Jennett, B. (1974). Assessment of coma and impaired consciousness. A practical scale. Lancet 2, 81–84.

Vagnozzi, R., Signoretti, S., Tavazzi, B., Floris, R., Ludovici, A., Marziali, S., Tarascio, G., Amorini, A.M., Di Pietro, V., Delfini, R., and Lazzarino, G. (2008). Temporal window of metabolic brain vulnerability to concussion: a pilot 1H-magnetic resonance spectroscopic study in concussed athletes—part III. Neurosurgery 62, 1286–1295; discussion 1295–1286.

Vagnozzi, R., Tavazzi, B., Signoretti, S., Amorini, A.M., Belli, A., Cimatti, M., Delfini, R., Di Pietro, V., Finocchiaro, A., and Lazzarino, G. (2007). Temporal window of metabolic brain vulnerability to concussions: mitochondrial-related impairment—part I. Neurosurgery 61, 379–388; discussion 388–379.

Vespa, P., Bergsneider, M., Hattori, N., Wu, H.M., Huang, S.C., Martin, N.A., Glenn, T.C., McArthur, D.L., and Hovda, D.A. (2005). Metabolic crisis without brain ischemia is common after traumatic brain injury: a combined microdialysis and positron emission tomography study. J. Cereb. Blood Flow Metab. 25, 763–774.

Vos, P.E., Battistin, L., Birbamer, G., Gerstenbrand, F., Potapov, A., Prevec, T., Stepan Ch., A., Traubner, P., Twijnstra, A., Vecsei, L., and von Wild, K. (2002). EFNS guideline on mild traumatic brain injury: report of an EFNS task force. Eur. J. Neurol. 9, 207–219.

Address correspondence to:
Antonio Belli, M.D., F.R.C.S., F.R.C.S. (S.N.), Ph.D.
Division of Clinical Neurosciences
University of Southampton
South Academic Block–MP806
Southampton General Hospital
Southampton, SO16 6YD, United Kingdom

E-mail: a.belli@soton.ac.uk

Investigation of microsphere-mediated cellular delivery by chemical, microscopic and gene expression analysis†

Lois M. Alexander,‡[a] Salvatore Pernagallo,‡[a] Alessandra Livigni,[b] Rosario M. Sánchez-Martín,[a] Joshua M. Brickman[b] and Mark Bradley*[a]

Received 20th July 2009, Accepted 22nd October 2009
First published as an Advance Article on the web 26th November 2009
DOI: 10.1039/b914428e

Amino functionalised cross-linked polystyrene microspheres of well defined sizes (0.2–2 μm) have been prepared and shown to be efficient and controllable delivery devices, capable of transporting anything from small dye molecules to bulky proteins into cells. However, the specific mechanism of cellular entry is largely unknown and widely variant from study to study. As such, chemical, biological and microscopic methods are used to elucidate the mechanism of cellular uptake for polystyrene microspheres of 0.2, 0.5 and 2 μm in mouse melanoma cells. Uptake is found to be wholly unreliant upon energetic processes, while lysosomal and endosomal tracking agents failed to show co-localisation with lysosomes/endosomes, suggesting a non-endocytic uptake pathway. To further explore the consequences of microsphere uptake, gene expression profiling is used to determine if there is a transcriptional response to "beadfection" in both murine and human cells. None of the common transcriptional responses to enhanced endocytosis are observed in beadfected cells, further supporting a non-endocytic uptake mechanism. Furthermore, the microspheres are noted to have a limited interaction with cells at a transcriptional level, supporting them as a non-toxic delivery vehicle.

Introduction

The development of cellular delivery devices, which includes cationic lipids, cell penetrating peptides (CPP's) and nanotubes and have been used to deliver anything from small dye molecules to large RNAs[1–3] into cells, has become a topic of zealous interest within the research community.

Some of the major hurdles that need to be overcome in order to develop an efficient delivery vehicle are ease of cargo loading to the delivery device, efficiency of delivery to the cytoplasmic region of the cell and controllability of cellular loading. However, a number of widely used delivery vehicles can have substantial, undesired cytotoxic effects, limiting their widespread use.[4,5]

In contrast, polymeric microspheres have been repeatedly demonstrated to be non-toxic and effective tools for cell biology, flow cytometry and medical diagnostics.[6–8] In addition, microspheres are able to enter a wide range of cell lines with high, but controllable loadings and can be easily functionalised with a range of moieties.

Despite the widespread utility of microspheres, the mechanism of microsphere uptake by non-phagocytic cells is poorly understood.[9] In general, two main uptake mechanisms may be considered: active endocytic processes[10] and/or passive diffusive mechanisms.[11] Insertion into the lipid bilayer and diffusion to the intracellular environment have previously been suggested for carbon nanotubes, amongst other mechanisms, after finding sodium azide, an inhibitor of adenosine triphosphate (ATP) hydrolysis, had a limited effect on uptake.[12] While some data support the notion that commercially available microspheres are taken up endocytically,[9,10,13,14] it is hard to reconcile this when their capacity to function as cytoplasmatic pH and calcium sensors has been demonstrated.[15,16] Microspheres have also been used to deliver siRNA intracellularly for the efficient gene silencing

[a] *Chemical Biology Section, School of Chemistry, University of Edinburgh, West Mains Road, Edinburgh, UK EH9 3JJ. E-mail: mark.bradley@ed.ac.uk; Fax: +44 (0)131 650 6453; Tel: +44 (0)131 651 3307*
[b] *MRC Center for Regenerative Medicine, Institute for Stem Cell Research, University of Edinburgh, West Mains Road, Edinburgh, UK EH9 3JJ*

† Electronic supplementary information (ESI) available: Fig. S1 shows the uptake of 2, 0.5 and 0.2 μm fluorescein microspheres by B16F10, E14 mES, HEK293T, HeLa, K562 and L929 cells as a function of time. Fig. S2 shows cellular viability by MTT assay following 24 hours incubation with microspheres. Fig. S3 shows the uptake of 2, 0.5 and 0.2 μm fluorescein microspheres by E14 mES, HEK293T, HeLa and L929 cells following treatment with 20 mM sodium azide. Fig. S4 shows the uptake of LacCer and transferrin controls under caveolae and clathrin-mediated endocytosis inhibition. Fig. S5 shows beadfected B16F10 cells pre-treated with mβ-CD and lovastatin. Fig. S6 shows cellular viability by MTT assay following treatment of B16F10 cells with chemical inhibitors. Fig. S7 shows beadfected B16F10 cells pre-treated with filipin III and genistein. Fig. S8 shows beadfected B16F10 cells pre-treated with chlorpromazine or under potassium depletion. Fig. S9 shows beadfected B16F10 cells pre-treated with DMA. Fig. S10 shows the uptake in B16F10 cells pre-treated with nocodazole. Fig. S11 shows real-time microscopy stills of a B16F10 cell ingesting 0.5 μm microspheres. Fig. S12 shows microscopy of cells treated with lysotracker red and microspheres. Fig. S13 shows the uptake of 2 and 0.5 μm microspheres in L929 and HEK293T cells after 48 hours and the cellular viability by MTT assay. Two real-time movies. Microarray data deposition: gene expression data have been deposited in ArrayExpress EBI (Experiment name: Bradley-Group_Microspheres for Cellular Delivery; ArrayExpress accession: E-MEXP-1845). See DOI: 10.1039/b914428e

‡ These authors contributed equally to this work.

of enhanced green fluorescent protein (EGFP) and functional proteins, such as β-galactosidase, which both require cytoplasmic localisation.[17,18] Taken together, these observations are inconsistent with an uptake mechanism that involves traditional endocytosis.

In this paper, the uptake of microspheres in several different cell lines was investigated as a function of microsphere diameter (0.2, 0.5 and 2 μm) and time of incubation (6–24 hours). Interestingly, microsphere uptake was found to be widely dependent on the microsphere diameter, with some cells taking up one size of microsphere better than others, with no logical patterns emerging. While these observations do not support endocytosis, this mechanism was investigated by both chemical modulation and sub-cellular localisation studies.

Microarray analysis was also used to determine whether significant gene expression changes occur in response to beadfection.[19,20] In particular, we show that there were no significant changes that occurred in response to microsphere uptake and that these changes did not include any of the known transcriptional responses to endocytosis. Moreover, this analysis showed no significant changes in genes associated with cell death using larger sized microspheres, suggesting that beads represent a highly effective, non-toxic method for cellular delivery.

Results

Cellular uptake of polystyrene microspheres

Uniform, monodisperse polystyrene amino-functionalised cross-linked microspheres (Fig. 1a and b) were synthesised by dispersion polymerisation as described previously, and coupled to different fluorophores as shown in Fig. 1c.[21]

In order to assess the uptake and toxicity patterns of 0.2, 0.5 and 2 μm amino-functionalised cross-linked polystyrene microspheres, and to assess their applicability as cellular delivery devices, fluorescein-conjugated microspheres were incubated with a range of cell lines (mouse melanoma (B16F10), human cervical cancer (HeLa), human embryonic kidney (HEK293T), mouse fibroblast (L929), erythroleukemic (K562) and feeder independent mouse embryonic stem cells (E14Tg2A)). As well as examining cell line dependence, microsphere uptake was assessed as a function of microsphere diameter (0.2, 0.5 or 2 μm) by flow cytometry (Fig. 2 upper).

Microsphere uptake was also confirmed by microscopy (Fig. 2a–c lower) and found to be high across all cell lines (approaching 95%), especially with use of the smaller sized microspheres (0.2 and 0.5 μm). Unsurprisingly, cellular uptake was also found to be time dependent, with longer incubations yielding higher uptakes across all sizes of microsphere (see Fig. S1 in ESI†).

To confirm that microsphere uptake did not affect viability in this range of cell lines, 3-(4,5-dimethylthiazol-2-yl)-2,5-diphenyltetrazolium bromide (MTT) cellular viability assays were used to estimate the percentage of viable cells in these cultures following treatment with a range of microspheres. Fig. S2 in ESI† shows that all cell lines contained greater than 90% viable cells following microsphere treatment, indicating that microspheres did not exert any cytotoxic effects on cells.

Chemical inhibition of uptake pathways

Uptake of microspheres is not energy dependent. Active mechanisms such as endocytosis are dependent on an energy source such as adenosine triphosphate (ATP).[22] If levels of ATP are depleted in cells then active mechanisms are consequently inhibited.[23] It was therefore examined whether microsphere uptake was energy dependent by incubating microspheres with cells that had been pre-treated with an inhibitor of ATP production, sodium azide (20 mM), which is known to block endocytosis.

Uptake of microspheres was measured by flow cytometry in 0.2% trypan blue in Hank's balanced saline solution (HBSS), designed to quench extracellular fluorescence so only cells containing microspheres intracellularly were detectable.[10,24]Fig. 3a shows that pre-treatment of cells with sodium azide had no effect on the uptake of microspheres in mouse melanoma B16F10 cells. Similar results were obtained with all other cell lines tested (see Fig. S3 in ESI†). In contrast, the uptake of FITC-conjugated transferrin and

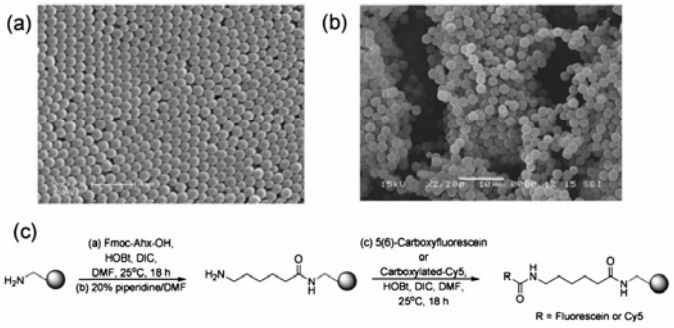

Fig. 1 Preparation of amino-functionalised polystyrene microspheres. Scanning electron microscopy images of (a) 0.5 μm and (b) 2 μm microspheres. (c) Chemical coupling of fluorescent dyes (fluorescein and Cy5) onto the microspheres. Fluorophore-coupled microspheres were prepared *via* an aminohexanoic unit to limit steric interactions and improve bioavailability.

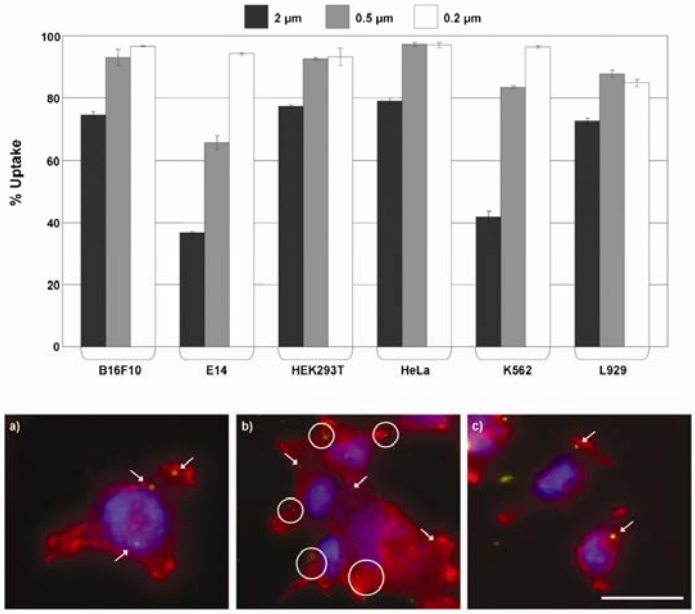

Fig. 2 Uptake of 2, 0.5 and 0.2 µm fluorescein labelled microspheres by cells. Top: uptake measured by flow cytometry after 24 h in B16F10, E14, HEK293T, HeLa, K562 and L929 cells (% uptake is the % of the total population containing microspheres where 0% is untreated cells). Bottom: images of B16F10 cells with: (a) 2 µm fluorescein microspheres; (b) 0.5 µm fluorescein microspheres; (c) 0.2 µm fluorescein microspheres. Actin filaments are stained with AlexaFluor 568-phalloidin and the cell nuclei are stained with Hoechst 33342. Scale bar is 25 µm.

BODIPY-labeled lactosyl ceramide (LacCer), which are known to be ingested by receptor-mediated endocytosis, was inhibited under these conditions (see Fig. S4 in ESI†).

The presence of cholesterol in the cellular membrane is also essential for energy dependent endocytosis and, as such, its depletion results in a general block on endocytic mechanisms.[25] We therefore sought to confirm that microsphere uptake was not reliant upon the presence of cholesterol by incubating microspheres with cells grown in a cocktail of cholesterol inhibitors that included mβ-cyclodextrin (mβ-CD) (to remove cholesterol already present in the membrane)[26] and lovastatin (to prevent the *de novo* synthesis of further cholesterol by inhibition of 3-hydroxy-3-methyl-glutaryl-CoA reductase).[25] Following pre-incubation of cells with mβ-CD (10 mM) and lovastatin (1 µg mL ^{1}), 0.2, 0.5 and 2 µm fluorescein microspheres were added and uptake was analysed by flow cytometry after 3 hours. Fig. 3b shows that incubation with these cholesterol inhibitors does not hinder microsphere uptake, while identical conditions blocked the endocytic uptake of both LacCer and transferrin. Microsphere uptake

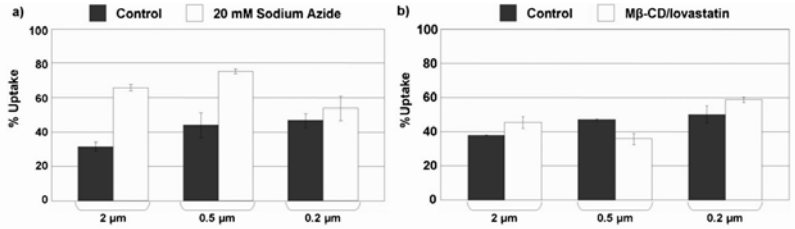

Fig. 3 Effect of ATP and cholesterol depletion on microsphere uptake. Uptake of 2, 0.5 and 0.2 µm fluorescein microspheres in B16F10 cells after 3 hours of (a) ATP depletion with sodium azide (20 mM); (b) cholesterol depletion with mβ-CD (10 mM) and lovastatin (1 µg mL^{-1}).

was additionally confirmed by microscopy (see Fig. S5 in ESI†), while MTT toxicity assays were undertaken to confirm mβ-CD and lovastatin did not significantly affect the number of viable, proliferating cells in these cultures (see Fig. S6 in ESI†).

Uptake of microspheres is not reliant upon caveolae. Although uptake was not found to be either ATP or cholesterol dependent, it was important to ensure that the uptake of microspheres did not occur by any form of endocytosis. As such, caveolae-mediated endocytosis, a mechanism known to be responsible for the uptake of LacCer, was selectively inhibited by the use of filipin III and genistein. Filipin III inhibits caveolae-mediated endocytosis by sequestering cholesterol in lipid rafts, which are essential for caveolae formation,[27] while genistein inhibits caveolae-mediated endocytosis by inhibiting a tyrosine kinase, which is required to phosphorylate proteins involved in caveolae formation.[28] B16F10 cells were incubated with filipin III (5 μg mL ^{1}) and genistein (200 μM), concentrations sufficient to inhibit the uptake of BODIPY FL C_5-lactosylceramide (LacCer)[29] (see Fig. S4 in ESI†), prior to the addition of microspheres. Fig. 4a shows that the uptake of microspheres by these cells, in which all caveolae-mediated endocytosis was blocked, was the same as in untreated cultures (measured by flow cytometry), demonstrating that caveolae-mediated endocytosis was unlikely to be responsible for microsphere entry in B16F10 cells.

Uptake was additionally confirmed by microscopy (see Fig. S7 in ESI†) and, as above, MTT assays were used to show that these inhibitors had no effect on cell viability at the doses used (see Fig. S6 in ESI†).

Uptake of microspheres is not reliant upon clathrin. As caveolae-mediated invaginations into the cellular membrane are generally 50–100 nm in diameter,[30] it may not be surprising that microspheres 4 to 40 times larger than these regions are not ingested *via* this mechanism. However, clathrin-mediated endocytosis can result in the formation of widely size variant endosomes, which are largely dependent on the cargo to be internalised.[31]

Clathrin-mediated endocytosis can be inhibited by chlorpromazine or depletion of potassium levels, known to disrupt the clathrin-mediated pathway by preventing coated pit assembly.[31,32] Inhibitor doses were established such that the endocytosis of FITC-conjugated transferrin was blocked[33] (see Fig. S4 in ESI†). Strikingly, cells that could not endocytose transferrin were still capable of taking up microspheres (Fig. 4b), indicating that clathrin coated pits were unlikely to be responsible for microsphere uptake (microscopy confirmed microsphere uptake under clathrin-coated pit inhibition, see Fig. S8 in ESI†). MTT assays showed that culturing cells under these conditions had little effect on the number of viable cells (see Fig. S6 in ESI†).

Uptake of microspheres is not reliant upon macropinocytosis. We also considered non-specific endocytic pathways, such as macropinocytosis, whereby a ruffling-like procedure by the cell membrane results in the formation of a vesicle, which may subsequently be internalised.[34] Membrane ruffling can be inhibited in two ways. Dimethylamiloride (DMA), an inhibitor of Na^+–H^+ exchange, blocks macropinocytosis by altering the concentrations of sodium ions, which are thought to be important to non-specific membrane ruffling. Alternatively, the underlying morphological rearrangements can be blocked by inhibiting F-actin elongation with cytochalasin D.

The effect of both these inhibitors on the uptake of microspheres (0.2, 0.5 and 2 μm) by B16F10 cells was analysed and quantified by flow cytometry and microscopy (Fig. 5 and Fig. S9 in ESI†). Interestingly, while DMA had little effect on microsphere uptake, cytochalasin D reduced microsphere uptake by 2–3-fold. Thus, while it appears unlikely that microspheres enter cells by macropinocytosis, there appears at least a partial requirement for actin polymerisation in the uptake process. This would suggest that uptake could involve some level of cytoskeletal rearrangement or may require an intact actin network for microsphere–cell interactions.

Uptake of microspheres is not reliant upon microtubule polymerisation. As actin polymerisation appeared relevant to uptake, the assessment of other cytoskeletal rearrangements known to be implicated in endocytosis was important. Lipid raft-mediated uptake and intracellular vesicular trafficking are thought to be dependent upon microtubule polymerisation and are blocked by nocodazole.[35] The capacity of nocodazole to inhibit microsphere uptake in B16F10 cells was therefore assessed. As with the other endocytosis inhibitors, nocodazole had little effect on microsphere uptake (see Fig. S10 in ESI†), suggesting that microtubule polymerisation is not required for either the interaction of the microspheres with the cellular membrane or their passage across the lipid bilayer. Thus

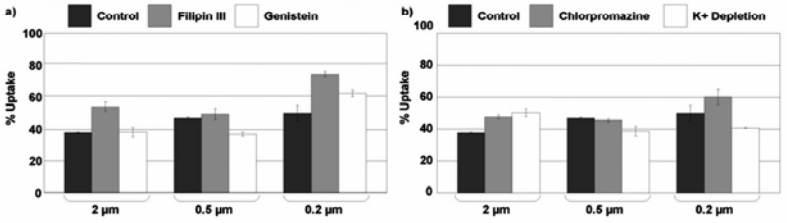

Fig. 4 Effect of inhibition on caveolae and clathrin-mediated endocytosis. Uptake of 2, 0.5 and 0.2 μm microspheres by B16F10 cells with a blockade on (a) caveolae-mediated endocytosis with filipin III (5 μg mL^{-1}) and genistein (200 μM); (b) clathrin-mediated endocytosis with potassium depletion (see Materials for buffer constituents) and chlorpromazine (10 μg mL^{-1}).

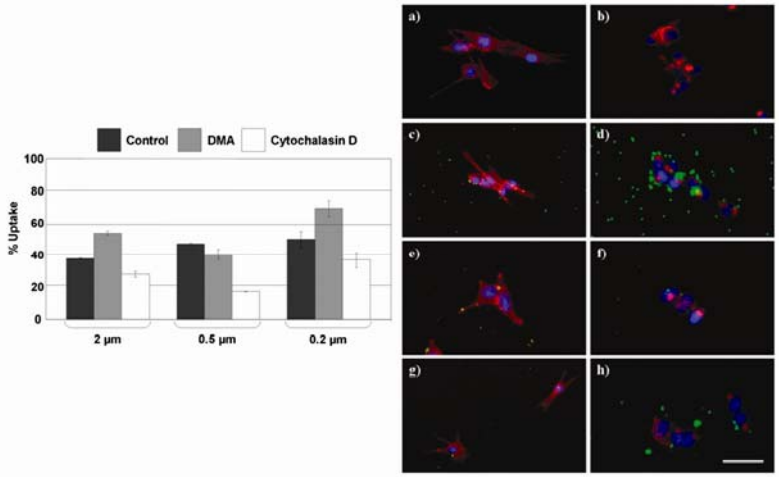

Fig. 5 Effect of macropinocytosis inhibition. Uptake of 2, 0.5 and 0.2 μm microspheres by B16F10 cells unable to undergo macropinocytosis. Left: DMA (10 μM) or cytochalasin D (10 μM) (% uptake is the % of the total population containing microspheres where 0% beadfection is untreated cell); right: microscopy of cells under standard incubation conditions (a, c, e and g) and in the presence of cytochalasin D (10 μM) (b, d, f and h). (a) and (b) are control cells with no microspheres; (c) and (d) are with 2 μm FAM-beads; (e) and (f) are with 0.5 μm FAM-beads; (g) and (h) are with 0.2 μm FAM-beads. Actin filaments are stained with AlexaFluor 568-phalloidin and the cell nuclei are stained with Hoechst 33 342. Scale bar is 140 μm.

despite a requirement for F-actin elongation and an intact cytoskeleton, lipid raft-mediated uptake is unlikely to be the mechanism by which microspheres are internalised.

Temperature dependence on uptake

Low temperatures have a substantial effect on cellular uptake processes, including endocytosis and passive diffusive mechanisms.[36] "Hardening" of the lipid bilayer at lowered temperatures would be expected to slow passive diffusive mechanisms due to increased membrane rigidity.[37] To examine the temperature dependence on uptake, B16F10 cells were incubated at 37, 20 and 4 °C and entry of microspheres into the cells was assessed after 3 hours by flow cytometry and microscopy (Fig. 6). In all cases, uptake was dramatically lowered at 20 °C and the effect was even more pronounced at 4 °C. At these low temperatures, microspheres do not extensively enter cells, but rather appear anchored to the cell membrane (Fig. 6a–c). Taken together with our inhibitor studies, these data suggest that the reduction in uptake is due to hardening of the lipid bilayer and a decrease in membrane fluidity, meaning passive movement across the membrane is hindered.

Endosomal and lysosomal markers

Although chemical inhibition of endocytic pathways had little effect on microsphere uptake, it is difficult to wholly rule out this mechanism. To further test whether microsphere uptake was in some way tied to endocytosis, the sub-cellular co-localisation of microspheres with endosomal and lysosomal markers was examined. FM4-64 is a commercially available lipophilic styryl dye, which through anchorage into the lipid bilayer labels the membrane of the cell and any subsequently formed endosomal compartments.[38] B16F10 mouse melanoma cells were pre-incubated with FM4-64 followed by 0.5 μm fluorescein microspheres and real-time confocal analysis carried out over a period of 30 minutes (see ESI† for the real-time movies).

Three microspheres were observed to have become anchored with the extracellular region of the cell and after repeated re-orientation of their alignment, the microspheres (still associated with one another) crossed the lipid bilayer rapidly and without the appearance of an endosome (see Fig. S11 in ESI†). However, disruption of the membrane was noted and evidenced by the association of the FM4-64 stain to one side of the microspheres, which gradually disassociated with time (it was no longer present after 15 minutes within the cell). Thus, microspheres appear to locally disrupt the membrane upon entering the cell and this observation would explain the reduction in uptake induced by inhibiting actin polymerisation.

To further confirm that this passage across the cell membrane does not result in lysosomal compartmentalisation, it was considered whether internalised microspheres co-localised with acidic organelles (lysosomes) following uptake.

As such, B16F10 cells were stained with LysoTracker Red, a dye capable of marking acidic compartments,[39] and analysed by confocal microscopy.

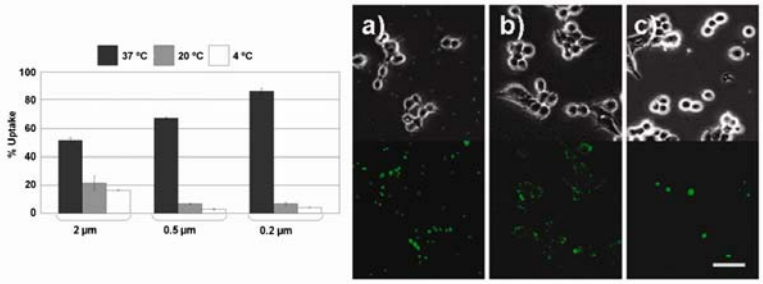

Fig. 6 Effect of temperature. Uptake of 2, 0.5 and 0.2 µm microspheres by B16F10 cells. Left: flow cytometry after 3 hours incubation; right: microscopy of cells with: (a) 2 µm microspheres incubated at 20 °C; (b) 0.5 µm microspheres incubated at 20 °C; (c) 0.2 µm microspheres incubated at 20 °C. Top are overlay images and bottom are fluorescence images. Scale bar is 300 µm.

Optical sections through cells containing internalised microspheres demonstrated that microspheres did not co-localise with lysosomes (Fig. 7 and Fig. S12 in ESI†), further supporting a mechanism which is not related to endocytosis.

Gene expression profiling

To further investigate the effect of microspheres on cells, the transcriptional consequences of uptake were analysed using gene profiling technology.[40] Agilent 4 × 44K whole human and mouse genome arrays were used to assess changes in gene expression levels that occurred as a result of the uptake of two differently sized microspheres (2 and 0.5 µm) in both mouse (L929 fibroblast) and human (HEK293T human embryonic kidney) cell lines. Transcriptional responses were examined in the hope of uncovering any significant and conserved changes in gene expression following beadfection (see Fig. S13 in ESI†).

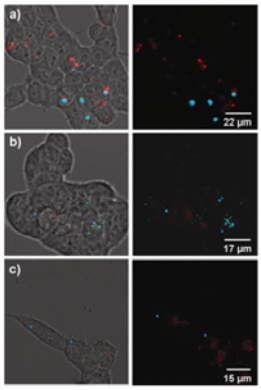

Fig. 7 Lysosomal staining. B16F10 cells incubated with Cy5 labelled microspheres (a) 2 µm; (b) 0.5 µm and (c) 0.2 µm microspheres (cyan) followed by LysoTracker Red (red). Images were collected on a Zeiss inverted confocal DM IRE2 microscope.

Preliminary analysis focused on the individual effect of microsphere size (0.5 or 2 µm) on HEK293T or L929 cells (see Tables SI–SIV in ESI†). In human HEK293T cells only 11 genes showed a greater than 2-fold expression change in response to 0.5 µm microspheres, while 21 genes changed their expression levels upon beadfection with 2 µm beads. In addition, only 5 genes were found to be in common between the two profiles (beadfection with 0.5 µm or beadfection with 2 µm).

Similar results were obtained with mouse L929 cells in which the expression levels of 28 genes were found to change in response to 0.5 µm microspheres and 13 genes were found to be up or down-regulated in response to 2 µm microspheres. In this case, only 3 genes were found to be common between the two sizes of microsphere. Strikingly, very few gene expression changes occurred upon treatment with either bead size, demonstrating how well tolerated the microspheres are by the cell. In addition, the genes altered were not conserved between species and significant homology was not evident.

To find any common changes between the two cell lines a more general analysis was performed, grouping the datasets irrespective of the microsphere diameter. In HEK293T cells, 38 genes appeared to be differentially expressed with over a 2-fold change in response to microsphere uptake, whereas, in mouse L929 cells, the expression levels of 74 genes were found to be altered (Fig. 8 and Tables SV and SVI in ESI†).

However, even with this less stringent approach the expression of only a small set of genes was found to change as a result of microsphere uptake and no homology could be found between the cell lines.

To determine if there were any core processes affected by microsphere uptake, gene ontology analysis was used to study their roles in biological processes that might be contained within any transcriptional response. In L929 cells, this confirmed that the addition of microspheres had no effect on cellular viability as the genes affected by beadfection were mainly related to cellular metabolism (Fig. 9, right). However, in HEK293T cells 2 genes out of 38 were noted to be involved in apoptosis or cell cycle arrest (Fig. 9, left), demonstrating the more sensitive nature of this cell line to beads over-loading.

Importantly, gene ontology analysis of both cell types generated results consistent with the chemical inhibitory

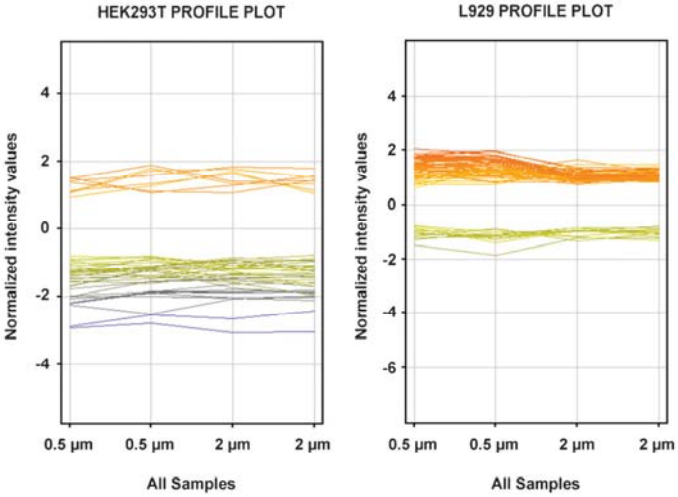

Fig. 8 Gene expression profiling. Profile plots of up and down-regulated genes across the 4 samples (normalised values in $\log_2$ scale). Analysis was made on four different subarrays. '0.5 µm' corresponds to subarrays hybridised with total RNA obtained from cells grown with 0.5 µm microspheres and '2 µm' corresponds to subarrays hybridised with total RNA obtained from cells grown with 2 µm microspheres.

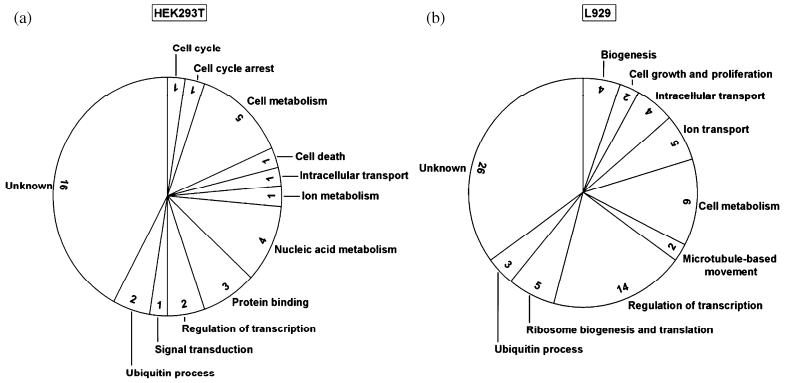

Fig. 9 Gene ontology. Pie graphs of gene ontology analysis. (a) HEK293T gene function of the 38 genes appeared to be differentially expressed with over a 2-fold change in response to the microspheres; (b) L929 cells, gene function of 74 genes found to be altered with a 2-fold change in the expression levels.

assays and microscopic analysis as none of the gene expression changes induced by microsphere uptake resembles those expected as a result of endocytosis.

Data validation

As no conserved patterns were observed in response to microsphere uptake, it appeared that both cell lines remained essentially unchanged in response to beadfection.

To confirm that these transcriptional profiles were accurate, the few statistically significant changes were validated by quantitative real-time PCR analysis. Transcripts showing a greater than 3-fold change in expression levels on the array chip were selected for further analysis (see Table SVII in ESI†). Independent biological samples from cells treated with microspheres under the same conditions, described for the microarray study, were used and a comparison was made

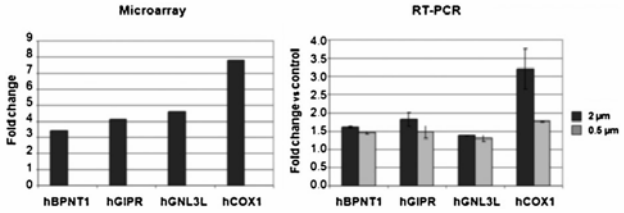

Fig. 10 Data validation. Comparison of the gene expression fold changes from microarray analysis (left panel) and quantitative real-time RT-PCR (right panel). For the real-time assay, HEK293T cells were incubated with 0.5 µm (grey) and 2 µm (black) microspheres. The *y*-axis represents the fold change relative to the untreated control cells. The transcripts number is normalised relative to human β-actin. The fold change value represents the mean of 2 experiments.

between the microarray and the quantitative PCR results (Fig. 10). In accordance with the microarray data, all the genes examined were found to be up-regulated in cells incubated with microspheres, although, overall, the fold changes seen were less dramatic than predicted by the microarray, however, the relative abundance of the transcripts was conserved.

None of the gene expression changes appear conserved between human and murine cell lines. The restricted number of transcripts moderately up-regulated in response to microsphere uptake having a role in metabolism, biogenesis and cell homeostasis. For example gastric inhibitory polypeptide receptor (GIPR) is a G-protein coupled receptor normally expressed in the fetal kidney and involved in glucose homeostasis.[41] Guanine nucleotide binding protein-like 3 (GNL3L) is a GTP-binding chaperone involved in ribosome biogenesis.[42] BPNT1 (bisphosphate 3′-nucleotidase) is a magnesium-dependent phosphomonoesterase that converts 3′(2′)-phosphoadenosine-5′-phosphate (PAP) to AMP, thus playing a role in nucleotide metabolism.[43] COX-1 (cytochrome oxidase subunit I)[44] is a mitochondrial transcript which encodes one of the major transmembrane subunits of cytochrome C oxidase, the last enzyme in the respiratory chain.

Discussion

In this paper, microspheres within a biologically relevant size range (0.2–2 µm) were shown to represent a highly efficient delivery system in a wide variety of cell lines, including mouse stem cells. The uptake of these microspheres was found to be size and time dependent (although cellular entry was high in all cases), but is independent of active transport. Moreover, the ingestion of these particles neither appears to impact on cell viability nor produce any significant changes in gene expression. As a result microspheres appear to represent a highly efficient, biologically inert delivery system.

Investigation of microsphere uptake was studied initially by chemical modulation and was found to be independent of both ATP and cholesterol depletion (both required for endocytosis). Moreover, a number of inhibitors were examined designed to block receptor-mediated (clathrin- or caveolae-mediated) endocytosis and they were found to have no impact on microsphere uptake at concentrations that significantly inhibited LacCer and transferrin uptake. Whilst these findings supported a non-endocytic mechanism, one inhibitor did appear to impact on uptake. Cytochalasin D, an inhibitor of F-actin polymerisation, yielded a decrease in uptake of up to 60% and microscopy revealed that microspheres could be seen to be 'sitting' on extracellular regions of the cells, unable to pass intracellularly. These observations suggest that microsphere uptake may require modulation of the actin cytoskeleton, in a process that does not require ATP hydrolysis.

Importantly, examination of the gene expression profile induced by microsphere uptake revealed no significant transcriptional changes in comparison to untreated control cells. Analysis performed using less stringent criteria identified small changes in a reduced number of transcripts (n = 38 and 74). Gene ontology of these subsets evidenced that none were typical transcriptional responses to endocytosis, further supporting a non-endocytic pathway.

Based on the absence of evidence for some form of endocytotic pathway, coupled to the requirement for actin polymerisation, we propose a mechanism whereby microspheres interact and anchor with the cell membrane. After a period of time that is dependant on bead microsphere diameter and cell line, membrane reorganisation occurs, facilitating the influx of the microsphere intracellularly. Such a mechanism must be wholly unreliant upon an energetic payload and would not result in the trapping of cargo within acidic organelles or result in cytotoxicity. As such, this renders microspheres as not only an efficient delivery vehicle, but also a device which may have wide ranging and versatile applications in a great number of areas of research.

Experimental procedures

Materials

Cellular uptake was assessed by flow cytometry using a BD Bioscience FACSAria equipped with the FACSDiva software. Cellular microscopy was performed on a Zeiss Axiovert 200M pseudo confocal microscope or a Leica inverted-confocal microscope and real-time microscopy was performed on a DeltaVision microscope. Real-time PCR was performed using a LightCycler 480 (Roche, UK) and a LightCycler 480 SYBR Green 1 Master (Roche, UK).

Styrene and *p*-divinylbenzene (DVB) were purchased from Sigma-Aldrich and *tert*-butylcatechol removed by washing

with 25% NaOH followed by water. 4-Vinylbenzylamine (VBAH) was prepared in-house from 4-vinylbenzylchloride (Sigma-Aldrich) as we have previously reported.[21] All other chemicals were used as received. Roswell Park Memorial Institute Medium (RPMI-CM) and Dulbecco's Modified Eagle Medium (DMEM) were purchased from Sigma-Aldrich and supplemented with 10% fetal bovine serum, 100 units per mL penicillin/streptomycin and 4 mM L-glutamine unless otherwise stated. Glasgow's Modified Eagle Medium (GMEM, Sigma-Aldrich) was supplemented with 10% fetal bovine serum; 0.25% sodium bicarbonate; 0.1% non-essential amino acids; 2 mM L-glutamine; 1 mM sodium pyruvate; 0.1 mM β-mercaptoethanol; 100 U mL $^{-1}$ leukaemia inhibitory factor (LIF).

Preparation of 0.2, 0.5 and 2 μm amino functionalised polystyrene-*co*-DVB microspheres

0.5 and 2 μm polystyrene microspheres were prepared by dispersion polymerisation as we have previously reported.[21] Briefly, AIBN (0.01 equiv.) was dissolved with VBAH (0.01 equiv.) in styrene (1 equiv.) with DVB (0.01 equiv.) and added to nitrogen degassed ethanol (or 93 : 7 ethanol–water to prepare 0.5 μm beads) with polyvinylpyrrolidone (M_w 40 000, 0.003 equiv.). The resulting solution was stirred (350 rpm) at 25 °C for 2 hours before the reaction mixture was heated to 70 °C and stirred for 18 h. The resulting microspheres were isolated by centrifugation (8500 rpm, 5–10 min) and washed sequentially with methanol and water. Microspheres were stored in sterile water at 4 °C.

0.2 μm polystyrene microspheres were prepared by emulsifier-free emulsion polymerisation as we have previously reported.[21] In brief, styrene (1 equiv.), DVB (0.02 equiv.), VBAH (0.01 equiv.) and magnesium sulfate (0.002 equiv.) were stirred in deoxygenated water for 30 min at 25 °C before heating to 80 °C and stirring at this temperature for 20 min. 2,2′-Azobis(2-amidinopropane) dihydrochloride (V-50, 0.003 equiv.) was added in a minimum volume of water and the emulsification was stirred at 80 °C for 2 h. Microspheres were subsequently isolated, washed and stored as described above.

Fluorophore labelling of amino functionalised polystyrene-*co*-DVB microspheres

0.2, 0.5 and 2 μm amino microspheres (30 mg) were washed in dimethylformamide (DMF, 3 × 1 mL) and isolated by centrifugation (13 000 rpm, 1–10 min dependent on the microsphere diameter). Fmoc-aminohexanoic acid (10 equiv.) was dissolved in DMF with 1-hydroxybenzotriazole hydrate (10 equiv.) and diisopropylcarbodiimide (10 equiv.) and stirred for 10 min at 25 °C before addition to the microspheres. The resulting suspension was mixed for 18 h at 25 °C and microspheres were then washed with DMF, methanol, water and then DMF. Fmoc deprotection was achieved *via* treatment with 20% piperidine–DMF and microspheres were subsequently washed sequentially with DMF–methanol–water. Carboxyfluorescein or Cy5-COOH (10 equiv.) was dissolved in DMF with (benzotriazol-1-yloxy)tripyrrolidinophosphonium hexafluorophosphate (PyBOP, 10 equiv.) and diisopropylethylamine (DIPEA, 10 equiv.), mixed for 1 min and then added to aminohexanoic microspheres suspended in DMF. The resulting suspension was mixed for 18 h at 25 °C and microspheres were then washed with DMF, methanol and water and finally stored in water at 4 °C.

Cell cultures

HeLa and K562 cells were cultured in RPMI; L929, HEK293T and B16F10 were cultured in DMEM; and E14Tg2A cells were cultured in GMEM on gelatine-coated flasks. Cells were grown to 70–80% confluency in a T75 flask at 37 °C/5% CO_2 prior to detachment, where appropriate, *via* trypsination. Cell pellets were collected by centrifugation (1100 rpm, 4 min) and re-suspended in the appropriate volume of culture medium before seeding onto polystyrene well plates (coated with gelatine for stem cell cultures).

Uptake of fluorophore labelled microspheres

Cells were cultured as described above in 24 well plates at a density of 3 × 10^4 cells per well. 24 h after seeding, labelled microspheres were added (86 μg mL $^{-1}$) and analysis was made as appropriate after 6, 12 and 24 h by flow cytometry in 0.2% trypan blue–Hank's balanced saline solution (HBSS) after cells were washed, trypsinised and centrifuged (1100 rpm, 4 min). Fluorescein fluorescence was excited using a 488 nm laser and emission collected using a 530/30 band pass filter.

Uptake under inhibition conditions

Cells were cultured as described above. Cells were pre-treated prior to the addition of microspheres with sodium azide (20 mM), mβ-CD (10 mM) with lovastatin (1 μg mL $^{-1}$), cytochalasin D (10 μM), DMA (10 μM), filipin III (5 μg mL $^{-1}$), genistein (200 μM), chlorpromazine (10 μg mL $^{-1}$), potassium depletion (140 mM NaCl, 20 mM Hepes, 1 mM $CaCl_2$, 1 mM $MgCl_2$, 1 mg mL $^{-1}$ D-glucose, pH 7.4) or nocodazole (10 μg mL $^{-1}$) in serum-free culture media for 1 h. Microspheres were then added and incubated with cells for 3 h. Cells were washed, trypsinised and collected by centrifugation before re-suspension in 0.2% trypan blue solution for flow cytometric analysis.

Cell viability studies (MTT assay)

Cells were cultured in a 96 well plate and microspheres were added (86 μg mL $^{-1}$ and 172 μg mL $^{-1}$) as described above. After 24 or 48 h the old media was removed and was replaced with phenol red-free culture media (100 μL) containing 3-(4,5-dimethylthiazol-2-yl)-2,5-diphenyltetrazolium bromide (MTT, 0.5 mg mL $^{-1}$). After 5 h, MTT solubilising solution (10% Triton X-100, 0.1 mol L $^{-1}$ HCl in anhydrous isopropanol, 100 μL per well) was added to dissolve the formazan crystals and the well plate was shaken overnight at 25 °C. Absorbance was measured at 570 nm and compared to that of untreated control cells.

Microscopy of cellular uptake

Cells were cultured and fluorescein-microspheres were added as described above. Cells were washed with PBS and the nuclei stained with Hoechst 33 342 (1 μg mL $^{-1}$) for 10 min. Cells were then fixed with 3% *p*-formaldehyde (20 min), washed (PBS) and the actin filaments stained with AlexaFluor 568-phalloidin

(1 unit per mL) for 15 min. Cells were washed with PBS prior to microscopy in 2% fetal bovine serum–PBS or 0.2% trypan blue–HBSS.

Real-time confocal microscopy

Cells were cultured on poly-lysine coated 24 mm glass coverslips and stained with FM4-64 as according to the manufacturer's instructions (Invitrogen). Fluorescein labelled 0.5 μm microspheres were added and incubated with cells for 10 min prior to mounting the glass coverslip on a deltavision RT microscope in an incubation chamber at 37 °C/5% CO_2 (exciting microspheres using a 490/20 nm excitation filter and collecting emission using a 528/38 nm band-pass filter and exciting FM4-64 using a 555/28 nm excitation filter and collecting emission using a 617/73 nm band-pass filter). Optical slices were repeatedly scanned over 30 min.

Microscopy of lysosomes

Cells were cultured and Cy5-microspheres were added as described above. LysoTracker Red DND-99 was used according to the manufacturer's instructions (Invitrogen). Microscopic evaluation was made on a Zeiss inverted confocal DM IRE2 microscope.

RNA isolation

Cells were cultured to a density of 2×10^5 cells per well in a 6 well plate. After 24 h, unlabelled amino-microspheres were added at a concentration of 86 μg mL^{-1} and incubated with cells for 48 h. Total RNA was isolated from both HEK293T and L929 cells grown with 0.5 and 2 μm microspheres and from untreated control cells. RNA extraction was performed using an RNeasy Mini Kit according to the manufacturer's protocol (QIAGEN, UK). The integrity and concentration of the total RNA were determined using an RNA 6000 Nano Assay Kit and a Bioanalyzer 2100 according to the manufacturer's protocols (Agilent, UK).

cRNA labelling

cRNA synthesis and labelling (fluorophores Cy3 and Cy5 both from PerkinElmer/NEN Life Sciences, UK) were performed using a Low RNA Input Linear Amplification Kit according to the manufacturer's protocol (Agilent, UK). cRNA was assessed using a NanoDrop® ND-3300 fluorospectrometer (Agilent, UK).

Hybridisation and scanning

Array hybridisation was performed using both 4 × 44K Whole Human Genome microarray (design 014850, Agilent) and 4 × 44K Whole Mouse Genome (design 014868, Agilent). Array hybridisation was achieved using a Gene Expression Hybridisation Kit from (Agilent, UK). The hybridised array was washed following the post-hybridisation washing step according to the manufacturer's Gene Expression Wash Buffer Kit protocol (Agilent, UK). The dried slides were scanned on an Agilent DNA microarray scanner (G2565AA, Agilent).

Data analysis

Datasets, pre-processed by Agilent's Feature Extraction 9.1, were analysed by Genespring GX 10. Datasets were filtered by flags given by the FE software (present, marginal and absent), only samples detected as present were used for the statistical analysis.

Two different data analyses were performed. Firstly, for each cell line, the data were grouped in two datasets, one for each size (0.5 μm and 2 μm) and independently analysed against the control (untreated cells). A second analysis was performed by grouping the two datasets together to analyse the more general interaction between microspheres and cells, irrespective of microsphere size, against the control (untreated cells). T-Test statistical analyses were carried out (T-test against zero) and *p*-values were computed asymptotically, where p-values < 0.01 were considered significant, meaning a probability of real changes in expression of 99.9%.

Quantitative real-time PCR analysis

Quantitative real-time PCR was used to validate the effect of the cell–polymer interactions on the gene expression profile. Total RNA was isolated from both HEK293T and L929 cells grown in the presence of 0.5 μm and 2 μm microspheres and untreated control cells. RNA extraction was performed using a RNeasy Mini Kit according to the manufacturer's protocol (QIAGEN, UK). The integrity and concentration of total RNA were determined using a RNA 6000 Nano Assay Kit and a Bioanalyzer 2100 (Agilent, UK). RNA (500 ng) was used for cDNA synthesis with Superscript III (Invitrogen), according to manufacturer's instructions. Real-time RT-PCR was performed using a LightCycler 480 (Roche) and a LightCycler 480 SYBR Green 1 Master (Roche). Primers were designed with the Roche ProbeFinder online and purchased from MWG-Operon. The following cycling conditions were used: denaturation: 95 °C 5 min, amplification: 95 °C 5 s, 58 °C 10 s, 72 °C 20 s (45 cycles), acquisition: 81 °C 1 s, melting curve: 95 °C 1 s, 65 °C 10 s, 95 °C—ramp 5 °C s^{-1} continuous, cool: −40 °C 10 s. Standard curves were generated from cDNA dilutions. Data were normalised relative to human β-actin.[45] PCR primers and annealing temperature (T_a) are listed in ESI† Table SVII.

Conclusions

In conclusion, microspheres of varying diameter have been analysed for uptake in a range of cell lines with a focus on their uptake in mouse melanoma cells. Uptake was not prevented following inhibition of either ATP hydrolysis or cholesterol synthesis or scavenging, nor slowed down by inhibitors of clathrin or caveolae mediated endocytosis or non-specific uptake *via* membrane ruffling. Although uptake by endocytosis is not limited to the mechanisms analysed here, microspheres appear not to be co-localised with acidic compartments and an endosome could not be observed by real-time confocal microscopy. This suggests that microspheres likely enter cells *via* a passive, but rapid mechanism. Furthermore, gene expression profiling of human and murine cells incubated with 2 μm and 0.5 μm microspheres revealed no significant changes in gene

expression. A handful of genes showed minimal changes and none of them was associated with a cell death or toxicity pathway, supporting the notion that the microspheres' presence within the cell is remarkably well tolerated and does not result in toxicity at the genetic level.

Acknowledgements

The authors would like to thank the BBSRC and the EPSRC for funding. R.S.M. would like to thank the Royal Society for a Dorothy Hodgkin Fellowship. The authors are grateful to Maria Lopalco for the Cy5 dye.

References

1 G. J. Nabel, E. G. Nabel, Z.-Y. Yang, B. A. Fox, G. E. Plautz, X. Gao, L. Huang, S. Shu, D. Gordon and A. E. Chang, *Proc. Natl. Acad. Sci. U. S. A.*, 1993, **90**, 11307–11311.
2 J. J. Díaz-Mochón, L. Bialy, J. Watson, R. Sánchez-Martín and M. Bradley, *Chem. Commun.*, 2005, 3316–3318.
3 Z. Liu, M. Winters, M. Holodniy and H. Dai, *Angew. Chem., Int. Ed.*, 2007, **46**, 2023–2027.
4 M. J. Parnham and H. Wetzig, *Chem. Phys. Lipids*, 1993, **64**, 263–274.
5 J. M. Wörle-Knirsch, K. Pulskamp and H. F. Krug, *Nano Lett.*, 2006, **6**, 1261–1268.
6 E. Boschetti and A. Schwarz, in *Medical and Biotechnology Applications: MML Series*, ed. R. Arshady, John Wiley & Sons, New York, 2nd edn, 1999, pp. 171–189.
7 A. Bernheim and M. A. Miglierina, *Biol. Cell*, 1986, **58**, 179–182.
8 S. Slomkowski, T. Basinska and B. Miksa, *Polym. Adv. Technol.*, 2002, **13**, 905–918.
9 W. Zauner, N. A. Farrow and A. M. R. Haines, *J. Controlled Release*, 2001, **71**, 39–51.
10 J. Rejman, V. Oberle, I. S. Zuhorn and D. Hoesktra, *Biochem. J.*, 2004, **377**, 159–170.
11 S. K. Banerji and M. A. Hayes, *Langmuir*, 2007, **23**, 3305–3313.
12 D. Pantarotto, J. Briand, M. Prato and A. Bianco, *Chem. Commun.*, 2004, 16–17.
13 P. Cherukuri, S. M. Bachilo, S. H. Litovsky and R. B. Weisman, *J. Am. Chem. Soc.*, 2004, **126**, 15638–15639.
14 S. Akhtar and K. J. Lewis, *Int. J. Pharm.*, 1997, **151**, 57–67.
15 R. M. Sánchez-Martín, M. Cuttle, S. Mittoo and M. Bradley, *Angew. Chem., Int. Ed.*, 2006, **45**, 5472–5474.
16 M. Bradley, L. Alexander, K. Duncan, M. Chennaoui, A. C. Jones and R. M. Sánchez-Martín, *Bioorg. Med. Chem. Lett.*, 2008, **18**, 313–317.
17 L. M. Alexander, R. M. Sánchez-Martín and M. Bradley, *Bioconjugate Chem.*, 2009, **20**, 422–426.
18 R. M. Sánchez-Martín, L. Alexander, M. Muzerelle, J. M. Cardenas-Maestre, A. Tsakiridis, J. M. Brickman and M. Bradley, *ChemBioChem*, 2009, **10**, 1453–1456.
19 J. Ziauddin and D. M. Sabatini, *Nature*, 2001, **411**, 107–109.
20 S. Pernagallo, J. J. Díaz-Mochón and M. Bradley, *Lab Chip*, 2009, **9**, 397–403.
21 R. M. Sánchez-Martín, M. Muzerelle, N. Chitkul, S. E. How, S. Mittoo and M. Bradley, *ChemBioChem*, 2005, **6**, 1341–1345.
22 S. L. Schmid and L. L. Carter, *J. Cell Biol.*, 1990, **111**, 2307–2318.
23 K. Sandvig and S. Olsnes, *J. Biol. Chem.*, 1982, **257**, 7504–7513.
24 V. L. Mosiman, B. K. Patterson, L. Canterero and C. L. Goolsby, *Cytometry, Part B*, 1997, **30**, 151–156.
25 I. S. Zuhorn, R. Kalicharan and D. Hoekstra, *J. Biol. Chem.*, 2002, **277**, 18021–18028.
26 E. P. Kilsdonk, P. G. Yancey, G. W. Stoudt, F. W. Bangerter, W. J. Johnson, M. C. Phillips and G. H. Rothblat, *J. Biol. Chem.*, 1995, **270**, 17250–17256.
27 P. A. Orlandi and P. H. Fishman, *J. Cell Biol.*, 1998, **141**, 905–915.
28 L. Pelkmans, D. Püntener and A. Helenius, *Science*, 2002, **296**, 535–539.
29 V. Puri, R. Watanabe, R. Deep-Singh, M. Dominguez, J. C. Brown, C. L. Wheatley, D. L. Marks and R. E. Pagano, *J. Cell Biol.*, 2001, **154**, 535–548.
30 J.-S. Shin and S. N. Abraham, *Microbes Infect.*, 2001, **3**, 755–761.
31 L.-H. Wang, K. G. Rothberg and R. G. W. Anderson, *J. Cell Biol.*, 1993, **123**, 1107–1117.
32 F. M. Brodsky, C. Y. Chen, C. Knuehl, M. C. Towler and D. E. Wakeham, *Annu. Rev. Cell Dev. Biol.*, 2001, **17**, 517–568.
33 E. M. Van Dam and W. Stoorvogel, *Mol. Biol. Cell*, 2002, **13**, 169–182.
34 S. Grimmer, B. Van Deurs and K. Sandvig, *J. Cell Sci.*, 2002, **115**, 2953–2962.
35 J. W. Murray and A. W. Wolkoff, *Adv. Drug Delivery Rev.*, 2003, **55**, 1385–1403.
36 S. C. Silverstein, R. M. Steinman and Z. A. Cohn, *Annu. Rev. Biochem.*, 1977, **46**, 669–722.
37 J. M. Hall, C. C. Parrish and R. J. Thompson, *Biol. Bull.*, 2002, **202**, 201–203.
38 W. J. Betz, F. Mao and C. B. Smith, *Curr. Opin. Neurobiol.*, 1996, **6**, 365–371.
39 D. R. Trollinger, W. E. Cascio and J. J. Lemasters, *Biophys. J.*, 2000, **79**, 39–50.
40 D. B. Wheeler, A. E. Carpenter and D. M. Sabatini, *Nat. Genet.*, 2005, **37**, S25–30.
41 V. Baldacchino, S. Oble, P. O. Décarie, I. Bourdeau, P. Hamet, J. Tremblay and A. Lacroix, *J. Mol. Endocrinol.*, 2005, **35**, 1–12.
42 X. Du, M. R. Rao, X. Q. Chen, W. Wu, S. Mahalingam and D. Balasundaram, *Mol. Biol. Cell*, 2006, **17**, 1–13.
43 T. Tsukihara, H. Aoyama, E. Yamashita, T. Tomizaki, H. Yamaguchi, K. Shinzawa-Itoh, R. Nakashima, R. Yaono and S. Yoshikawa, *Science*, 1996, **272**, 1136–1144.
44 B. D. Spiegelberg, J. Dela Cruz, T. H. Law and J. D. York, *J. Biol. Chem.*, 2005, **280**, 5400–5405.
45 V. S. Subramanian, Z. M. Mohammed, A. Molina, J. S. Marchant, N. D. Vaziri and H. M. Said, *J. Physiol.*, 2007, **582**, 73–85.